2015

# Functionalized Single Walled Carbon Nanotube / Polyamide Nanocomposite Membranes for Water Desalination

By
Wai-Fong Chan

Dissertation submitted to the faculty of the Virginia Polytechnic Institute and State University in partial fulfillment of the requirements for the degree of

Doctor of Philosophy
In
Chemical Engineering

Stephen M. Martin, Chair
Eva Marand
Donald G. Baird
Richey M. Davis
Andrea M. Dietrich

November 20, 2015
Blacksburg, VA

Keywords: Nanocomposite Membrane, Carbon Nanotube, Polyamide, Zwitterion, Functionalization, Desalination, Biofouling.

# Functionalized Single Walled Carbon Nanotube / Polyamide Nanocomposite Membranes for Water Desalination


## ABSTRACT

Cost-effective purification and desalination of water is a global challenge. Reverse osmosis (RO), the current method of choice, requires high pressure drops across the membranes in order to achieve acceptably high flow rates. Conventional polymer membranes are limited in their performance by a trade-off between water permeability and water/salt selectivity. Biofilm fouling is another critical problem in RO applications. Recent simulations and experiments suggest that properly functionalized carbon nanotubes (CNTs) can be used to construct RO membranes that have high permeation flux as well as complete ion rejection, and that are resistant to biofilm formation.

The objective of this research was to combine zwitterion-functionalized carbon nanotubes with traditional thin film polyamide (PA) to fabricate a novel desalination membrane which has both high permeability as well as selectivity. Zwitterion functional groups in CNTs act as molecular gatekeepers at the entrance of the nanotubes to enhance blockage for salt ions. Functionalized CNTs were oriented on a membrane support by high vacuum filtration. These oriented CNTs were sealed by a polyamide film via interfacial polymerization. Cross-sectional image of the nanocomposite membrane taken by scanning electron microscopy (SEM) showed semi-aligned zwitterion-CNTs on top of a porous support covered by a thin PA film with an overall thickness of approximately 250 nm.

When the concentration of zwitterion-CNTs in the membrane increased, the nanocomposite membranes experienced significant improvement in permeation flux while the ion rejection increases slightly or remains unchanged. This indicated that the increased water flux is not due to an increase in nonspecific pores in the membrane, but rather due to an additional transport mechanism resulting from the presence of the functionalized CNTs. Significant increase of flux was also observed in separating cations other than sodium. The separation of the PA skin layer dominated the ion rejection mechanism by size exclusion even when the carbon nanotubes were introduced into the polyamide coating.

The zwitterion functional groups exposed at the membrane surface also interacted with the feed water to form a strong hydration layer, which results in improved surface biofouling resistance. The adsorption rate of protein foulants on the nanocomposite membrane surface was significantly reduced compared to the control membrane without CNTs, and the adsorbed fouling layer could be easily removed by flushing with water. After washing, the nanocomposite membrane recovered 100% of the decreased water flux whereas the control membrane only recovered 10% of the decreased flux resulting in a permanent loss of 30% in water permeation. We have therefore demonstrated that advanced materials like CNTs can be synthesized with desired functional groups, and can be embedded into traditional RO membranes to simultaneously resolve the challenge of low flux and surface fouling in the current desalination process.

## *Acknowledgement*

"Save the world", I said to Dr. John Walz, our former department head, when he asked me what my ultimate goal is in research. It has been five and half years since then. I did not get a chance to save the world like the Marvel heroes do, but I have entered this unforgettable journey of innovation study in membrane science that changed my life completely. It is a total transformation one can only get from being on the path of doctor of philosophy. It is even more amazing when all the good and bad things that have happened to me work together and eventually lead me to a better future. I am truly thankful to have Dr. Eva Marand to be my advisor. She gave me a project that I love so much, and helped me fulfill part of my dream in saving the world, at least on the topic of making clean drinking water for civilizations around the globe. From her, I learned to treat my research as part of my own project and personal interest, not an assignment other people have given to you. I learned that when she was not around, I would have to be my own advisor and take care the business in the lab. I learned that when I think things are impossible to deal with, there is always a way out.

I was once lost in this journey, drifting by the flow and did not know what would happen to me tomorrow. Day in and day out, I wondered what I have gained through these trainings. Was this a training of independency? I wondered. Was it a training of patience? Patience in facing mind-battling questions regarding to the health of my advisor, my future, decision on keeping my own project alive or not, and comments others have given to me on job searching and research goals. I still remembered the toughest time when Dr. Marand passed away, I had to move my laboratory from the old Randolph Hall to the new building—Goodwin on the exact same week. The fatigue and emptiness was very hard to cope with. But I survived. Not just survived, I have also discovered that I was not disconnected from the surrounding. There were great love and care poured into me from everyone in the family and ChemE department.

Therefore, I can only be humble and thankful to this PhD degree that I have today. I did not earn this by my own hand, but by many support and comfort that I got from my friends. I want to say "thank you" to Dr. Stephen Martin, for helping me out step-by-step so I can walk towards the possibility of graduation. It is difficult for him so words cannot say enough of my gratitude. I want to thank Dr. Karl Johnson for giving me advices on my research project when Dr. Marand was not physically able to do so. I want to thank Dr. David Cox for the understanding of my struggling on research funding, and offered me the resource I needed to continue my work. I want to thank Dr. William Ducker for working me on my new research idea, and being so patient on teaching me about surface science, something that I do not have much experience before. I want to thank Diane, Tina and Brittany for preparing every document I need to sign to

continue my study in the department. I want to thank Jody Smiley form the Civil and Environmental Engineering department for helping me on measurement of testing solution. I will also need to thank my committee members for all the supports on my research projects. The discussion I have with them always fascinates me and become part of my main driving force on this research.

At the end, I want to thank my funding agency, which is the department of Chemical Engineering, the graduate school of Virginia Tech, and the US Bureau of Reclamation.

Thank You!

# Table of Contents

# List of Figures

# List of Tables

# Chapter 1. Introduction

## 1.1. Problem Statement

In 2012, the United Nations (UN) announced that water scarcity already affects every continent.[1] Around 700 million people in 43 countries are facing water shortages or lack of access to clean drinking water today. By 2025, 1.8 billion people will be living in countries or regions with absolute water scarcity, and two-third of the world's population could be living under water stressed conditions. Water scarcity is mainly caused by overwhelming human consumption, from growing water-thirsty meat and vegetables, to raising industries, urbanization and biofuel crops.[2] The scale of the water scarcity makes it an interconnected global issue, and minimizing the gap between water supply and demand is critical.

Although over 70% of the surface of the earth is covered with water, less than 3% of that water is fresh, while the rest is seawater and undrinkable. Moreover, the distribution of fresh water is not even over the globe. Fewer than 10 countries possess 60% of the world's available fresh water supply.[3] The importance of discovering ways to generate freshwater from seawater relates directly to the regional stability and sustainable growth of civilization, and the concept was well illustrated by President John F. Kennedy. In 1961, he told the Washington press corps that "if we could even competitively, at a cheap rate, get freshwater from saltwater, that would really dwarf any other scientific accomplishments."

Desalination, a technique that converts saline water into drinkable water, is one of the most important solutions for water scarcity.[4] The total global desalination capacity has been growing exponentially for the last decade and is expected to be over 100 million cubic meters ($m^3$) per day by 2016, twice the rate of global water production by desalination in 2008.[5–7] Reverse Osmosis (RO) is by far the most popular method in desalinating seawater into clean water. Other methods such as muti-stage flash (MSF) distillation and multiple-effect distillation (MED) are energy-intensive and will soon be out of the market.[8] Figure 1.1 shows the global fresh water capacity by different desalination processes and RO fulfills more than half of the supply. The majority of new desalination plants are based on RO membrane technology, and they have been built in Spain, which has the largest desalination capacity in the Mediterranean region, as well as in Singapore and Israel. These produce potable water that can meet 20 to 30% of the total demands.[9,10]

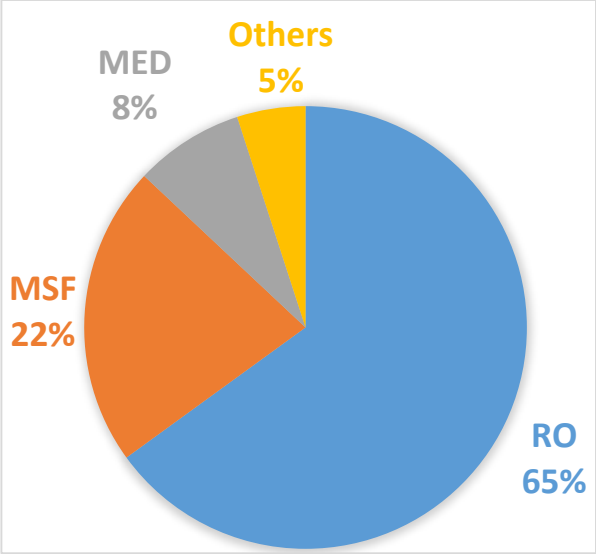


**Figure 1.1.** Total global desalination capacity by technology in 2013.[11]

RO technology utilizes semipermeable membranes to separate salt ions from water at the molecular level. This process has received tremendous improvement since the first commercial RO membrane was invented in 1959.[12] Significant cost reductions were achieved using advanced membrane materials, module design, process design and energy recovery. However, most of the RO membranes are made out of synthetic polymers, which show a tradeoff between water permeability and water/salt selectivity.[13] This fundamentally limits the performance of the desalination because higher water generation rates leads to lower salt rejection and water quality. Larger sizes of desalination plants and higher energy consumption will be required to insure that enough clean water is produced to meet the increasing demand. In fact, energy consumption is the major portion of the total cost of water desalination (~45% of the total cost).[8] More advanced technology is needed in synthesizing the next generation of RO membranes.

From the engineer's point of view, permeability and selectivity are the two most critical properties for studying and optimizing the performance of polymeric membranes. These two intrinsic properties are controlled by several factors, such as chain stiffness, degree of chemical crosslinking and water uptake properties. At steady state, the diffusive permeability of a penetrant $i$, $P_i$, can be written in terms of a sorption, or partition, coefficient, $K_i$, and an effective, concentration averaged diffusion coefficient, $D_i$.

$$P_i = K_i \times D_i \tag{1-1}$$

To improve the performance of an RO membrane, the diffusivity and partitioning of water molecules in the polymer matrix should be maximized, while that of salt ions are minimized. Although increasing the free volume and pore size of the membranes can increase the permeability of water, it could also reduce the resistance for salt transport and decrease the salt rejection of the membrane. In recent decades, new types of hybrid membranes which are made of out of inorganic

materials dispersed in a continuous organic polymer phase termed "mixed matrix membranes" (MMM) have emerged.[14] MMMs combine excellent properties provided from the additives with the easy processibility of polymeric membranes. Some of the additives like zeolites and carbon nanotubes have been used recently to fabricate hybrid RO membranes, due to their superior selectivity and transport velocity, respectively. Research studies on hybrid RO membranes show promising results that the embedded nanomaterials improve the permeability of water molecules while preventing salt ions from transporting through the membranes. Thus, they change the inherent trade-off relationship between permeability and selectivity in most of the polymeric membranes. Detailed information about the pros and cons of different designs and additives can be found in chapter 3.

Among all the inorganic nanomaterials, carbon nanotubes (CNTs) have caught the attention of many researchers in water filtration due to the similarity between their fluid transport properties and those of aquaporin biological channels.[15] Carbon nanotubes have exceptional transport properties because of the unprecedented smoothness of the potential energy surface inside the CNTs. Molecular dynamics (MD) simulations by Corry *et al*.[16] have shown that carbon nanotubes with pore diameters less than 9 Å can completely reject ions while allowing transport of water. Furthermore, recent experimental and computational studies both suggest that ion exclusion can be controlled by electrostatic interactions between the ions and fixed charges on the carbon nanotubes.[17–20] In this study, we fabricated polyamide nanocomposite membranes containing zwitterion-functionalized single wall nanotubes (Z-SWNTs). Membrane characterization and permeation experiments were conducted in order to fully understand the separation mechanism and the microstructure of this nanocomposite membrane. We also considered the applicability of functionalized CNTs in making large-scaled RO membranes for commercial purposes.

## 1.2. Research Studies

A summary of the research studies described in this is presented below.

1. **Synthesis of zwitterion functionalized carbon nanotubes.** The functionalization of CNTs with a zwitterionic group is described. The goal of this investigation is to improve the permselectivity of CNTs as well as their dispersion in the polymer matrix. Zwitterions are chemical groups that contain both positive and negative charges. They possess high dipole moments that improve the adhesion between the carbon nanotubes and the polymer

matrix and creates a defect-free mixed-matrix membrane. The zwitterionic group also protects the membrane surface from non-specific protein adhesion and prevents biofouling, one of the key issues in reverse osmosis applications. The zwitterion functional group we chose in this study has a length of approximately 1.1–1.2nm. This is very close to the pore diameter of CNTs we functionalized. These large chemical groups can greatly reduce the pore size of the carbon nanotubes can separate solvated ions from water molecules more effectively through size exclusion. The functionalized CNTs show higher nitrogen and oxygen content and lower in carbon content, indicating that the surface and tips of the CNTs are covered by zwitterionic groups.

2. **Reverse Osmosis of Zwitterionic CNTs/Polyamide Membranes.** The fabrication and characterization of zwitterion functionalized CNTs/polyamide membranes was studied. Zwitterionic CNTs were embedded in an all-aromatic polyamide layer by interfacial polymerization. RO Experiments were conducted to demonstrate that the addition of zwitterionic CNTs in the polyamide layer increases the water flux and salt rejection of the membrane. The rejection mechanism of the membranes was also studied using different types of salt ions and with different ionic strength in the feed solution.
3. **Anti-Biofouling Properties:** The surface fouling properties were studied for the zwitterionic CNT/polyamide membrane. Protein solutions were used to foul the membrane over a period of time in order to prove the hypothesis that zwitterionic groups present on the CNTs can reduce the adsorption rate of biofoulants on the membrane surface, and improve the performance and life-time of the membranes.

## 1.3. Outline of Chapters

**Chapter 2** consists of the background and theory of desalination membranes. The history of development of the semi-permeable reverse osmosis membranes is discussed briefly, followed by the study of the minimum energy required for overcoming the osmotic pressure. The transport principles of membranes described by the "solution-diffusion" model, and the selectivity in terms of diffusivity and solubility are discussed in detail. Other membrane types and transport models are also discussed in this chapter.

**Chapter 3** is a literature review of RO membranes, which summarizes the performance of commercial desalination membranes, different choices of monomers for growing the barrier layer on the membrane, surface modifications on desalination membranes, and finally the use of

nanomaterials in thin-film composite membranes and their relative performance. This chapter describes the emerging challenges for today's RO industry, and the research methods being used to resolve the issues. The chapter also contains a short comparison between reverse osmosis and nanofiltration membranes.

**Chapter 4** presents the computational and experimental studies of zwitterion-CNTs/polyamide nanocomposite membranes for desalination applications. Zwitterion carbon nanotube has been studied using molecular dynamics simulations and shows perfect salt rejection when two functional groups are attached at both ends of the nanotubes. A dispersion of zwitterion functionalized CNTs was filtered through a porous polyethersulfone support to partially align the CNTs. Aligned CNTs were then embedded in a polyamide thin layer to form a thin-film nanocomposite membrane with the overall thickness of the barrier layer approximately 250 nm. The water permeation flux and salt rejection have been examined in terms of the concentration of carbon nanotubes present in the membrane as well as the salt concentration in the feed solution. Water flux of the polymeric membrane has been improved by more than 3-fold while salt rejection increased slightly, indicating that new transport mechanism was introduced into the membrane so that the membrane did not show any trade-off between water permeability and water/salt selectivity.

**Chapter 5** presents more detailed experimental studies of the zwitterion-CNTs/polyamide nanocomposite membrane. Improvement in water flux was observed when other feed solutions containing different cations and anions were used in testing the nanocomposite membranes. Experimental studies also demonstrated that salt ions were rejected mainly by size exclusion rather than electrostatic repulsion. The trade-off between the degree of crosslinking and the amount of carbon nanotube embedded in the thin layer is studied extensively. The hypothesized existence of nanochannels at the interface between CNTs and the polymer phase is discussed. The pore size and its distribution for the membrane was measured in order to clarify the possible pathways within the nanocomposite membranes for water transport. Zwitterionic groups attached on the CNTs also demonstrated the ability to improve the surface biofouling resistance by reducing the adsorption rate of protein at the surface. The deposited foulant layers were also less strongly adhered than on the control membrane, and could be easily removed by water cleansing.

**Chapter 6** contains a discussion of experimental considerations for fabricating thin-film nanocomposite membranes with desired properties. Different fabrication methods, including the

types of monomer, pH condition of the aqueous phase, organic solvent, contact time, and thermal treatments, are discussed. This serves as a future guide for those who wants to replicate this work, develop new thin-film nanocomposite membranes, or optimize the performance of existing nanocomposite membranes.

**Chapter 7** contains a summary of the research, and describes proposed areas for future work including:

- Study the adhesion force between polyamide chains and the carbon nanotubes with different functional groups.
- The force can be measured by AFM tip that is coated with polyamide short chain. The chain can then be brought close to the CNTs and measure the force curve it generates during the contact.

## 1.4. Common Terminology

RO [=] Reverse Osmosis

NF [=] Nanofiltration

TFN [=] Thin-film Nanocomopsite

TFC [=] Thin-film Composite

CNT [=] Carbon Nanotubes

SWNT [=] Single-walled Carbon Nanotubes

## References


(1) UN-Water. *Managing Water under Uncertainty and Risk*; United Nations Educational, Scientific and Cultural Organization, 2012; Vol. 1.

(2) Lee, K. P.; Arnot, T. C.; Mattia, D. A Review of Reverse Osmosis Membrane Materials for desalination—Development to Date and Future Potential. *Journal of Membrane Science* **2011**, *370*, 1–22.

(3) Fry, A.; Martin, R. Facts and Trends: Water. *World Business Council for Sustainable Developement* **2006**.

(4) Gleick, P.; Cooley, H.; Cohen, M.; Morikawa, M. The World's Water 2008-2009: The Biennial Report on Freshwater Resources. **2008**.

(5) New Desalination Capacity, 1980-2009-Chart, Global Water Intelligence, 10. **2009**.

(6) Desalination: A National Perspective, National Academies Press. **2009**.

(7) The Big Dipper: Contracted Desalination Capacity Forecast-Chart, Global Water Intelligence, 10. **2009**.

(8) Buonomenna, M. Nano-Enhanced Reverse Osmosis Membranes. *Desalination* **2013**, *314*, 73–88.

(9) Hoek, E. M. V.; Tarabara, V. V. *Encyclopedia of Membrane Science and Technology*; 2013.

(10) Talbot, D. Megascale Desalination: The world's largest and cheapest reverse-osmosis desalination plant is up and running in Israel. http://www.technologyreview.com/featuredstory/534996/megascale-desalination/.

(11) International Desalination Association. Global Data Report DesalData (2013-2014). *IDA desalination yearbook* **2013**.

(12) Reid, C. E.; Breton, E. J. Water and Ion Flow across Cellulosic Membranes. *Journal of Applied Polymer Science* **1959**, *1*, 133–143.

(13) Geise, G. M.; Park, H. B.; Sagle, A. C.; Freeman, B. D.; McGrath, J. E. Water Permeability and Water/salt Selectivity Tradeoff in Polymers for Desalination. *Journal of Membrane Science* **2011**, *369*, 130–138.

(14) Kulprathipanja, S. *Zeolites in Industrial Separation and Catalysis*; 2010.

(15) Zhu, F.; Tajkhorshid, E.; Schulten, K. Theory and Simulation of Water Permeation in Aquaporin-1. *Biophysical journal* **2004**, *86*, 50–57.

(16) Corry, B. Designing Carbon Nanotube Membranes for Efficient Water Desalination. *Journal of Physical Chemistry B* **2008**, *112*, 1427–1434.

(17) Corry, B. Water and Ion Transport through Functionalised Carbon Nanotubes: Implications for Desalination Technology. *Energy & Environmental Science* **2011**, *4*, 751.

(18) Fornasiero, F.; Park, H. G.; Holt, J. K.; Stadermann, M.; Grigoropoulos, C. P.; Noy, A.; Bakajin, O. Ion Exclusion by Sub-2-Nm Carbon Nanotube Pores. *Proceedings of the National Academy of Sciences of the United States of America* **2008**, *105*, 17250–17255.

(19) Majumder, M.; Chopra, N.; Hinds, B. J. Effect of Tip Functionalization on Transport through Vertically Oriented Carbon Nanotube Membranes. *Journal of the American Chemical Society* **2005**, *127*, 9062–9070.

(20) Majumder, M.; Zhan, X.; Andrews, R.; Hinds, B. J. Voltage Gated Carbon Nanotube Membranes. *Langmuir : the ACS journal of surfaces and colloids* **2007**, *23*, 8624–8631.

# Chapter 2. Theory and Background of Reverse Osmosis

## 2.1. Introduction and History

Reverse osmosis (RO) is a water purification process using membranes that are permeable to water but essentially impermeable to the dissolved salts. The salt solution is pressurized and fed to one side of the membrane. Water is withdrawn from the feed solution and permeate through the membrane, leaving as a low-pressure permeate, while the depleted salts/impurity stay in feed stream and become a concentrated brine.

The discovery of using membranes to separate small solutes from water can be dated back to 1748 by Jean-Antoine Nollet. Pfeffer, Traube and others were, however, the first to study osmotic phenomena with ceramic membranes around the 1850s. In 1931, the process was recognized officially as a method of desalting water[1] and patented by the term reverse osmosis. It did not obtain much interest in generating fresh drinking water until the first cellulose acetate film was synthesized by Reid and Breton at the University of Florida in 1959.[2] The flux of their membranes was very low due to the excess thickness (5–20 μm thick) required to form a free-standing membrane. However, by pressurizing the feed solution to 1000 psi, the membrane could provide salt removals better than 98 %. A breakthrough discovery by Sidney Loeb at the University of California at Los Angeles and Srinivasa Sourirajan at the National Research Council of Canada, Ottawa in 1962 made reverse osmosis a practical desalting process. The Loeb-Sourirajan anisotropic cellulose acetate membrane[3] was characterized by an effectively thin "skin" layer supported atop a highly porous and much thicker substrate, which resulted in 10 times the flux of the best Reid and Breton membrane with equivalent rejections. With this design water desalination by RO become a practical process and small demonstration plants were installed in the next few years. Different types of module design (tubular, spiral-wound, and hollow fiber) were also developed in order to utilize the membranes in a large-scale filtration system.[4–6]

Anisotropic cellulose acetate membranes became the industry standard through the 1960s to the mid-1970s, until John Cadotte, of Dow FilmTec® Corporation, developed the interfacial polymerization method for producing composite membranes.[7] Ultra-thin aromatic polymer layers with thicknesses < 200 nm were coated atop porous ultrafiltration membrane substrates via the interfacial polymerization process, and acted as a skin barrier that had extremely high salt rejections and fast water fluxes.[8,9] The high durability contributed by the aromatic structure made it the new industry standard. This interfacial composite membrane was commercialized in 1975

and installed in a large reverse osmosis seawater desalination plant at Jiddah, Saudi Arabia.[10] As the focus moved toward the removal of trace amounts of salts and other dissolved solutes from brackish and waste water, recent developments beginning in the mid-1980s, resulted in the synthesis of super-thin nanofiltration (NF) membranes able to operate under low pressures[11,12]. These membranes are used to treat already good-quality water to produce ultra-pure water for the electronics industry. Under this influence, more and more nanofiltration membranes have been synthesized and fully developed into large-scale processes in the 2000s.

In the 1990s, along with investments in large-scale desalination plants within the US and Europe, improvements in water desalination have been shifted towards better energy recovery devices (such as "turbochargers", "pressure exchangers" or "work exchangers"), designs of membrane modules and configurations of membrane arrays, water pretreatment and post-treatment. Energy consumption for Reverse Osmosis desalination processes have been significantly reduced down to approximately 1.8 kWh per cubic meters of fresh water generated from seawater in 2015, compared to over 6 kWh/$m^3$ in the 1980s.[13] The development in new membrane materials or designs, however, has been greatly reduced, letting the interfacial composite membranes by FilmTec® dominate most of the market. In 2007, a new concept of dispersing zeolite nanoparticles in thin film composite membranes was proposed by Hoek *et al.*[14] Since then, numerous studies on using nanomaterials with superior properties to enhance the performance of RO active layer were conducted and have had significant impacts on the conventional desalination process. This has resulted in a new type of RO membranes called thin-film nanocomposite (TFN) membranes. In 2011, a start-up water company named Nano$H_2O$ (since purchased by LG) commercialized the first TFN membrane, with water flux over 2 times faster than other commercial seawater desalination membranes. The current desalination industry involves multi-billion dollar investments worldwide, with half of the facilities installed in the United States, Europe, North Africa, and Japan. The remainder are installed in the Gulf region in Middle East. The global desalination capacity is expected to be over 100 million $m^3$ per day by 2016. In some regions where fresh water relies on imports from other countries, such as Singapore and Israel, better and faster desalination plants also mean economic reform because it can provide a significant amount of the potable water supply for daily usage and agriculture. Some of the milestones in the development of the RO industry are summarized in Figure 2.1.

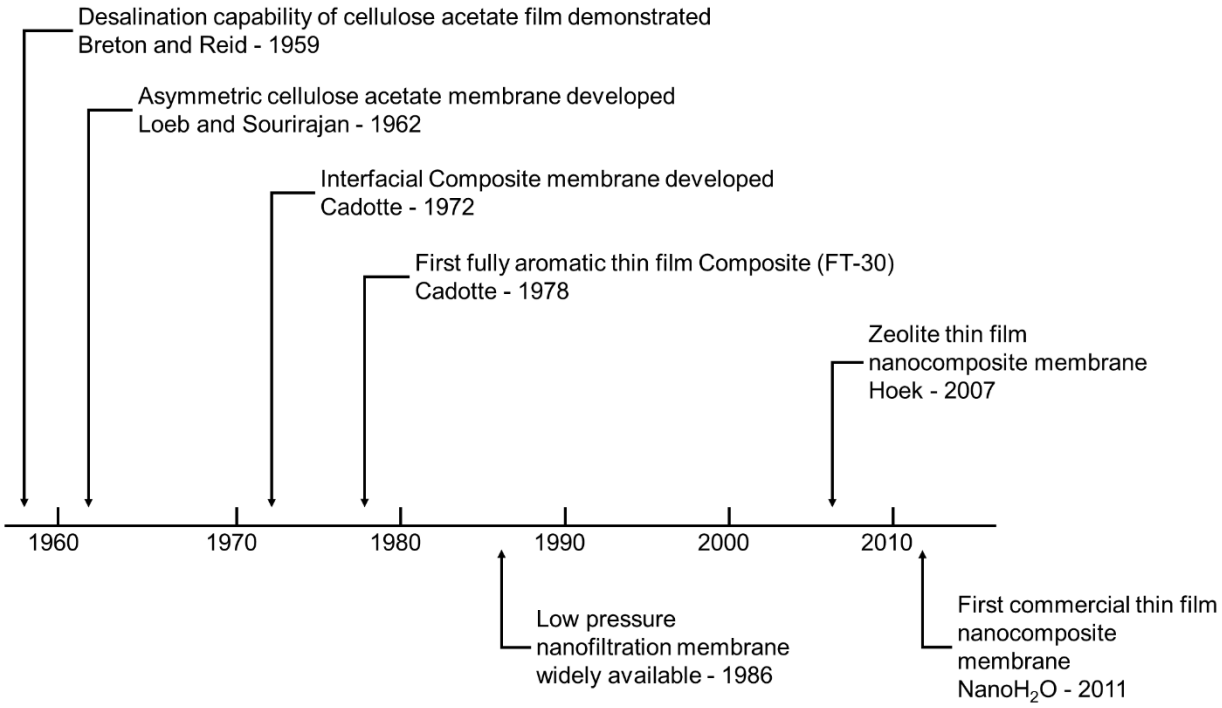


**Figure 2.1.** Milestones in the development of RO membranes, modified from Richard W. Baker, *Membrane Technology and Applications*, 2nd edition, p. 192, copyright 2004.[15]

## 2.2. Theoretical Background of Reverse Osmosis

When a semipermeable membrane is placed between a salt solution and pure water, normal osmosis occurs spontaneously to equalize the solute concentrations on both sides. Water permeates the membrane from the pure water side into the salty side to dilute the concentration of salt. If a hydrostatic pressure is applied to the salt side of the membrane, the flow of water can be retarded and, when the applied pressure is sufficient (equivalent to the osmotic pressure), the water ceases to flow across the membrane. The hydrostatic pressure required to stop the water flow is called the osmotic pressure ($\Pi_s$). If pressures greater than the osmotic pressure are applied to the salt side of the membrane as shown in Figure 2.2, then the flow of water can be reversed, and begins to flow from the side of salt solution to pure water side. This process is called reverse osmosis.

### 2.2.1. Minimum Energy for RO

The ideal desalting process for seawater is equivalent to the reversed thermodynamic process of mixing between salt and water.[16] The energy for the separation will thus be equal in magnitude but opposite sign to the free energy of mixing.

Van't Hoff's equation gives

$$w_{thO} \cong \Pi_s V_w \tag{2-1}$$

where $w_{thO}$ is the theoretical work of separation per unit water product for infinitesimal recoveries, $\Pi_s$ is the osmotic pressure, and $V_w$ is the infinitesimally small volume of desalted water across a semipermeable membrane.

The close relationship between the free energy of mixing and the osmotic pressure can then be[13]:

$$-d(\Delta G_{mix}) = -RTlna_w dn_w = \Pi_s \overline{V_w} dn_w \tag{2-2}$$

where $\Delta G_{mix}$ is the free energy of mixing, R is the ideal gas constant, T is the absolute temperature, $a_w$ is the activity of water, $n_w$ is the number of moles of water , and $\overline{V_w}$ is the molar volume of water. This is consistent with our understanding of reverse osmosis, that the minimum applied pressure to drive infinitesimally small volume of water across the membrane must be equal to the osmotic pressure of seawater.

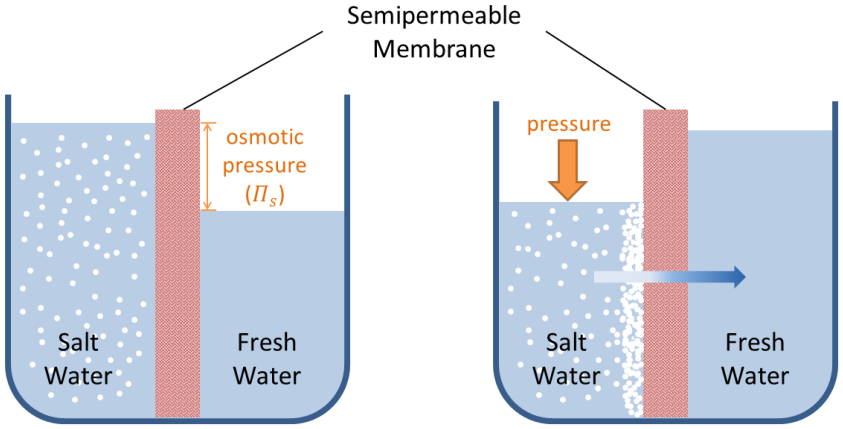


**Figure 2.2.** Reverse Osmosis happens when hydrostatic pressure applies on solvent-rich side. Water permeates through the semi-permeable membrane leaving salt ions as the retentate.

The theoretical minimum energy for desalination is a function of the percent recovery of fresh water.

$$\text{recovery rate} = \frac{\text{product flow rate}}{\text{feed flow rate}} = \frac{Q_P}{Q_F} \tag{2-3}$$

Figure 2.3 shows the ideal desalting process, where the product is assumed to be pure water. In reality, there will always be trace amount of salt present in the product stream (< 0.5%). The mass and mole balances for the system are as follows:

$$Q_F = Q_P + Q_R \tag{2-4}$$

$$Q_F C_F = Q_P C_P + Q_R C_R \tag{2-5}$$

Since $C_P$ is assumed to be zero, all the salt ions in the feed are rejected and carried away through the retentate stream. The higher the recovery rate, the more pure water is drawn out from the feed, and the higher the salt concentration will be in the retentate. Furthermore, since the concentration at the feed side in the RO system, $C_{in}$, is described as the average of feed and retentate concentration, $C_{in}$ increases as the recovery rate goes up. Eventually, the osmotic pressure in the feed side, as described in equation (2-6), will also increase significantly.

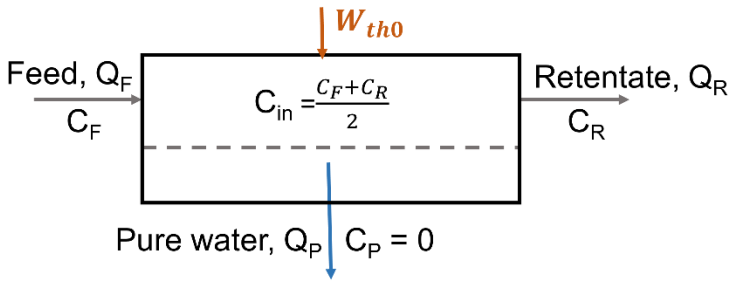


**Figure 2.3.** Ideal desalting process

$$\Pi_s = \Delta C_s RT = C_{in} RT \tag{2-6}$$

where $\Delta C_s$ is the concentration difference between the feed and permeation sides. As the salinity of seawater or the desired water recovery increases, so does the minimum energy required for desalination in order to overcome the rising osmotic pressure. For example, the theoretical minimum energy of desalination for seawater at 35,000 parts per million (ppm) salt and at a typical recovery of 50% is 0.8 kWh/m$^3$. The minimum energy increases to 1.0 kWh/m$^3$ at 45,000 ppm of salt under the same recovery rate (depicted in Figure 2.4). The actual energy consumption would be approximately 1 kWh/m$^3$ larger due to the finite size of the desalination process, heat loss in irreversible thermodynamic processes, and other energy consumption in the intake, pretreatment and posttreatment steps.[13]

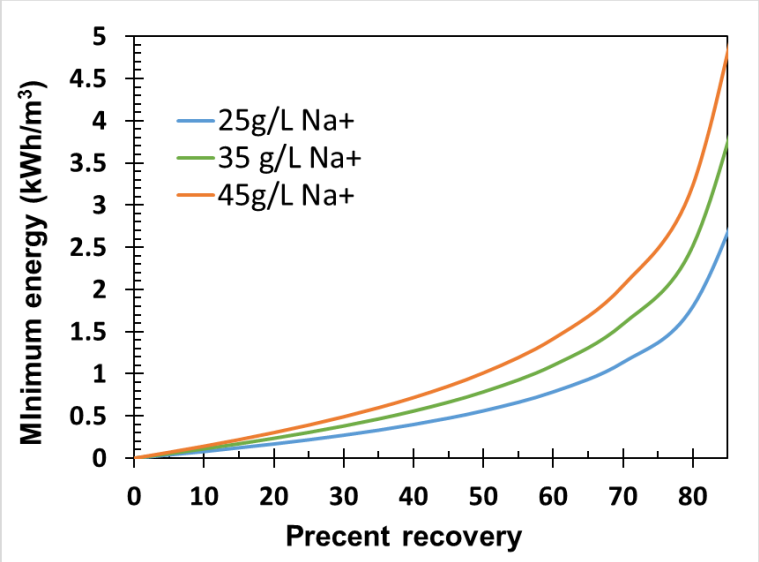


**Figure 2.4.** Theoretical minimum energy for desalination as a function of recovery rate of common seawaters: 25 g/L is typical of the less saline seawater drawn from the Tampa Bay estuary. 35 g/L is the average value for seawater, and 45 g/L is characteristic of water from the Arabian Gulf.

### 2.2.2. Solution-Diffusion Model

The properties of the semi-permeable membrane are the most important factors in controlling the performance of the reverse osmosis process. RO membranes are usually made out of synthetic polymers such as cellulose acetate and polyamide, and are characterized as dense nonporous membranes with fluid transport across the polymer described by the solution-diffusion model. This is the same model applied to pervaporation and gas separation membranes. According to this model, pressure, temperature, and the composition of fluids on either side of the membrane determine the concentration of the diffusing species at the membrane surface in equilibrium with the fluids. Once dissolved in the membrane, individual permeating molecules move by the same random process of molecular diffusion no matter whether the membrane is being used in reverse osmosis, pervaporation, or gas permeation. Figure 2.5 provides a schematic of the chemical potential, concentration, and pressure gradients assumed in a solution-diffusion membrane. Both salt and water molecules dissolve at the interface and diffuse through the membrane from the high to low chemical potential side. The higher chemical potential at the feed side is due to the applied hydraulic pressure, $P_o$, that overcomes the osmotic pressure and increases the overall activity of the feed solution. The pressure within the membrane is assumed to be constant at the high-pressure value, and there is a discontinuity in pressure at the permeate side of the membrane, where the pressure falls suddenly from $P_o$ to $P_L$. It is unlike the situation in a porous polymer film, where the pressure of the fluid within the pores decreases continuously through the film. Nonporous

membranes require the hydrostatic pressure to be constant throughout the film thickness to maintain mechanical equilibrium.[17]

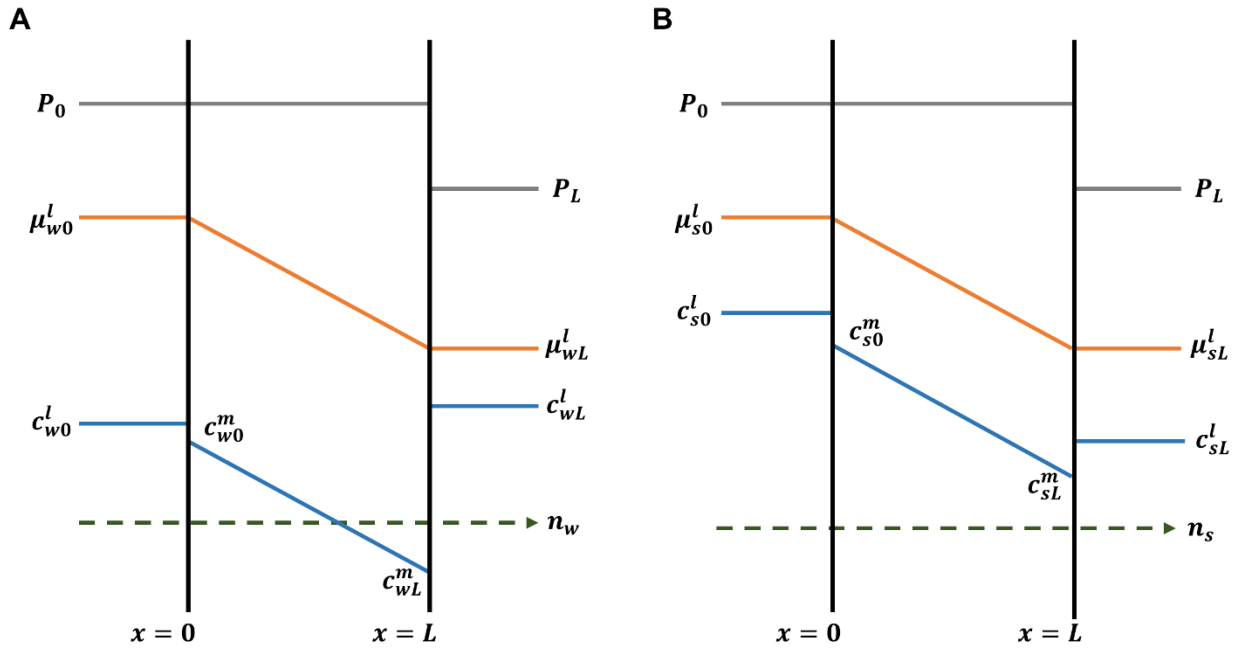


**Figure 2.5.** Profiles of the hydrostatic pressure, $p$, chemical potential, $\mu$, and concentration, $c$, in a dense, non-porous polymer film of thickness L for water (A), subscript $w$, and salt (B), subscript $s$. The permeation direction of the flux, $n$, is indicated. Superscripts $l$ and $m$ refers to the external solution and membrane phases, respectively, and the subscripts $0$ and $L$ refer to the feed and permeate sides of the film, respectively.

The second step in this process, diffusion through the membrane matrix, is the rate limiting step.[18] The diffusion, furthermore, is governed by the opening and closing of transient gaps, as shown in Figure 2.6, to allow penetrants to execute diffusional jumps within the matrix. This phenomenon is due to the thermally stimulated, local segmental dynamics of the polymer chains[19,20]. At steady state, the diffusive permeability of a penetrant $i$, $P_i$, can be written in terms of a sorption, or partition, coefficient, $K_i$, and an effective, concentration averaged diffusion coefficient, $D_i$.

$$P_i = K_i \times D_i \tag{2-7}$$

This relationship describes both water and ion transport through polymers.

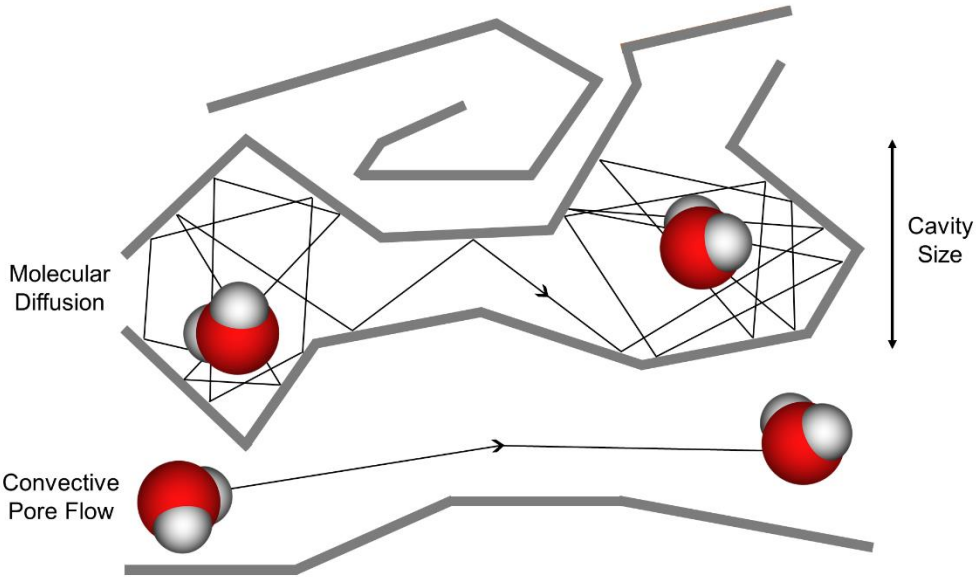


**Figure 2.6.** Illustration of the motion of a water molecule in a polymer matrix. Molecular diffusion happens when the molecule jumps from one cavity to another. Interconnected cavity within the membrane phase may also allow convective pore flow for faster water transport.

Using solution-diffusion model, water flux through the membrane is described as below.[21]

$$J_w = \frac{D_w K_w c_{w_o} v_w (\Delta p - \Pi_s)}{\ell RT} \tag{2-8}$$

where $J_w$ is the steady state volumetric flux of water
$D_w$ is the diffusion coefficient of water
$K_w$ is the sorption coefficient at the interface
$c_{w_o}$ is the water concentration in the feed solution
$v_w$ is the molar volume
$\Delta p$ is the applied hydrostatic pressure
$\ell$ is the membrane thickness

This equation can be simplified to

$$J_w = A(\Delta p - \Pi_s) \tag{2-9}$$

where $A$ is a constant equal to the term $D_w K_w c_{w_o} v_w / \ell RT$. In the reverse osmosis literature, the constant $A$ is usually called the water permeability constant.

For salt ions in solution, the effect of the pressure gradient on their transport is very small. Therefore, the salt flux is essentially independent of pressure.

$$J_s = \frac{D_s K_s (c_{s_o} - c_{s_l})}{\ell} \tag{2-10}$$

where $c_{s_o}$ is the salt concentration in the feed solution side and $c_{s_l}$ is the salt concentration in the permeation side.

This equation can be simplified to

$$J_s = B(c_{s_o} - c_{s_l}) \tag{2-11}$$

where $B$ is usually called the salt permeability constant and has the value of $D_s K_s / \ell$.

The rejection coefficient, $R$, is generally used in quantifying the overall performance of the RO membrane, and it is defined as

$$R = \left(1 - {}^{c_{s_o}}/_{c_{s_l}}\right) \times 100\ \% \tag{2-12}$$

Although the salt rejection is a parameter generally used in grading RO membranes, it is not an intrinsic material property but a result of permeability selectivity of a membrane towards water and salt molecules, which will be discussed subsequently. Rejection increases with applied pressure as shown in Figure 2.7, because the water permeation flux increases with pressure while salt flux does not.

Since the water flux is directly proportional to the difference between the applied hydrostatic pressure and the osmotic pressure in equation (2-9), the increase of salt concentration in feed solution will increase $\Pi_s$, and thus lower the deviation between $\Delta P$ and $\Pi_s$, and eventually decrease the salt rejection due to the slow permeation flux of water. In order to counteract this phenomenon, high hydrostatic pressure is often required when separating solutions with high salinity not only to overcome the osmotic pressure, but also to maintain the desired salt rejection. In most desalination processes, $\Delta P$ is often 100 to 200 psi higher than the osmotic pressure built up at the feed side in order to recover fresh water with high purity.

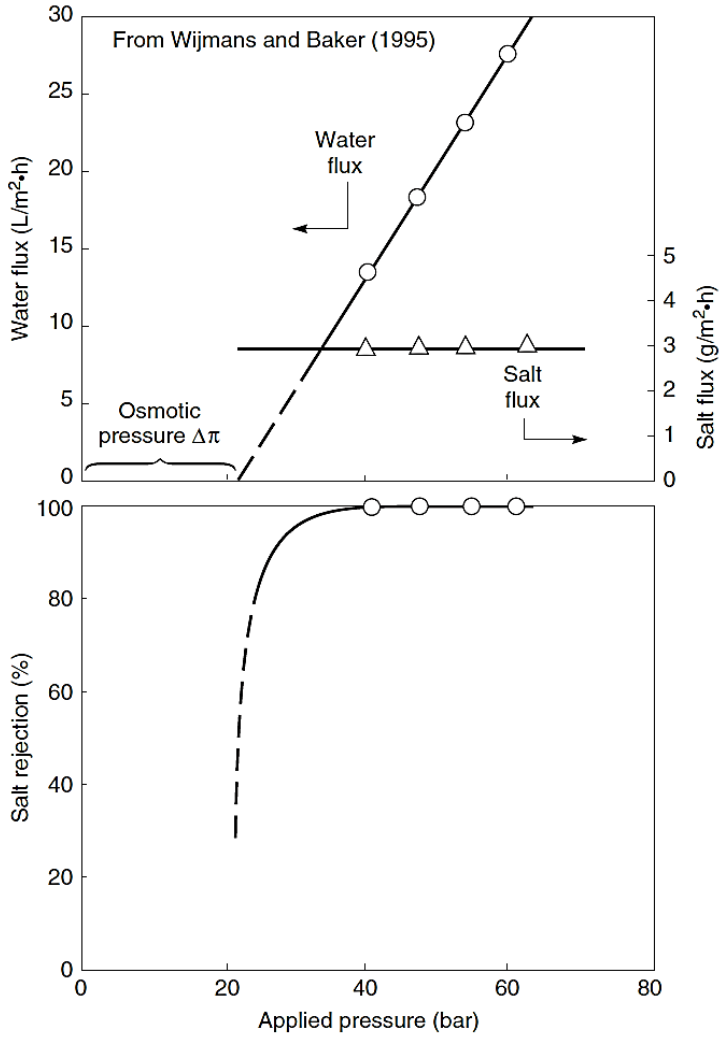


**Figure 2.7.** Flux of water and salt along with the rejection data for a reverse osmosis membrane (FilmTec Corp. FT-30) as a function of pressure[21]. Feed solution was a model of seawater with 3.5 wt% sodium chloride.

Water filtration membranes aimed at separating impurities with sizes of 1 nm and above (i.e. nanofiltration, ultrafiltration and microfiltration) usually contain well-defined pores that can be measured experimentally. Water transport across the membranes can then be described as a continuous water flow insides the pores (illustrated in Figure 2.6), instead of molecular diffusion within polymer chains. The crosslinked polyamide thin film used for reverse osmosis membranes, however, contains pores, or free volumes, that are less than 0.3 nm in diameter, which is very close to the range of thermal segmental motion of the polymer chains. Therefore, the free volumes in the polymer matrix are 1) not continuous cylindrical pores stretched across the membrane, and 2) do not have a well-defined size and stationary position. Although interconnected voids that may allow conviction of water molecules were observed within RO membranes in some studies, the transport can more suitably be characterized as molecular diffusion through a dense polymer matrix. Nevertheless, the structure of interfacially polymerized aromatic polyamide membranes

introduced another conundrum. These membranes could not be readily prepared as freestanding films of well-defined thickness, but rather form globular ridge-and-valley structures with uneven thickness at different spots on the membrane. Therefore, it has been difficult to characterize the fundamental water and salt transport properties (e.g. water and salt solubility, diffusivity, and permeability) in such materials. Although the solution-diffusion model with well-developed structure/property correlations have been widely used to guide the development of gas separation membranes, much remains unknown about the influence of polymer chemical and morphological structure on the water/salt transport properties in desalination membranes.

### 2.2.3. Water/salt Trade-off Relationship in Polymeric Membranes

A common measure of the ability of a polymer membrane to separate two mixed components is the permeability selectivity, $\alpha$, which is defined as the ratio of the permeability of the more permeable penetrant to that of the less permeable penetrant. Permeability selectivity is commonly viewed as a material property,[22] and for water/salt separation can be written as follows

$$\alpha = \frac{P_W}{P_s} = \frac{K_W}{K_s} \times \frac{D_w}{D_s} \tag{2-13}$$

where the sorption, or solubility, selectivity is $K_w/K_s$, and the diffusivity, or mobility, selectivity is $D_w/D_s$. For most membrane applications, polymers with combinations of high permeability and high selectivity properties are desirable. However, polymers with lower hindrance to one penetrant also permit the others to permeate with less resistance. This is true in most synthetic polymer membranes, and the tradeoff between permeability and selectivity has been systematically studied by Robeson.[23] Recently, Freeman and McGrath *et al.*[22] have recognized the empirical trade-off of water/salt permeability, sorption, and diffusivity as well. The relationship between water/sodium chloride permeability selectivity and water permeability, depicted in Figure 2.8, is produced from available data for polymer-based desalination membranes (including RO and nanofiltration (NF) membranes). An upper bound is observed indicating that polymers with higher water permeability are less effective in separating salt ions from water, and *vice versa*. The trade-off relationship of sorption and diffusivity were also observed in this study, and have shown that trade-off between water diffusivity and water/NaCl diffusivity selectivity is the dominant factor in the behavior shown in Figure 2.8. The sorption coefficient of salt into a polymer matrix generally depends on polymer water uptake, and the sorption selectivity values, $K_w/K_s$, vary insignificantly at

equivalent water uptake across different membranes. This indicates that the polymer properties affects salt sorption in materials proportional to the water uptake (i.e. higher water uptake will surely increase the salt sorption despite the polymer materials).[18] The sorption selectivity can, however, be impacted strongly if the polymer is charged and can reject ions by an electrostatic potential built up at the interface as in the case of nanofiltration membranes.

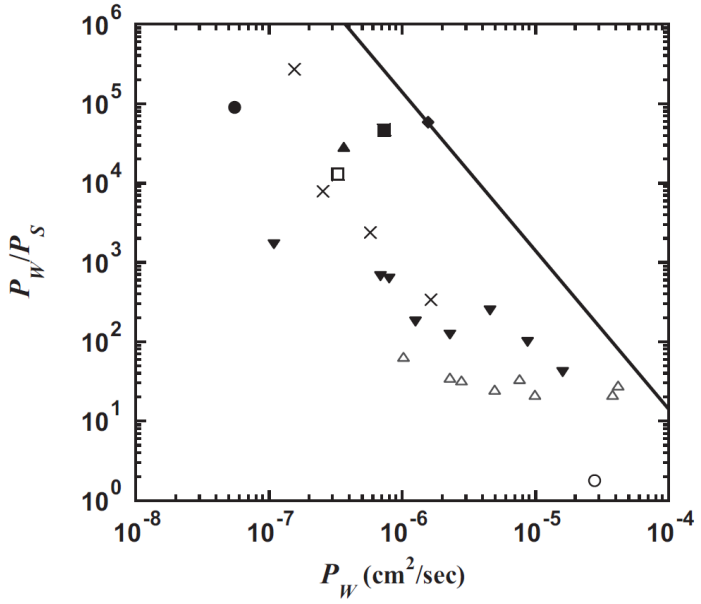


**Figure 2.8.** Correlation between water/NaCl permeability selectivity, $P_w/P_s$ , and water permeability, $P_w$ , for seven different types of seawater RO, brackish water RO and NF membranes.[22] The symbol (○) correspond to a hypothetical membrane composed of water. The water permeability of such a membrane is taken to be the product of self-diffusion coefficient of water and water sorption coefficient for pure water. Copyright 2011. Reprint with permission from Elsevier Ltd.

Literature data for the transport of water and NaCl through polymer membranes reveals the existence of and upper-bound relationship similar to those observed in polymers considered for gas separation. The upper bound for performance is observed in all the polymeric membranes and limits the productivity of fresh water in desalination plants, leading to higher capital cost and energy consumption. In fact, the energy consumption is a major portion of the total cost of water desalination and can reach values as high as ~45 % of the total production cost. The remainder of the costs are mostly labour.[24,25] Membrane replacement and related issues are only 5% of the total cost. Research in low pressure or low energy membranes technology is therefore the fastest-growing niche in recent decades.

## 2.3. Thin Film Nanocomposite Membranes (TFN)

Polymer composite membranes have been widely studied over the past few decades. The characteristic of low cost, small energy footprint to manufacture, and high flexibility for compact module design gives rise to megascale desalination plants running in the Middle-East and Europe[26]. The design of membranes, however, is restricted by several challenges such as the trade-off relationship between water permeability and water/salt selectivity, as well as low resistance to surface bio-fouling. It is therefore necessary to develop a new generation of membranes with high permselectivity, good antifouling properties, and resistance to chemical attack in the fashion of energy efficiency and cost effectiveness.

The emerging of using nanomaterials in thin film applications such as sensors, batteries and fuel cells,[27–30] encourages the separation industry to look across the spectrum of material choices, and stimulated the concept of making nanocomposite membranes (originated by Jia *et. al.*[31]) in the 1990s. Jia's group incorporated a hydrophobic zeolite into polydimethylsiloxane (PDMS) membranes to improve both permeability and selectivity of the film for the purpose of overcoming the Robeson upper boundary[23] in the field of gas separation. Nowadays, mixed-matrix membrane (MMM) with nanomaterials dispersed in polymer matrix have found in applications for gas–gas, liquid–liquid, and liquid–solid separations.[14,32–38]

For conventional composite membranes, three different locations on the membranes have been investigated for the deposition of nanomaterials: (1) the membrane surface (i.e. nanoparticles grafted-on); (2) dispersion in the bulk phase of polymer matrix, or so-called thin-film nanocomposite (TFN); and (3) thin-film composite (TFC) membranes with nanocomposite substrates. Different sizes and shapes of nanoparticles (NPs), as well as nanotubes, nanofibers and nanosheets have been studied recently with promising results. To date, nanomaterials that have been explored in fabricating TFN membranes include zeolites, CNTs, silica, Ag and $TiO_2$. The common fabrication method is the in-situ interfacial polymerization (IP) process between aqueous m-phenylenediamine (MPD) and trimesoyl chloride (TMC) organic solution as depicted in Figure 2.9. The nanofillers can be dispersed either in the aqueous or organic phase. A more detailed introduction of TFN membranes can be found in Chapter 3 in terms of the background and the choices of nanomaterial.

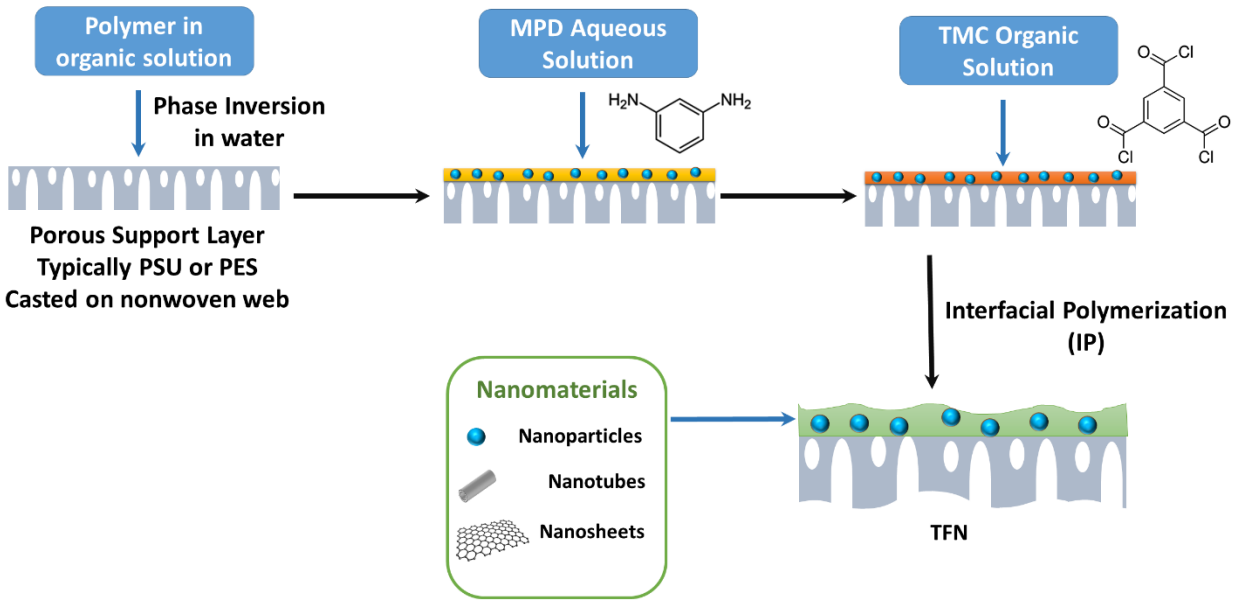


**Figure 2.9.** Schematic of the common fabrication for thin-film nanocomposite membranes.

### 2.3.1. Effects of Nanomaterials on the Trade-off Relationship

The polyamide (PA) skin layer acts as the barrier in a TFC membrane, and controls the performance and properties of the membrane in terms of permeability, selectivity, and fouling resistance. The incorporation of nanomaterials into the PA layer could modify physicochemical properties of the membrane such as hydrophilicity, charge density, porosity, chemical crosslinking, and could even provide special water channels that may overcome the permeability/selectivity trade-off relationship.[32,37–41] Nanomaterials can also be functionalized with desired properties before being inserted into the thin film, giving extra degrees of freedom in designing the membrane. For example, zeolite nanoparticles synthesized with super-hydrophilicity greatly reduced the contact angle of the resulting zeolite-PA TFN membrane from around 70º to 40º with an increase of zeolite loading from 0% to 0.4% (w/v) in the organic crosslinking solution.[14] According to the solution-diffusion model, the increase in hydrophilicity of the membranes could facilitate both the water sorption and diffusion through the polymer matrix. The embedded zeolite is low in concentration and well-dispersed within the matrix, minimizing defects created through the disruption of polymer chains. It thus leads to greater permeability without sacrificing the permeability selectivity between water and salt ions.

## 2.4. New Approach in Studying Reverse Osmosis Membranes

### 2.4.1. Pore-Flow (PF) Model

Although TFC membranes are generally described as a dense nonporous layer, and the penetrant is believed to permeate through the membrane by diffusion, interconnected voids for fast water transport have been observed in some studies on cellulose acetate RO membranes.[42] Furthermore, with advanced materials such as nanotubes and nanofibers being introduced to the PA layer to generate TFN membranes, sub-nanometer-sized pores with rigid cylindrical structures could possibly exist within the matrix and provide selective water channels across the membrane. Continuous pore flow of water in advanced RO membranes could dominate the transport across the film, and it would be incorrect to define the transport using a large value of the diffusion coefficient in the solution-diffusion model.

Another interesting fact is that the determination of the pore size and its distribution has been widely practiced for grading nanofiltration (NF) membranes,[43,44] the type of filtration membrane that is commonly synthesized by interfacial polymerization just as that for RO membranes, but with loose polymer chains, or lower degree of chemical crosslinking. The size of solutes a NF membrane can separate from its solvent are about 2 to 3 Å larger than that for an RO membrane, and yet the transport models for these two types of membranes are significantly different. NF membranes are studied as a porous membranes and are described by the pore flow (PF) model. This model was proposed by Okada and Matsuura[45] in 1991 to describe transport in pervaporation membranes, and is based on three assumptions: (1) fluids on either side of membrane are in equilibrium with the membrane at the interface, meaning that there is a continuous gradient of chemical potential ($\mu$) across the membrane, (2) the solute and solvent concentration gradients across the membrane are zero and the chemical potential gradient across the membrane can be expressed as a pressure gradient, and (3) straight cylindrical pores exist across the thickness of the membrane.

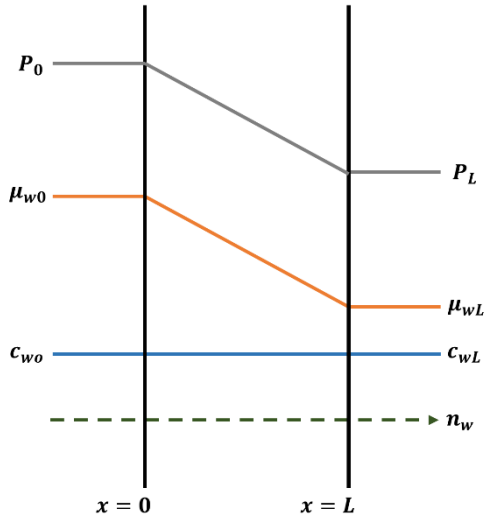


**Figure 2.10.** Profiles of the chemical potential ($\mu$), pressure ($P$) and concentration gradients of the fluid based on the pore-flow model.

The liquid transport in porous membranes is described by Darcy's equation and the water flux ($J_w$) is as:[46]

$$J_w = \frac{A}{\delta}(P_f - P_p) \quad \textbf{(2-14)}$$

where the solute flux ($J_s$) is expressed as:

$$J_s = \frac{B}{\delta}(P_f^2 - P_p^2) \quad \textbf{(2-15)}$$

where $A$ is the solvent phase transport parameter, $B$ is the solute phase transport parameter, $P_f$ and $P_p$ are the pressure in the feed and permeate side of the membrane, respectively, and $\delta$ is the pore length. The PF model has not been widely used to describe solute transport in membrane technology. Geise *et al.*[18] argue that the concentration profile of water in the RO membrane does not appear to be constant across the film, but has been shown experimentally to gradually decrease along the flow direction.[47] This agrees with the water profile proposed by the solution-diffusion model as previously discussed. In addition, the pore-flow model only considers axial solute concentration gradients, and the effect of pore's shape and tortuosity in solute rejection and transport has not been clearly stated in present PF models.

### 2.4.2. Mixed-Matrix Membrane Model

The mixed-matrix model describes the transport of fluids through both the matrix phase and the filler phase of a composite film. Since the 1960s, studies on mixed-matrix membranes have been conducted experimentally and theoretically[48] in terms of the permeability in the filler phase, the influence of filler concentration, and the transport at the interface between the bulk polymer and the fillers[49]. An analog of transport in mixed-matrix membranes in dielectrics (the Maxwell model) has also been studied comprehensively.[48,50,51] The effective composite membrane permeability is determined as

$$P_{eff} = P_m\left[\frac{P_d + 2P_m - 2\theta_d(P_m - P_d)}{P_d + 2P_m + \theta_d(P_m - P_d)}\right] \quad \textbf{(2-16)}$$

where $P$ is the single component permeability, $\theta_d$ is the fraction of dispersed filler material in the membrane, and the subscripts $d$ and $m$ refer to the dispersed and matrix phases, respectively. The model only describes a dilute dispersion of spherical fillers in the matrix with the orientation along the axis of the applied pressure difference. Equation (2-16) can be rewritten in the form of relative permeability as[46]

$$\frac{P_{eff}}{P_m} = \frac{\frac{P_d}{P_m}(1 + 2\theta_d) + (2 - 2\theta_d)}{\frac{P_d}{P_m}(1 - \theta_d) + (2 + \theta_d)} \quad \textbf{(2-17)}$$

At extreme ratios of filler permeability to matrix permeability, $\frac{P_d}{P_m}$ (greater than 100 or less than 0.1), the effective permeability of the membrane becomes less sensitive to the presence of the filler. In the case of high $P_d$ (dispersed phase) the permeate flux is mostly through the filler particle, while in case of a low $P_d$ the local fluxes preferentially go around the filler particle. Furthermore, if an impermeable or less permeable filler material (i.e. $P_d \cong 0$) is embedded, there will be no increase in the effective permeability of the material, but rather a decrease unless defects are formed at the dispersed–continuous phase interface.[32,49]

### 2.4.3. Structural Studies of the Polyamide Active Layer

The PA skin layer of TFC membranes has been described as a continuous dense nonporous film using the solution-diffusion model; or with voids at sub-nanometer size interconnecting each other to form continuous pores stretch across the active layer within an otherwise dense structure, according to pore-flow model. In contrast to these conceptualizations of the active layer, recent studies[52–54] suggest that globular features visible in cross-sectional transmission electron microscopy (TEM) images of PA layers, as depicted in Figure 2.11, correspond to voids (i.e., regions without polymer) having tens of nanometers in diameter. Notice that the voids observed in the images do not provide any selectivity to the membrane, as the size of the space is much larger than the effective pores (~0.5 nm) described in PF model.

Pacheco *et al.*[55] proposed the idea of polymer nodules to explain the formation of globular features observed in cross-sectional TEM images of PA active layers. Polymer homologs form at the interface between aqueous MPD solution and organic TMC solution during the IP. Small sheets of PA film form at different spots of the interface, and ready to spread out and crosslink with other small films. These dense polymer films effectively prevent any diffusion of MPD monomers beneath to the organic phase for further crosslinking with TMC. MPD then concentrates at the interface where PA has not yet been fully developed, and creates local pressure to extend the aqueous phase outward into the organic phase in order to maximize the surface for active crosslinking. This results in the formation of the common ridge-and-valley structure observed in the PA layer.

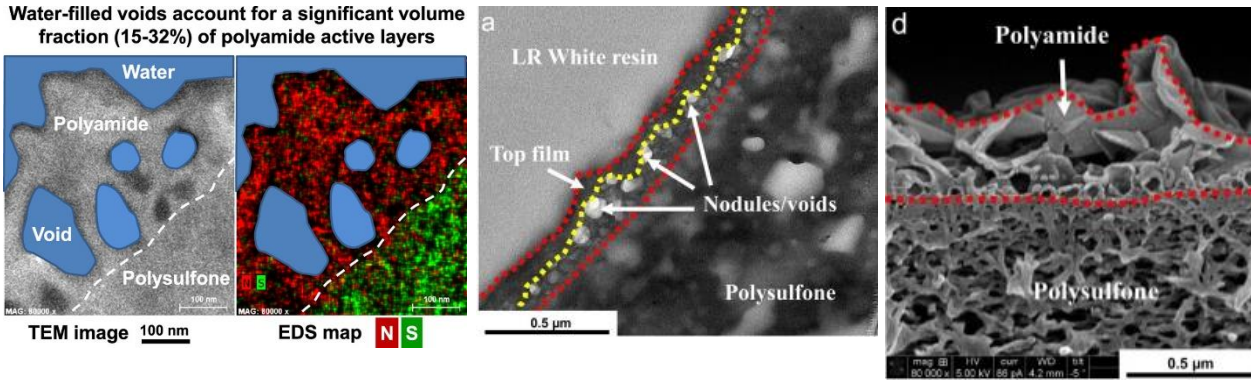


**Figure 2.11.** Cross-sectional TEM and SEM images of samples of the (a) NF90, (d) ESPA3 membranes.[56] All images above reveal the nodules/voids structure in the "dense" PA active layer visibly. Copyright 2015. Reprint with permission from Elsevier Ltd.

Orlando *et al.*[56] demonstrated that the nodules present in the active layer are actually filled with water during the RO process, suggesting that water molecules first diffuse through the top thin skin of the void where the thickness ranges from 10 to 60 nm. It then transports freely within the voids and eventually reaches the bottom where water molecule then once again dissolves into the PA matrix to exit the nodule to reach the porous substrate via molecular diffusion. This idea can utterly revolutionize the concept of transport in reverse osmosis membranes, in that the distance for the diffusion of water and salt ions in the membrane would be redefined from the overall thickness of the membrane of 100 to 200 nm, down to the thin skin layer of the nodules of 10 to 60 nm. The rest of the resistance is from the self-diffusion of water and ions within the void space. This also suggests that the optimization of RO membrane should no longer focus on minimizing the overall thickness of the skin layer, but should aim to maximize the void space inside the barrier layer.

## References


(1) Horvath, A. Water Softening. *US Patent 1,825,631* **1931**.

(2) Reid, C. E.; Breton, E. J. Water and Ion Flow across Cellulosic Membranes. *Journal of Applied Polymer Science* **1959**, *1*, 133–143.

(3) SIDNEY, L.; SRINIVASA, S. Sea Water Demineralization by Means of an Osmotic Membrane. In *Saline Water Conversion?II*; Advances in Chemistry; AMERICAN CHEMICAL SOCIETY, 1963; Vol. 38, pp. 117–132 SE – 9.

(4) Westmoreland, J. Spirally Wrapped Reverse Osmosis Membrane Cell. *US Patent 3,367,504* **1968**.

(5) Bray, D. Reverse Osmosis Purification Apparatus. *US Patent 3,417,870* **1968**.

(6) Shields, C. P. Five Year's Experience with Reverse Osmosis Systems Using Du Pont "Permasep" Permeators. *Desalination* **1979**, *28*, 157–179.

(7) Cadotte, J. Evolution of Composite Reverse Osmosis Membranes. *Materials science of synthetic membranes* **1985**.
(8) Larson, R. E.; Cadotte, J. E.; Petersen, R. J. The FT-30 Seawater Reverse Osmosis Membrane--Element Test Results. *Desalination* **1981**, *38*, 473–483.
(9) Cadotte, J. Interfacially Synthesized Reverse Osmosis Membrane. *US Patent 4,277,344* **1981**.
(10) Muirhead, A.; Beardsley, S.; Aboudiwan, J. Performance of the 12,000 m3/d Seawater Reverse Osmosis Desalination Plant at Jeddah, Saudi Arabia January 1979 through January 1981. *Desalination* **1982**, *42*, 115–128.
(11) Eriksson, P. Water and Salt Transport through Two Types of Polyamide Composite Membranes. *Journal of Membrane Science* **1988**, *36*, 297–313.
(12) Kamiyama, Y.; Yoshioka, N.; Matsui, K.; Nakagome, K. New Thin-Film Composite Reverse Osmosis Membranes and Spiral Wound Modules. *Desalination* **1984**, *51*, 79–92.
(13) Elimelech, M.; Phillip, W. The Future of Seawater Desalination: Energy, Technology, and the Environment. *Science* **2011**, *333*, 712–718.
(14) Jeong, B.-H.; Hoek, E. M. V.; Yan, Y.; Subramani, A.; Huang, X.; Hurwitz, G.; Ghosh, A. K.; Jawor, A. Interfacial Polymerization of Thin Film Nanocomposites: A New Concept for Reverse Osmosis Membranes. *Journal of Membrane Science* **2007**, *294*, 1–7.
(15) Baker, R. W. *Membrane Technology and Applications*; 2nd ed.; 2004; Vol. 23.
(16) Spiegler, K. S.; El-Sayed, Y. M. The Energetics of Desalination Processes. *Desalination* **2001**, *134*, 109–128.
(17) Paul, D. R. The Role of Membrane Pressure in Reverse Osmosis. *Journal of Applied Polymer Science* **1972**, *16*, 771–782.
(18) Geise, G. M.; Paul, D. R.; Freeman, B. D. Fundamental Water and Salt Transport Properties of Polymeric Materials. *Progress in Polymer Science* **2014**, *39*, 1–24.
(19) Smit, E.; Mulder, M. H. V; Smolders, C. A.; Karrenbeld, H.; Van Eerden, J.; Feil, D. Modelling of the Diffusion of Carbon Dioxide in Polyimide Matrices by Computer Simulation. In *Journal of Membrane Science*; 1992; Vol. 73, pp. 247–257.
(20) Freeman, B. D. Basis of Permeability/Selectivity Tradeoff Relations in Polymeric Gas Separation Membranes. *Macromolecules* **1999**, *32*, 375–380.
(21) Wijmans, J. G.; Baker, R. W. The Solution-Diffusion Model: A Review. *Journal of Membrane Science* **1995**, *107*, 1–21.
(22) Geise, G. M.; Park, H. B.; Sagle, A. C.; Freeman, B. D.; McGrath, J. E. Water Permeability and Water/salt Selectivity Tradeoff in Polymers for Desalination. *Journal of Membrane Science* **2011**, *369*, 130–138.
(23) Robeson, L. M. The Upper Bound Revisited. *Journal of Membrane Science* **2008**, *320*, 390–400.
(24) Wilf, M.; Bartels, C. Optimization of Seawater RO Systems Design. *Desalination* **2005**, *173*, 1–12.
(25) Zhu, A.; Christofides, P. D.; Cohen, Y. Effect of Thermodynamic Restriction on Energy Cost Optimization of RO Membrane Water Desalination. *Industrial & Engineering Chemistry Research* **2008**, *48*, 6010–6021.
(26) Talbot, D. Megascale Desalination: The world's largest and cheapest reverse-osmosis desalination plant is up and running in Israel. http://www.technologyreview.com/featuredstory/534996/megascale-desalination/.

(27) Chen, Z.; Holmberg, B.; Li, W.; Wang, X.; Deng, W.; Munoz, R.; Yan, Y. Nafion/zeolite Nanocomposite Membrane by in Situ Crystallization for a Direct Methanol Fuel Cell. *Chemistry of Materials* **2006**, *18*, 5669–5675.
(28) Jalani, N. H.; Dunn, K.; Datta, R. Synthesis and Characterization of Nafion-MO (M=Zr, Si, Ti) Nanocomposite Membranes for Higher Temperature PEM Fuel Cells. *Electrochimica Acta* **2005**, *51*, 553–560.
(29) Jiang, C.; Markutsya, S.; Pikus, Y.; Tsukruk, V. V. Freely Suspended Nanocomposite Membranes as Highly Sensitive Sensors. *Nature materials* **2004**, *3*, 721–728.
(30) Croce, F.; Croce, F.; Appetecchi, G. B.; Appetecchi, G. B.; Persi, L.; Persi, L.; Scrosati, B.; Scrosati, B. Nanocomposite Polymer Electrolytes for Lithium Batteries. *Nature* **1998**, *394*, 456–458.
(31) Jia, M.; Peinemann, K. V.; Behling, R. D. Molecular Sieving Effect of the Zeolite-Filled Silicone Rubber Membranes in Gas Permeation. *Journal of Membrane Science* **1991**, *57*, 289–296.
(32) Chan, W.-F.; Chen, H.; Surapathi, A.; Taylor, M. G.; Shao, X.; Marand, E.; Johnson, J. K. Zwitterion Functionalized Carbon Nanotube/polyamide Nanocomposite Membranes for Water Desalination. *ACS Nano* **2013**, *7*, 5308–5319.
(33) Peng, F.; Pan, F.; Sun, H.; Lu, L.; Jiang, Z. Novel Nanocomposite Pervaporation Membranes Composed of Poly(vinyl Alcohol) and Chitosan-Wrapped Carbon Nanotube. *Journal of Membrane Science* **2007**, *300*, 13–19.
(34) Surapathi, A.; Chen, H.; Marand, E.; Karl Johnson, J.; Sedlakova, Z. Gas Sorption Properties of Zwitterion-Functionalized Carbon Nanotubes. *Journal of Membrane Science* **2013**, *429*, 88–94.
(35) Kim, S.; Marand, E. High Permeability Nano-Composite Membranes Based on Mesoporous MCM-41 Nanoparticles in a Polysulfone Matrix. *Microporous and Mesoporous Materials* **2008**, *114*, 129–136.
(36) Kim, S.; Chen, L.; Johnson, J. K.; Marand, E. Polysulfone and Functionalized Carbon Nanotube Mixed Matrix Membranes for Gas Separation: Theory and Experiment. *Journal of Membrane Science* **2007**, *294*, 147–158.
(37) Lee, S.; Kim, H.; Patel, R.; Im, S. J.; Kim, J. H.; Min, B. R. Silver Nanoparticles Immobilized on Thin Film Composite Polyamide Membrane: Characterization, Nanofiltration, Antifouling Properties. *Polymers for Advanced Technologies* **2007**, *18*, 562–568.
(38) De Lannoy, C.-F.; Jassby, D.; Gloe, K.; Gordon, A. D.; Wiesner, M. R. Aquatic Biofouling Prevention by Electrically Charged Nanocomposite Polymer Thin Film Membranes. *Environmental science & technology* **2013**.
(39) KURTH, C.; KOEHLER, J. IMPROVED HYBRID TFC RO MEMBRANES WITH NITROGEN ADDITIVES. *WO Patent …* **2011**, *1*.
(40) HOEK, E.; YAN, Y.; JEONG, B. NANOCOMPOSITE MEMBRANES AND METHODS OF MAKING AND USING SAME. *WO Patent 2,006,098,872* **2006**.
(41) Lee, H. S.; Im, S. J.; Kim, J. H.; Kim, H. J.; Kim, J. P.; Min, B. R. Polyamide Thin-Film Nanofiltration Membranes Containing TiO2 Nanoparticles. *Desalination* **2008**, *219*, 48–56.
(42) Chan, K.; Liu, T. Effect of Shrinkage on Pore Size and Pore Size Distribution of Cellulose Acetate Reverse Osmosis Membranes. *Industrial & Engineering Chemistry …* **1984**, 124–133.

(43) Bowen, W. R.; Welfoot, J. S. Modelling the Performance of Membrane Nanofiltration — Critical Assessment and Model Development. *Chemical Engineering Science* **2002**, *57*, 1121–1137.
(44) Otero, J. a.; Mazarrasa, O.; Villasante, J.; Silva, V.; Prádanos, P.; Calvo, J. I.; Hernández, a. Three Independent Ways to Obtain Information on Pore Size Distributions of Nanofiltration Membranes. *Journal of Membrane Science* **2008**, *309*, 17–27.
(45) Okada, T.; Matsuura, T. A New Transport Model for Pervaporation. *Journal of Membrane Science* **1991**, *59*, 133–150.
(46) Wang, J.; Dlamini, D. S.; Mishra, A. K.; Pendergast, M. T. M.; Wong, M. C. Y.; Mamba, B. B.; Freger, V.; Verliefde, A. R. D.; Hoek, E. M. V. A Critical Review of Transport through Osmotic Membranes. *Journal of Membrane Science* **2014**, *454*, 516–537.
(47) Rosenbaum, S.; Cotton, O. Steady-State Distribution of Water in Cellulose Acetate Membrane. *Journal of Polymer Science Part A: Polymer Chemistry* **1969**, *7*, 101–109.
(48) Noble, R. D. Perspectives on Mixed Matrix Membranes. *J. Memb. Sci.* **2011**, *378*, 393–397.
(49) Cay-Durgun, P.; Fink, S. G.; Shabilla, A.; Yin, H.; Sasaki, K. a.; Lind, M. L. Analysis of the Water Permeability of Linde Type A Zeolites in Reverse Osmosis. *Separation Science and Technology* **2014**, *49*, 2824–2833.
(50) Bouma, R. H. B.; Checchetti, A.; Chidichimo, G.; Drioli, E. Permeation through a Heterogeneous Membrane: The Effect of the Dispersed Phase. *Journal of Membrane Science* **1997**, *128*, 141–149.
(51) Chung, T. S.; Jiang, L. Y.; Li, Y.; Kulprathipanja, S. Mixed Matrix Membranes (MMMs) Comprising Organic Polymers with Dispersed Inorganic Fillers for Gas Separation. *Progress in Polymer Science (Oxford)*, 2007, *32*, 483–507.
(52) An, Q.; Hung, W. S.; Lo, S. C.; Li, Y. H.; De Guzman, M.; Hu, C. C.; Lee, K. R.; Jean, Y. C.; Lai, J. Y. Comparison between Free Volume Characteristics of Composite Membranes Fabricated through Static and Dynamic Interfacial Polymerization Processes. *Macromolecules* **2012**, *45*, 3428–3435.
(53) Kong, C.; Koushima, A.; Kamada, T.; Shintani, T.; Kanezashi, M.; Yoshioka, T.; Tsuru, T. Enhanced Performance of Inorganic-Polyamide Nanocomposite Membranes Prepared by Metal-Alkoxide-Assisted Interfacial Polymerization. *Journal of Membrane Science* **2011**, *366*, 382–388.
(54) Kong, C.; Kanezashi, M.; Yamomoto, T.; Shintani, T.; Tsuru, T. Controlled Synthesis of High Performance Polyamide Membrane with Thin Dense Layer for Water Desalination. *Journal of Membrane Science* **2010**, *362*, 76–80.
(55) Pacheco, F. A.; Pinnau, I.; Reinhard, M.; Leckie, J. O. Characterization of Isolated Polyamide Thin Films of RO and NF Membranes Using Novel TEM Techniques. *Journal of Membrane Science* **2010**, *358*, 51–59.
(56) Lin, L.; Lopez, R.; Ramon, G. Z.; Coronell, O. Investigating the Void Structure of the Polyamide Active Layers of Thin-Film Composite Membranes. *Journal of Membrane Science* **2015**.

# Chapter 3. Literature Review of RO Membrane Technology

## 3.1. Introduction

Development on today's membrane technology focuses on three major challenges: 1) high permselectivity for seawater and brackish water desalination; 2) Low surface biofouling; and 3) Resistance to chemical attack such as Chlorine used in disinfecting wastewater. Thin-film composite membranes synthesized by interfacial polymerization (IP) process forms polyamide (PA) barrier layer with thickness of 100 to 200 nm atop of porous substrate. It offers excellent fast water flux, and dominate the design of most of the RO membranes, despite it was a technique developed over 40 years ago. The dominant effect also restrain the possibility of further development in resolving the major challenges because the performance is heavily relied on the physiochemical properties of the PA layer. The amide bonding on the backbone of PA chain can be attacked by chlorine radicals and break down to short chains. Regular PA membrane can start to degrade only after 12 hours of exposure in solution with chlorine concentration at 2 g/L,[1] and experience significant decrease in salt rejection. Furthermore, the surface of PA is negatively-charged at normal pH because of the carboxylic functional groups present on the polymer backbone, which is formed from the hydrolysis of unreacted acid chloride group on the crosslinking agent during IP. This charged surface is prompt to protein and bacteria adsorption, and subsequently increase the chance of biofouling.

On the other hands, boron removal is another challenge for desalination process and has recently been under the scientific spotlight. Boron exists in the environmental water in the form of boric acid, and the average concentration of boric acid in seawater is approximately 4.6 mg/L.[2] The problem of high boron concentration was first recognized in late 1990s when farmers in Israel noticed poisoning of crops and partially discolored leaves, and identified that the trace amount of boron in the reclaimed wastewater was responsible for these damages.[3] Adequate boron removal from seawater thus became essential in desalination applications for potable water production. However, boron rejection by current seawater RO membranes still remains considerably lower than that of sodium chloride, the main inorganic salt in seawater.

To resolve these challenges, recent development in the RO industries have approached each problem separately and commercialized different types of membrane modules, such as seawater RO membranes with high boron removal, low surface fouling, or energy saving

membrane that runs at ultra-low pressure. Table 3.1 and Figure 3.1 summarizes the performance of some of the commercial membranes available in the market.

**Table 3.1.** Comparison of membrane performance between different manufacturers in terms of the permeation flux and rejection.

| Name | RO Membrane Type | Solution Concentration (NaCl ppm) | Applied Pressure (bar) | Permeance (L/(m$^2$ h)/bar) | Rejection (%) |
|---|---|---|---|---|---|
| [4]**DOW FILMTEC**™ | | | | | |
| SW30HR-380 | Seawater | 32,000 | 55 | 0.50 | 99.7 |
| SW30XHR-400i | Seawater + Boron Removal | 32,000 | 83 | 0.31 | 99.8 |
| BW30HR-440i | Brackish Water | 2,000 | 15.5 | 2.82 | 99.7 |
| [5]**Hydranautics**™ | | | | | |
| SWC®-5-LD | Seawater + Low Fouling | 32,000 | 55.2 | 0.69 | 99.8 |
| ESPA®-1 | Ultra-Low Pressure | 1,500 | 10.3 | 4.95 | 99.3 |
| [6]**TORAY™** | | | | | |
| TM840M-1760 | Seawater | 32,000 | 55.2 | 0.53 | 99.8 |
| TM740-1760 | Brackish Water | 2,000 | 15.5 | 2.77 | 99.7 |
| [7]**FLUID SYSTEM**™ | | | | | |
| SW 8 | Seawater | 32,800 | 55.2 | 0.55 | 99.8 |
| FR 8 | Fouling Resistant | 2,000 | 15.5 | 3.01 | 99.6 |
| [8]**LG NanoH2O**™ | | | | | |
| SW 400 ES | Seawater | 32,000 | 55 | 1.06 | 99.7 |
| BW 400 ES | Brackish Water | 2,000 | 10.3 | 4.34 | 99.6 |

It should be noticed that the property of permeance for each membrane shown in Table 3.1 was calculated by dividing the total flux, in the unit of cubic meter per day ($m^3$/d), of a membrane module, by the total effective area of the membrane and the applied hydrostatic pressure. The permeance is not the permeability of water through the membrane because it has not been normalized by the film thickness. The active thickness of the barrier layer in each membrane, however, is not provided. Thus, Figure 3.1 does not show the trade-off relationship of the water permeability and water/salt selectivity of the commercial membranes, but rather a comparison of the extinct properties of the membrane across different brands and applications. In spite of the lack of information in order to calculate the true material properties for each membrane, a general upper bound can still be observed in the chart, where membranes with have higher water permeance shows lower salt rejection toward sodium chloride, and *vice versa*.

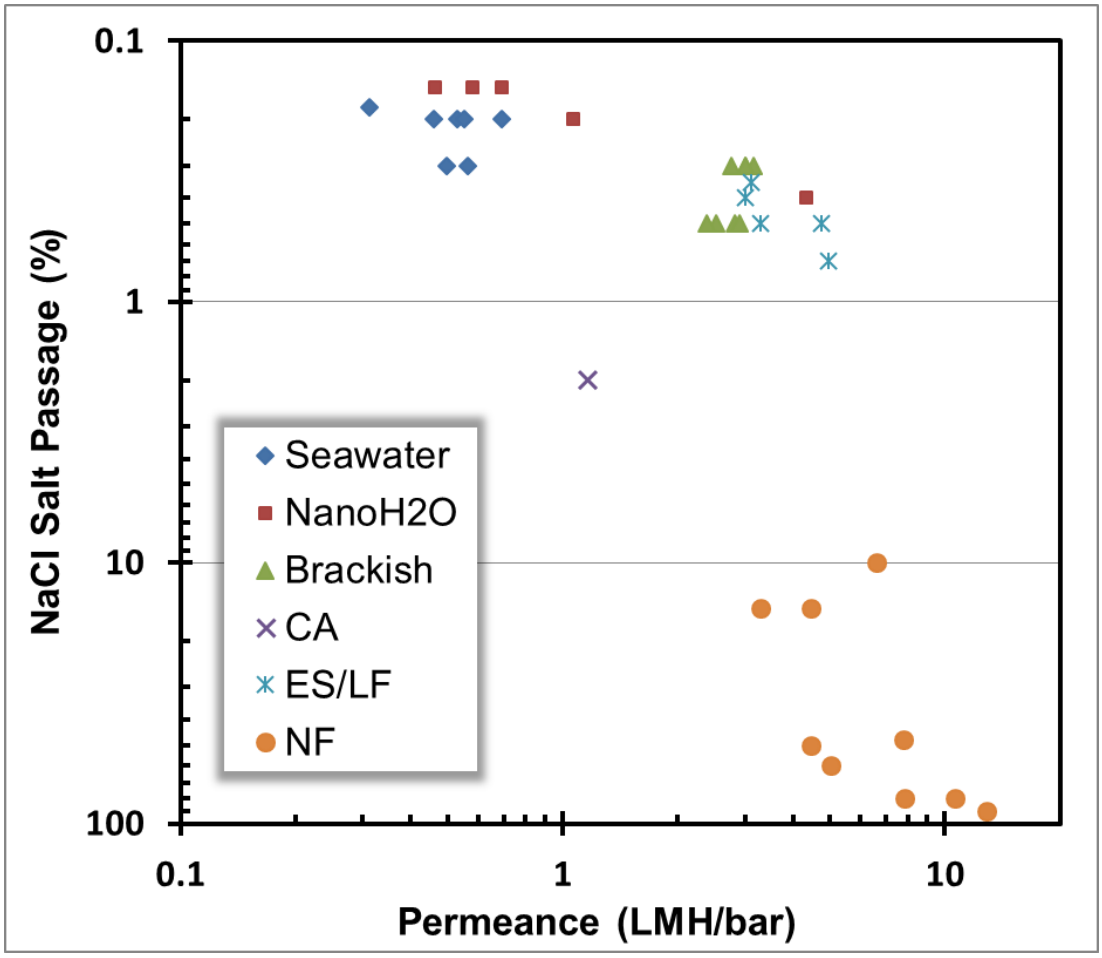


**Figure 3.1.** Trade-off relationship between permeance of water and salt rejection. Salt Passage is *(100% – salt rejection)*, which also indicates the amount if salt that permeates through the membrane. Permeance is in the unit of Liter pre squared Meter per Hour (LMH) per bar of applied transmembrane pressure. The legend of *CA* is cellouse acetate RO membrane, and *ES/LF* stands for energy saving and low fouling, respectively. *NF* stands for nanofiltration membrane. *NanoH2O* is the company that commercializes thin film nanocomposite membranes for seawater and brackish water RO.

In this chapter, we will be discussing various scientific approaches in improving the RO membranes, including the choices of polymers for the barrier layer other than aromatic polyamide, the post-treatment of contemporary RO and NF membranes by surface modification. We will also discuss the thin-film nanocomposite (TFN) membranes fabricated by dispersing nanofillers (i.e. nanoparticles, nanotubes or nanofibers) with variety of properties in the barrier layer to enhance the separation performance. A short comparison will also be provided to differentiate between RO and NF membranes, in terms of their usage and rejection mechanism. Finally, we will compare RO application with other desalting processes, such as Forward Osmosis (FO), in order to open up more possibilities in generating fresh water in a "greener" and cost-effective way.

### 3.1.1. Choice of Materials for Thin Film Composite

After the revolutionary success of the introduction of thin-film composite (TFC) RO membranes into the market, chemically-crosslinked, fully aromatic polyamide became the choice for the majorities, and the research and development towards new polymeric materials for RO membranes has declined dramatically. The number of patents by membrane manufacturers reduced greatly at the end of 1990s, but the secret about the chemical composition and post-treatment performed on commercial RO membranes has been revealed by advanced analytical techniques emerged at the meantime, such as XPS, ATR-FTIR and TEM, etc. One of the major research area has been to provide membranes the ability to withstand exposure to chlorine or chlorine-induced oxidants, because chlorine is commonly added to water as a disinfectant and bactericide.[1] Nitrogen-based functional groups such as amines and secondary amines linkages is very sensitive to chlorine radicals dissolved in solution. The structure of polyamide, therefore, will be slowly degraded by the aqueous chlorine and shorten the life-time of the membrane. The degradation mechanism of PA membrane is depicted in Figure 3.2.

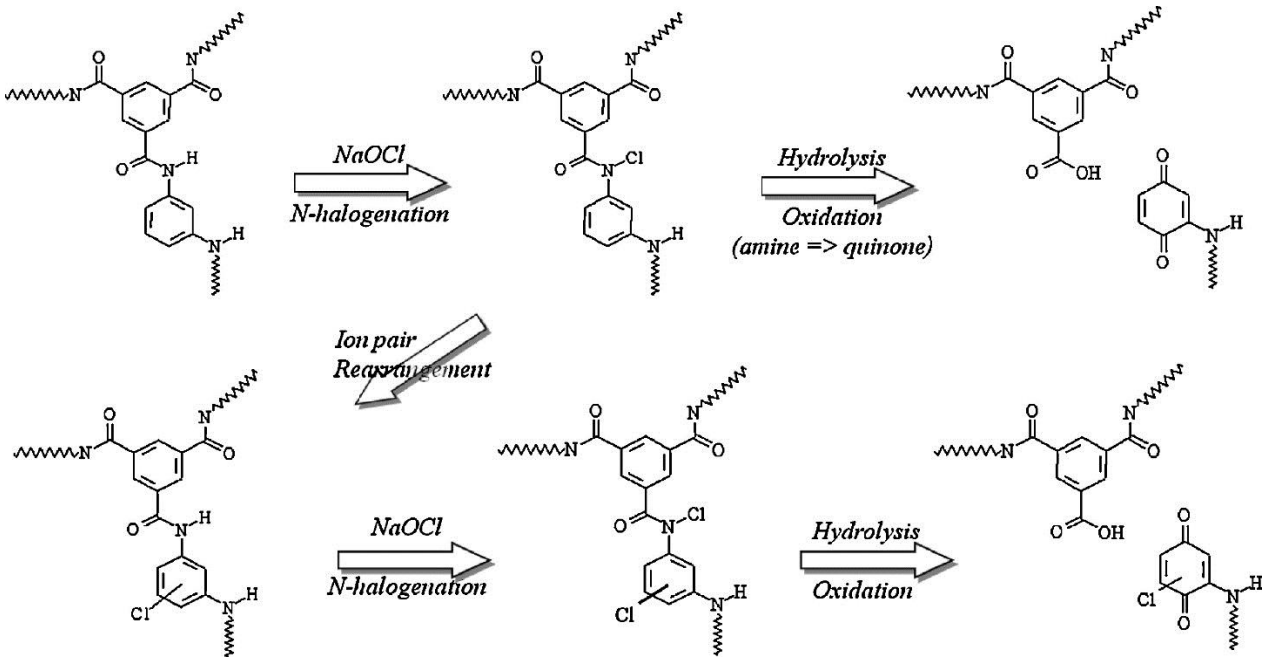


**Figure 3.2.** Mechanism of degradation of polyamide RO membrane by aqueous chlorine.[1] Copyright 2011. Reuse with permission from Elsevier Ltd.

The aqueous chlorine in the form of hyperchlorite (–OCl) attacks the amide bonds (–O═C–N–H–) within the polymer matrix. Aromatic rings bonded to the N–H group of amide linkages are electrophilic and tend to accept electrons from the chlorine radicals. Consequently, the N–H group is converted to an N–Cl group by N-halogenation, and the attacked linkage undergoes an intermolecular rearrangement to form various aromatic substitution products. This lower the crosslinking density of PA membrane, and eventually fail to separate salt ions from water, resulting in decreased salt rejection and increased water flux after chlorination.[9,10]

Several approaches have been taken to minimize the chlorine attack. Piperazine consists of a six-membered ring with two secondary amine groups at opposite position in the ring. It has been used to replace m-phenylenediamine (MPD) to crosslink with trimesoyl chloride (TMC), and forms a tertiary amine at the amide linkage.[11] The absence of N–H group reduces the chlorine attack and prolong the membrane's life. Another approach is to substitute majority of the polymer chains with disulfonated polysulfone-based polymers, which have been reported to be more tolerant to aqueous chlorine than PA-based polymers.[12,13] McGrath and Freeman *et al.*[14] synthesized new disulfonated diamine called S-BAPS, and crosslinked it with TMC to form TFC membrane with the presence of both sulfone and amide groups. The use of other monomers and additives for TFC RO membranes can be found in Table 3.2, where it shows the membrane performance in terms of water permeation and salt rejection, as well as the solvents and curing process used by different studies.

| | |
|---|---|
| 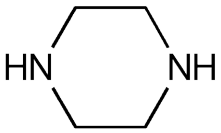 | 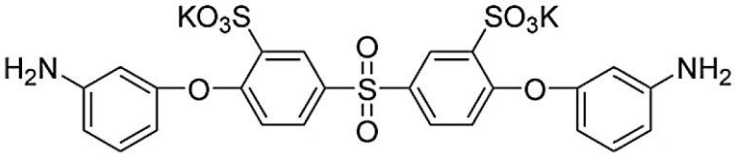 |
| Piperazine | Disulfonated bis[4-(3-aminophenoxy)phenyl]sulfone (S-BAPS) |

**Table 3.2.** Choice of Monomers in Interfacial Polymerization for Thin Film Composite

| Ref. | Aqueous Phase | Organic Phase | Applied Pressure (psi) | Permeation Flux (L/(m$^2$ h)) | Rejection (%) | Aqueous and organic solvents | Curing temp. and time |
|---|---|---|---|---|---|---|---|
| 15 | ▪ m-phenylenediamine *[2wt%]*<br>▪ Triethylamine *[3wt%]*<br>▪ Camphor sulfonic acid *[4wt%]* | ▪ 5-isocyanato-phthaloyal chloride *[0.1~0.33%]*<br>▪ Isophthaloyal chloride *[0~0.66%]* | 232 | 30~40 | 99~95.5 | Water/ IP1016 | 70 - 80°C 10min |
| 16 | ▪ m-phenylenediamine *[1wt%]*<br>▪ m-phenylenediamine-5-Sulfonic acid *[1wt%]*<br>▪ TEA & CSA *[3wt%]* | ▪ Trimesoyl chloride *[0.1% w/v]* | 217.5 | 31 | 90 | Water/ IP1016 | 80°C 5min |
| 11 | ▪ Piperazine *[5%, w/v]* | ▪ Trimesoyl chloride *[0.1% w/v]* | 150 | 92 | 72 | Water/ hexane | 80°C 5min |
| | ▪ Piperazine *[2%, w/v]* | ▪ Isophthaloyal chloride *[0.1% w/v]* | 150 | 25 | 40 | | |
| | ▪ 3,5-diaminobenzoic acid *[1%, w/v]* | ▪ Isophthaloyal chloride *[0.1% w/v]* | 250 | 228 | 23 | | |
| | ▪ 3,5-diaminobenzoic acid *[1%, w/v]* | ▪ Trimesoyl chloride *[0.1% w/v]* | 250 | 96 | 67 | | |
| | ▪ m-phenylenediamine *[2%]* | ▪ Trimesoyl chloride *[0.1%]* | 150 | 71 | 95 | | |
| | ▪ m-phenylenediamine *[0.9%]*<br>▪ Piperazine *[0.1%]* | ▪ Trimesoyl chloride *[0.1%]* | 150 | 48 | 90 | | |
| | ▪ N-(2-aminoethyl)-piperazine *[1.5% w/v]* | ▪ Isophthaloyal chloride *[0.7% w/v]*<br>▪ Trimesoyl chloride *[0.3% w/v]* | 150 | 13 | 60 | | |
| 14 | ▪ Disufonated bis[4-(3-Aminophenoxy)phenyl]sulfone (S-BAPS) *[2% w/v]* | ▪ Trimesoyl chloride *[1% w/v]* | 225 | 150 | 80 | Water/ n-dodecane | 80°C 10min |
| 17 | Two Steps:<br>1) 4-methyl-phenylene-diamine *[2wt%]*<br>2) N,N'-dimethyl-m-phenylenediamine *[1wt%]*<br>▪ Triethylamine *[3wt%]*<br>▪ Camphor sulfonic acid *[4wt%]*<br>▪ SDS *[0.15wt%]* | ▪ 5-choroformyloxyisophaloyl chloride *[0.15wt%]* | 225 | ~46 | ~95 | Water/ hexane | 100°C 8min |

All tested feed solution is 2000 ppm of Sodium Chloride (NaCl)

### 3.1.2. Surface Fouling and Post-treatment of membranes

Besides chemical attack and oxidation, fouling is another major obstacles for the aromatic polyamide RO membrane. It deteriorates the separation performance and shorten membrane lifetime, which eventually increase the cost of the RO process. Different approaches have been performed, which includes pretreatment of the RO feed solution (e.g. filtration, lime softening, acidification, etc.), and periodic cleaning by osmotic back-washing or chemical cleaning.[17] Another approach is to develop RO membranes that has higher surface fouling resistance by modifying the commercial RO membranes, which often involves chemical post-treatments of the membrane surface to increase its hydrophilicity, and thus increase the water permeability and improve chlorine resistance. Post-treatment is easy to scale-up and preferred by the industries. Various chemical and physical techniques have been developed for membrane post-treatment in the last two decades.

Water soluble solvents such as acids and alcohols have been used to treat the membrane, which partially hydrolyze the surface to improve flux and rejection.[18] Surface coating with more hydrophilic compounds is another common approach to achieve membrane hydrophilization. Ishigami *et al.*[19] alternatively grafted polycation and polyanion on the surface of RO membranes via layer-by-layer deposition, and significantly increase the surface hydrophilicity and prevent adsorption of protein at the surface. Sarkar *et al.*[20] has patented a new technique that involves grafting brush-like dendrimers atop of a RO membrane, and is then crosslinked with hydrophilic polymers such as polyethylene glycol. The results show great reduction on surface contact angle, and the constant movement of the brush-like polymer grafted on the surface makes it unfavorable for foulants to attach onto. Table 3.3 shows some other additives used in membrane post-treatments, as well as the fabrication methods used to attach variety of polymers to the surface. The table also shows the percent changes of the permeation flux before and after the post-treatment process. Despite there are great increase in hydrophilicity, some of the modified membranes experienced significant drop in water permeation flux, due to the extra thickness of coating at the surface. The diffusion coefficient of water and salt within the coating may also be altered, slowing down the overall transport of water across the membranes. Other surface modification techniques, including free radical-, photochemical-, radiation-, redox- and plasma-induced grafting, have also been used to covalently attach useful monomers onto the membrane surface.[21]

**Table 3.3.** Choice of Surface Modifiers for RO Membranes

| Ref. | Additives | Fabrication Methods | Salts in Feed | Flux Change (%) | Rejection (%) | Advantages |
|---|---|---|---|---|---|---|
| 22 | Methacrylic acid *[10%]*<br>PEG-methacrylate *[16%]* | Grafted on surface of commercial RO membranes | NaCl<br>1500 ppm | - 9.2<br>- 5.0 | 98.0<br>94.6 | ▪ The presence of charges on the surface provided by the grafted polymer protects the surface from foulants. |
| 20 | Hydrophilic PAMAM dendrimer (G2) +<br>PEG dynamic brush +<br>Silver ions | Grafted on polyamide surface | NaCl<br>1000 ppm | - 21.4 | 98.6 | ▪ Surface contact angle was drastically decreased, which help to remove or minimize any remaining bio-foulants without leaching in the permeation. |
| 23 | Hydrophilic surface modifying macromolecule, contained PEG and PPG *[0.25wt%]* | Dispersed in aqueous phase | NaCl<br>3.5wt% | - 25 | 96.1 ± 2.03 | ▪ Additives are supposed to change the surface-foulant affinity of the membrane and thus create better antifouling RO membrane. |
| 24 | Dimethyl Sulfoxide *[1wt%]* | Dispersed in aqueous phase | NaCl<br>2000 ppm | + 208.14 | 95.1 | ▪ Addition of DMSO increased the size of the aggregate pores, and thus enhanced the water permeability significantly. The cross-linking of the resulting membrane was also improved. |
| 19 | **Polycation**<br>Poly(sodium 4-styrene sulfonate)<br>**Polyanion**<br>poly(allylamine hydrochloride) | Layer by layer film deposition on RO membrane | NaCl<br>500 ppm | - 30.4 | 99.0 | ▪ After 6 layers of deposition, membrane surface became negatively charged and the absorption of protein at the surface decreased significantly. |
| 25 | **Thermal-Responsive Polymer**<br>Poly(N-isopropylacrylamide-co-acrylamide) | Hydrogen-bonded to non-crosslinked functional groups on RO membrane | NaCl<br>2000 ppm | ± 10 | 98.5 | ▪ Surface contact angle decreased<br>▪ Surface foulant resistance improved<br>▪ Flux recovery improved at higher temperature; easier to clean |
| 26 | **Zwitterionic Amino Acid**<br>3-(3,4-dihydroxyphenyl)-l-alanine | Hydrogen-bonded to the membrane surface and oxidative polymerized to form a continuous layer | N/A | + 15.1 | 97.6 | ▪ Significant surface contact angle decreased<br>▪ Increase of permeation flux with unchanged salt rejection<br>▪ Protein adsorption decreased more than 2-fold<br>▪ High water flux recovery |

- PEG: Poly(ethylene glycol)
- PPG: Poly(propylene glycol)

## 3.2. Thin-Film Nanocomposite Membranes (TFNs)

The advantage of modifying the surface of TFC membrane is that the cost of the materials is fractional compared to the entire process, and can easily be scaled-up for industrial applications. However, the in-situ grafting or hydrogen-bonding polymers to the membrane surface lowers the freedom on tuning the properties of the membrane. Majority of the surface coating, as previously mentioned, were only able to provide higher hydrophilicity to the membrane for better fouling resistance, and may meanwhile sacrifice the performance in water permeation. A unique field in improving water treatment using nanotechnology has immerged recently. The original idea is to separate solute from solvent at the molecular level using either nano-scaled particle embedded in TFC membranes, or internal nanostructure (i.e. nanopores) of the membrane. Membranes with internal nanostructures, such as zeolite membranes and aligned carbon nanotube membranes have been studied both theoretically and experimentally[27–40]. Thin film nanocomposite (TFN) RO membranes, first introduced by Hoek *et al*.[41] in 2007, also show excellent results in enhancing the membrane performance. The idea is to embed nanoparticles throughout the polycondensed polymer thin film layer, and the most prominent nanoparticles being investigated are zeolites, carbon nanotubes (CNTs)[42] as well as other nanofillers such as silver[43], $TiO_2$[44], silica particles[45] and metal-organic frameworks.[46] Most TFN membranes showed higher water flux without decreasing salt rejection. The proposed mechanisms of the enhanced desalination performance of TFN membranes include: (i) faster water transport within the porous nanomaterials[34,42,47]; (ii) increased membrane affinity to water[34,44]; (iii) PA structure change[45,48,49]. Nanomaterials may also improve some physical membrane properties, such as thermal stability, mechanical strength or fouling resistance.[43] Table 3.4 shows some of the recent development in TFN membranes using different nanomaterials, with the performance of the resulting membranes and advantages offered by the nanofillers.

### 3.2.1. Choices of Nanomaterials

- **Zeolite**

Zeolite is a crystalline aluminosilicate material with uniform sub-nanometer- or nanometer-scale pores. Its three-dimensional framework structure forms uniform pores with identical pore size, and can act as sieves on a molecular scale. Zeolites with desire pore size can be manufactured under controlled synthesis, and offer extremely high selectivity in gas-gas and water/salt separations. Zeolite membranes were previously applied solely for gas separations but shows promising

separation for RO applications as well with different synthesis approach. Lee's group synthesized MFI-type zeolite membranes with high aluminum contents and reported about 1 – 4 kg/m$^2$ h in flux and 92.9 – 97.3 % in salt rejections.[50–52] Zeolite nanoparticles with super-hydrophilicity has been introduced into thin-film composite membranes and have greatly reduced the contact angle of the resulting zeolite-PA TFN membrane with an increase of zeolite loading from 0% to 0.4% (w/v) in the organic crosslinking solution.[34] The permeation flux shows about 80% increase with no decrease in salt rejection.

- **Graphene and Graphene Oxide**

Graphene is a two-dimensional nanomaterial comprising of a sheet of carbon atoms arranged in a hexagonal configuration. The unique properties of graphene and graphene oxide (GO) sheets such as high surface area and excellent mechanical strength encouraged researchers to study its possibility in replacing conventional membrane materials. Studies using molecular dynamic simulation have demonstrated that nanoporous graphene can function as a thin barrier layer that has fast water flux and meanwhile maintains high ion rejection.[53–56] Simulation study also shows that graphene sheets with nanopores' diameter no larger than 5.5 Å can effectively separate salt from water.[54] GO sheet that contains oxygen-rich functional groups has also exhibited enhanced water permeability, anti-fouling and anti-bacterial properties and good chlorine resistance when exploited in separation membranes. Recently, Perreault *et al*. have reported the use of GO sheets on the surface of a TFC RO membrane, and have strongly enhanced the antimicrobial property of the membrane.[57] Goh *et al*. also reported immobilizing GO nanosheets onto the surface of ultrafiltration hollow fiber membranes by electrostatic interaction, and form novel nanofiltration (NF) that can offer higher water permeability without compromising membrane selectivity.[58]

- **Carbon nanotubes (CNTs)**

CNTs comprise of a sheet of graphene that are rolled into hallow smooth cylindrical tubes, and can offer incredible aspect ratio that the inner diameter of the tube can be less than 1 nm but the length of tube is up to microns. CNTs has been discovered to be exceptional in structural and functional properties, such as mechanical, tensile, and electrical characteristics that rendered them a great potential for various technological applications.[59] There are two types of carbon nanotubes: single-walled carbon nanotubes (SWNT) and multi-walled carbon nanotubes (MWNT), which differ by the number of cylindrical arrays arranged around the hallow nanotube core. Among all the choices of nanomaterials, CNTs have caught many attention for potential applications in water

purification and desalination, due to their similarity to aquaporin biological channels. MD simulation have extensively been used to study the transport behavior of water molecules in CNT channels.[40,60–64] Simulations done by Hummer *et al*. showed that hydrogen-bonded water molecules form chain-like structure within the CNT, which is not only facilitated the entrance and permeation of water in CNT, but also experience fast frictionless conduction through the tubes.[60] This is the result of the chain of water molecules travels inside a hydrophobic, defect-free inner core of CNT tube which has minimal interactions with the water molecules in the interior. The fluid and ion transports in the inner core of CNT will be discussed subsequently in this chapter.

In 2010, Ratto *et al*.[42] have patented a method to produce composite membranes from open-ended nanotubes embedded in a polyamide matrix. The matrix forms a layer that the thickness is substantially less than the average length of the nanotubes, allowing the nanotubes to be randomly oriented through the matrix while providing channels extending through the layer for the selective passage of molecular species or particles based on size. The method consists of dispensing single-walled CNTs (1.2–1.4 nm in diameter) into one of the two liquid phases of conventional interfacial polymerization. A microporous support is first wetted in an aqueous diamine solution, and then contact with a second non-aqueous phase with isophthaloyl chloride, followed by a third non-aqueous phase with trimesoyl chloride. CNTs suspended in one or more of the three phases, while the thin polyamide layer serves as matrix that withhold the randomly-orientated CNTs. This procedure does not require costly steps or equipment to synthesize in-situ CNTs on the membrane. CNTs can be grown separately and functionalized with different functional group, and then embed into the membranes using existing techniques. Table 3.5 shows most of the recent CNT-TFN membranes that are fabricated using similar techniques, but with CNTs functionalized with various functional groups.

Lannoy *et al.* demonstrated the use of carboxylic functionalized CNTs in polyamide membrane to form electrically conductive nanocomposite membrane that can offer high salt rejection and prevents biofilm formation at the membrane surface when electric potential is applied to the membrane.[65] Chan *et al*. introduced zwitterionic functional groups to the tips and surface of SWNTs and embedded them into PA skin layer to greatly enhance the water permeation flux without sacrificing the salt rejection of the resulting TFN membranes. Zwitterionic groups can potentially improve the anti-biofouling resistance of the membrane as well, reducing the formation of biofilm at the interface without any electric potential flowing across the membrane.[47]

**Table 3.4.** Choice of Nanomaterials for Nanocomposite Desalination Membranes

| Ref. | Nanoparticles | Aqueous Phase | Salts in Feed | Applied Pressure (Psi) | Permeation Flux ($L/(m^2 h)$) | Rejection (%) | Advantages |
|---|---|---|---|---|---|---|---|
| 65 | Multi-walled CNT; <8nm in diameter; 10-30μm length | MPD *[2wt%]* | NaCl 1000ppm | 100 | *Applied potential: 1.5V* 22.0 ± 2.8 | 92.1±1.3 | Applied potential significantly increases anti-biofouling property. 1 min-flushing can recover almost 92% of flux. |
| 66 | Halogen reactive nitrogen from amines, imides, sulfonamides, and more | MPD *[4wt%]* | N/A | N/A | 54 | >99 | Chloromines was formed on the surface when chlorinated water comes in contact with reactive nitrogen. It protects the surface from Chlorine attack and biofouling. |
| 41 | Zeolite A nanoparticles *[0.4 % w/v]* **(in organic phase)** | MPD *[2wt%]* | NaCl 2000 ppm | 180 | 16.5±1.3 | 91.2±0.5 | Zeolite A increases surface hydrophilicity which improves water permeability, solute rejection and fouling resistance. |
| 48 | Linde type A (LTA) zeolite nanocrystals | MPD *[2-3% w/v]* TEACSA *[6% w/v]* SLS *[0.02% w/v]* IPA *[0-20% w/v]* | NaCl 2000 ppm | 224.8 | 20.4 to 108.8 | 90 to 95 | Microporous defects were observed in nanocomposite membranes, indicating that nanoparticles change bulk polyamide structure and reducing cross-linking |
| 44 | $TiO_2$ **(in organic phase)** | MPD *[2 wt%]* NaOH *[0.05 wt%]* | $MgSO_4$ 2000 ppm | 87 | 9.1 | 95 | TiO2 nanoparticles in PA produced the increase of water flux due to the enhanced hydrophilicity in the membranes |
| 43 | Silver Nanoparticles | MPD *[2 wt%]* NaOH | $MgSO_4$ 2000 ppm | 125 to 250 | ~90 | 96 to 97 | With Ag nanoparticles on the membranes colonies of Pseudomonas were almost all dead |
| 67 | Polyhedral Oligomeric Silsequioxane (POSS) **(in organic phase)** | MPD *[2 wt%]* | NaCl 2000 ppm | 225 | 22 to 33 | >98 | POSS acts as cross-linkers and increases free volume of the PA film, which thus increases permeation. |

- Crosslinking agents are all TMC

**Table 3.5.** The Use of Carbon Nanotubes in Thin-Film Nanocomposite Desalination Membranes

| Ref. | Type | Loading | Dimension | Application | Salts in Feed | Applied Pressure (Psi) | Permeation Flux ($L/(m^2 h)$) | Rejection (%) |
|---|---|---|---|---|---|---|---|---|
| 68 | Oxidized MWNTs | ▪ 0-0.2% (w/v) in aqueous phase<br>▪ 0-5% in organic phase | N/A | Reverse Osmosis | NaCl 2000 ppm | 100 | 71 | Obviously Decrease |
| 47 | Zwitterionic SWNTs | ▪ 20 wt%; Direct deposit onto membrane substrate | OD = ~1.5nm<br>L= ~1μm | Reverse Osmosis | NaCl 2500 ppm | 530 | 48.8 | 98.6 |
| 65 | Carboxylic MWNTs | ▪ 3 mg per membrane sample; Direct deposit onto substrate | OD <8nm<br>L= 10–30μm | Reverse Osmosis | NaCl 1000 ppm | 100 | *Applied potential: 1.5V*<br>22.0 ± 2.8 | 92.1±1.3 |
| 69 | PMMA modified MWNTs | ▪ 0.67, 1.33, 2.0 g/L in organic phase | OD= 20–30nm | Nanofiltration | $Na_2SO_4$ 2000 ppm | 145 | 69.7 | 99.0 |
| 70 | Amine functionalized MWNTs | ▪ 0.01%, 0.05%, 0.1% in aqueous phase | OD = ~5nm<br>L= ~50μm | Forward Osmosis | NaCl 10mM feed 2M draw | N/A | 95.7 | 89.3 |
| 71 | Aminosilanized SWNTs | ▪ 0.05%, 0.1%, 0.2% (w/v) in organic phase | OD = ~2.7nm<br>L= ~150nm | Low pressure Reverse Osmosis | NaCl 34mM | 232 | ~22 | ~96 |
| 72 | Functionalized MWNTs | ▪ 0.01–0.06% in aqueous or organic phase | OD = ~30nm<br>L= 10–30μm | Nanofiltration | Brilliant blue | N/A | Increase | No Change |

Introducing nanomaterials in the polymer matrix can also change the membrane structure and property. The integrity and stability of the resulting TFN membrane, therefore, becomes a critical factor for the overall membrane performance, which strongly relies on the good dispersion of nanomaterials in the casting solution, or interfacial adhesion between the crosslinked matrix and the embedded nanomaterials. Many efforts were devoted to improve the dispersion and adhesion forces of nanofillers either through modifying nanomaterial surface or applying surfactant. Materials such as CNTs with inherently hydrophobic surface are specifically studied, and a common strategy is to oxidize the CNTs to generate hydroxyl and carboxyl functional groups on their surface as well as at the tip opening.[73] Other strategies such as grafting poly(methyl methacrylate) (PMMA)[69] or amine[70] on the CNT's surface also showed improvement in dispersing the CNTs in the TFN membranes. Poor dispersion may cause disruption of the polymer chains, or lowers the degree of crosslinking of PA during the IP process.

### 3.2.2. Fluid Transport through Carbon Nanotubes (CNTs)

As previously mentioned, vertically-aligned carbon nanotubes with both ends open can offer high-speed fluid transport in a TFN membrane due to its unprecedented smoothness and regularity of rigid cylindrical pores. Studies suggest that the transport of water through sub-nanometer CNTs occurs via a cooperative, pulse-like movement of hydrogen-bonded molecules within the channels, similar to what has been observed in aquaporin biological channels.[74] This transport mechanism has been shown to lead to flow rates that are much faster than what is predicted by classical hydrodynamics.[75,76] In fact, the flow rates of water in CNTs depend strongly on the slip length, which is commonly quoted in the nanofluidics literature and is a useful property for a given flow system of fluid-solid combination. Numerous experimental and simulation studies have been conducted in verifying the flow enhancement of CNTs but no unified result has been discovered yet. Generally the flux differs by 1–5 orders of magnitude compared to the classical no-slip flow predictions. The slip length $L_s$ and flow enhancement $E$ for Hagen-Poiseuille flow are defined as follows:[61]

$$u_s = u(R) = L_s \left| \left( \frac{\partial u(r)}{\partial r} \right)_{r=R} \right| \tag{3-1}$$

$$E = \frac{Q_{slip}}{Q_{no\text{-}slip}} = \left( 1 + \frac{8L_s}{D} \right) \tag{3-2}$$

where $u_s$ is the slip velocity (fluid velocity at the wall), $Q_{slip}$ is the observed flow rate, $Q_{no\text{-}slip}$ is the expected flow rate using the no-slip boundary condition, and $D$ is the diameter of the tube. Using Equation (3-2) one can estimate the flow enhancement given the slip length. Theoretically the slip length is independent of the channel size when it is above a certain width/tube diameter.[61] However, simulation studies tend to show that the slip length of water molecule inside CNTs changes as the diameter of the nanotube varies. In 2005, experimental studies from Majumder *et al.*[77] showed a slip length of 39–68 μm for a 7 nm diameter CNT, and results in a flow enhancement of (44–77)×$10^3$. Using a 10 nm diameter CNT membrane, Du *et al.*[78] found 485 μm slip length. Qin *et al.*[79] found that for narrow CNTs with diameters of 0.81, 0.87, 0.89, 1.10, 1.42, 1.52, 1.59 nm, their corresponding slip lengths are 53, 44.6, 29.3, 56.6, 13.5, 8.4, 7.9 nm, respectively.

### 3.2.3. Functionalization of CNTs

In terms of ion separation, molecular dynamics (MD) simulation studies[63,64] have examined the ability of CNTs in filtering ions from water with their diameters ranging from 6 to 11 Å. They reported almost complete ion exclusion from pores up to 9 Å in diameter due to ion desolvaion energy barriers. By contrast, water faces relatively low energy barriers and is able to pass through these narrow nanotubes. However, producing CNTs with diameter < 9 Å is not currently practical economically, due to the cost in separating narrow nanotubes from others with wide range of diameter distribution. Larger diameter CNTs have much higher water flux, but do not have the ability to reject ions. For example, Yu *et al*. studied ion transport through CNT membranes using large diameter (3 nm) CNTs,[80] and the results showed no ion rejection properties as long as a continuous water channel forms inside the CNTs. To enhance the molecular selectivity of CNT beyond steric effects, their surface chemistry can also be modified through functionalization. This alternative approach is to start from a non-ion-selective CNT with large diameter, and attach multiple functional groups at the CNT tip to reduce the effective pore sizes either by steric hindrance or charge repulsions. Holt *et al*. studied the ion exclusion of CNTs by using nanotubes with pore diameter below 2 nm, and functionalized it with hydroxyl groups in order to reject ions through charge-charge interaction between the tip functional groups and the dissolved salt ions, while allowing non-charge water molecules to pass through the tubes with fast permeation flux.[81] Similarly, tip and core functionalization of large diameter CNTs has been shown to modulate the flux of water, both experimentally[37,82] and from simulations[83].

## 3.3. TFN membranes for Other Applications

### 3.3.1. Forward Osmosis

Forward osmosis (FO), as one of the subset osmotically driven membrane processes, has been extensively investigated in the past decade. The driving force in FO process is provided by a concentrated draw solution (DS), rather than applied hydraulic pressure as in RO. DS at the permeation side generates osmotic pressure that drives the water across the membrane from a low concentration feed solution to DS. The permeated water can then be recovered by removing the thermally-decomposable salts in the DS using waste-heat from chemical plants.[84] FO, therefore, becomes a system that can potentially offer exceptional advantages in desalination process, such as low operating cost and wide range of feed solutions due to operation with low temperature and pressure.[70] One of the main obstacles in the FO process, however, is internal concentration polarization (ICP). The ICP is a natural phenomenon which occurs when the water that withdrew from the feed solution dilutes the DS around the support layer, and significantly reduces the osmotic pressure and retards the desalting process. In order to minimize the ICP, Amini *et al.*[70] synthesized TFN membrane with functionalized MWNTs embedded in the active barrier layer in order to lower the structural parameter, such as the film thickness, tortuosity and porosity. The resulting TFN membranes exhibited higher water permeation flux with acceptable salt rejection.

The biggest challenge for FO, however, remains in the choices of draw solution. Elimelech *et al.* argues that there is no "free lunch" in desalination process, and energy is always required to demix the salts from water, which reduce the entropy of the system.[85] Meanwhile, the magic draw solution which can utilize thermal treatment to be vaporized, and at the meantime offers good osmotic pressure to the system just does not exist. The best salt for DS would be NaCl or other monovalent salts, and the most efficient way to separate monovalent salts from water remains to be RO. This dilemma was also brought up by McGovern *et al.*[86], who argued that reverse osmosis is significantly more energy efficient than FO, and research for FO would best be fully oriented towards alternate applications for desalination.

### 3.3.2. Pressure Retarded Osmosis

Similar to FO, pressure retarded osmosis (PRO) extracts osmotic energy by allowing water to flow through a semi-permeable membrane from a low-salinity feed solution to a high-salinity draw solution. The flowing process is against an applied hydraulic pressure, and the work that is

done by the osmotic pressure will be used to generate electricity using hydraulic turbine. Most of PRO studies nowadays are focused on mixing of seawater and river water, which up to 2.6 TW of osmotic energy is projected to be extracted globally.[87] However, the seawater–river water PRO system has a low energy density due to its low osmotic pressure difference. In order to maximize the osmotic energy, Chung *et al*. proposed to combine seawater brine that is generated by the seawater RO plants, to the wastewater retentate from the city water plant. Their experimental study showed that high power density of 21.1 $W/m^2$ (square meter of membrane) could be generated by such system,[87] and is much higher than the previously proposed value of 5 $W/m^2$ in the regular seawater-river water system. In terms of the design of PRO membranes, similar problems such as ICP remains to be a challenge for PRO, and so far, based on the best of my knowledge, there is no significant movement towards using TFN membranes to resolve such issues.

### 3.4. The differences between RO and NF membrane

The goal of most of the early work on reverse osmosis was to produce desalination membranes with sodium chloride rejections greater than 98%. However, since late 1990s, membranes with lower NaCl rejections but much higher water permeability have been produced. These membranes, which fall into a transition region between pure reverse osmosis and pure ultrafiltration membranes, are called loose reverse osmosis, low-pressure reverse osmosis, or more commonly, nanofiltration membranes (NF). Typically, NF membranes have NaCl rejections between 20 and 80%.[88] Moreover, they have distinct differences in terms of their membrane structure, water transport theory and salt rejection mechanism compared to RO membranes. While RO membranes usually has nominal pore diameter down to the size of a few Å, the pore size for NF membranes are ranging from subnanometer to nanometer size.

The transport mechanism for RO, as previously mentioned, follows solution-diffusion model, which postulates that solvent (water) and solute (salt) molecules are adsorbed into the polymer at the interface and diffuse through the polymeric structure. The permeselectivity depends upon the degree of crosslinking of the polymer, the film hydrophilicity, solvent and solute diffusivities, etc. However, NF membranes generally follows the modified version of Pore-Flow model, which assumes: (1) the membrane is micro-porous with cylindrical pores, (2) water transports through the membrane by viscous flow, (3) solute transports through the membrane by both diffusion and convection in pores, and (4) transport through the membrane pores is

determined by interaction forces, friction forces, and chemical potential gradients of the water and solute.[89] Since most of the NF membranes are composed of polymers with charged functional groups at the backbone, they provide electrostatic potential along the pores of the membrane to reject salt ions. Therefore, the consideration of membrane–solute interactions gives this model a potential to provide more accurate prediction results.

Although polyamide RO membrane is also negatively charged at neutral pH, due to the carboxylic acid group present on the backbone of the polymer, the charge does not provide any salt rejection but rather just increase the surface hydrophilicity of the membrane. Figure 3.3 shows the polymer structure of the PA in a RO membrane, where the –COOH functional group in the repeating unit is from the hydrolysis of unreacted acid chloride functional groups during the interfacial polymerization. PA was determined to generally contain 72% of the crosslinked structure (repeating unit of *n*) and 28% with the –COOH group (repeating unit of *m*).[90] NF membranes, on the other hand, can be neutrally, positively and negatively charged. Neutral NF membrane simply rejects salt by size sieving, while anionic NF membranes contain positively-charged functional groups that repel positive cations while attracting negative anions through electrostatic force. It can offer better rejection if the valence of the cation is larger (e.g. $CaCl_2$ > NaCl). Cationic NF membranes work in a reverse fashion and offer better rejection towards anions with larger valence (e.g. $Na_2SO_4$ > NaCl).

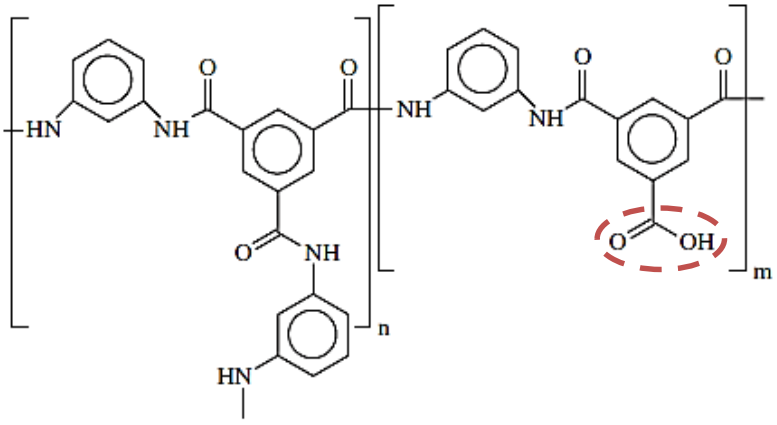


**Figure 3.3.** Chemical structure of aromatic polyamide RO membrane.

The rejection mechanism of charged NF membranes depends on both the molecular size of salt ions and the Donnan exclusion effects. When a charged NF membrane is in contact with an electrolyte solution, Donnan potential is formed by an electrochemical equilibrium. Because electrostatic forces with the fixed charges on the membrane counteract the tendency of the co-ion

(ions having the same charge sign of the pore charges) to move in the direction of their concentration gradient, charged species distribute unevenly between membrane and solution phase. This results in the membrane being enriched with counterions and depleted of co-ions. As a consequence, a potential difference is established at the solution/membrane interphase. When a pressure gradient is applied across the membrane, the Donnan potential tends to exclude co-ions from the membrane. Because of the electroneutrality requirement, which arises from the energetic cost of charge separation, counterions have to be rejected as well. This is the separation mechanism known as Donnan charge exclusion.

NF membranes are usually two- to five-fold more permeable than brackish and seawater RO membranes because of the fast water diffusion rate in these loose-chain, low chemically crosslinked composite structures. However, at higher feed concentrations (i.e., ≥ 2000 ppm) the Donnan exclusion effect is negated by electrostatic screening of the fixed charges. When the feed solution becomes more concentrated, the ionic strength in the solution increases and affects the Debye length, $\lambda_d$, of the functional groups in the membrane. The Debye length can be described as follow:

$$\lambda_d = \sqrt{\frac{\varepsilon_0 \varepsilon_r k_B T}{2 N_A e^2 I}} \tag{3-3}$$

where $I$ is the ionic strength, $\varepsilon_0$ and $\varepsilon_r$ is the vacuum and relative permittivity respectively. $T$ is the absolute temperature, $e$ is elementary charge, and $N_A$ is the Avogadro number. Therefore, as the ionic strength of the feed solution increase, $\lambda_d$ decreases. Once the Debye length falls shorter than the pore diameter of the membrane (i.e. feed concentration >2000ppm), salt ions can freely transport through the membrane and results in the loss of salt rejection. NF membranes are therefore used to remove low levels of salt from already relatively-clean water. Since there is no high osmotic pressure to overcome, the membranes are usually operated at very low pressures of 50-200 psig.

RO membranes reject salt ions mostly based on their molecular sizes, despite the charge of the ions. Therefore, as depicted in Figure 3.4, when the feed salt concentration is similar to the level in brackish water (100 to 2000 ppm), the rejection of salt ions tends to increase as the feed concentration increases. However, as the concentration continues to increase up to the level close to sea water, the salt rejection could drop from 98% to ~91%, with the water permeation flux decreasing significantly as well. Unlike NF membranes, however, the decrease of rejection in RO

membranes is strictly due to the increase of osmotic pressure across the membrane, which leads to the decrease of the water permeation flux. Consequently, it results in lower salt rejection, because for the same amount of salts permeating through the membrane, there is less driving force for water to transport to the other side of the membrane at high salinity. Therefore, the operating condition for RO is usually at 225 psi for brackish water, and 600 – 800 psi for sea water in order to maintain the high salt rejection.

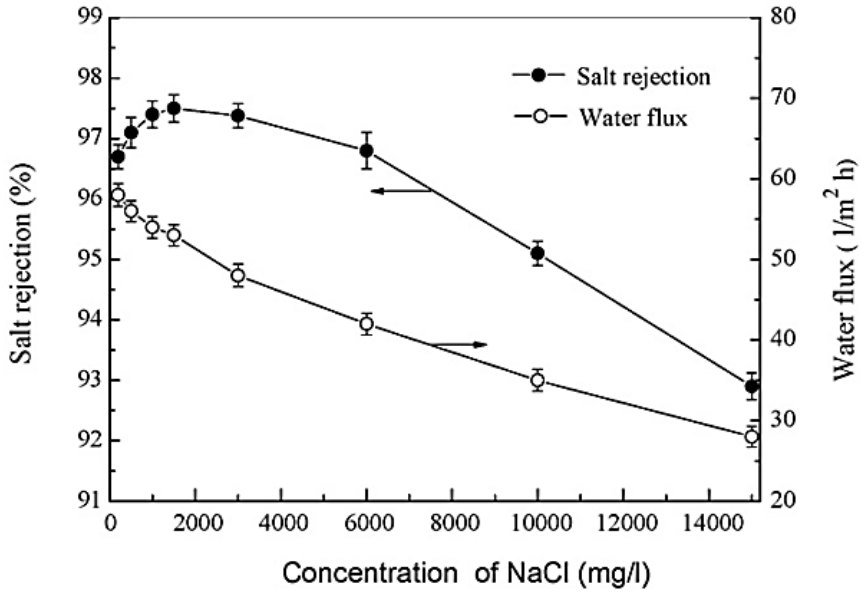


**Figure 3.4.** Effects of feed concentration on the salt rejection and water flux of thin-film composite membrane tested with feed solution of NaCl at 25˚C and pH 7, and at transmembrane pressure of 1.5MPa. Copyright 2009.[91] Reuse with permission from Elsevier Ltd.

## References


(1) Shin, D. H.; Kim, N.; Lee, Y. T. Modification to the Polyamide TFC RO Membranes for Improvement of Chlorine-Resistance. *Journal of Membrane Science* **2011**, *376*, 302–311.

(2) Argust, P. Distribution of Boron in the Environment. *Biological trace element research* **1998**.

(3) Tu, K. L.; Nghiem, L. D.; Chivas, A. R. Boron Removal by Reverse Osmosis Membranes in Seawater Desalination Applications. *Separation and Purification Technology* **2010**, *75*, 87–101.

(4) DOW FILMTEC™ Membranes, Midland, Michigan U.S.A. 48674.

(5) Hydranautics Corporate, 401 Jones Road, Oceanside, CA 92058.

(6) TORAY Membrane USA, Inc., 13435 Danielson Street, Poway CA 92064, U.S.A.

(7) Koch Membrane Systems, Inc., 850 Main Street Wilmington, Massachusetts 01887-3388 USA.

(8) LG NanoH2O, Inc. El Segundo, California, 90245. **2015**.

(9) Light, W. G.; Chu, H. C.; Tran, C. N. Reverse Osmosis TFC Magnum Elements for Chlorinated/dechlorinated Feedwater Processing. *Desalination* **1987**, *64*, 411–421.
(10) Watters, J. C.; Klein, E.; Fleischman, M.; Roberts, J. S.; Hall, B. Rejection Spectra of Reverse Osmosis Membranes Degraded by Hydrolysis or Chlorine Attack. *Desalination* **1986**, *60*, 93–110.
(11) Saha, N. K.; Joshi, S. V. Performance Evaluation of Thin Film Composite Polyamide Nanofiltration Membrane with Variation in Monomer Type. *Journal of Membrane Science* **2009**, *342*, 60–69.
(12) Xie, W.; Park, H.-B.; Cook, J.; Lee, C. H.; Byun, G.; Freeman, B. D.; McGrath, J. E. Advances in Membrane Materials: Desalination Membranes Based on Directly Copolymerized Disulfonated Poly(arylene Ether Sulfone) Random Copolymers. *Water Science and Technology* **2010**, *61*, 619–624.
(13) McGrath, J. E.; Freeman, B. D.; Lee, C. H.; Cook, J.; Xie, W.; Park, H. B. Fundamental Salt and Water Transport Properties in Directly Copolymerized Disulfonated Poly(arylene Ether Sulfone) Random Copolymers. *Polymer* **2011**, *52*, 2032–2043.
(14) Xie, W.; Geise, G. M.; Freeman, B. D.; Lee, H.-S.; Byun, G.; McGrath, J. E. Polyamide Interfacial Composite Membranes Prepared from M-Phenylene Diamine, Trimesoyl Chloride and a New Disulfonated Diamine. *Journal of Membrane Science* **2012**.
(15) Zhou, Y.; Yu, S.; Liu, M.; Chen, H.; Gao, C. Effect of Mixed Crosslinking Agents on Performance of Thin-Film-Composite Membranes. *Desalination* **2006**, *192*, 182–189.
(16) Yong, Z.; Sanchuan, Y.; Meihong, L.; Congjie, G. Polyamide Thin Film Composite Membrane Prepared from M-Phenylenediamine and M-Phenylenediamine-5-Sulfonic Acid. *Journal of Membrane Science* **2006**, *270*, 162–168.
(17) Liu, L.-F.; Cai, Z.-B.; Shen, J.-N.; Wu, L.-X.; Hoek, E. M. V.; Gao, C.-J. Fabrication and Characterization of a Novel Poly(amide-Urethane@imide) TFC Reverse Osmosis Membrane with Chlorine-Tolerant Property. *Journal of Membrane Science* **2014**, *469*, 397–409.
(18) Mukherjee, D.; Kulkarni, A.; Gill, W. N. Chemical Treatment for Improved Performance of Reverse Osmosis Membranes. *Desalination* **1996**, *104*, 239–249.
(19) Ishigami, T.; Amano, K.; Fujii, A.; Ohmukai, Y.; Kamio, E.; Maruyama, T.; Matsuyama, H. Fouling Reduction of Reverse Osmosis Membrane by Surface Modification via Layer-by-Layer Assembly. *Separation and Purification Technology* **2012**, *99*, 1–7.
(20) Sarkar, A.; Dvornic, P. Surface Modification of Polyamide Reverse Osmosis Membranes. *US Patent 8,505,743* **2013**, *1*.
(21) Li, D.; Wang, H. Recent Developments in Reverse Osmosis Desalination Membranes. *Journal of Materials Chemistry* **2010**, *20*, 4551.
(22) Belfer, S.; Purinson, Y.; Fainshtein, R. Surface Modification of Commercial Composite Polyamide Reverse Osmosis Membranes. *Journal of Membrane Science* **1998**, *139*, 175–181.
(23) Tarboush, B. J. A.; Rana, D.; Matsuura, T.; Arafat, H. a.; Narbaitz, R. M. Preparation of Thin-Film-Composite Polyamide Membranes for Desalination Using Novel Hydrophilic Surface Modifying Macromolecules. *Journal of Membrane Science* **2008**, *325*, 166–175.
(24) Kim, S.; Kwak, S.; Suzuki, T. Positron Annihilation Spectroscopic Evidence to Demonstrate the Flux-Enhancement Mechanism in Morphology-Controlled Thin-Film-Composite (TFC) Membrane. *Environmental science & technology* **2005**, *39*, 1764–1770.

(25) Yu, S.; Liu, X.; Liu, J.; Wu, D.; Liu, M.; Gao, C. Surface Modification of Thin-Film Composite Polyamide Reverse Osmosis Membranes with Thermo-Responsive Polymer (TRP) for Improved Fouling Resistance and Cleaning Efficiency. *Separation and Purification Technology* **2011**, *76*, 283–291.
(26) Azari, S.; Zou, L. Using Zwitterionic Amino Acid L-DOPA to Modify the Surface of Thin Film Composite Polyamide Reverse Osmosis Membranes to Increase Their Fouling Resistance. *Journal of Membrane Science* **2012**, *401-402*, 68–75.
(27) Li, L.; Lee, R. Purification of Produced Water by Ceramic Membranes: Material Screening, Process Design and Economics. *Separation Science and Technology* **2009**, *44*, 3455–3484.
(28) Misdan, N.; Lau, W. J.; Ismail, A. F. Seawater Reverse Osmosis (SWRO) Desalination by Thin-Film Composite membrane—Current Development, Challenges and Future Prospects. *Desalination* **2012**, *287*, 228–237.
(29) Fathizadeh, M.; Aroujalian, A.; Raisi, A. Effect of Added NaX Nano-Zeolite into Polyamide as a Top Thin Layer of Membrane on Water Flux and Salt Rejection in a Reverse Osmosis Process. *Journal of Membrane Science* **2011**, *375*, 88–95.
(30) Perego, C.; Bagatin, R.; Tagliabue, M.; Vignola, R. Zeolites and Related Mesoporous Materials for Multi-Talented Environmental Solutions. *Microporous and Mesoporous Materials* **2013**, *166*, 37–49.
(31) Li, L.; Liu, N.; McPherson, B.; Lee, R. Influence of Counter Ions on the Reverse Osmosis through MFI Zeolite Membranes: Implications for Produced Water Desalination. *Desalination* **2008**, *228*, 217–225.
(32) Covarrubias, C.; García, R.; Arriagada, R.; Yánez, J.; Ramanan, H.; Lai, Z.; Tsapatsis, M. Removal of Trivalent Chromium Contaminant from Aqueous Media Using FAU-Type Zeolite Membranes. *Journal of Membrane Science* **2008**, *312*, 163–173.
(33) Li, L.; Dong, J.; Nenoff, T. M.; Lee, R. Desalination by Reverse Osmosis Using MFI Zeolite Membranes. *Journal of Membrane Science* **2004**, *243*, 401–404.
(34) Jeong, B.-H.; Hoek, E. M. V.; Yan, Y.; Subramani, A.; Huang, X.; Hurwitz, G.; Ghosh, A. K.; Jawor, A. Interfacial Polymerization of Thin Film Nanocomposites: A New Concept for Reverse Osmosis Membranes. *Journal of Membrane Science* **2007**, *294*, 1–7.
(35) Kim, S.; Chen, L.; Johnson, J. K.; Marand, E. Polysulfone and Functionalized Carbon Nanotube Mixed Matrix Membranes for Gas Separation: Theory and Experiment. *Journal of Membrane Science* **2007**, *294*, 147–158.
(36) Majumder, M.; Chopra, N.; Hinds, B. J. Effect of Tip Functionalization on Transport through Vertically Oriented Carbon Nanotube Membranes. *Journal of the American Chemical Society* **2005**, *127*, 9062–9070.
(37) Majumder, M.; Chopra, N.; Hinds, B. J. Mass Transport through Carbon Nanotube Membranes in Three Different Regimes: Ionic Diffusion and Gas and Liquid Flow. *ACS nano* **2011**, *5*, 3867–3877.
(38) Holt, J. K. Carbon Nanotubes and Nanofluidic Transport. *Advanced Materials* **2009**, *21*, 3542–3550.
(39) Holt, J. K.; Noy, A.; Huser, T.; Eaglesham, D.; Bakajin, O. Fabrication of a Carbon Nanotube-Embedded Silicon Nitride Membrane for Studies of Nanometer-Scale Mass Transport. *Nano Letters* **2004**, *4*, 2245–2250.

(40) Kalra, A.; Garde, S.; Hummer, G. Osmotic Water Transport through Carbon Nanotube Membranes. *Proceedings of the National Academy of Sciences of the United States of America* **2003**, *100*, 10175–10180.
(41) HOEK, E.; YAN, Y.; JEONG, B. NANOCOMPOSITE MEMBRANES AND METHODS OF MAKING AND USING SAME. *WO Patent 2,006,098,872* **2006**, *1*.
(42) RATTO, T.; HOLT, J.; SZMODIS, A. MEMBRANES WITH EMBEDDED NANOTUBES FOR SELECTIVE PERMEABILITY. *WO Patent 2,010,002,805* **2010**.
(43) Lee, S.; Kim, H.; Patel, R.; Im, S. J.; Kim, J. H.; Min, B. R. Silver Nanoparticles Immobilized on Thin Film Composite Polyamide Membrane: Characterization, Nanofiltration, Antifouling Properties. *Polymers for Advanced Technologies* **2007**, *18*, 562–568.
(44) Lee, H. S.; Im, S. J.; Kim, J. H.; Kim, H. J.; Kim, J. P.; Min, B. R. Polyamide Thin-Film Nanofiltration Membranes Containing TiO2 Nanoparticles. *Desalination* **2008**, *219*, 48–56.
(45) Jadav, G. L.; Singh, P. S. Synthesis of Novel Silica-Polyamide Nanocomposite Membrane with Enhanced Properties. *Journal of Membrane Science* **2009**, *328*, 257–267.
(46) Kurth, C. J.; Koehler, J. A.; Zhou, M.; Holmberg, B. A. Hybrid Nanoparticle TFC Membranes. *US patent 0261344A1* **2012**.
(47) Chan, W.-F.; Chen, H.; Surapathi, A.; Taylor, M. G.; Shao, X.; Marand, E.; Johnson, J. K. Zwitterion Functionalized Carbon Nanotube/polyamide Nanocomposite Membranes for Water Desalination. *ACS Nano* **2013**, *7*, 5308–5319.
(48) Lind, M. L.; Ghosh, A. K.; Jawor, A.; Huang, X.; Hou, W.; Yang, Y.; Hoek, E. M. V. Influence of Zeolite Crystal Size on Zeolite-Polyamide Thin Film Nanocomposite Membranes. *Langmuir : the ACS journal of surfaces and colloids* **2009**, *25*, 10139–10145.
(49) Lind, M. L.; Jeong, B.-H.; Subramani, A.; Huang, X.; Hoek, E. M. V. Effect of Mobile Cation on Zeolite-Polyamide Thin Film Nanocomposite Membranes. *Journal of Materials Research* **2009**, *24*, 1624–1631.
(50) Lu, J.; Liu, N.; Li, L.; Lee, R. Organic Fouling and Regeneration of Zeolite Membrane in Wastewater Treatment. *Separation and Purification Technology* **2010**, *72*, 203–207.
(51) Liu, N.; Li, L.; McPherson, B.; Lee, R. Removal of Organics from Produced Water by Reverse Osmosis Using MFI-Type Zeolite Membranes. *Journal of Membrane Science* **2008**, *325*, 357–361.
(52) Li, L.; Liu, N.; McPherson, B.; Lee, R. Enhanced Water Permeation of Reverse Osmosis through MFI-Type Zeolite Membranes with High Aluminum Contents. *Industrial & Engineering Chemistry Research* **2007**, *46*, 1584–1589.
(53) Gahlot, S.; Sharma, P. P.; Gupta, H.; Kulshrestha, V.; Jha, P. K. Preparation of Graphene Oxide Nano-Composite Ion-Exchange Membranes for Desalination Application. *RSC Advances* **2014**, 24662–24670.
(54) Cohen-Tanugi, D.; Grossman, J. C. Water Desalination across Nanoporous Graphene. *Nano Letters* **2012**, *12*, 3602–3608.
(55) Nicolaï, A.; Sumpter, B. G.; Meunier, V. Tunable Water Desalination across Graphene Oxide Framework Membranes. *Physical chemistry chemical physics : PCCP* **2014**, *16*, 8646–8654.
(56) Cohen-Tanugi, D.; Grossman, J. C. Water Permeability of Nanoporous Graphene at Realistic Pressures for Reverse Osmosis Desalination. *The Journal of chemical physics* **2014**, *141*, 074704.

(57) Perreault, F.; Tousley, M. E.; Elimelech, M. Thin-Film Composite Polyamide Membranes Functionalized with Biocidal Graphene Oxide Nanosheets. *Environmental Science & Technology Letters* **2014**, *1*, 71–76.
(58) Goh, K.; Setiawan, L.; Wei, L.; Si, R.; Fane, A. G.; Wang, R.; Chen, Y. Graphene Oxide as Effective Selective Barriers on a Hollow Fiber Membrane for Water Treatment Process. *Journal of Membrane Science* **2015**, *474*, 244–253.
(59) Daer, S.; Kharraz, J.; Giwa, A.; Hasan, S. W. Recent Applications of Nanomaterials in Water Desalination: A Critical Review and Future Opportunities. *Desalination* **2015**, *367*, 37–48.
(60) Hummer, G.; Rasaiah, J. C.; Noworyta, J. P. Water Conduction through the Hydrophobic Channel of a Carbon Nanotube. *Nature* **2001**, *414*, 188–190.
(61) Kannam, S. K.; Todd, B. D.; Hansen, J. S.; Daivis, P. J. How Fast Does Water Flow in Carbon Nanotubes? *The Journal of chemical physics* **2013**, *138*, 094701.
(62) Liu, H.; Murad, S.; Jameson, C. J. Ion Permeation Dynamics in Carbon Nanotubes. *The Journal of chemical physics* **2006**, *125*, 084713.
(63) Song, C.; Corry, B. Intrinsic Ion Selectivity of Narrow Hydrophobic Pores. *The Journal of Physical Chemistry B* **2009**, *113*, 7642–7649.
(64) Corry, B. Designing Carbon Nanotube Membranes for Efficient Water Desalination. *Journal of Physical Chemistry B* **2008**, *112*, 1427–1434.
(65) De Lannoy, C.-F.; Jassby, D.; Gloe, K.; Gordon, A. D.; Wiesner, M. R. Aquatic Biofouling Prevention by Electrically Charged Nanocomposite Polymer Thin Film Membranes. *Environmental science & technology* **2013**.
(66) KURTH, C.; KOEHLER, J. IMPROVED HYBRID TFC RO MEMBRANES WITH NITROGEN ADDITIVES. *WO Patent …* **2011**, *1*.
(67) Duan, J.; Litwiller, E.; Pinnau, I. Preparation and Water Desalination Properties of POSS-Polyamide Nanocomposite Reverse Osmosis Membranes. *Journal of Membrane Science* **2015**, *473*, 157–164.
(68) Zhang, L.; Shi, G.-Z.; Qiu, S.; Cheng, L.-H.; Chen, H.-L. Preparation of High-Flux Thin Film Nanocomposite Reverse Osmosis Membranes by Incorporating Functionalized Multi-Walled Carbon Nanotubes. *Desalination and Water Treatment* **2011**, *34*, 19–24.
(69) Yu, C. C.; Yu, H. W.; Chu, Y. X.; Ruan, H. M.; Shen, J. N. Preparation Thin Film Nanocomposite Membrane Incorporating PMMA Modified MWNT for Nanofiltration. *Key Engineering Materials* **2013**, *562-565*, 882–886.
(70) Amini, M.; Jahanshahi, M.; Rahimpour, A. Synthesis of Novel Thin Film Nanocomposite (TFN) Forward Osmosis Membranes Using Functionalized Multi-Walled Carbon Nanotubes. *Journal of Membrane Science* **2013**, *435*, 233–241.
(71) Baroña, G. N. B.; Lim, J.; Choi, M.; Jung, B. Interfacial Polymerization of Polyamide-Aluminosilicate SWNT Nanocomposite Membranes for Reverse Osmosis. *Desalination* **2013**, *325*, 138–147.
(72) Roy, S.; Ntim, S. A.; Mitra, S.; Sirkar, K. K. Facile Fabrication of Superior Nanofiltration Membranes from Interfacially Polymerized CNT-Polymer Composites. *Journal of Membrane Science* **2011**, *375*, 81–87.
(73) Yin, J.; Deng, B. Polymer-Matrix Nanocomposite Membranes for Water Treatment. *Journal of Membrane Science* **2014**, *479*, 256–275.
(74) Zhu, F.; Tajkhorshid, E.; Schulten, K. Theory and Simulation of Water Permeation in Aquaporin-1. *Biophysical journal* **2004**, *86*, 50–57.

(75) Thomas, J.; McGaughey, A. Water Flow in Carbon Nanotubes: Transition to Subcontinuum Transport. *Physical Review Letters* **2009**, *102*, 184502.
(76) Thomas, J.; McGaughey, A. Reassessing Fast Water Transport through Carbon Nanotubes. *Nano letters* **2008**.
(77) Majumder, M.; Chopra, N.; Andrews, R.; Hinds, B. J. Nanoscale Hydrodynamics: Enhanced Flow in Carbon Nanotubes. *Nature* **2005**, *438*, 43–44.
(78) Du, F.; Qu, L.; Xia, Z.; Feng, L.; Dai, L. Membranes of Vertically Aligned Superlong Carbon Nanotubes. *Langmuir* **2011**, *27*, 8437–8443.
(79) Qin, X.; Yuan, Q.; Zhao, Y.; Xie, S.; Liu, Z. Measurement of the Rate of Water Translocation through Carbon Nanotubes. *Nano Lett* **2011**, *11*, 2173–2177.
(80) Yu, M.; Funke, H. H.; Falconer, J. L.; Noble, R. D. Gated Ion Transport through Dense Carbon Nanotube Membranes. *Journal of the American Chemical Society* **2010**, *132*, 8285–8290.
(81) Fornasiero, F.; Park, H. G.; Holt, J. K.; Stadermann, M.; Grigoropoulos, C. P.; Noy, A.; Bakajin, O. Ion Exclusion by Sub-2-Nm Carbon Nanotube Pores. *Proceedings of the National Academy of Sciences of the United States of America* **2008**, *105*, 17250–17255.
(82) Hinds, B. J.; Chopra, N.; Rantell, T.; Andrews, R.; Gavalas, V.; Bachas, L. G. Aligned Multiwalled Carbon Nanotube Membranes. *Science (New York, N.Y.)* **2004**, *303*, 62–65.
(83) Majumder, M.; Corry, B. Anomalous Decline of Water Transport in Covalently Modified Carbon Nanotube Membranes. *Chemical communications (Cambridge, England)* **2011**, *47*, 7683–7685.
(84) Elimelech, M.; Phillip, W. The Future of Seawater Desalination: Energy, Technology, and the Environment. *Science* **2011**, *333*, 712–718.
(85) Shaffer, D. L.; Werber, J. R.; Jaramillo, H.; Lin, S.; Elimelech, M. Forward Osmosis: Where Are We Now? *Desalination* **2014**.
(86) McGovern, R. K.; Lienhard V, J. H. On the Potential of Forward Osmosis to Energetically Outperform Reverse Osmosis Desalination. *Journal of Membrane Science* **2014**, *469*, 245–250.
(87) Wan, C. F.; Chung, T.-S. Osmotic Power Generation by Pressure Retarded Osmosis Using Seawater Brine as the Draw Solution and Wastewater Retentate as the Feed. *Journal of Membrane Science* **2015**, *479*, 148–158.
(88) Baker, R. W. *Membrane Technology and Applications*; 2nd ed.; 2004; Vol. 23.
(89) Wang, J.; Dlamini, D. S.; Mishra, A. K.; Pendergast, M. T. M.; Wong, M. C. Y.; Mamba, B. B.; Freger, V.; Verliefde, A. R. D.; Hoek, E. M. V. A Critical Review of Transport through Osmotic Membranes. *Journal of Membrane Science* **2014**, *454*, 516–537.
(90) Zhao, L.; Chang, P. C.-Y.; Yen, C.; Ho, W. S. W. High-Flux and Fouling-Resistant Membranes for Brackish Water Desalination. *Journal of Membrane Science* **2013**, *425-426*, 1–10.
(91) Yu, S.; Liu, M.; Lü, Z.; Zhou, Y.; Gao, C. Aromatic-Cycloaliphatic Polyamide Thin-Film Composite Membrane with Improved Chlorine Resistance Prepared from M-Phenylenediamine-4-Methyl and Cyclohexane-1,3,5-Tricarbonyl Chloride. *Journal of Membrane Science* **2009**, *344*, 155–164.

# Chapter 4. The Study of Using Zwitterion Functionalized Carbon Nanotube in Thin-Film Nanocomposite Membranes for Water Desalination

The contents of this chapter have been previously published, and are reprinted with permission[1]: W.-F. Chan, H. Chen, A. Surapathi, M.G. Taylor, X. Shao, E. Marand and Karl Johnson. Zwitterion functionalized carbon nanotube/polyamide nanocomposite membranes for water desalination, *ACS Nano*. **7(6),** 2013, pp.5308–5319.

## 4.1. Introduction

The increasing demand for fresh water has become one of the global challenges for human being in this century. Approximately 800 million people, or almost one-sixth of the world's population living on parts of the earth that do not have access to safe drinking water.[2] Although over 70% of the surface of the earth is covered with water, access to clean water remains a critical issue worldwide.[3] Conventional methods for desalination include distillation and reverse osmosis. The first method is unavoidably energy intensive as water has a very high heat of vaporization. Reverse osmosis (RO) with semipermeable polymer membrane is another way to meet the demand.[4] Thin film composite membranes based on aromatic polyamides are predominantly used as RO materials. However, these materials are far from optimum.[5] There is a need to improve the permeance of water while keeping the salt rejection at acceptable levels.

Carbon nanotubes are promising materials for use in membranes because they have shown remarkably high water transport rate.[6–13] Molecular simulations and experimental studies have demonstrated that the transport of fluids through CNTs is orders of magnitude faster than through other nanoporous materials due to the unprecedented smoothness and regularity of the CNT pores.[5,8,10,13–16] The transport of water in CNTs has been shown to give flow rates that are faster than predicted by classical hydrodynamics.[17,18] However, simulation studies suggest that only CNTs with diameter less than 0.9 nm has the ability to filter salt ions from water molecules.[19] CNTs with larger diameter have much higher water flux but do not reject ions.[20] Even though fabrication of CNTs with extremely small pore diameter (~0.4 nm) has been reported,[21] producing desalination membrane with CNTs having diameter < 0.9 nm is not economical. An alternate approach is to tune the effective diameter of the CNT entrance by attaching functional groups, narrowing the mouth of regular CNTs down to desirable sizes.

Hinds *et al.*[22] showed that biotin functionalized CNTs have a marked transport reduction of $Ru(NH_3)_6^+$ ion. Fornasiero *et al.*[23] showed ion exclusion using CNTs functionalized with hydroxyl, carbonyl and carboxylic groups. The pore diameter of CNTs was in sub-2 nm (much

larger than the average diameter of salt ions), but the resulted CNTs membrane showed significant salt rejection with fast water flux. Their results suggest a Donnan-type exclusion mechanism, dominated by electrostatic interactions between the fixed $COO^-$ charges on the ends of the CNTs and mobile ions. However, this also means that the salt rejection decrease along with the increase of ion concentration in feed solution. When electrostatic repulsion from the functional groups is completely retarded by the strong ionic strength in the solution, CNTs alone did not provide any sorts of size exclusion and thus rejection dropped significantly. For some of the ions with small hydrated size their rejections reached zero.

Our group has focused on using functionalized single-walled CNTs (SWNTs) with zwitterion groups which act as molecular gatekeepers at the entrance of CNTs to enhance the blockage of salt ions. Our hypothesis is that chain-like zwitterion groups will be more effective at rejecting both positive and negative ions than CNTs having singly charged functional groups. We postulate that this enhanced performance will be due to a combination of Donnan-type rejection and size exclusion by steric hindrance, because the zwitterion is larger and has more conformational degrees of freedom than the functional groups considered in previous simulations.[24] Moreover, zwitterion groups should prevent biofouling of the membrane since zwitterion-treated surfaces have shown good resistance to cell adhesion.[25–27] In this study, we have synthesized zwitterionic SWNTs (Z-SWNTs) using the functional group with the following structure: $–COO–(CH_2)_3–N^+(CH_3)_2–(CH_2)_2COO^-$.[28] The pore diameter of CNTs before functionalization was 1.5 nm on the average. We then fabricated Z-SWNTs/polyamide nanocomposite membranes using a protocol that partially aligns the CNTs within the polyamide thin film through flow filtration.[7] We have measured the performance of the membranes as a function of the concentration of the CNTs. Other common salts rather than sodium chloride were also tested to study the separation mechanism of Z-SWNTs. Both the change of ions' hydrated size and their valence charge show noticeable effect to their rejection. Note that the synthesis method we have developed can be used for large-scale manufacture of CNT membranes, in contrast to previous methods in synthesizing CNT membranes,[22,23] which require CNTs to be grown on a substrate in a CVD reactor, and therefore, are non-scalable.

## 4.2. Experimental

### 4.2.1. Modeling

Johnson's group has performed molecular dynamics simulations for hypothetical single-walled CNT membrane shown in Figure 4.1. A membrane composed of (20,0) CNTs with diameter and length of 15.6 Å and 41.18 Å respectively was built in a simulation box. The CNTs were embedded in two graphene sheets to form a membrane, with the ends of each tube functionalized with 0, 1, or 2 zwitterionic groups. The membrane was immersed into a water box containing NaCl or KCl with periodic boundary conditions along three dimensions. The sizes of the simulation boxes were 54.1 Å × 55.38 Å × 114 Å. The nominal concentration of salt in seawater of 0.6 M was used for most of the calculations. All calculations were performed with the LAMMPS package[29] using a time step of 1 fs. In the flux calculation, a pressure drop was introduced to generate the flux through the membrane using the method developed by Zhu *et al.*[30] Following the approach of Corry,[19,24] a constant force was applied to each water molecule in the force region of the saltwater box from 45 to 69 Å.

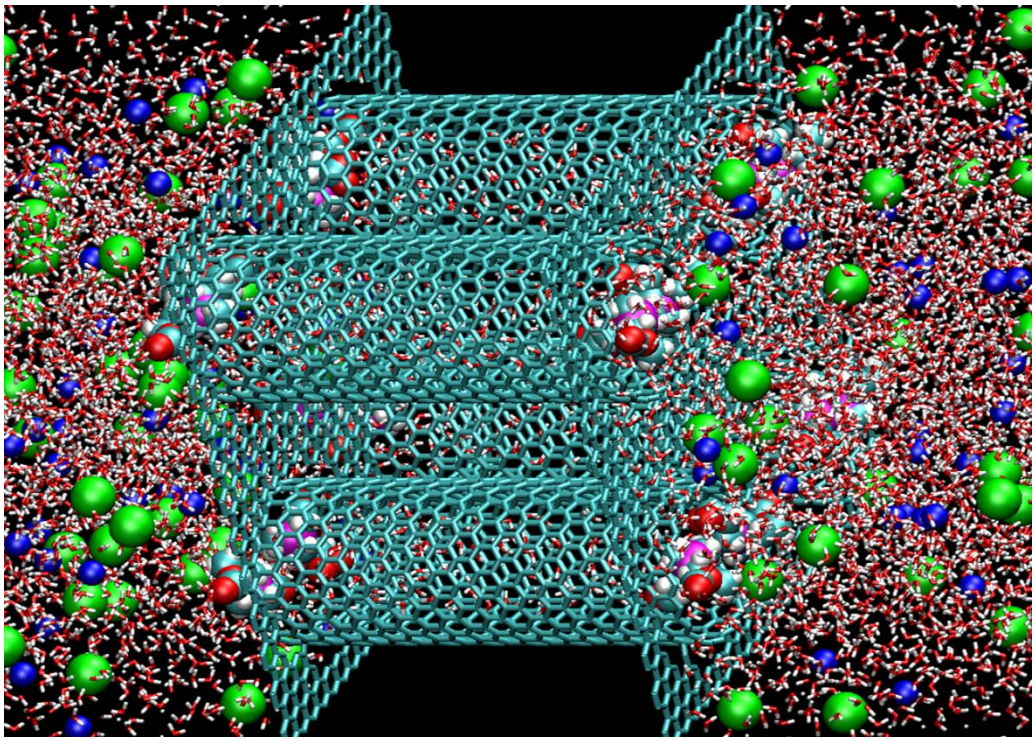

**Figure 4.1.** View of the section for simulation cell containing a membrane composed of four CNTs embedded between two graphene sheets with saltwater on either side of the membrane. Each end of each tube is functionalized with two zwitterionic groups. The carbons of the CNTs and graphene sheets are shown as cyan lines. Water molecules are shown as red and white sticks, Cl-

and Na+ ions are shown as green and blue spheres, respectively, and the atoms of the zwitterions are shown as space filling models, cyan for C, red for O, white for H, and magenta for N.

### 4.2.2. Materials

The following chemicals were purchased from Sigma-Aldrich: 1,3,5-benzenetricarbonyl trichloride (trimesoyl chloride, TMC), 1,3-phenylenediamine (m-phenylenediamine, MPD) and sodium dodecylbenzenesulfonate (SDBS) were used as received. All chemical were of analytical grade. Polyethersulfone (PES) ultrafiltration membranes were provided by Trisep Corporation (Goleta, CA). The salts used in this study were potassium chloride (KCl, ≥ 99.5%; FisherChemical), sodium Chloride (NaCl, ≥ 99.5%; Sigma-Aldrich), magnesium chloride hexahydrate ($MgCl_2 \cdot 6H_2O$; EK industries), magnesium sulfate ($MgSO_4$, ≥ 99%; Spectrum Chemical MFG. Corp.) and calcium chloride ($CaCl_2$, ≥ 99%; Sigma-Aldrich).

### 4.2.3. CNT Functionalization

Carboxylate functionalized CNTs of outer diameter 15 Å and length 1 μm were purchased from Nano Lab Inc. (Waltham, MA).[31] The COOH– functionalized CNTs were produced by chemical vapor deposition (CVD). Concentration of –COOH groups in the CNTs was approximately 2–7 wt % (as determined by titration). These functionalized CNTs were reacted with thionyl chloride ($SOCl_2$) at 65 °C for 36 h and the –COOH groups were replaced by COCl groups. The acylated CNTs were then esterificated using 3-dimethylamino-1-propanol, $(CH_3)_2$- N-$C_3H_6$-OH.This was followed by a ring-opening reaction of lactone, in which β-propiolactone was opened to form an acid group and attached to the tertiary amine on the functional group.[32,33] The resulting zwitterionic group had a positive charge at the tertiary amine group and negative charge at the carboxylated group.

### 4.2.4. Membrane Fabrication

**Functionalized CNT Nanocomposite Membranes.** The interfacial polymerization (IP) of polyamide (PA) is very sensitive to the operating condition and reaction time. Moreover, there are many ways to carry out the procedure. Different publications report different recipes in terms of the concentration of monomers, contact time, air-drying time, curing temperature, etc.[34–37] Using this sensitive membrane to embed carbon nanotubes is rarely done and involved many trial-and-error approaches. Our fabrication process was divided into three steps, as shown schematically in Figure 4.2. First, the PES support was pretreated by soaking in 0.5 wt % SDBS solution for two

days to open the pores and to increase the hydrophilicity. The support was then soaked in deionized (DI) water for one day to remove any excess surfactants. This soaking pretreatment guaranteed that there was no SBDS solution left in the pores. The absence of this step may introduce air bubbles underneath the later PA layer. Afterward, a predetermined amount of functionalized CNTs was poured on the support. We used high-vacuum filtration to disperse the CNTs on the support in a semi-aligned orientation[7] and to remove the solvent. The support with aligned CNTs was then dried for an hour in a vacuum oven to insure that all water was removed from the nanotubes before the interfacial polymerization took place. The support was then sandwiched between two round poly(tetrafluoroethylene) (PTFE) frames. The third step in the membrane fabrication process was interfacial polymerization of PA. IP was carried out on the CNT covered support by wetting the fabrication side (with CNTs) with an aqueous diamine solution containing 2 wt% MPD and 0.2 wt% of SDBS at ambient temperature for 2 min and then the membrane was unclamped and immediately placed on a glass plate. A glass roller was rolled over the membrane once to remove all the excess MPD solution. The membrane was then sandwiched again into the holder and wetted by an n-hexane solution containing 0.5% (w/v) TMC for 90 seconds. The resulting PA thin film nanocomposite membrane was subsequently heat cured at 68°C for 5 min. After the membrane had cooled down, it was washed thoroughly with DI water, submersed in fresh DI water and stored in a laboratory refrigerator at 4°C. Field emission scanning electron microscopy (FESEM) was used to examine the surface of the support, as shown and described in Section 4.3.2.

**End-Capped CNT Nanocomposite Membranes.** The end-capped SWNTs were purchased from NanoLab, Inc.[31] and used as received without any further purification. They were produced by CVD method, with diameter of 15 Å and length of 1 to 5 μm. Unlike the zwitterionic functionalized SWNTs, end-capped SWNTs required the presence of surfactant in the solution to maintain a well-dispersed phase. In this case, 10 mg of SBDS was added into 40 mL of deionized water to create a 0.025 wt % SBDS solution. A certain amount of end-capped SWNTs, depending on the desired concentration of SWNTs in the membrane, was then dispersed in the SBDS solution by sonication. Using the identical fabrication method outline above, end-capped SWNTs were deposited and semi-aligned on a pretreated membrane support by filtration, followed with an interfacial polymerization of the polyamide carried out on the CNTs-attached support. After 5 min of oven curing, the fresh nanocomposite membrane was washed thoroughly with DI water, submersed in fresh DI water and stored in a laboratory refrigerator at 4 °C.

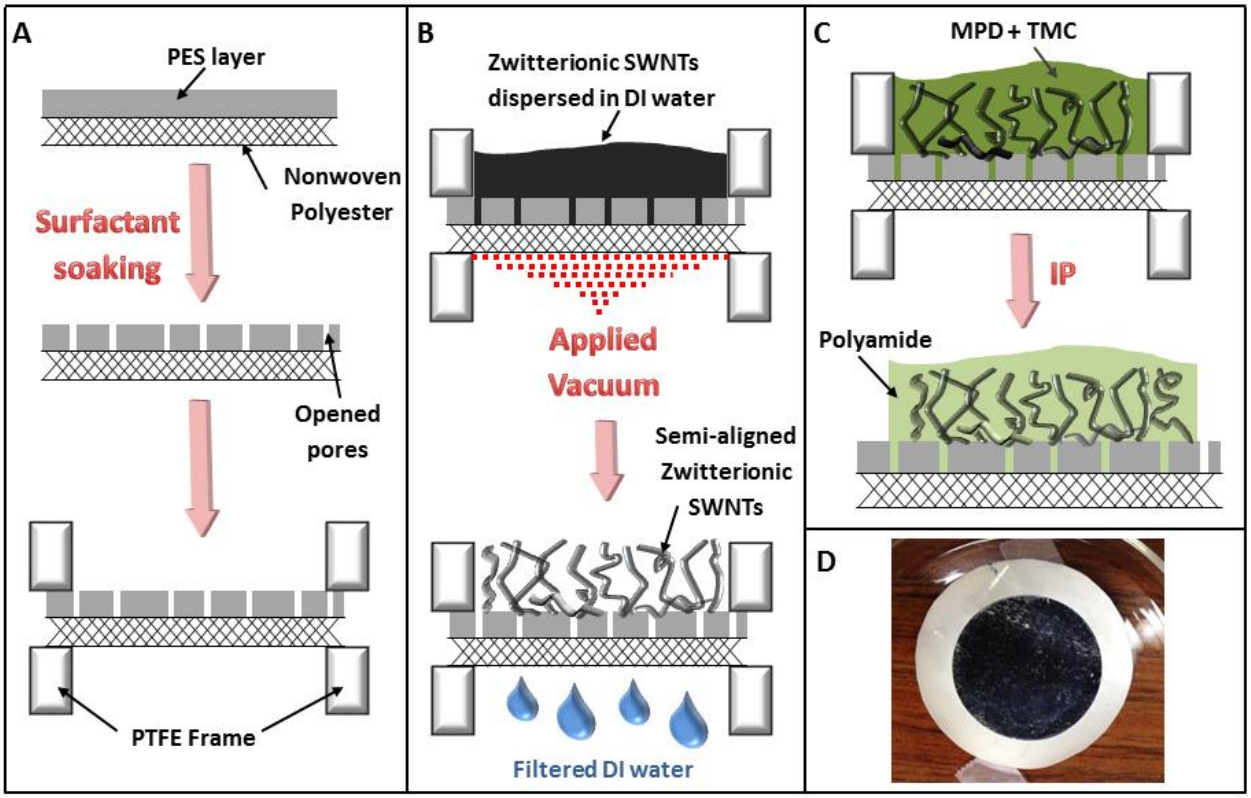


**Figure 4.2.** Cross-section schematics of the fabrication procedure for Z-SWNTs nanocomposite membrane. (A) PES ultrafiltration membrane, composed of a thin PES layer cast on a nonwoven polyester web, soaked in surfactant solution to cleanse the pores and to increase hydrophilicity. The membrane was then sandwiched by two round frames made out of PTFE. (B) Zwitterion functionalized SWNTs, deposited onto the pretreated PES support, through vacuum filtration. (C) Interfacial polymerization of polyamide carried out between functionalized CNTs at which MPD presented in the aqueous solution crosslinks with TMC in non-aqueous solution. (D) Photograph of the top of Z-SWNTs nanocomposite membrane that is exposed to the feed.

### 4.2.5. Membrane Characterization

The surfaces and cross-section of the membranes were characterized by field emission scanning electron microscopy (FESEM, LEO 1550). A small piece of fabric-free membrane sample was frozen in liquid nitrogen and fractured cryogenically. Pressure-driven experiments were carried out on a laboratory-scale cross-flow membrane test unit as shown schematically in Figure 4.3, capable of pressures from 25 to 1000 psi. This test unit is comprised of a stainless steel membrane cell, high pressure pump (Hydra-cell pump, Warner Engineering), back-pressure regulator (US Paraplate), bypass valve (Swagelock), feed water reservoir (Nalgene), operated in closed loop mode with retentate being circulated into the feed water reservoir. Feed solutions were kept between 25 to 30 °C. The ion concentration analysis of the permeant was measured by sodium

ion-selective electrode (Thermo Scientific; 8611NWP, MA) for sodium ion, and atomic adsorption spectrophotometry (AAS; Perkin Elmer 5100, Wellesley, MA) for other cations.

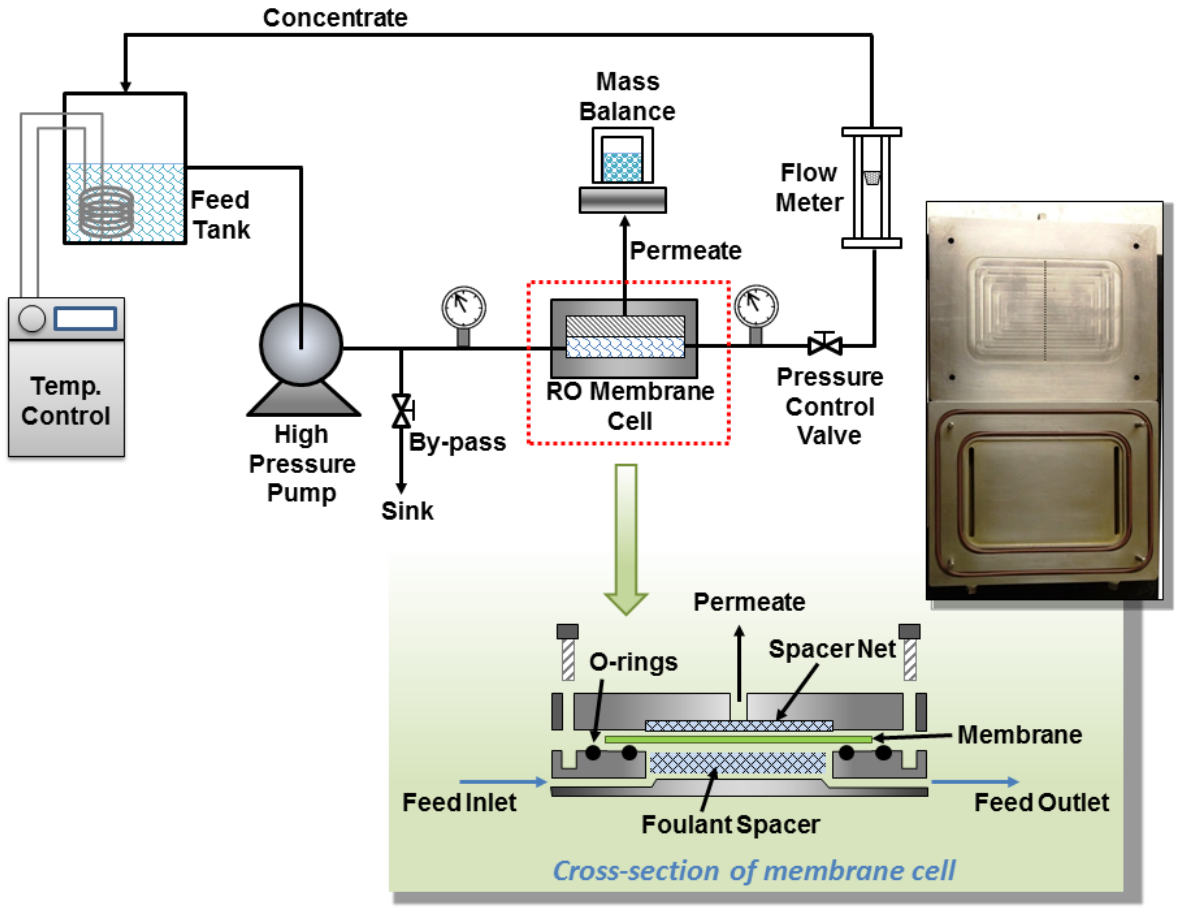


**Figure 4.3.** Schematic diagram of the RO membrane system and the cross-section of membrane test cell. The photograph on the right is the stainless stain cell, where the upper half is the permeation side and the lower part is the feed side.

### 4.2.6. Membrane Permeation Tests

The membrane cell was pressurized to the designated hydraulic pressure by adjusting the speed of the pump and the flow rate of the retentate. For each testing pressure the permeation flux was allowed to equilibrate for 30 min before any permeant collection. A known amount of permeant was collected in a glass vial within a given period of time. The density of water was taken to be 0.997 g/cm$^2$ at ambient temperature, the volumetric flow rate was calculated from $Q = \frac{\Delta V}{t \cdot A}$, where $\Delta V$ is the permeate volume (liter), $t$ is the permeation time (hour) and $A$ is the effective membrane area (m$^2$). The flow rate, $Q$, was recorded both in the units of liter per square meter per hour (LMH) and gallon per square foot per day (GFD). The sodium ion electrode was

calibrated using a standard solution with concentration of 1000 ± 5 ppm $Na^+$. The atomic absorption spectrophotometer (AAS) was calibrated using standard solutions, which contained 5, 10, 15 and 20 ppm of the specific cations. Thus, the concentrations of cations in the feed, $C_f$, and the permeant, $C_p$, were measured and the salt rejection ratio (in percent) was calculated from

$$\Re(\%) = \left(1 - \frac{C_p}{C_f}\right) \times 100 \qquad (4\text{-}1)$$

## 4.3. Results and Discussion

### 4.3.1. Flux and Rejection from Simulation Studies

Molecular simulations clearly show that zwitterion functionalized CNTs reject ions, while allowing an acceptable flux of water. The conductance of water and ions for NaCl solutions was calculated at a pressure drop of 208 MPa through pristine and functionalized CNTs. The large pressure drop used in this study improves the sampling statistics in the simulations, because the time scales accessible in simulations were only on the order of tens of nanoseconds. We note that extrapolation to lower pressure drops can be made since the flux of water has been shown to be a linear function of the pressure drop for both nanotubes[19] and for graphene nanopores.[38] The conductance of water and ions through CNTs as a function of simulation time is shown in Figure 4.4, where the linear increase in conductance with time indicates that the simulations are at steady state. We note from Figure 4.4 that as the number of zwitterion functional groups per tube increases, the conductance of both water and ions decreases. When each tube end was functionalized with two zwitterions, the conductance of ions decreased to zero while the flow rate of water was reduced, although its magnitude was still significant at about 100 water molecules per tube per nanosecond. The calculated ion rejection was 100% for the system with two zwitterions per tube end; no ions passed through the CNTs over a total simulation time of 8 ns. We have carried out simulations with 0.6 M KCl for the zwitterion functionalized CNTs and have found results very similar to those for NaCl. The diameter distribution of CNTs used in experiments ranges from 10 to 20 Å, with an average diameter of 15 Å. One or two zwitterions groups should be adequate to block all ion transport in CNTs having diameters less than 15 Å (vide supra).

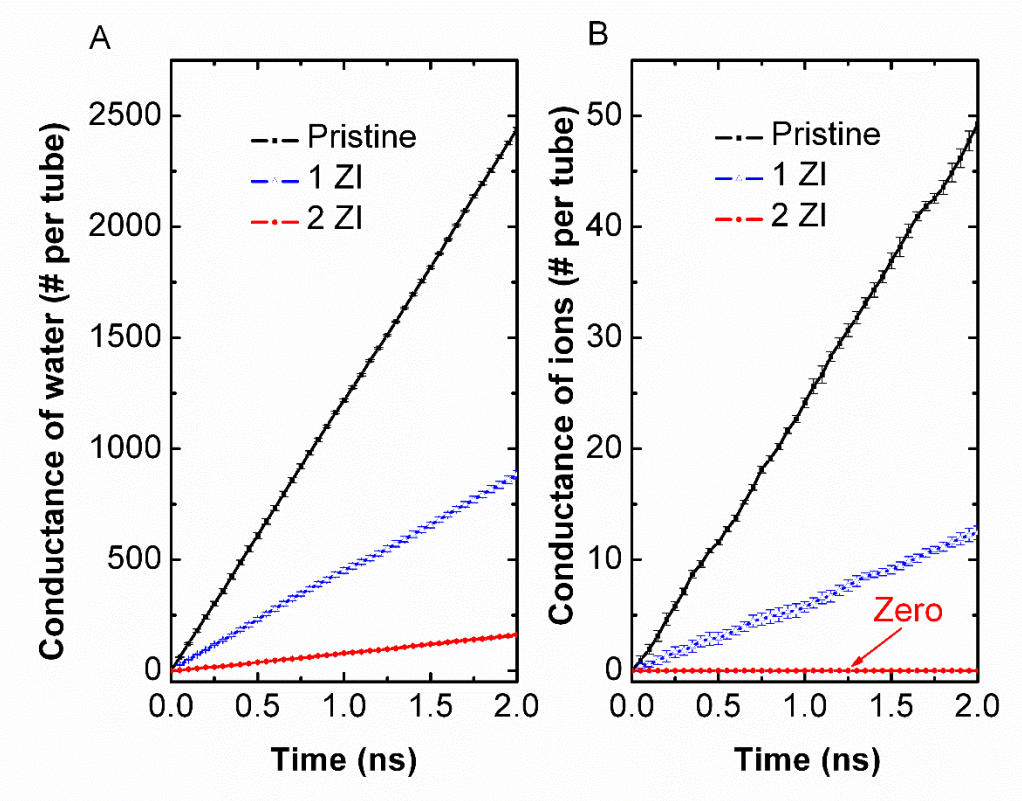


**Figure 4.4.** Conductance of (A) water and (B) ions per CNT (20,0) for pristine (non-functionalized) nanotubes (black line with solid square), CNTs with one zwitterion (1 ZI) at each end (blue line with empty triangle), and with two zwitterions (2 ZI) at each end (red line with solid circle) for a bulk concentration of 0.6 M NaCl and a pressure drop of 208 MPa. Error bars show the standard deviation based on four independent simulations

### 4.3.2. Membrane Microstructure

The surface morphologies of the PES support, PA and Z-SWNTs/PA nanocomposite membranes were studied using FESEM and images are shown in Figure 4.5, parts A, B, and C, respectively. The cross-sectional view of the Z-CNTs/PA membrane, also taken by FESEM, is shown in Figure 4.5(D). The neat PES support (A) has a relatively smooth and porous surface with pore sizes ranging approximately from 6 to 20 nm. After interfacial polymerization, a thin PA skin layer with ridge-valley shape was formed on the top of the PES substrate (B) and acted as a barrier layer in separating salt ions from water. In the Z-CNTs/PA nanocomposite membrane image (C), all the nanotubes are covered by interfacially polymerized PA. Due to the random packing of Z-CNTs, the surface roughness of the nanocomposite membrane is greatly increased relative to plain PA. The cross-section of the Z-CNTs/PA membrane (D) shows that nanotubes are embedded in

PA with semi-aligned orientation (examples indicated by arrows). The overall thickness of the nanocomposite layer is approximately 250 nm.

**(A)**

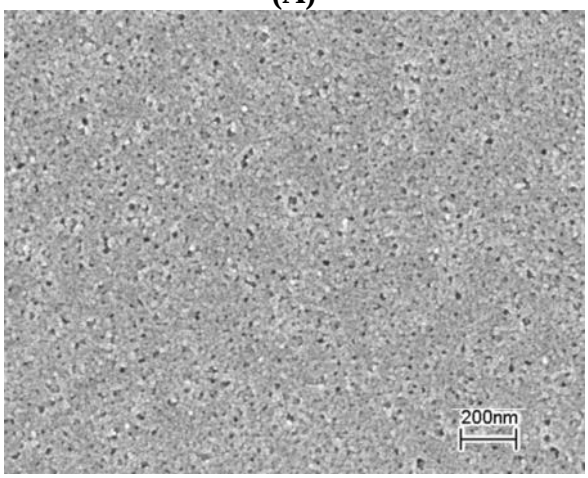


**(B)**

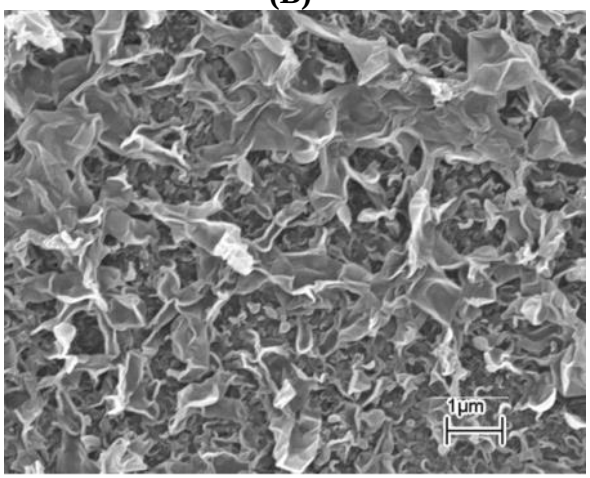


**(C)**

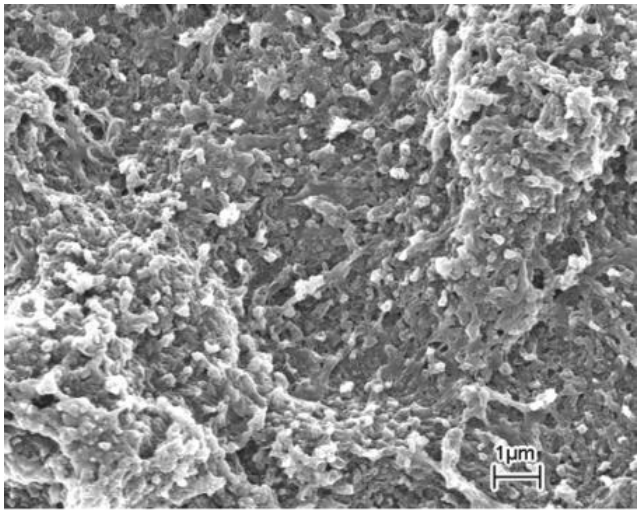


**(D)**

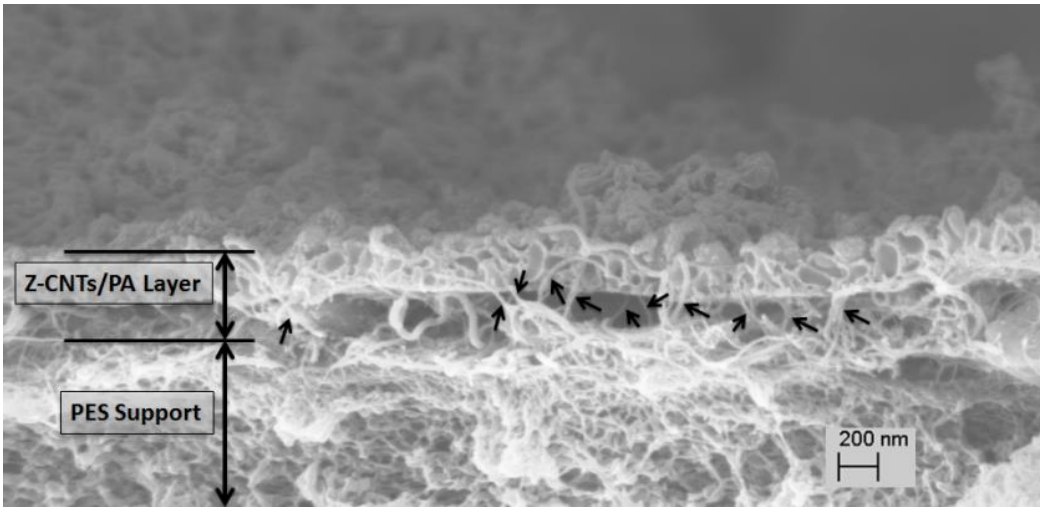

**Figure 4.5.** Field view of a Z-SWNTs emission scanning microscopy images of the PES support, plain PA and Z-SWNTs/PA membranes. The surface morphologies of (A) PES support, (B) PA and (C) Z-SWNTs/PA. (D) shows the cross-sectional /PA membrane.

### 4.3.3. Effect of Z-SWNTs to Water Flux and Ion Rejection

Three polyamide (PA) membranes were fabricated with 0 (0 wt %), 0.25 (9 wt %) and 0.75 (20 wt %) mg of zwitterion functionalized SWNTs deposited in a plain PA matrix with total area of 17.35 $cm^2$. As a control, a fourth nanocomposite membrane containing 20 wt % end-capped SWNTs was also fabricated. The area of each PA membrane that contained the CNTs was 10.75 $cm^2$ and was located in the center of the PA membrane. The weight percentage reflects the percentage of CNTs in the selective PA layer. These membranes were tested for water and ion flux by using a pressure drop of 3.65 MPa (530 psi) with a feed solution containing 1000 ppm of $Na^+$ (or ~2500 ppm NaCl or 43.5 mM). The transport results are shown in Figure 4.6. Adding 0.25 mg CNTs to the PA membrane resulted in the water flux increasing more than 2-fold, from 11.6 LMH (liters per square meter per hour) to 23.9 LMH, while the rejection of NaCl increased by approximately 1% from 97.6% to 98.5%. Increasing the amount of CNTs to 0.75 mg, the water flux increased by about a factor of 4 (to 48.6 LMH) over the plain PA membrane and the ion rejection remained about constant at 98.6%. Figure 4.6 also shows that a significant increase in flux was achieved when 20 wt% end-capped SWNYs were incorporated into the polyamide matrix. However, this increase in water flux was accompanied by a significant drop in salt rejection down to 93%, which is lower than the salt rejection of the neat polyamide membrane.

Each membrane was tested for three consecutive days to examine the membrane stability. All membranes showed stable performance with <1% variability over three days. We note that commercial PA membranes have significantly better performance than our membranes due to differences in the synthetic procedure.[37] Our purpose at this time is not to produce an optimized PA membrane, but rather show that PA membranes can be significantly improved by the addition of functionalized CNTs. Because there is no trade-off between selectivity and permeability, the experimental results suggest that the functionalized CNTs impart an additional transport mechanism to the membrane.

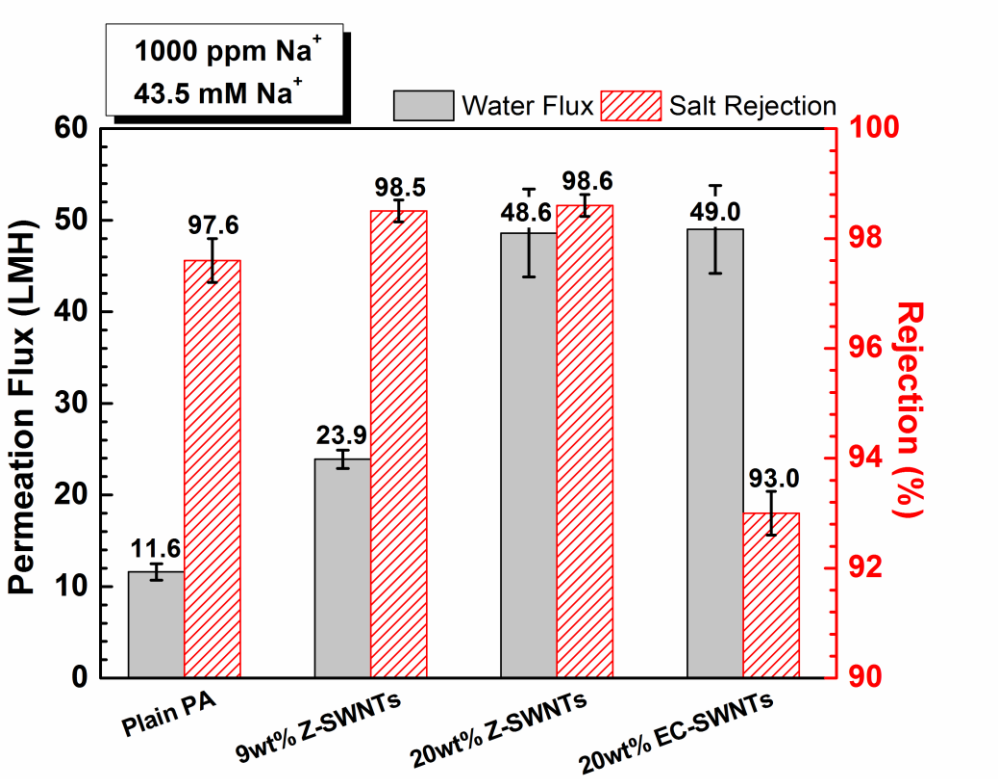


**Figure 4.6.** Water flux (solid) and salt rejection (hatched) as a function of CNT concentration in the selective PA layer of the nanocomposite membrane. The concentrations of zwitterions functionalized single-walled CNTs (Z-SWNTs) are 0 wt% (0 mg), 9wt% (0.25mg) and 20 wt% (0.75 mg), respectively. The concentration of end-capped single-walled CNTs (EC-SWNTs) is 20wt%. The concentration of $Na^+$ is 1000 ppm (43.5 mM NaCl). Pressure of 530 psi was applied for each membrane test. Error bars were computed from the standard deviations of the fluxes over a three day period.

We hypothesize that this mechanism consists of fast fluid flow through the functionalized CNTs, whose zwitterionic groups block the entry of ionic species into the CNT pores, thereby enhancing (or at least preserving) the salt rejection. Increasing the concentration of CNTs provided more channels for the transport of water through the PA membrane, while ions were still blocked due to the zwitterionic groups attached at tube ends. We note that the CNTs are entirely embedded within the PA membrane and are not completely aligned within the PA. This means that there is considerable room for improvement in the synthesis of the composite membrane. An ideal membrane would have CNTs perfectly aligned with the direction of fluid flow and would percolate completely through the membrane, so that no fluid would have to permeate through the polymer. Our membranes are far from optimal by this measure, but they do provide a proof of concept that functionalized CNTs can enhance both water flux and salt rejection.

The fact that the water flux of the end-capped CNT composite membrane also increases significantly in comparison to the neat polyamide membrane suggests the formation of nanoscaled voids at the interface between the carbon nanotubes and the polymer matrix, at least for the pristine CNTs. These nanochannels allow water and salt ion molecules to travel through the membrane close to the external surface of the CNTs at faster rates than across the polyamide thin layer, leading to a higher water flux but lower selectivity for water/salt ion. It is possible that these nanochannels also exist in the case of the zwitterion-functionalized CNT composite membranes. Since the zwitterionic functional groups are attached not only at the pore entrance of the carbon nanotubes, but also along the wall of SWNTs, they can reject salt ions by size exclusion and Donnan exclusion at the entrance as well as inside the nanochannels. Therefore, it is possible that water molecules travel both inside the SWNTs and around them in the nanochannels. In the case of functionalized carbon nanotubes, both of the paths could be blocked by the zwitterionic groups, which offer good water/ions selectivity. An alternate scenario is that the end-capped CNTs induce voids in the PA membrane while the zwitterion-functionalized CNTs do not. This is based on the following differences between the end-capped and zwitterion-functionalized CNTs: (1) The end-capped CNTs are about a factor of 5 longer than the zwitterion-functionalized tubes, the former being as long as 5 μm, while the latter are about 1 μm in length.[31] It is reasonable to assume that these very long CNTs will disrupt the PA membrane structure to a much larger degree than the shorter CNTs. (2) The end-capped CNTs likely have pristine surfaces with very few functional groups covalently bound to them. In contrast, we estimate that each zwitterion functionalized CNT will have about $6.4\times10^3$ zwitterions or an average of about one zwitterion for every 30 carbon atoms on the CNT (See Appendix information). This means that most of the zwitterions will be bound to and distributed along the sidewalls of the CNTs because the ends can only accommodate a small number of functional groups. For example, a (20,0) CNT could have a maximum of 20 zwitterions on each end. Hence, the interfacial surface energies of the end-capped and zwitterion-functionalized CNTs will be very different. We assume that the zwitterions will impart a greater degree of compatibility with the PA; hence, there may not be voids around the zwitterion-functionalized CNTs. This hypothesis is consistent with experiments showing that the pristine end-capped CNTs required the addition of surfactant to be dispersed in the PA, while the zwitterion functionalized CNTs were dispersible in the absence of surfactant (see Section 4.2.4).

### 4.3.4. Salt Concentration Effects

We have studied the effect of salt concentration on the ion rejection from both simulations and experiments. Johnson's group studied the system with one zwitterion group per tube in simulations because two zwitterions per tube end showed total rejection, dominated by steric effects (Figure 4.6), and would therefore be less sensitive to changes in ion concentration. Flux simulations was carried out for 0.6 and 0.3 M NaCl and KCl solutions (35000 and 17500 ppm for NaCl, 44700 and 22350 ppm for KCl), both with a pressure drop of 208 MPa. The simulations was run for 36 ns in order to gather accurate statistics for the ion rejection as a function of concentration. The results are given in Table 4.1. The simulations indicate that the salt concentration has no effect on the ion rejection, at least for concentrations in the range 0.3 to 0.6 M. Simulations at much lower concentrations, as those used in experiments, were not feasible because of the low flux of ions and resulting poor statistics.

**Table 4.1.** Water and ion flow rate (number per ns per CNT) and ion rejection as a function of salt concentration for flow through a (20,0) CNT having one zwitterion functional group at each end.

| Concentration | Cation conductance | Anion conductance | Total ion conductance | Water conductance | Ion rejection |
|---|---|---|---|---|---|
| 0.6 M NaCl | 3.8 ± 0.2 | 3.6 ± 0.1 | 7.4 ± 0.2 | 460.0 ± 10.7 | 24.7 % ± 4.3 % |
| 0.3 M NaCl | 2.1 ± 0.2 | 1.9 ± 0.2 | 3.9 ± 0.4 | 500.3 ± 20.3 | 27.4 % ± 9.2 % |
| 0.6 M KCl | 2.7 ± 0.2 | 3.0 ± 0.4 | 5.7 ± 0.6 | 489.9 ± 6.3 | 45.3 % ± 6.3 % |
| 0.3 M KCl | 1.3 ± 0.1 | 1.7 ± 0.2 | 3.0 ± 0.2 | 520.4 ± 10.1 | 45.9 ± 5.4 % |

The concentration of $Na^+$ in experiments was varied between 50 and 2000 ppm (2.2–43.5 mM) to test for ion concentration effects. We performed experiments with both the plain PA membrane (no CNTs) and the nanocomposite membrane with 20 wt % CNTs in order to test for differences in concentration dependence inherent in the PA membrane as opposed to the functionalized CNTs. The results of these experiments, plotted in Figure 4.7, show an increase in the salt rejection with ion concentration for both the plain PA membrane and the nanocomposite membrane with 20 wt% CNTs.

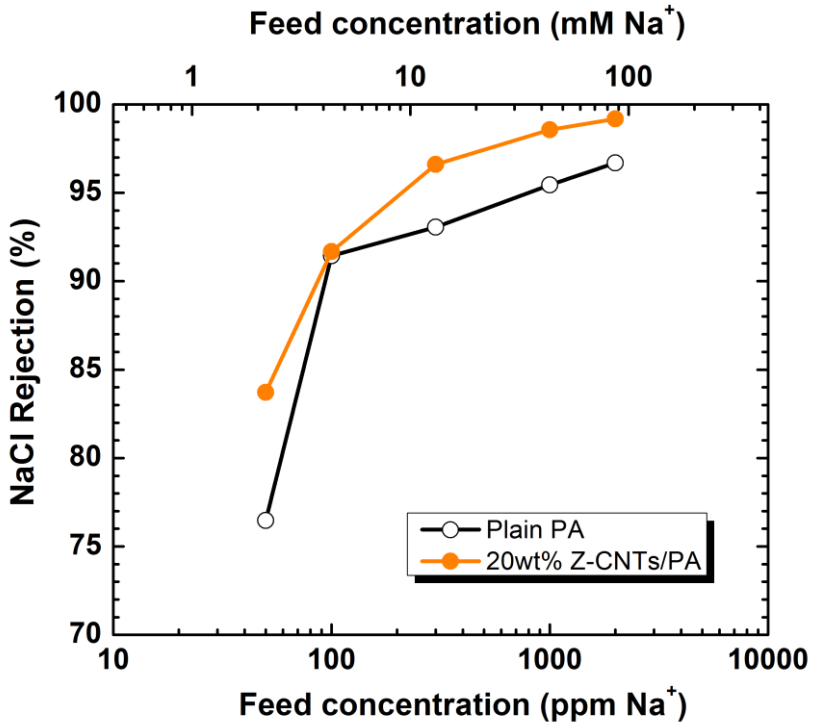


**Figure 4.7.** Salt rejection as a function of NaCl feed concentration in plain PA (black curve with open circle) and a nanocomposite membrane with 20wt% Z-SWNTs (orange curve with solid circle). Feed pressure was 3.65 Mpa (530 psi).

The increase in rejection with increasing ion concentration is an unexpected result; indeed, the opposite effect was observed by Fornasiero *et al.*[23], who found that the ion rejection decreased with increasing ion concentration in the feed, and dropped to zero when the ion concentration was equal to 10 mM for KCl. The difference in the performance between their membranes and ours is due to the mode of ion rejection. Fornasiero *et al*. used negatively charged CNTs membranes, which rejected ions in accordance with the Donnan equilibrium theory. Many nanofiltration membranes are negatively charged and exhibit electrostatic screening effects.[39–41] Therefore, ion rejection is sensitive to salt concentrations in charged membranes. In contrast, Ji *et al.*[42] showed that addition of zwitterionic groups counteracts the effects of ion concentration. They demonstrated that the ion rejection decreased from 96.5 to 65% as salt concentration was increased from 100 to 3500 ppm $MgCl_2$ for a membrane without zwitterions. However, the addition of zwitterion groups to the membrane gave very stable rejection ratios that were independent of salt concentration.[42] Note that our plain PA membrane, which is uncharged inside the pores, exhibits an increase in the rejection with increasing concentration of NaCl (over a narrow range of concentrations). This same trend has been observed for other PA-type membranes.[43,44] We

therefore attribute the increase in salt rejection with increasing NaCl concentration observed for the nanocomposite membrane in Figure 4.7 to both the PA component and zwitterion functional groups on the CNTs. This agrees with molecular simulations done by Dr. Johnson's group,[1] showing no effect of concentration on the rejection ratio of Z-SWNTs.

## 4.4. Conclusions

We have shown that zwitterion functionalized CNTs can be embedded in a PA membrane and that the performance of the nanocomposite membrane increases as the fraction of CNTs is increased. The water flux increases significantly and the ion rejection increases or remains about the same, indicating that the increased water flux is not due to an increase in nonspecific pores in the membrane, but rather due to an additional transport mechanism resulting from the presence of the functionalized CNTs. Molecular simulations show that the addition of only two zwitterions per nanotube end results in complete rejection of ions, while allowing significant water flux for nanotubes with diameters the same as those used in the experiments. The nanocomposite membrane did not experience any electrostatic screening effect, which confirmed that the ion separation mechanism is dominated by size exclusion instead of charge repulsion as is predicted by corresponding MD simulation studies. Assuming a membrane containing 20 wt % CNTs, having lengths of 1 μm, and assuming all CNTs are perfectly aligned (which is not the case in our experiments), we estimate a flux of 34,000 LMH for a membrane with a pressure drop of 530 psi (see Appendix). This is 3 orders of magnitude greater than our experimentally observed flow rate of 48.6 LMH, indicating that there is ample opportunity to optimize this first-generation membrane.

## References


(1) Chan, W.-F.; Chen, H.; Surapathi, A.; Taylor, M. G.; Shao, X.; Marand, E.; Johnson, J. K. Zwitterion Functionalized Carbon Nanotube/polyamide Nanocomposite Membranes for Water Desalination. *ACS Nano* **2013**, *7*, 5308–5319.

(2) UNDCWS. The 2030 Water Resources Group Annual Report. **2015**.

(3) Gleick, P. H. Water Resources. In Encyclopedia of Climate and Weather Schneider, S. H., Ed. *Oxford University Press: New York* **1996**, *2*, 817–823.

(4) Lee, K. P.; Arnot, T. C.; Mattia, D. A Review of Reverse Osmosis Membrane Materials for desalination—Development to Date and Future Potential. *Journal of Membrane Science* **2011**, *370*, 1–22.

(5) Holt, J. K.; Park, H. G.; Wang, Y.; Stadermann, M.; Artyukhin, A. B.; Grigoropoulos, C. P.; Noy, A.; Bakajin, O. Fast Mass Transport through Sub-2-Nanometer Carbon Nanotubes. *Science (New York, N.Y.)* **2006**, *312*, 1034–1037.

(6) Kim, S.; Chen, L.; Johnson, J. K.; Marand, E. Polysulfone and Functionalized Carbon Nanotube Mixed Matrix Membranes for Gas Separation: Theory and Experiment. *Journal of Membrane Science* **2007**, *294*, 147–158.

(7) Kim, S.; Jinschek, J. R.; Chen, H.; Sholl, D. S.; Marand, E. Scalable Fabrication of Carbon Nanotube/Polymer Nanocomposite Membranes for High Flux Gas Transport. *Nano Letters* **2007**, *7*, 2806–2811.

(8) Majumder, M.; Chopra, N.; Hinds, B. J. Effect of Tip Functionalization on Transport through Vertically Oriented Carbon Nanotube Membranes. *Journal of the American Chemical Society* **2005**, *127*, 9062–9070.

(9) Skoulidas, A. I.; Ackerman, D. M.; Johnson, J. K.; Sholl, D. S. Rapid Transport of Gases in Carbon Nanotubes. *Physical Review Letters* **2002**, *89*, 185901.

(10) Skoulidas, A. I.; Sholl, D. S.; Johnson, J. K. Adsorption and Diffusion of Carbon Dioxide and Nitrogen through Single-Walled Carbon Nanotube Membranes. *The Journal of chemical physics* **2006**, *124*, 054708.

(11) Surapathi, A.; Herrera-Alonso, J.; Rabie, F.; Martin, S.; Marand, E. Fabrication and Gas Transport Properties of SWNT/polyacrylic Nanocomposite Membranes. *Journal of Membrane Science* **2011**, *375*, 150–156.

(12) Majumder, M.; Chopra, N.; Hinds, B. J. Mass Transport through Carbon Nanotube Membranes in Three Different Regimes: Ionic Diffusion and Gas and Liquid Flow. *ACS nano* **2011**, *5*, 3867–3877.

(13) Holt, J. K. Carbon Nanotubes and Nanofluidic Transport. *Advanced Materials* **2009**, *21*, 3542–3550.

(14) Holt, J. K.; Noy, A.; Huser, T.; Eaglesham, D.; Bakajin, O. Fabrication of a Carbon Nanotube-Embedded Silicon Nitride Membrane for Studies of Nanometer-Scale Mass Transport. *Nano Letters* **2004**, *4*, 2245–2250.

(15) Skoulidas, A. I.; Sholl, D. S. Transport Diffusivities of CH4, CF4, He, Ne, Ar, Xe, and SF6 in Silicalite from Atomistic Simulations. *The Journal of Physical Chemistry B* **2002**, *106*, 5058–5067.

(16) Kalra, A.; Garde, S.; Hummer, G. Osmotic Water Transport through Carbon Nanotube Membranes. *Proceedings of the National Academy of Sciences of the United States of America* **2003**, *100*, 10175–10180.

(17) Thomas, J.; McGaughey, A. Water Flow in Carbon Nanotubes: Transition to Subcontinuum Transport. *Physical Review Letters* **2009**, *102*, 184502.

(18) Thomas, J.; McGaughey, A. Reassessing Fast Water Transport through Carbon Nanotubes. *Nano letters* **2008**.

(19) Corry, B. Designing Carbon Nanotube Membranes for Efficient Water Desalination. *Journal of Physical Chemistry B* **2008**, *112*, 1427–1434.

(20) Yu, M.; Funke, H. H.; Falconer, J. L.; Noble, R. D. Gated Ion Transport through Dense Carbon Nanotube Membranes. *Journal of the American Chemical Society* **2010**, *132*, 8285–8290.

(21) Qiang, L. Creating the Narrowest Carbon Nanotubes. *Nature* **2000**.

(22) Hinds, B. J.; Chopra, N.; Rantell, T.; Andrews, R.; Gavalas, V.; Bachas, L. G. Aligned Multiwalled Carbon Nanotube Membranes. *Science (New York, N.Y.)* **2004**, *303*, 62–65.

(23) Fornasiero, F.; Park, H. G.; Holt, J. K.; Stadermann, M.; Grigoropoulos, C. P.; Noy, A.;

Bakajin, O. Ion Exclusion by Sub-2-Nm Carbon Nanotube Pores. *Proceedings of the National Academy of Sciences of the United States of America* **2008**, *105*, 17250–17255.

(24) Corry, B. Water and Ion Transport through Functionalised Carbon Nanotubes: Implications for Desalination Technology. *Energy & Environmental Science* **2011**, *4*, 751.

(25) Cheng, G.; Li, G.; Xue, H.; Chen, S.; Bryers, J. D.; Jiang, S. Zwitterionic Carboxybetaine Polymer Surfaces and Their Resistance to Long-Term Biofilm Formation. *Biomaterials* **2009**, *30*, 5234–5240.

(26) Ladd, J.; Zhang, Z.; Chen, S.; Hower, J. C.; Jiang, S. Zwitterionic Polymers Exhibiting High Resistance to Nonspecific Protein Adsorption from Human Serum and Plasma. *Biomacromolecules* **2008**, *9*, 1357–1361.

(27) Li, G.; Cheng, G.; Xue, H.; Chen, S.; Zhang, F.; Jiang, S. Ultra Low Fouling Zwitterionic Polymers with a Biomimetic Adhesive Group. *Biomaterials* **2008**, *29*, 4592–4597.

(28) Surapathi, A.; Chen, H.; Marand, E.; Karl Johnson, J.; Sedlakova, Z. Gas Sorption Properties of Zwitterion-Functionalized Carbon Nanotubes. *Journal of Membrane Science* **2013**, *429*, 88–94.

(29) Plimpton, S. Fast Parallel Algorithms for Short – Range Molecular Dynamics. *J. Comput. Phys.* **1995**, *117*, 1–19.

(30) Zhu, F. Q.; Tajkhorshid, E.; Schulten, K. Pressure-Induced Water Transport in Membrane Channels Studied by Molecular Dynamics. **2002**, *83*, 154–160.

(31) Nano Lab Inc.,179 Bear Hill Road, Waltham, MA 02451.

(32) Zhang, Z.; Chen, S.; Jiang, S. Dual-Functional Biomimetic Materials: Nonfouling Poly(carboxybetaine) with Active Functional Groups for Protein Immobilization. *Biomacromolecules* **2006**, *7*, 3311–3315.

(33) Surapathi, A.; Chen, H.; Marand, E.; Karl Johnson, J.; Sedlakova, Z. Gas Sorption Properties of Zwitterion-Functionalized Carbon Nanotubes. *Journal of Membrane Science* **2013**, *429*, 88–94.

(34) Ghosh, A. K.; Hoek, E. M. V. Impacts of Support Membrane Structure and Chemistry on Polyamide–polysulfone Interfacial Composite Membranes. *Journal of Membrane Science* **2009**, *336*, 140–148.

(35) Saha, N. K.; Joshi, S. V. Performance Evaluation of Thin Film Composite Polyamide Nanofiltration Membrane with Variation in Monomer Type. *Journal of Membrane Science* **2009**, *342*, 60–69.

(36) Kong, C.; Kanezashi, M.; Yamomoto, T.; Shintani, T.; Tsuru, T. Controlled Synthesis of High Performance Polyamide Membrane with Thin Dense Layer for Water Desalination. *Journal of Membrane Science* **2010**, *362*, 76–80.

(37) Xie, W.; Geise, G. M.; Freeman, B. D.; Lee, H.-S.; Byun, G.; McGrath, J. E. Polyamide Interfacial Composite Membranes Prepared from M-Phenylene Diamine, Trimesoyl Chloride and a New Disulfonated Diamine. *Journal of Membrane Science* **2012**.

(38) Cohen-Tanugi, D.; Grossman, J. C. Water Desalination across Nanoporous Graphene. *Nano letters* **2012**, *12*, 3602–3608.

(39) Bellona, C.; Drewes, J.; Xu, P.; Amy, G. Factors Affecting the Rejection of Organic Solutes during NF/RO Treatment—a Literature Review. *Water Research* **2004**.

(40) Chung, C.; Buu, N.; Chau, N. Influence of Surface Charge and Solution pH on the Performance Characteristics of a Nanofiltration Membrane. *Science and Technology of*

*Advanced …* **2005**.

(41) Peeters, J.; Boom, J. Retention Measurements of Nanofiltration Membranes with Electrolyte Solutions. *Journal of Membrane …* **1998**.

(42) Ji, Y.-L.; An, Q.-F.; Zhao, Q.; Sun, W.-D.; Lee, K.-R.; Chen, H.-L.; Gao, C.-J. Novel Composite Nanofiltration Membranes Containing Zwitterions with High Permeate Flux and Improved Anti-Fouling Performance. *Journal of Membrane Science* **2012**, *390-391*, 243–253.

(43) Yu, S.; Liu, M.; Lü, Z.; Zhou, Y.; Gao, C. Aromatic-Cycloaliphatic Polyamide Thin-Film Composite Membrane with Improved Chlorine Resistance Prepared from M-Phenylenediamine-4-Methyl and Cyclohexane-1,3,5-Tricarbonyl Chloride. *Journal of Membrane Science* **2009**, *344*, 155–164.

(44) Bandini, S.; Drei, J.; Vezzani, D. The Role of pH and Concentration on the Ion Rejection in Polyamide Nanofiltration Membranes. *Journal of Membrane Science* **2005**, *264*, 65–74.

# Chapter 5. Novel Zwitterion Functionalized Carbon Nanotube Nanocomposite Membranes for Improved RO performance and Surface Anti-Biofouling Resistance

The contents of this chapter have been submitted for publication to the Journal of Membrane Science: W.-F. Chan, E. Marand and Stephen Martin, *Novel Zwitterion Functionalized CNT Nanocomposite Membrane for Improved RO performance and Surface Anti-Biofouling Resistance*.

## 5.1. Introduction

The demand for fresh water is rising globally and the trend has accelerated continuously in the past decade accompanied with population overgrowth, rapid industrialization in developing countries, contamination of available water resources, and climate change.[1] However, the supply for fresh water is not sustainable with current global development, and more than one-third of the world's population is currently living in water-stressed countries.[2] Reverse osmosis (RO) is the leading desalination technique and can alleviate global water scarcity by retrieving high quality of fresh water from non-drinkable water resources (i.e. sea, brackish and waste water).[3] Desalination by RO is expected to reach 38 billion $m^3$ per year by 2016,[2] which is nearly 1% of global fresh water consumption. Aromatic polyamide (PA) based thin film composite membranes (TFC) are the main type RO membranes currently in use.[4–6] Many recent studies have focused on modifying TFC membranes to achieve high energy-efficiency, ultra-low surface fouling and robustness against chemical attack. While industries have developed different types of membrane materials to target these problems separately, nanotechnology provides a new route to address the issues at the same time. By building novel membranes with either internal nano-structures (i.e. nanopores) or incorporation of nanoparticles or nanotubes, size sieving can be achieved down to sub-nanometer scales, and can render membranes resistant to reactive chemicals and surface protein adsorption.[7–10]

Among the choices of nanomaterials, carbon nanotubes (CNT) show promising results as building blocks for nano-engineered membranes. Molecular simulations and experimental studies have shown that the transport of fluid through CNT is orders of magnitude faster than through other nanoporous materials due to the unprecedented atomic smoothness and regularity of the CNT pores.[11–13] Molecular dynamics (MD) simulation studies[14,15] have examined water and ion transport through CNTs with a range of pore sizes (diameters) through which water passes rapidly but ions do not. These studies demonstrate that the degree of selectivity towards different ion types

varies with pore radius, and pores of radius ranging from 3.4 to 6.1 Å exhibit rejection of even monovalent ions. CNTs with functional groups attached at both ends were also explored computationally and exhibited outstanding filtration ability.[16] Tip functional groups reduce the CNTs' effective pore size, granting separation ability to CNTs with larger diameters, potentially decreasing materials costs. Functional groups improve dispersion and the compatibility of CNTs in composite materials and minimizes defects during membrane synthesis.[17–19] Membranes with vertically-aligned CNTs (VACNT) embedded in a polymer composite were synthesized experimentally, with inner diameters ranging from 1.6 to 10 nm.[10,11,20,21] As expected, liquid flow through the non-interacting hydrophobic cores of the CNT is found to be significantly enhanced, with velocities at least 1000 times faster than that predicted by conventional no-slip hydrodynamic theory.[13,22] The ion rejection in these membranes, however, is often provided by the functional groups attached at the CNTs' opening rather than sieving by the size of the CNT pores. Fornasiero *et al.* studied ion exclusion in CNTs functionalized with hydroxyl, carbonyl and carboxylic groups,[10] and their results demonstrated that rejection was dominated by electrostatic interactions between the fixed $COO^-$ charges on the ends of CNTs and the co-ions in the feed. This is a Donnan-type exclusion mechanism and is subject to electrostatic screening effects at higher electrolyte concentrations, leading to a total loss of rejection ability. In addition, the fabrication of CNT-based nanocomposite membranes often involves sophisticated in-situ processes like surface etching[11] which is not easily scalable for large scale manufacturing.

Thin-film-nanocomposite (TFN) membranes employ a different approach to building novel RO membranes. Nanomaterials such as zeolite, silver and titanium oxide particles, silica and CNTs with excellent properties (e.g., super-hydrophilicity, fast water transport, biocide) are directly blended in the PA skin layer and dispersed within the polymer matrix to enhance membrane permselectivity or introduce new properties.[9,17,18,23–27] Many researchers reported improved performance (Table 5.1) in terms of water permeation flux and fouling resistance, but the degree of crosslinking of the polymer skin layer is reduced during the process, leading to a decrease in selectivity and mechanical stability. As shown in Figure 5.1 and Figure **5.2**, all-aromatic polyamides are chemically crosslinked to form rigid chains with self-assembled networks of pores for water uptake and transport.[28] When nanomaterials, illustrated as spheres A and B in Figure 5.2, are present during the polymerization, part of the crosslink network is disrupted when polymer end groups were prevented from reacting with other monomers and were terminated with

carboxylic acid groups. When crosslinking is possible by detouring around the nanomaterials, the rigid aromatic backbones in PA restrict the segmental motion of chains. The lack of chain rotation results in nanosized defects (shown as blue ovals) around the sphere surface and also lowers the selectivity. Nanomaterials that are incompatible with polyamide (sphere B) open up larger defects and destroy the stability of the layer. A performance comparison can be seen in Table 5.1. Ordinary PA membranes exhibit salt rejections as high as 99.8%, but all the reported TFN membranes fall below this value. All the PA fabrication methods shown in the table use the same monomeric aromatic amines and crosslinking agent, with different recipes in terms of pH in monomer solution, cure temperature, crosslinking time, etc. Kim *et al.* demonstrated the impact of the interaction between nanomaterials and the PA on the membrane selectivity.[18] Functionalized CNTs with higher interaction forces with Atomic Force Microscopy (AFM) tips coated with PA film exhibited improved water flux and salt rejection when added into the PA layer, when compared to other types of CNT with lower interaction forces.

**Table 5.1.** Research studies on thin film nanocomposite membranes using different nanomaterials.

| **Nanomaterials** | **Applied Pressure (MPa)** | **Permeation Flux ($L/(m^2 h)$)** | **Rejection (%)** | **Advantages** |
|---|---|---|---|---|
| No additive [29] | 1.55 | 43.0 | 99.8 | |
| Multi-walled CNT; ~8nm inner diameter [30] | 0.69 | 22.0 | 92.1 | • Applied potential significantly increases fouling resistance<br>• 1 min-flushing can recover almost 92% of flux. |
| Zeolite A nanoparticles [31] | 1.24 | 16.5 | 91.2 | • Increases surface hydrophilicity<br>• Improves water permeability, solute rejection and fouling resistance. |
| Linde type A (LTA) zeolite nanocrystals [32] | 1.55 | 108.8 | 90 | • Reduces polymer cross-linking<br>• Microporous defects were observed |
| Titanium Oxide ($TiO_2$) [33] | 0.60 | 9.1 | 95[l] | • Enhances hydrophilicity; higher water flux |
| Silver Nanoparticles [9] | 1.38 | 90 | 96.5[l] | • Colonies of Pseudomonas on membrane surface were almost all dead. |
| Polyhedral Oligomeric Silsequioxane (POSS) [34] | 1.55 | 27.5 | ~98 | • Acts as cross-linkers and increases free volume of the PA film, which thus increases permeation. |

[l] Salt in the feed solution is magnesium chloride ($MgCl_2$)

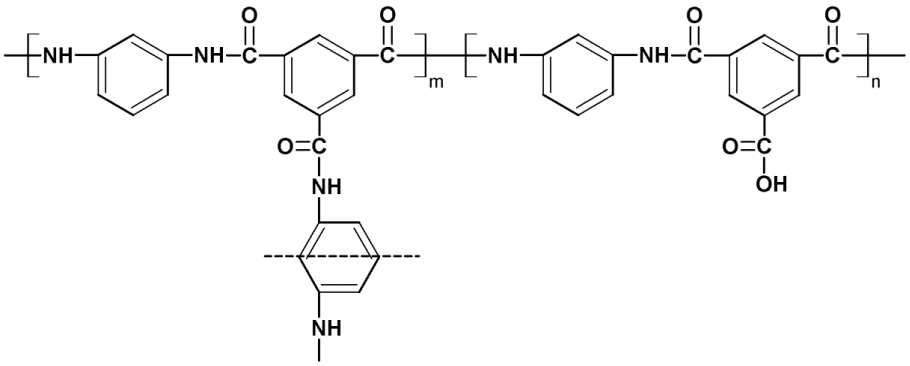

**Figure 5.1.** Polymer structure of all-aromatic polyamide in thin-film composite RO membrane.

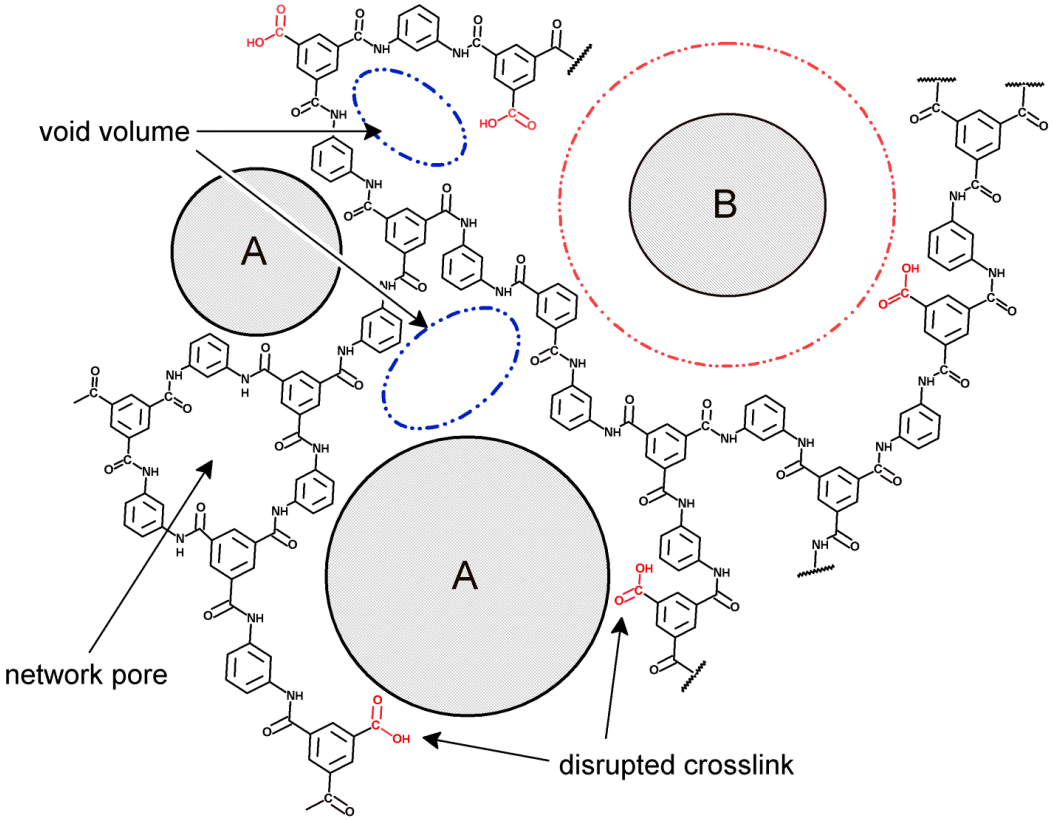


**Figure 5.2.** Schematic illustrates the disruption of PA chains in TFN membranes when nanomaterials (sphere A and B) present in the skin layer. Sphere A is chemically compatible to PA but B is not due to poor interfacial interaction. The red circle represents the closest distance PA chains can be around sphere B.

A thin, durable and scalable nanocomposite membrane with properties that can operate at high salt concentration is highly desirable. Previous work in our laboratory has focused on using zwitterion-functionalized single-walled CNTs (Z-SWNT) as the nanomaterial in fabricating TFN membranes.[17] The alternation of charges in the zwitterion results in a very strong dipole moment,

which greatly enhances the interaction between the Z-SWNT and the PA matrix. Moreover, zwitterion-treated surfaces have also shown good resistance to protein adhesion in several studies.[35–37] MD simulations have predicted that CNTs having a diameter of 1.5 nm with two or more zwitterionic groups attached at both ends reject salt ions completely.[17] We have previously reported the synthesis of PA membranes embedded with a high weight percentage of partially-aligned Z-SWNT.[17] These membranes exhibited significant improvements in water permeation and similar or improved salt rejection as the weight percentage of the nanotubes in the membrane increased. Both simulation and experiment suggested that the zwitterionic groups act as a gatekeeper at the entrance of the CNTs, rejecting ions via steric effects instead of charge repulsion. Herein we report on the impact of chemical structure, surface morphology, and separation mechanism on the performance of Z-SWNT/PA TFN membranes. We also report on improved resistance to surface biofouling in the TFN membranes due to the incorporation of Z-SWNTs.

## 5.2. Materials and Methods

### 5.2.1. Materials

The following chemicals were purchased from Sigma-Aldrich (St. Louis, MO): 1,3,5-benzenetricarbonyl trichloride (trimesoyl chloride, TMC), 1,3-phenylenediamine (m-phenylenediamine, MPD) and sodium dodecylbenzenesulfonate (SDBS). D-(+)-raffinose pentahydrate, α-cyclodextrin, D-(+)-galactose, D-(+)-maltose monohydrate and β-D-lactose were purchased from Alfa Aesar (Ward Hill, MA). Cyclohexanone was purchased from Cole-Parmer (Vernon Hills, IL) and bovine serum albumin (BSA) from BioWorld Inc. (Dublin, OH). Alginic acid, sodium salt (AAS) was from Scientific Polymer Products, Inc. (Ontario, NY). All chemicals were used as received without further purification. Polyethersulfone (PES) ultrafiltration membranes were provided by Trisep Corporation (Goleta, CA). The salts used in this study were potassium chloride (KCl; FisherChemical), sodium chloride (NaCl; Sigma-Aldrich), magnesium chloride hexahydrate (MgCl2·6H2O; EK industries), magnesium sulfate (MgSO4; Spectrum Chemical MFG. Corp.) and calcium chloride ($CaCl_2$; Sigma-Aldrich).

### 5.2.2. CNT Functionalization

Carboxylate functionalized SWNTs of outer diameter 15 Å and length 1 μm were purchased from Nano Lab Inc. (Waltham, MA).[38] We used the same functionalization procedure described in our prior work.[17,39] The COOH functionalized SWNTs were produced by chemical

vapor deposition (CVD). The concentration of –COOH groups in the SWNTs was approximately 2–7 wt % (as determined by titration). These functionalized SWNTs were reacted with thionyl chloride ($SOCl_2$) at 65 °C for 36 h and the –COOH groups were replaced by COCl groups. The acylated SWNTs were then esterified using 3-dimethylamino-1-propanol, $(CH_3)_2–N–C_3H_6–OH$. This was followed by a ring-opening reaction of lactone, in which β-propiolactone was opened to form an acid group and attached to the tertiary amine on the functional group.[40,41] The resulting zwitterionic group had a positive charge at the tertiary amine group and a negative charge at the carboxylated group. The final chemical structure is illustrated in Figure 5.3.

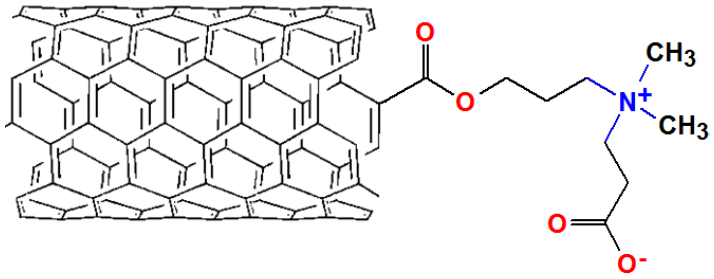


**Figure 5.3.** Schematic of the chemical structure of zwitterionic functional group attached on the SWNTs.

### 5.2.3. Membrane Fabrication

The interfacial polymerization (IP) of polyamide is very sensitive to operating conditions and reaction time. Different publications report different recipes in terms of the concentration of monomers, contact time, air-drying time, curing temperature, etc.[42–44,29] Our fabrication process was divided into two steps: deposition and alignment of CNTs, and interfacial polymerization of PA, as shown schematically in Figure 5.4. The PES support used in this fabrication was first immersed in a 0.5 wt % SDBS solution for two days and then in deionized (DI) water for one more day to open the pores and increase the hydrophilicity. A predetermined quantity of zwitterion functionalized SWNTs were dispersed in DI water through ultrasonication. The pretreated PES membrane was placed in the filtration system and the dispersed Z-SWNTs solution was poured on top of it. We then used vacuum filtration to deposit the SWNTs on the support in a semi-aligned orientation[45] and to remove the solvent. The SWNT coated support was then dried for an hour in a vacuum oven to insure that all water was removed from the nanotubes and the support pores before interfacial polymerization (IP) took place.

The second step in the membrane fabrication process was interfacial polymerization of PA. The SWNT coated PES support was sandwiched between two circular poly(tetrafluoroethylene) (PTFE) frames. IP was carried out on the support by wetting the SWNT coated side with an aqueous diamine solution containing 2 wt% MPD and 0.2 wt% of SDBS at ambient temperature for 2 min. The membrane was then unclamped from the PTFE frames and immediately placed on a glass plate. A glass roller was used to roll over the membrane to remove all the excess MPD solution. The membrane was then sandwiched again between the frames and wetted by an n-hexane solution containing 0.34% (v/v) TMC for 90 seconds. The resulting PA thin film nanocomposite membrane was then heat cured at 68 °C for 5 min. After the membrane had cooled down, it was washed thoroughly with DI water, submersed in fresh DI water and stored in a laboratory refrigerator at 4 °C.

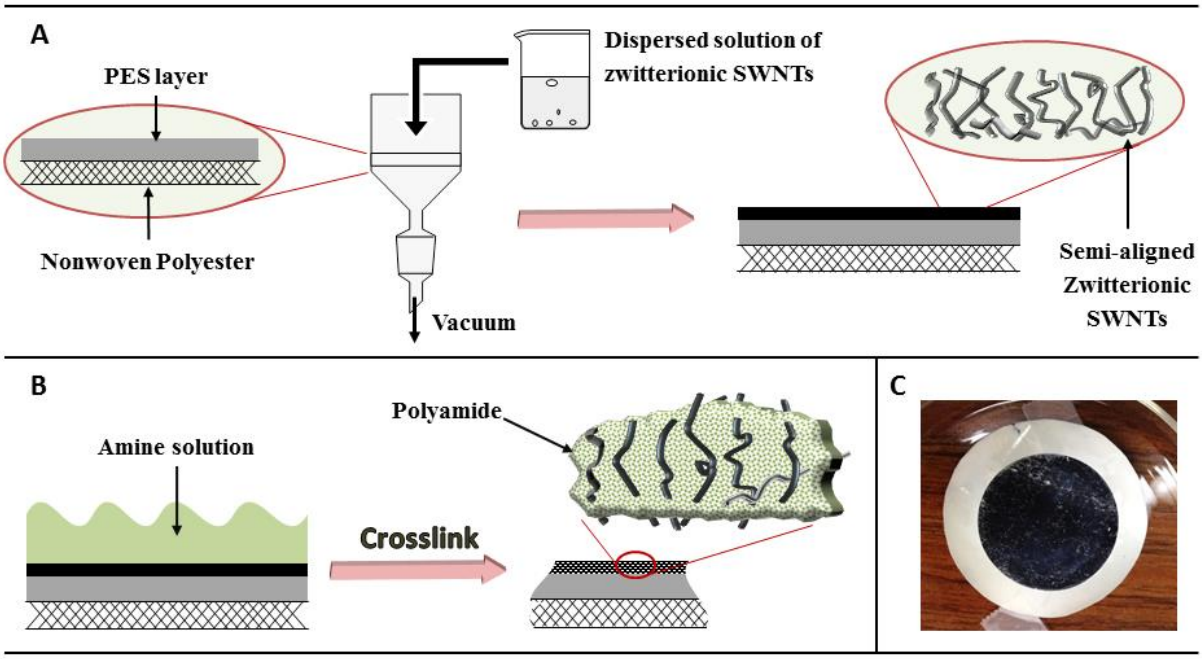


**Figure 5.4.** Cross-sectional schematics of the fabrication procedure for Z-SWNT/PA nanocomposite membrane. (A) PES ultrafiltration membrane is composed of a thin PES layer covered on a non-woven polyester web, and has been pretreated in surfactant solution. Zwitterion functionalized SWNTs was then deposited onto the PES membrane support through vacuum filtration. (B) Aromatic polyamide formed in between the semi-aligned functionalized SWNTs via interfacial polymerization, at which aqueous solution containing MPD monomers came in contact with nonaqueous solution containing TMC crosslinker. (C) Photograph of the top of Z-SWNT nanocomposite membrane that is the effective side exposed to the feed solution.

### 5.2.4. Membrane Characterization

The surface roughness of the membranes was measured by Atomic Force Microscopy (AFM; Asylum Research® Cypher scanning probe microscope) using contact mode, with a 5 $\mu m^2$ scanned area. The roughness parameters were estimated from the AFM images and calculated with the AFM surface analysis software (MFP-3D, Igor Pro v.6.3.4.1). The hydrophilicity of the membrane surface was measured through contact angle experiments (KSV Instruments LTD Cam 200) using test droplets composed of deionized water. Static water contact angles were determined from side-view pictures captured after the value of contact angle stabilized. The chemical structure of the plain polyamide and Z-SWNT nanocomposite membranes were characterized by attenuated total reflectance Fourier transform infrared spectroscopy (ATR-FTIR; Varian 670-IR FT-IR Spectrometer). Spectra were collected in air in the mid-infrared region (800─4000 $cm^{-1}$), using 256 scans at resolution 1 (0.4821 $cm^{-1}$ spacing). Before each measurement, a background spectrum was obtained and subtracted from that of the membrane to remove any atmospheric absorbance peaks.

### 5.2.5. Membrane Permeation Test

Pressure-driven permeation experiments were carried out on a laboratory-scale cross-flow membrane test unit, shown schematically in Figure 4.3 in Chapter 4, capable of withstanding pressures from 0.17 to 6.9 MPa. This test unit is comprised of a 316 stainless steel membrane cell, a high pressure pump (Hydra-cell pump, Warner Engineering), and a feed tank operated in closed loop mode with the retentate being circulated back to the feed water reservoir. Feed solutions contained common cations ($Na^+$, $Mg^{2+}$, $K^+$ and $Ca^{2+}$) at predetermined concentrations, and were kept at room temperature by a temperature controlled chiller (VMR; 1150S). The applied transmembrane pressure and the circulation flow rate were adjusted to 2.41 MPa and 2.5 L/min, respectively. The Reynolds number for this module geometry was estimated from the formula applied for a rectangular duct and was calculated to be 1633, which falls within the laminar flow region (see Appendix). However, the mesh design of the feed spacer placed inside the cell helps to create local turbulence when water flows through the cavity of the cell. The permeation flux was allowed to equilibrate for 30 min before any permeant collection. A known amount of permeant was collected in a glass vial within a given period of time. The density of water was taken to be 0.997 $g/cm^2$ at ambient temperature, the volumetric flow rate was calculated from

$Q = \frac{\Delta V}{t \cdot A}$, where $\Delta V$ is the permeate volume (liter), $t$ is the permeation time (hours) and $A$ is the effective membrane area ($m^2$). The flow rate, $Q$, was then calculated in the units of liter per square meter per hour (LMH). The concentration analysis of the cations present in the permeant was measured by atomic adsorption spectrophotometry (AAS; Perkin Elmer 5100, Wellesley, MA). The concentrations of cations in the feed, $C_f$, and the permeant, $C_p$, were then measured and used to calculate salt rejections using the equation shown below.

$$\Re(\%) = \left(1 - \frac{C_p}{C_f}\right) \times 100 \tag{5-1}$$

### 5.2.6. Pore Size Distribution Test

The pore size distribution in the RO membranes was measured using the method developed by Otero *et al*.[46] as follows: six solutes (i.e., ethanol, galactose, lactose, maltose, raffinose, and α-cyclodextrine) with different Stokes' radii were each dissolved in DI water to prepare different feed solutions with concentrations of 500 ppm. The testing conditions and procedure were identical to the cross-flow filtration test described in the previous section. The concentration of carbon content in the feed and permeate solution were measured by a total organic carbon (TOC) analyzer to obtain the rejection. The results were analyzed using the equation

$$f = {J_{W,t}}/{J_W} = 1 - \frac{1}{1 + (r_P / B)^c} \tag{5-2}$$

where $f$ and $r_P$ are the number fraction of pore size and pore size, respectively. $J_{W,t}$ and $J_W$ are the pure water flux passing through the transmitting pores and the total pure water flux, respectively. B and C are constants that were obtained through non-linear fitting of the permeation data using Origin 9.0 software. In this study, the plot of $\frac{df}{dr}$ versus $r$ was used to determine the pore size distribution of the RO membrane based on equation (5-2).

### 5.2.7. Surface Fouling Experiment

A series of cross-flow filtration experiments were also conducted to investigate the surface fouling of the RO membranes. Initially, membrane samples were used to filter DI water for 12 h. Then a solution containing model organic foulants was introduced into the feed tank. The

membrane permeation flux was then recorded for the next 10 h. BSA (model protein) and AAS (model polysaccharide) were the organic foulants added in the feed solution in different concentrations. BSA fouling has been proven to be significantly enhanced with the presence of AAS.[47] The temperature of the feed solution was kept at 20 ± 0.5˚C and the circulation flow rate was kept at 1.0 L/min for all the testing. The circulation flow was significantly slower than that in the ion filtration experiment in order to facilitate the adsorption of the foulant on the membrane surface. To obtain a better comparison across different membranes, the applied transmembrane pressure was adjusted from membrane to membrane so that all the trials have a similar initial permeation flux. When the fouling tests were completed, the membranes were then washed again with water to determine their flux recovery capability. DI water was circulated in the RO system for 12 h with flow rate at 2 L/min under a transmembrane pressure of 0.34 MPa. After cleaning, the tank was refilled with new DI water and the filtration test continued for another hour under the same conditions as in the fouling test. The permeation flux after the wash was also recorded.

## 5.3. Results and Discussions

### 5.3.1. Membrane Morphology

The overall thickness of the skin layer of the Z-SWNT/PA membranes was reported in our prior publication[17] and was approximately 250 nm. AFM imaging of the membrane surfaces, depicted in Figure 5.5, showed that the surface roughness increased significantly after polymerization of PA on the PES support. The root mean square deviation of the surface roughness increased from 5.86 nm to 27.03 nm after plain PA was coated on the support, and to 27.62 nm when both the functionalized SWNT and PA were coated on the support. The increased surface roughness was at least partly due to the ridge-and-valley microstructure of the PA coating, as shown previously,[1,2,33,48] as well as in our SEM image in Figure 5.5(B). The AFM image for Z-SWNT/PA has a very similar surface roughness to the control sample, thus it is difficult to tell whether the Z-SWNTs are exposed on the surface of the membrane. The surface contact angles of plain PA and nanocomposite membranes are shown in Table 5.2 and their values are also very close to each other. This suggests that the Z-SWNT/PA membrane surface is covered by PA, and that the addition of Z-SWNTs has little effect on the membrane surface. An ideal nanocomposite membrane, however, would have CNTs perfectly aligned with the direction of fluid flow and would percolate completely through the membrane, so that no fluid would have to permeate

through the polymer matrix. The surface properties of such a membrane would be expected to be different from a PA coating. In contrast, SEM images (Figure 5.5D) show that some bundles of SWNT percolate through the top of the PA layer and extend above the surface. This could allow the tip functional groups on the CNTs to interact directly with the solutes dissolved in the feed solution, as demonstrated in protein fouling experiments (vide infra).

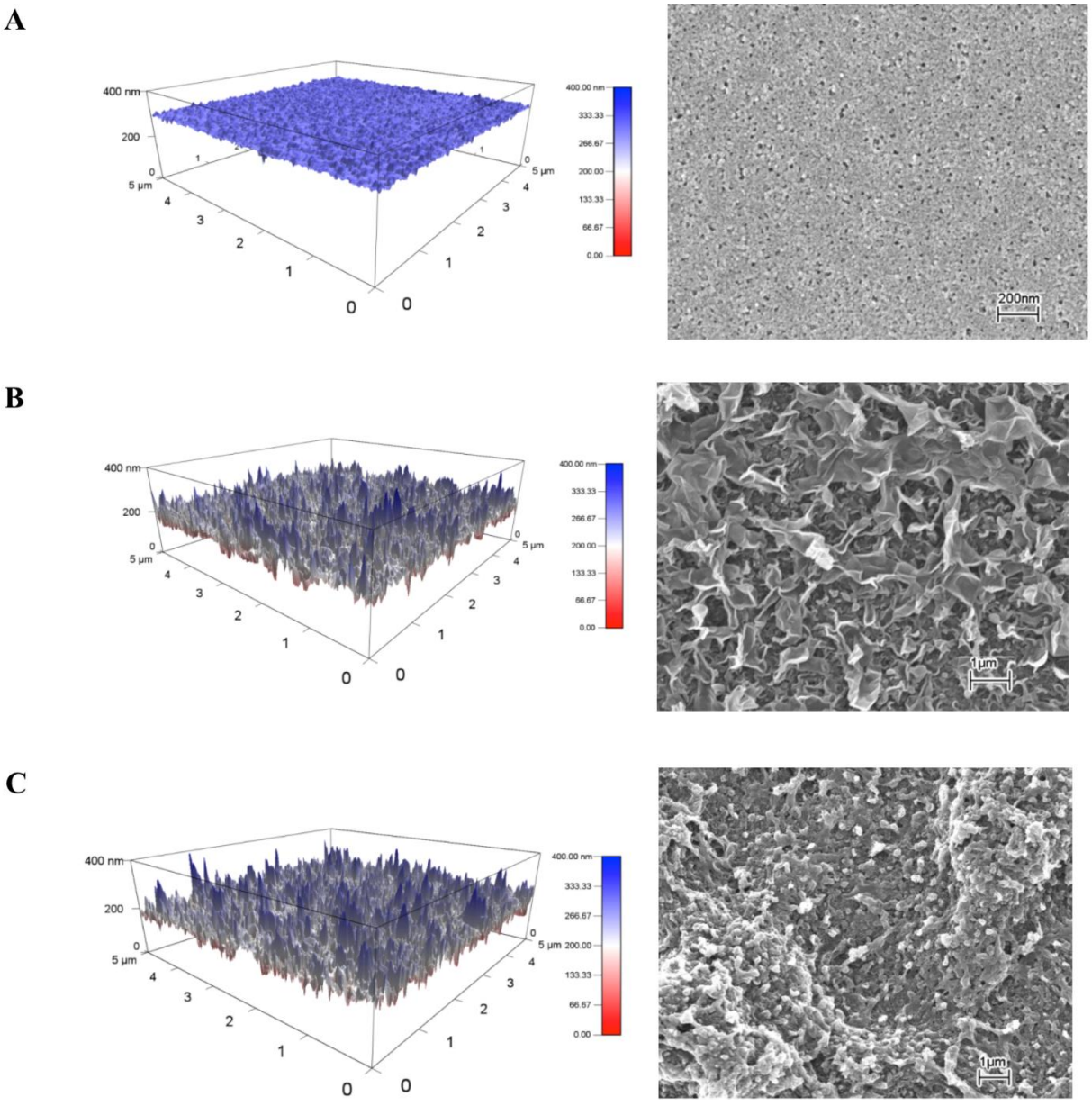

D

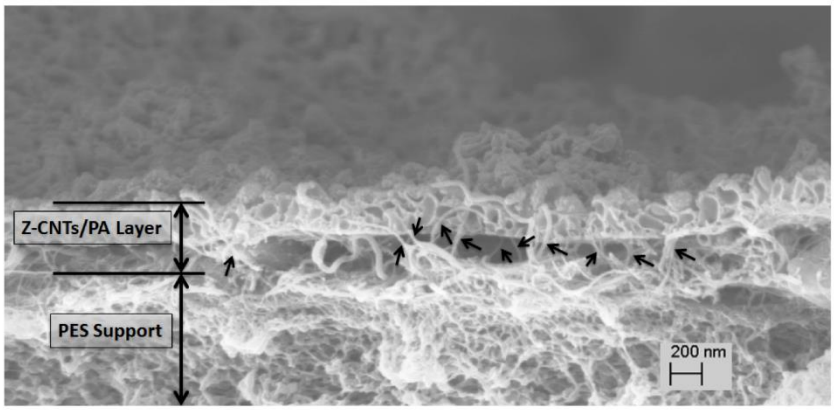


**Figure 5.5.** AFM and SEM images of the surface of (A) polyethersulfone (PES) ultrafiltration membrane support, (B) Plain polyamide membrane, and (C) 20wt% Z-SWNT/PA membrane. The root mean square of surface roughness of (A), (B) and (C) are 5.86, 27.03 and 27.62 nm, respectively. (D) shows the cross-sectional view of the Z-SWNT/PA membrane, where black arrows indicate the CNTs with semi-aligned orientation. SEM images are adapted with permission from ACS Nano.[17]

**Table 5.2.** Contact angles for polyamide and 20wt% Z-CNT nanocomposite membrane.

| | Left contact angle | Right contact angle |
|---|---|---|
| Polyamide (PA) | 45.05° | 44.42° |
| 20wt% Z-SWNT/PA | 46.14° | 48.88° |

### 5.3.2. ATR-FTIR analysis

ATR-FTIR measurements were employed to analyze the chemical composition of the skin layer of the PA and Z-SWNT/PA membranes. The expanded view of the IR spectrum (wavenumber 1800 to 1050 $cm^{-1}$) is shown in Figure 5.6, where it shows the bonding stretch of the signature peaks for the PES support, plain PA, and Z-SWNT/PA membranes. The spectrum of PES shows medium and strong S=O stretches at 1325 and 1140 $cm^{-1}$, which is a contribution from the sulfone group. After a thin layer of PA was coated on top of it, the S=O peaks diminished but strong amide C=O and aromatic amide C=C ring stretches were observed at 1660 and 1610 $cm^{-1}$. The N–H in-plane bending and N–C stretching vibration of the –CO–NH– group was also observed at 1543 $cm^{-1}$.[30] The degree of crosslinking of the polyamide can be estimated using the amount of carbonyl groups present, determined using the C=O bond in COOH (1700 – 1725 $cm^{-1}$). Low crosslinking results in more unreacted acid chloride groups in the solution, which are easily hydrolyzed and turned to carboxylic acid groups (COOH). The peak detected around 1720 $cm^{-1}$ was very weak, indicating that the PA coating was highly crosslinked. The spectrum of Z-

SWNT/PA also contains the same strong amide peaks, showing that the nanocomposite membrane consists primarily of the PA matrix. A comparison of the in-ring C–C stretch (1500 to 1400 $cm^{-1}$) between PA and Z-SWNT/PA was conducted to quantify the addition of CNTs in the thin film. The signal for this peak in the PA control sample is solely due to the aromatic structure of PA, whilst the signal in the TFN membrane contains contributions from both the ring structure in the SWNTs and the PA. The peak at 1543 $cm^{-1}$ was chosen as a reference peak since it did not show up in the spectrum of the PES substrate (more discussion about the choice of the reference peak can be found in the supporting information). Following normalization with respect to the reference peak, the concentration of C–C (in-ring) stretch in Z-SWNT/PA membrane is 44.9% higher than that in the plain PA membrane. This result shows that a high weight percentage of hexagonal carbon rings was introduced to the PA skin layer due to the addition of the CNTs during the membrane fabrication process.

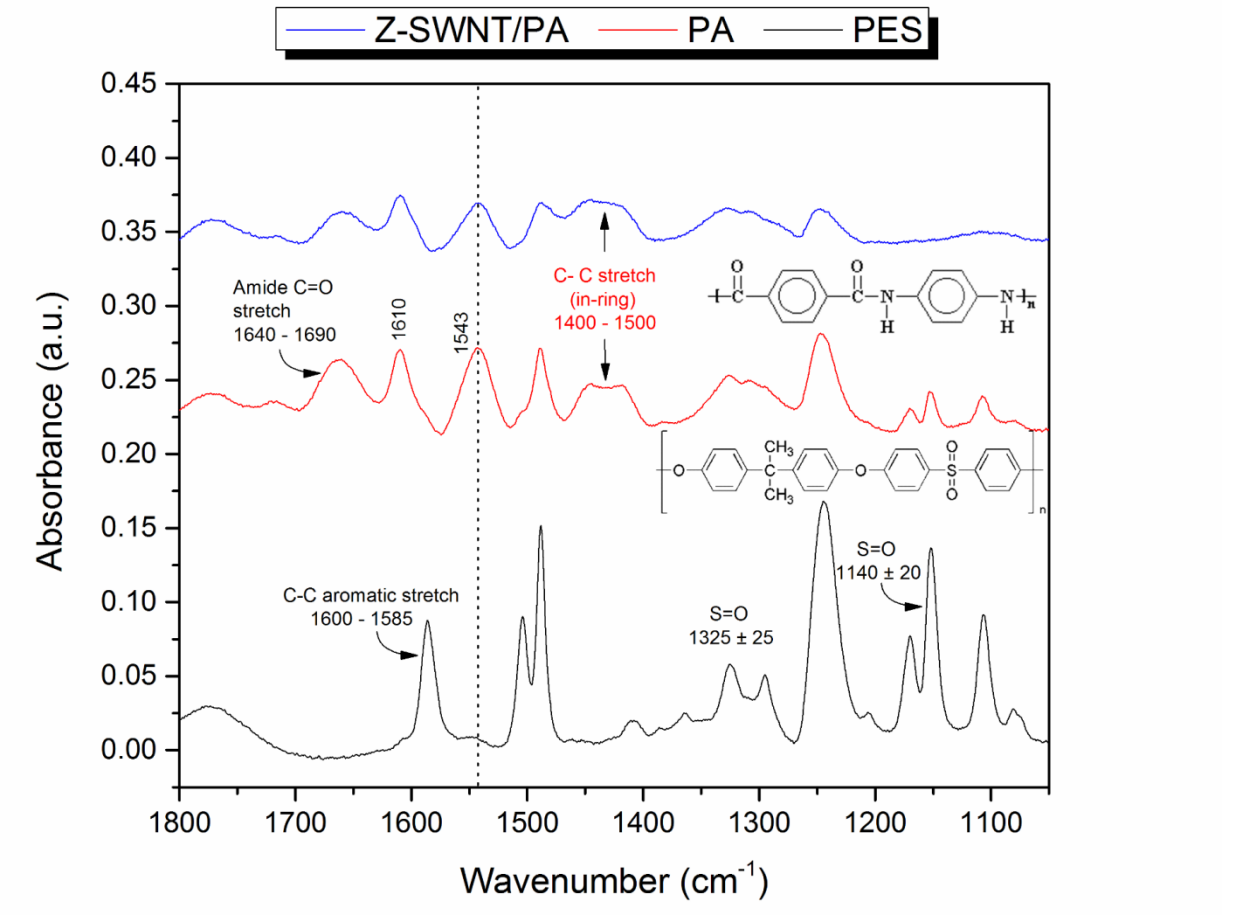


**Figure 5.6.** Expanded view of ATR-FTIR spectra at the bonding stretch region (1800 to 1050 $cm^{-1}$). Spectra include PES support (black), plain PA membrane (red) and Z-SWNT/PA membrane

(blue). The polymer structure of aromatic PA (top) and PES (bottom) are also shown in the graph for identification of their bonding. Dash line at 1543 $cm^{-1}$ indicates the reference peak used for normalizing other bonding peaks for cross comparison.

### 5.3.3. Composition study of the Z-SWNT/PA membranes

As discussed earlier, the degree of polyamide crosslinking can be disrupted easily by the presence of nanomaterials and this can reduce the high salt selectivity of the PA skin layer. By increasing the concentration of TMC, the concentration of the electrophilic carbonyl functional groups is increased in the solution, which initiates more local step-growth polymerization and forms low-molecular-weight homologs. The more homologs grown around the embedded nanomaterials, the higher the chance for these homologs to be crosslinked together to form a PA backbone close to the surface of the nanomaterials. Increased TMC increases the overall reaction rate and yields a higher degree of crosslinking at the end of the polymerization, and more importantly, it minimizes void volume formed at the interface between PA matrix and the nanomaterials. Increasing the TMC concentration also substantially increases the density of PA and forms a more durable but less permeable skin layer around the embedded nanomaterials.[49] A series of trade-off experiments were conducted to study the correlation between the loading of CNTs and the integrity of the nanocomposite skin layer by adjusting the concentration of Z-SWNTs deposited onto the membrane and the TMC content in the hexane solution. Figure 5.7 depicts the permeation results for each membrane with the permeation flux tagged in the figure in the units of LMH.

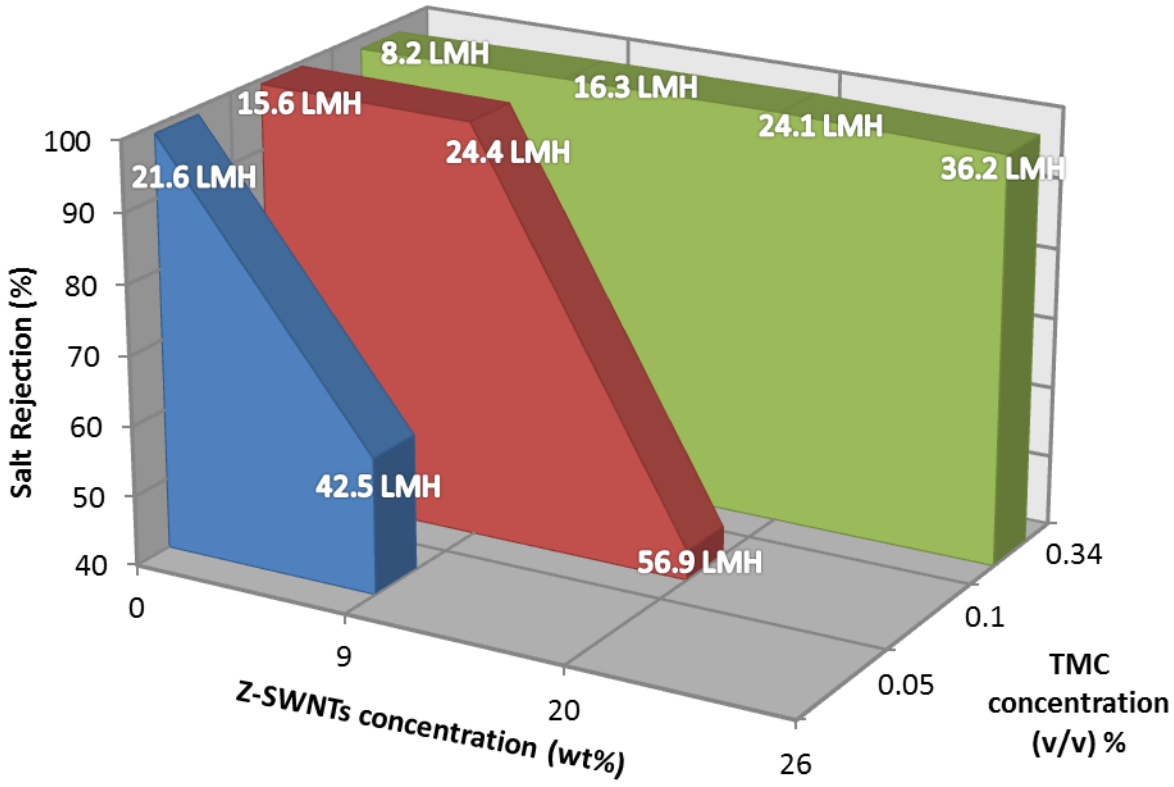


**Figure 5.7.** Trade-off between the density of polyamide skin layer, controlled by the concentration of crosslinking agent, TMC (Y-axis), and the concentration of Z-SWNTs embedded in the skin layer (X-axis). The Z-axis shows the salt rejection of the TFN membranes, and the numbers within the graph show the permeation flux of each membrane in units of liter per $m^2$ per hour (LMH). All the membranes were operated under the same applied transmembrane pressure at 2.41MPa. The feed solution contained 2000 ppm of $Na^+$ from dissolved sodium chloride.

Increasing the concentration of TMC reduces the water permeation in the membrane in the absence of Z-SWNTs, which agrees with results reported by Ahmad *et al.*[49] that the rate of reaction for polymerization is increased tremendously as the TMC content was increased, reducing the pore size and free volume of the skin layer, and hence lowering the permeation. Plain PA membranes fabricated with 0.05 (v/v)% of TMC had looser polymer chains and larger pore sizes, offering high salt rejection (98.9%) and permeation flux (21.6 LMH). However, when 9 wt% of Z-SWNTs was added into this loose membrane, the rejection decreased drastically to 59%. This shows that the skin layer structure is disrupted by the inclusion of nanotubes. When a higher concentration of TMC was used during the fabrication the PA layer was better able to accommodate high loadings of nanotubes. When the concentration of TMC was increased to 0.34 (v/v)% the skin layer was able to accommodate up to 26 wt% CNT without a significant decrease in salt rejection. Among

all the TFN membranes studied, we found the optimal condition to be at 0.34 (v/v)% of TMC and 26 wt% of Z-SWNTs. These conditions resulted in the highest water flux (36.2 LMH) and salt rejection (greater than 98%.)

### 5.3.4. Feed concentration effects (RO or Charged NF)

Holt *et al.*[10] fabricated nanofiltration (NF) membranes using –COOH functionalized CNTs. Their results show that the salt rejection of the membranes declined drastically when the salt concentration in the feed solution increased from 1 mM to 10 mM. This phenomenon generally occurs in charged NF membranes, where the average pore size of the separation skin layer is significantly larger than the species being separated. In these cases the fixed charges from the functional nanoparticles or acid groups on the polymer backbone induces an electrostatic repulsion to exclude ions of the same charge. This reduces the effective pore size of the membrane, a separation mechanism known as Donnan charge exclusion. However, at higher feed concentrations (i.e., $\geq$ 2000 ppm) the Donnan exclusion effect is negated by electrostatic screening of the fixed charges. In the case of Holt *et al.*[10], the Debye length, $\lambda_D$, of the charged functional groups on the CNTs decreased as the ionic strength of the solution increased. Salt rejection decreased rapidly when $\lambda_D$ fell below the CNT diameter.

In our previous simulation and experimental study, zwitterion functionalized SWNTs reject ions via a different separation mechanism than singly-charged functionalized CNTs. Simulations suggested that increasing the feed concentration of NaCl from 0.3M to 0.6M would not affect the salt rejection ability of the zwitterion functionalized CNT membranes.[17] The water flux and salt rejection of a 20wt% Z-SWNT/PA membrane was studied in order to determine whether the Z-SWNT/PA membranes reject ions based on size or Donnan exclusion. The feed solution contains $MgSO_4$ or $MgCl_2$ with concentration of $Mg^{2+}$ ranging from 100 to 5000 ppm (4.1 mM to 205.7 mM). We used $Mg^{2+}$ as the feed cation because its divalent charge increases the ionic strength much faster than a monovalent salt and retards Donnan exclusion rapidly. As shown in Figure 5.8, the overall salt rejection for $Mg^{2+}$ stayed above 97% and varied only by ± 1% between different membrane samples. The rejection increased slightly as the feed concentration increased for both $MgSO_4$ and $MgCl_2$, and was as high as 99.7% even at the highest feed concentration of 5000 ppm. This indicates that the effective pore size of Z-SWNTs remains unchanged regardless of the ionic strength of the feed. In other words, the electrostatic screening due to dissolved salt

ions does not impact the selectivity of the membrane. There is no significant differences in rejection between $MgCl_2$ and $MgSO_4$.

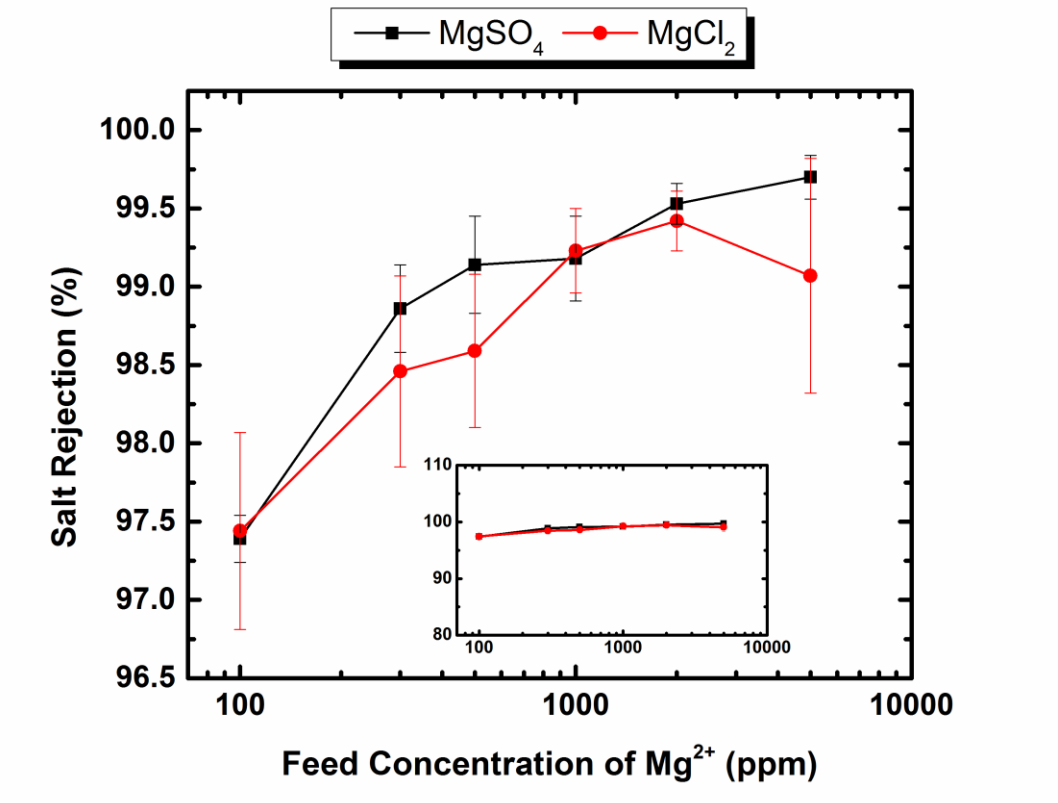


**Figure 5.8.** Salt rejection for $MgSO_4$ and $MgCl_2$ as a function of $Mg^{2+}$ concentration in the feed solution. Solution concentration varies from 100 to 5000 mg/L. Three membrane samples of 20 wt% Z-SWNT/PA were tested, and the error bar shows the standard deviation between trials. The applied transmembrane pressure is 2.41 MPa. The secondary plot within the figure shows that the change of salt rejection is relatively small, while the expanded plot enlarges the initial and final drop of the rejection.

**Table 5.3.** Hydrated radii[50] for the ions tested in this study.

| Cation | Hydrated Radii (Å) | Anion | Hydrated Radii (Å) |
|---|---|---|---|
| $K^+$ | 3.31 | $Cl^-$ | 3.32 |
| $Na^+$ | 3.58 | $SO4^{2-}$ | 3.79 |
| $Ca^{2+}$ | 4.12 | | |
| $Mg^{2+}$ | 4.38 | | |

Francesco *et al*.[10] suggest that the larger the valence number difference between cation and anion ($z^+$ and $z^-$) the better the salt rejection will be for a charged NF membrane. This is because charged membranes will exhibit a stronger repulsive force toward the oppositely charged ions relative to the attractive force to the similarly charged ions. This results in more counterions being rejected by the membrane than co-ions transported through. For a negatively-charged membrane, if the $z^-/z^+$ ratio in the feed solution decreases from 1 to 0.5 (e.g. $CaSO_4$ to $CaCl_2$), the rejection of the cation could drop from approximately 40 % to less than 15 %.[10] In contrast, the Z-SWNT/PA membrane reported here did not experience any significant reduction in salt rejection when the $z^-/z^+$ ratio decreased from 1 to 0.5 ($MgSO_4$ to $MgCl_2$). This further demonstrates that the electrostatic screening effect is negligible in the Z-SWNTs membranes.

### 5.3.5. Permselectivity for common cations

Z-SWNT/PA membranes were also tested using other common alkali ions present in seawater. Plain PA and 20 wt% Z-SWNT/PA membranes were tested for water and ion flux with feed solutions containing 2000 ppm of $Na^+$, $Mg^{2+}$, $K^+$ or $Ca^{2+}$ cations from NaCl, $MgCl_2$/$MgSO_4$, KCl or $CaCl_2$ respectively. A second set of experiments was conducted with all the feed solutions maintained at an ionic strength of 87 mM. The permeation flux and ion rejection are shown in Figure 5.9. The water flux for all five salt solutions increased approximately three-fold after adding Z-SWNTs to the PA matrix. For example, the water flux increased from 14.7 to 34.7 LMH for the NaCl solution and from 7.4 to 30 LMH for the $MgCl_2$ solution. A similar trend was observed in both sets of experiments (i.e. constant concentration and constant ionic strength). Based on our previous study[17], water transport in the Z-SWNT/PA membrane could occur through the core of the nanotubes as well as through "nanochannel" defects at the interface between the CNT outer wall and the polymer matrix. The increase in permeation flux could be due to the presence of either or both of these transport paths. The zwitterionic functional groups used in this study have been demonstrated to have strong water sorption properties[41], which attracts more water to the tip of the CNTs and facilitates water entry into the nanotubes. However, the bulky size of the functional groups was also shown to greatly decrease the water permeation rate in CNTs. If nanochannels are present next to every CNT, water could possibly be transported through them rather than through the CNT cores.

The cation rejection data for different salts with constant feed concentration or ionic strength are shown in Figure 5.9(B). The first four salts in the graph have the same anion group

($Cl^-$) to allow for direct comparison. In the plain PA membrane, divalent cations experienced ~1% higher rejection than monovalent cations at the same mass concentration. This could be due to the stronger bonding energy between the divalent metal ions and water molecules in the feed solution, which results in a larger diameter for the hydrated ions. However, this increase in rejection also corresponds to an increase in the ionic strength of the feed solutions. In contrast, the Z-SWNT/PA membrane exhibited no discernable trend in salt rejection with regard to the hydrated radius of the cations, as any differences in the measured rejection values are within the experimental error. In the constant ionic strength experiment, the charge screening effect of the dissolved ions on the membrane is the same for all salt solutions. By factoring out differences in electrostatics, any differences in the rejection should be due to the size sieving and should correlate with the size of the hydrated ions. However, no discernible trend in the cation rejection is observed for the constant ionic strength test in either the PA or Z-SWNT/PA membranes. The nearly constant rejection values (as a function of hydrated radius and ionic strength) suggest that the pores in both the PA and Z-SWNT/PA membranes are smaller than the hydrated radius of the smallest cation ($K^+$).

**A**

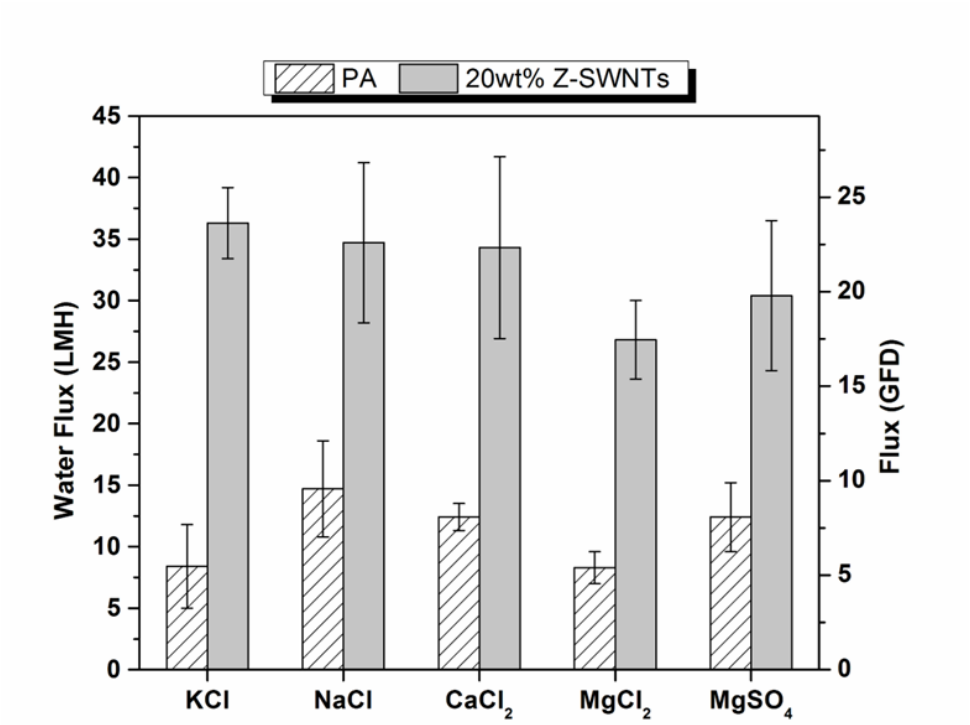

**B**

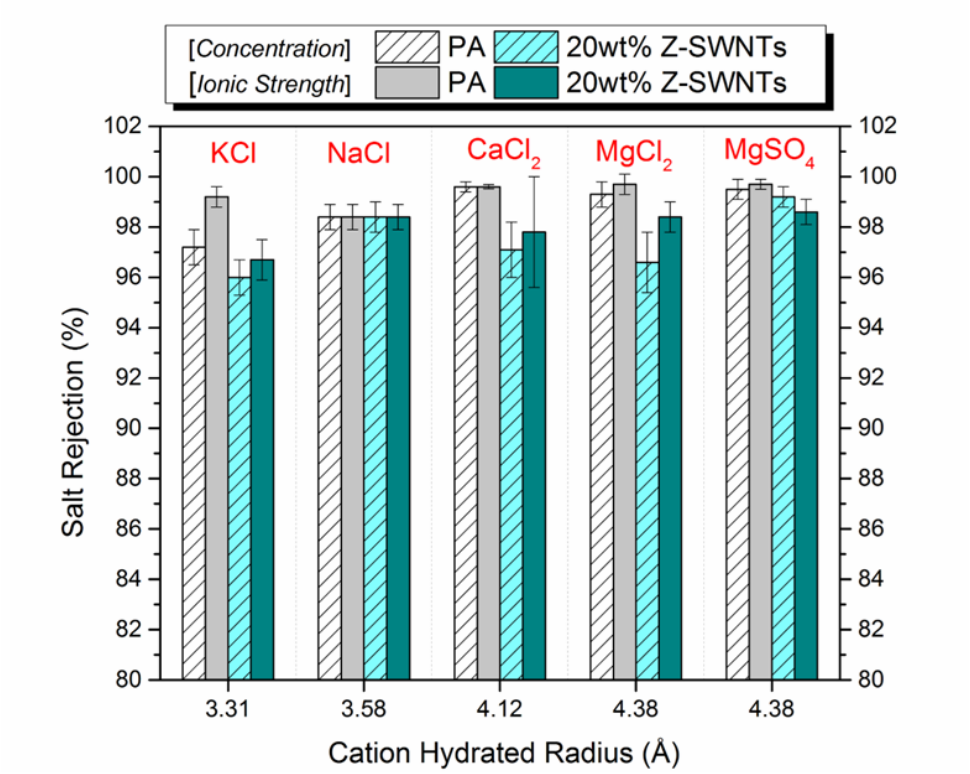


**Figure 5.9.** (A) Permeation flux of plain PA (white hatched) and Z-SWNT/PA membrane (grey solid). All cation concentrations in feed solutions were maintained at 2000 ppm. (B) Salt rejection for both constant cation concentration experiment (Concentration) and constant ionic strength experiment (Ionic strength). Results for PA are shown in white hatch and grey bars. Results for nanocomposite membrane are shown in light cyan with hatch and dark cyan bars. Results are the average of tests on three different membranes. The transmembrane pressure was 2.41MPa and the feed flow rate was at 2.5 LPM.

The selectivity of the membranes showed a consistent trend upon the addition of the Z-SWNTs into the PA matrix. The salt rejection values for $Na^+$ are identical in the plain PA and nanocomposite membranes. However, the average rejection of $Ca^{2+}$ and $Mg^{2+}$ was slightly higher in the PA membrane than in the Z-SWNT membrane, although this difference was within the experimental error. The addition of Z-SWNT generally increased the variation in selectivity measurements between membranes. This is likely due to the difficulty in achieving consistent orientation, dispersity, and density of Z-SWNTs in the PA film from membrane to membrane, resulting in a larger fluctuation in salt rejection compared to the pure PA membranes. Some of the nanocomposite membranes exhibited $Ca^{2+}$ rejection values as high as 99.3% while others exhibited values below 96%.

During the functionalization of the Z-SWNTs, the zwitterionic functional groups can react both at the CNT ends as well as at reactive defect sites along the length of the CNT. These randomly distributed zwitterionic groups attract polymer chains during the interfacial polymerization via electrostatic interactions and hydrogen bonding, and could serve to decrease the formation of nanochannels outside the CNTs. Molecular simulations by Johnson *et al.*[17] have shown that zwitterion functionalized CNTs at the tube end can greatly reduce or even stop the transport of ions through the core of CNT, while still allowing acceptable levels of water molecule transport. More than 6000 zwitterionic groups are estimated to react on the outside walls of each CNT. These defect-site zwitterion groups may also serve to reject ion transport through nanochannels outside the CNTs. Therefore, we can posit three possible paths for selective water transport: through the core of CNTs, through nanochannels outside the CNTs, and through the PA matrix. Other research studies on mixed-matrix membranes agree with this theory that fluid flows through thin-film nanocomposite membranes via these three pathways.[51,52] As discussed previously, when the embedded CNT concentration remains constant, increasing the crosslink density of the PA matrix results in a decrease in the permeation flux. This could be caused by a decrease in the presence of nanochannels due to stronger interactions with the polymer, forcing more water to be transported slowly through the PA matrix. In addition, the diffusivity in the polymer matrix decreases with increasing crosslink density, so any water transport through the PA matrix is further slowed. The lack of change in salt rejection upon the addition of CNTs suggests that the combination of the three transport mechanisms present in the Z-SWNT/PA membranes results in a pore size distribution similar to that of the PA membranes.

### 5.3.6. Pore size distribution of thin film nanocomposite membrane

Water and salt ions are commonly understood to permeate through nonporous polymeric films via a solution-diffusion mechanism. However, some studies show that RO membranes can be treated as a porous separator with sub-nanometer pores created by irregular packing of randomly kinked stiffed chains.[53] These voids are interconnected and form tortuous channels 0.6 to 0.9 nm in diameter, through which the majority of water flows. Only 1% of the water is carried by homogeneous diffusion in the polymer matrix.[54] The Z-SWNT/PA membranes contain CNTs that act as channels for water flux, so it is reasonable to describe the transport using the pore flow model. Both the pore size and pore size distribution (PSD) are of interest, as they could give insight into the presence of defects (i.e. nanochannels outside the CNTs). The pore size and PSD were

determined based on the permeation of a series of uncharged solutes with known molecular size (the molecular radii of the solutes are listed in Table A.1 in Appendix). The uncharged solutes have no specific interactions with the membrane constituents, and their retention behavior was assumed to be a result of size exclusion only. In addition, the rejection of a given solute was assumed to be equal to the fraction of hydrated pores in the membranes that were smaller than the molecular size of the organic solute. Otero *et al.*[46] derived the correlation between the actual membrane pore size and the stokes' radii of the solute used, and the results showed that the pore radius is, on average, 0.14 nm greater than the solute radii (see supporting information). This is the closest approach distance between a solute and the pore walls and can be interpreted as the thickness of hydration layer of the pore. Wang *et al.*[55] have suggested that the pore radius is equal to the Stokes' radii of the rejected solutes, and that there is no hydration layer present in the pores. Based on these assumptions, the PSD curve was obtained by fitting the rejection of the solutes to equation (5-2).

The cumulative PSD and the corresponding PSD for plain PA and Z-SWNT/PA are shown in Figure 5.10(A) and (B), respectively. There is no significant difference in the distribution curves between PA and Z-SWNT/PA, and their average pore radii are both around 2.5 Å. The PSD of Z-SWNT/PA calculated without the hydration layer of the pore walls is also shown in Figure 5.10. The average pore radius in this case is approximately 1.3 Å, which is too small for water molecules to penetrate. This suggests that it is more accurate to account for the presence of a hydration layer. In either case, the pore size did not change after adding Z-SWNTs into the PA matrix, and the effective pore size of the Z-SWNT and its surrounding nanochannels is very similar to the pore size of the PA matrix. In other words, the zwitterionic groups at the tip of the CNT have reduced the effective pore size from an initial diameter of 15 Å to ~2.5 Å. This result agrees with the ion rejection measurements, where similar values of salt rejection were observed for both PA and Z-SWNT/PA membranes. The primary difference between the membranes is the geometry of the pores: water and ions travel through tortuous and interconnected nanovoids in the PA matrix, but in straighter and more continuous CNT cores and nanochannels in the Z-SWNT/PA membrane. Another possible explanation is that most of the sieving of the uncharged solutes occurs in a layer of PA covering the CNTs, and the CNTs then provide fast channels for water permeation after the sieving occurs. All the permeation fluxes in this experiment increased significantly when the CNT content in the film increased. However, it is unclear whether the ends of the Z-SWNTs pierce the

upper surface of the membrane, so the selectivity could be due to a thin PA top layer. This would account for the similar salt rejection values observed in the PA and Z-SWNT/PA membranes.

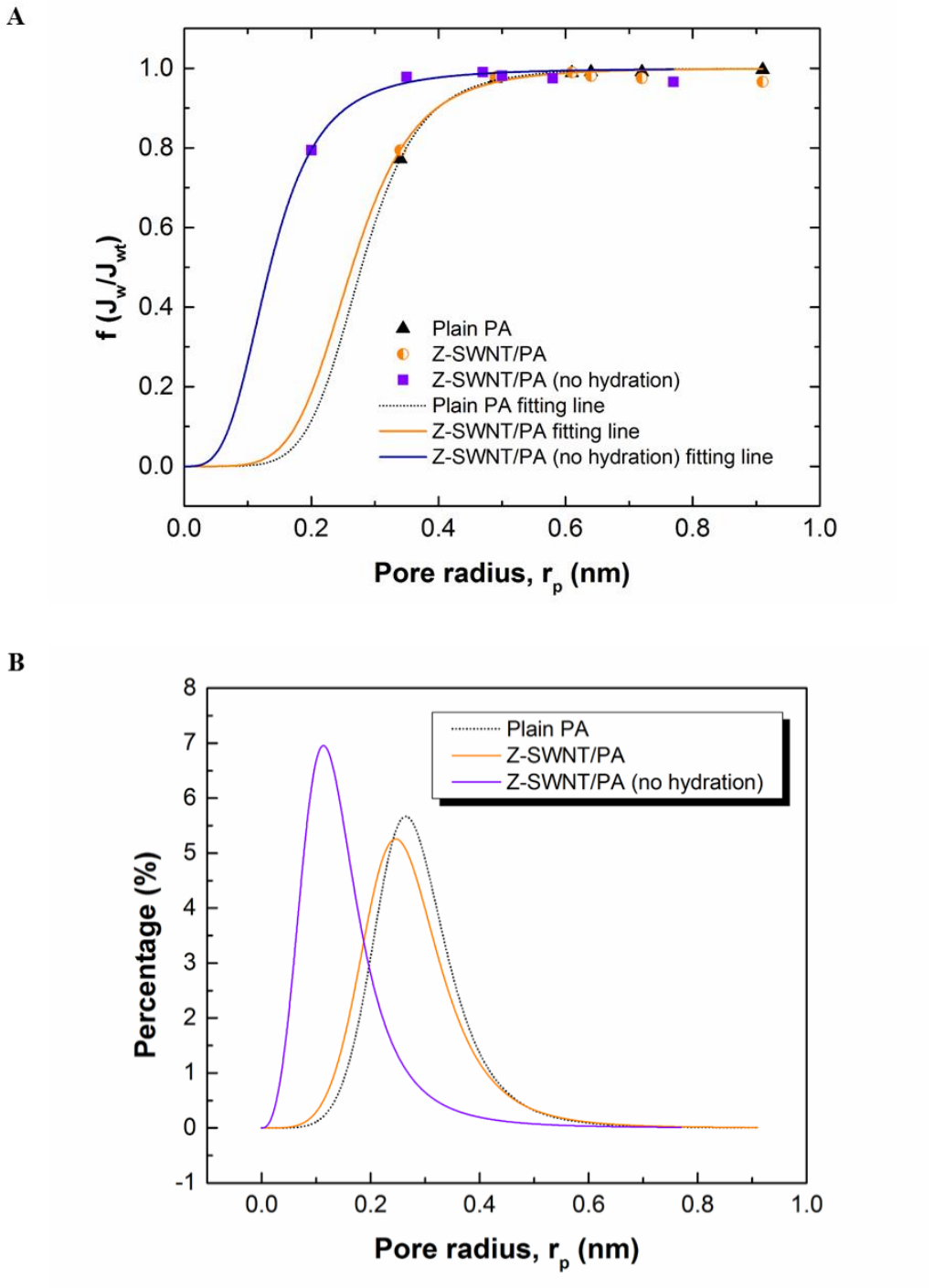


**Figure 5.10.** (A) Cumulative pore size distribution as obtained from rejection of uncharged solutes in RO membranes. (B) Pore size distribution as derived from the derivatives of the fitting lines in (A).

### 5.3.7. Analysis of surface biofouling

The surface biofouling behavior of the PA and Z-SWNT/PA membranes was studied by exposing the membranes to a bovine serum albumin (BSA) solution and measuring the decrease in water flux over time. Exposed zwitterionic groups on the functionalized CNTs are expected to improve the surface biofouling properties of the Z-SWNT/PA membranes. Zwitterions, possessing both positive and negative charges, create stronger and more stable electrostatic interactions with water than uncharged hydrophilic materials. This results in a hydration layer at the membrane surface and makes it difficult for foulants to displace water molecules and bind to the surface. Polyamide RO membranes possess surface charges[56] due to the presence of carboxylic groups on the polymer backbone. Common foulant species (e.g. proteins) are also charged in solution and are thus attracted to the membranes and can bind strongly due to specific interactions between functional groups, an effect that increases surface fouling.[47] We expect that the PA surface studied here had a low surface charge due to the high degree of chemical crosslinking in the film,[49] making it is less prone to foulant adsorption. The conditions of the feed solution, therefore, were adjusted to enhance the fouling ability of the BSA in solution. Elimelech *et al.*[47] reported that increasing the ionic strength in the feed solution reduces the electrostatic repulsion between BSA molecules and between the BSA molecules and the membrane. The addition of calcium ion to the feed solution also promotes the formation of complexes composed of the constituent of organic foulants and then assists with BSA adsorption. In our study, 2.0 mM of $Ca^{2+}$ and 4.0 mM of NaCl were added to the feed solution to make up a total ionic strength of 10 mM. The electrostatic repulsion between BSA molecules is further reduced when the pH of the solution is close to the isoelectric point of BSA. Thus, the pH of the feed solution was maintained at 4.7, the isoelectric point of BSA when the ionic strength is 10mM.

A 20wt% Z-SWNT/PA membrane was placed in the filtration system, and the permeation flux was recorded every 20 minutes over the course of 10 hours. The membrane was then flushed with pure DI water for 2 hours before the permeation was tested again. The results are shown in Figure 5.11, where the y-axis shows the ratio of the flux, $J$, to the initial flux, $J_0$. The effect of ionic strength and the concentration of BSA can be seen in Figure 5.11A, while the flux recovery rate of the membranes is depicted in Figure 5.11B. There was no significant decline in permeation fluxes at low concentrations of BSA (0.1g/L.) When the ionic strength in solution increased, the flux decreased slightly and fluctuated, but stayed above 90% of the initial flux. This suggests that

some BSA was deposited on the surface but that the adsorption rate was slow due to the low BSA concentration in solution, and the adsorbed BSA could be easily displaced by the crossflow in the system. Significant decreases in permeation were only observed when the concentrations of BSA were greater than 1.0 g/L (flux data for additional operating conditions can be found in the supporting information). A 1.0 g/L solution of BSA was then used to foul both the PA and Z-SWNT/PA membranes (Figure 5.11B). Both membranes exhibited two stages of fouling: at short times, the flux of the plain PA membrane decreased rapidly; after 100 min the rate of flux decrease gradually slowed down and the flux reached a quasi-steady state at a relative flux of $J/J_0 \sim 0.61$. In contrast, the Z-SWNT/PA membrane exhibited a slower loss of flux at short times (less than 300 minutes) before plateauing at a higher relative flux value ($J/J_0 \sim 0.72$). Thus, the initial adsorption of BSA on the PA membrane surface is faster than on the Z-SWNT/PA surface, and the flux reduction due to fouling is decreased for the Z-SWNT/PA membrane.

The PA membrane retained 60% of its initial flux after 10h of fouling, whilst the Z-SWNT/PA membrane retained 70% of its initial flux. After the DI-water cleaning procedure, the PA membrane flux returned to a value of 69% of the initial flux, whereas the Z-SWNT/PA membrane flux returned to 100% of the initial flux. The observed water flux in the Z-SWNT/PA membrane after cleaning was slightly higher than the initial flux, and this is attributed to a slight drift in the feed temperature and applied transmembrane pressure. Although both PA and Z-SWNT/PA membranes lost 30-40% of their initial flux due to surface fouling, the recovery of flux in the Z-SWNT/PA membrane indicates that BSA is only weakly adsorbed and is easily removed. This result agrees with reports that surfaces functionalized by zwitterionic group exhibited slower flux reduction rates during fouling and high water flux recovery after washing with clean water.[37]

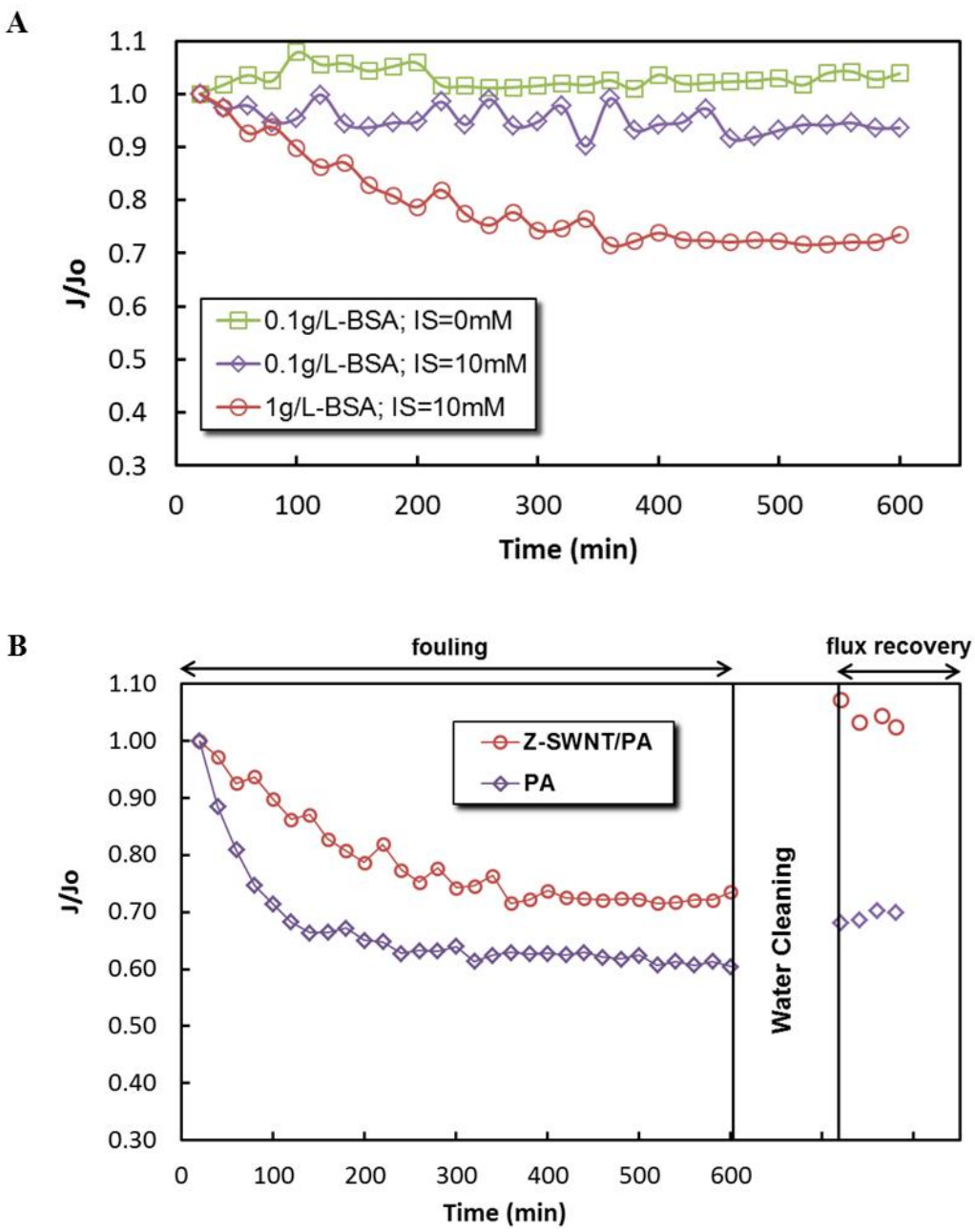


**Figure 5.11.** Normalized flux of the membranes as a function of time during BSA fouling. (A) Effect of ionic strength (IS) and BSA concentration on fouling of 20wt% Z-SWNT/PA membrane. Total ionic strength of the feed solution was adjusted by varying $Ca^{2+}$ and NaCl concentration. (B) Comparison of flux change between the control PA and nanocomposite membranes. The concentration of BSA was kept at 1g/L, and the solution pH was constantly adjusted to 4.7. AAS (100 mg/L) was added to the solution in every testing.

## 5.4. Conclusion

We have fabricated a novel nanocomposite desalination membrane using zwitterionic functionalized carbon nanotubes incorporated into a polyamide thin film composite. The semi-

aligned CNTs in the polyamide layer offer channels for fast water transport, and maintain high salt rejection due to the steric hindrance of the zwitterionic groups located at the ends of the CNTs. The mechanical stability of the polyamide matrix can be improved by increasing the degree of chemical crosslinking. In this way, nanocomposite membranes can be produced with high CNT loadings without introducing defects that lead to decreased salt rejection. The pore size distribution of the nanocomposite membrane was found to be very similar to that of a pure polymer membrane, indicating that the pores created by the functionalized CNTs in the polymer matrix have effective sizes similar to the original polyamide membrane. The flux improvement in the nanocomposite membranes is due to the reduced tortuosity and increased interconnectivity of the water transport channels created by the inclusion of CNTs. The nanocomposite membranes exhibited increased surface fouling resistance, likely due to zwitterionic groups exposed at the membrane surface interacting with the water molecules to prevent strong binding of the foulant. After washing, the nanocomposite membrane regained 100% of the original water flux, indicating that foulants were not strongly adsorbed on the hydrated surface and were easily removed when flushed with clean water. We have demonstrated that advanced materials like CNTs can be synthesized with desired functional groups, and can be embedded into traditional RO membranes to simultaneously resolve the challenge of low flux and surface fouling in the current desalination process.

## 5.5. Acknowledgement

The authors would like to thank Jody Smiley for her help in the AAS and TOC measurements. We also like to acknowledge Dr. Karl Johnson from the Department of Chemical and Petroleum Engineering at University of Pittsburgh for his writing assistance and proof reading of this article. We gratefully appreciate the Graduate School Assembly at Virginia Tech for financial support of this project.

## References

(1) Lee, K. P.; Arnot, T. C.; Mattia, D. A Review of Reverse Osmosis Membrane Materials for desalination—Development to Date and Future Potential. *Journal of Membrane Science* **2011**, *370*, 1–22.

(2) Elimelech, M.; Phillip, W. The Future of Seawater Desalination: Energy, Technology, and the Environment. *Science* **2011**, *333*, 712–718.

(3) Mezher, T.; Fath, H.; Abbas, Z.; Khaled, A. Techno-Economic Assessment and Environmental Impacts of Desalination Technologies. *Desalination* **2011**, *266*, 263–273.

(4) Wang, J.; Dlamini, D. S.; Mishra, A. K.; Pendergast, M. T. M.; Wong, M. C. Y.; Mamba,

B. B.; Freger, V.; Verliefde, A. R. D.; Hoek, E. M. V. A Critical Review of Transport through Osmotic Membranes. *Journal of Membrane Science* **2014**, *454*, 516–537.

(5) Yin, J.; Deng, B. Polymer-Matrix Nanocomposite Membranes for Water Treatment. *Journal of Membrane Science* **2014**, *479*, 256–275.

(6) Cadotte, J. E.; Petersen, R. J.; Larson, R. E.; Erickson, E. E. A NEW THIN-FILM COMPOSITE SEAWATER REVERSE OSMOSIS MEMBRANE Advantages over Polysaccharides in Such Areas of Performance as Flux , Salt. *Desalination* **1980**, 25–31.

(7) Saleh, T. a.; Gupta, V. K. Synthesis and Characterization of Alumina Nano-Particles Polyamide Membrane with Enhanced Flux Rejection Performance. *Separation and Purification Technology* **2012**, *89*, 245–251.

(8) Kim, E. S.; Hwang, G.; Gamal El-Din, M.; Liu, Y. Development of Nanosilver and Multi-Walled Carbon Nanotubes Thin-Film Nanocomposite Membrane for Enhanced Water Treatment. *Journal of Membrane Science* **2012**, *394-395*, 37–48.

(9) Lee, S.; Kim, H.; Patel, R.; Im, S. J.; Kim, J. H.; Min, B. R. Silver Nanoparticles Immobilized on Thin Film Composite Polyamide Membrane: Characterization, Nanofiltration, Antifouling Properties. *Polymers for Advanced Technologies* **2007**, *18*, 562–568.

(10) Fornasiero, F.; Park, H. G.; Holt, J. K.; Stadermann, M.; Grigoropoulos, C. P.; Noy, A.; Bakajin, O. Ion Exclusion by Sub-2-Nm Carbon Nanotube Pores. *Proceedings of the National Academy of Sciences of the United States of America* **2008**, *105*, 17250–17255.

(11) Holt, J. K.; Park, H. G.; Wang, Y.; Stadermann, M.; Artyukhin, A. B.; Grigoropoulos, C. P.; Noy, A.; Bakajin, O. Fast Mass Transport through Sub-2-Nanometer Carbon Nanotubes. *Science (New York, N.Y.)* **2006**, *312*, 1034–1037.

(12) Holt, J. K. Carbon Nanotubes and Nanofluidic Transport. *Advanced Materials* **2009**, *21*, 3542–3550.

(13) Kalra, A.; Garde, S.; Hummer, G. Osmotic Water Transport through Carbon Nanotube Membranes. *Proceedings of the National Academy of Sciences of the United States of America* **2003**, *100*, 10175–10180.

(14) Corry, B. Designing Carbon Nanotube Membranes for Efficient Water Desalination. *Journal of Physical Chemistry B* **2008**, *112*, 1427–1434.

(15) Song, C.; Corry, B. Intrinsic Ion Selectivity of Narrow Hydrophobic Pores. *The Journal of Physical Chemistry B* **2009**, *113*, 7642–7649.

(16) Corry, B. Water and Ion Transport through Functionalised Carbon Nanotubes: Implications for Desalination Technology. *Energy & Environmental Science* **2011**, *4*, 751.

(17) Chan, W.-F.; Chen, H.; Surapathi, A.; Taylor, M. G.; Shao, X.; Marand, E.; Johnson, J. K. Zwitterion Functionalized Carbon Nanotube/polyamide Nanocomposite Membranes for Water Desalination. *ACS Nano* **2013**, *7*, 5308–5319.

(18) Kim, H.; Choi, K.; Baek, Y.; Kim, D. High-Performance Reverse Osmosis CNT/Polyamide Nanocomposite Membrane by Controlled Interfacial Interactions. *ACS applied materials & interfaces* **2014**, 2819–2829.

(19) Ma, H.; Yoon, K.; Rong, L.; Shokralla, M.; Kopot, A.; Wang, X.; Fang, D.; Hsiao, B. S.;

Chu, B. Thin-Film Nanofibrous Composite Ultrafiltration Membranes Based on Polyvinyl Alcohol Barrier Layer Containing Directional Water Channels. *Industrial and Engineering Chemistry Research* **2010**, *49*, 11978–11984.

(20) Kim, S.; Fornasiero, F.; Park, H. G.; In, J. Bin; Meshot, E.; Giraldo, G.; Stadermann, M.; Fireman, M.; Shan, J.; Grigoropoulos, C. P.; *et al.* Fabrication of Flexible, Aligned Carbon Nanotube/polymer Composite Membranes by in-Situ Polymerization. *Journal of Membrane Science* **2014**, *460*, 91–98.

(21) Majumder, M.; Chopra, N.; Hinds, B. J. Mass Transport through Carbon Nanotube Membranes in Three Different Regimes: Ionic Diffusion and Gas and Liquid Flow. *ACS nano* **2011**, *5*, 3867–3877.

(22) Skoulidas, A. I.; Ackerman, D. M.; Johnson, J. K.; Sholl, D. S. Rapid Transport of Gases in Carbon Nanotubes. *Physical Review Letters* **2002**, *89*, 185901.

(23) Park, J.; Choi, W.; Kim, S. H.; Chun, B. H.; Bang, J.; Lee, K. B. Enhancement of Chlorine Resistance in Carbon Nanotube Based Nanocomposite Reverse Osmosis Membranes. *Desalination and Water Treatment* **2010**, *15*, 198–204.

(24) Rana, D.; Kim, Y.; Matsuura, T.; Arafat, H. A. Development of Antifouling Thin-Film-Composite Membranes for Seawater Desalination. *Journal of Membrane Science* **2011**, *367*, 110–118.

(25) Jadav, G. L.; Singh, P. S. Synthesis of Novel Silica-Polyamide Nanocomposite Membrane with Enhanced Properties. *Journal of Membrane Science* **2009**, *328*, 257–267.

(26) Lind, M.; Jeong, B. Effect of Mobile Cation on Zeolite-Polyamide Thin Film Nanocomposite Membranes. *Journal of Materials …* **2009**.

(27) Zhang, L.; Shi, G.-Z.; Qiu, S.; Cheng, L.-H.; Chen, H.-L. Preparation of High-Flux Thin Film Nanocomposite Reverse Osmosis Membranes by Incorporating Functionalized Multi-Walled Carbon Nanotubes. *Desalination and Water Treatment* **2011**, *34*, 19–24.

(28) Kim, S.; Kwak, S.; Suzuki, T. Positron Annihilation Spectroscopic Evidence to Demonstrate the Flux-Enhancement Mechanism in Morphology-Controlled Thin-Film-Composite (TFC) Membrane. *Environmental science & technology* **2005**, *39*, 1764–1770.

(29) Xie, W.; Geise, G. M.; Freeman, B. D.; Lee, H.-S.; Byun, G.; McGrath, J. E. Polyamide Interfacial Composite Membranes Prepared from M-Phenylene Diamine, Trimesoyl Chloride and a New Disulfonated Diamine. *Journal of Membrane Science* **2012**.

(30) de Lannoy, C.-F.; Jassby, D.; Gloe, K.; Gordon, A. D.; Wiesner, M. R. Aquatic Biofouling Prevention by Electrically Charged Nanocomposite Polymer Thin Film Membranes. *Environmental science & technology* **2013**.

(31) HOEK, E.; YAN, Y.; JEONG, B. NANOCOMPOSITE MEMBRANES AND METHODS OF MAKING AND USING SAME. *WO Patent 2,006,098,872* **2006**, *1*.

(32) Lind, M. L.; Ghosh, A. K.; Jawor, A.; Huang, X.; Hou, W.; Yang, Y.; Hoek, E. M. V. Influence of Zeolite Crystal Size on Zeolite-Polyamide Thin Film Nanocomposite Membranes. *Langmuir : the ACS journal of surfaces and colloids* **2009**, *25*, 10139–10145.

(33) Lee, H. S.; Im, S. J.; Kim, J. H.; Kim, H. J.; Kim, J. P.; Min, B. R. Polyamide Thin-Film Nanofiltration Membranes Containing TiO2 Nanoparticles. *Desalination* **2008**, *219*, 48–

56.

(34) Duan, J.; Litwiller, E.; Pinnau, I. Preparation and Water Desalination Properties of POSS-Polyamide Nanocomposite Reverse Osmosis Membranes. *Journal of Membrane Science* **2015**, *473*, 157–164.

(35) Cheng, G.; Li, G.; Xue, H.; Chen, S.; Bryers, J. D.; Jiang, S. Zwitterionic Carboxybetaine Polymer Surfaces and Their Resistance to Long-Term Biofilm Formation. *Biomaterials* **2009**, *30*, 5234–5240.

(36) Jiang, S.; Cao, Z. Ultralow-Fouling, Functionalizable, and Hydrolyzable Zwitterionic Materials and Their Derivatives for Biological Applications. *Advanced Materials* **2010**.

(37) Azari, S.; Zou, L. Using Zwitterionic Amino Acid L-DOPA to Modify the Surface of Thin Film Composite Polyamide Reverse Osmosis Membranes to Increase Their Fouling Resistance. *Journal of Membrane Science* **2012**, *401-402*, 68–75.

(38) Nano Lab Inc.,179 Bear Hill Road, Waltham, MA 02451.

(39) Surapathi, A.; Chen, H.; Marand, E.; Karl Johnson, J.; Sedlakova, Z. Gas Sorption Properties of Zwitterion-Functionalized Carbon Nanotubes. *Journal of Membrane Science* **2013**, *429*, 88–94.

(40) Zhang, Z.; Chen, S.; Jiang, S. Dual-Functional Biomimetic Materials: Nonfouling Poly(carboxybetaine) with Active Functional Groups for Protein Immobilization. *Biomacromolecules* **2006**, *7*, 3311–3315.

(41) Surapathi, A.; Chen, H.; Marand, E.; Karl Johnson, J.; Sedlakova, Z. Gas Sorption Properties of Zwitterion-Functionalized Carbon Nanotubes. *Journal of Membrane Science* **2013**, *429*, 88–94.

(42) Ghosh, A. K.; Hoek, E. M. V. Impacts of Support Membrane Structure and Chemistry on Polyamide–polysulfone Interfacial Composite Membranes. *Journal of Membrane Science* **2009**, *336*, 140–148.

(43) Saha, N. K.; Joshi, S. V. Performance Evaluation of Thin Film Composite Polyamide Nanofiltration Membrane with Variation in Monomer Type. *Journal of Membrane Science* **2009**, *342*, 60–69.

(44) Kong, C.; Kanezashi, M.; Yamomoto, T.; Shintani, T.; Tsuru, T. Controlled Synthesis of High Performance Polyamide Membrane with Thin Dense Layer for Water Desalination. *Journal of Membrane Science* **2010**, *362*, 76–80.

(45) Kim, S.; Jinschek, J. R.; Chen, H.; Sholl, D. S.; Marand, E. Scalable Fabrication of Carbon Nanotube/Polymer Nanocomposite Membranes for High Flux Gas Transport. *Nano Letters* **2007**, *7*, 2806–2811.

(46) Otero, J. a.; Mazarrasa, O.; Villasante, J.; Silva, V.; Prádanos, P.; Calvo, J. I.; Hernández, a. Three Independent Ways to Obtain Information on Pore Size Distributions of Nanofiltration Membranes. *Journal of Membrane Science* **2008**, *309*, 17–27.

(47) Ang, W.; Elimelech, M. Protein (BSA) Fouling of Reverse Osmosis Membranes: Implications for Wastewater Reclamation. *Journal of Membrane Science* **2007**, *296*, 83–92.

(48) Petersen, R. J.; Cadotte, J. E. Thin Film Composite Reverse Osmosis Membranes.

*Handbook of Industrial Membrane Technology* **1990**, 307–348.

(49) Ahmad, a; Ooi, B. Properties–performance of Thin Film Composites Membrane: Study on Trimesoyl Chloride Content and Polymerization Time. *Journal of Membrane Science* **2005**, *255*, 67–77.

(50) Nightingale, E. R. Phenomenological Theory of Ion Solvation. Effective Radii of Hydrated Ions. *The Journal of Physical Chemistry* **1959**, *63*, 1381–1387.

(51) Turgman-Cohen, S.; Araque, J. C.; Hoek, E. M. V; Escobedo, F. a. Molecular Dynamics of Equilibrium and Pressure-Driven Transport Properties of Water through LTA-Type Zeolites. *Langmuir* **2013**, *29*, 12389–12399.

(52) Cay-Durgun, P.; Fink, S. G.; Shabilla, A.; Yin, H.; Sasaki, K. a.; Lind, M. L. Analysis of the Water Permeability of Linde Type A Zeolites in Reverse Osmosis. *Separation Science and Technology* **2014**, *49*, 2824–2833.

(53) Košutić, K.; Kaštelan-Kunst, L.; Kunst, B. Porosity of Some Commercial Reverse Osmosis and Nanofiltration Polyamide Thin-Film Composite Membranes. *Journal of Membrane Science* **2000**, *168*, 101–108.

(54) Chan, K.; Liu, T. Effect of Shrinkage on Pore Size and Pore Size Distribution of Cellulose Acetate Reverse Osmosis Membranes. *Industrial & Engineering Chemistry …* **1984**, 124–133.

(55) Wang, X.; Fang, D.; Hsiao, B. S.; Chu, B. Nanofiltration Membranes Based on Thin-Film Nanofibrous Composites. *Journal of Membrane Science* **2014**, *469*, 188–197.

(56) Hadidi, M.; Zydney, A. L. *Fouling Behavior of Zwitterionic Membranes: Impact of Electrostatic and Hydrophobic Interactions*; Elsevier, 2013.

# Chapter 6. Guidelines of the Fabrication Procedure for Thin-Film Nanocomposite Membranes

Many parameters need to be considered when fabricating a thin-film composite membrane by interfacial polymerization (IP), including the concentration of reactants, partition coefficients of the reactants, reactivity ratios where blends of reactants are employed, solubility of nascent polymer in the solvent phase, the overall kinetics and diffusion rates of the reactants, presence of by-products, hydrolysis, cross linking and post treatment.[1] A fraction of recipes from the literature are shown in Table 6.1, including the choices of monomer, the pH condition of the aqueous phase, the organic solvent, the contact time, and thermal treatments. These are varied depending on the application being pursued.

**Table 6.1.** Choices of monomers, crosslinking agent, and fabrication methods from different literatures. The numbers shown at the first column refer to its reference number.

| | **Monomer solution** | **Crosslinking agent solution** | **Solvent (Aqueous / Organic)** | **Aqueous solution removal method** | **Contact time (Monomer / Crosslinker)** | **Cure time and temperature** |
|---|---|---|---|---|---|---|
| 2 | MPD [2wt%]<br>TEA [3wt%]<br>CSA [4wt%] | IPC [0.1~0.33%]<br>ICIC [0~0.66%] | Water / IP1016 | Not mentioned | 120 sec / N/A | 10 min & 70~80°C |
| 3 | Piperazine [5% w/v] | TMC [0.1% w/v] | Water / Hexane | Air Drying [5 min] | 120 sec / 90 sec | 5 min & 80°C |
| | 3,5-diamino benzoic acid [1%, w/v] | TMC [0.1% w/v] | | | | |
| | MPD [0.9%]<br>Piperazine [0.1%] | IPC [0.7% w/v]<br>TMC [0.3% w/v] | | | | |
| 4 | MPD [2wt%]<br>TEA [2wt%]<br>CSA [4wt%] | TMC [0.1%] | Water / Hexane | Air Knife with pressure 5-7 psi | 15 sec / 15 sec | 10 min & 68°C |
| 5 | MPD [1.5% w/v] | TMC [0.05% w/v] | Water / N-dodecane | Rubber Roller; Roll across surface one time | 5 min / 1 min | In air 10 min & 80°C **or** In boiling water for 10 min |

MPD: m--phenylenediamine
TEA: triethylamine
CSA: (+)-10-camphor sulfonic acid
ICIC: 5-isocyanato-isophthaloyal chloride
IPC: isophthaloyal chloride
TMC: Trimesoyl chloride
IP1016: isoparaphin type hydrocarbon oil

The formation mechanism of Polyamide (PA) thin films by IP can be explained by the work of Freger[6] on PA film formation kinetics and Nadler and Srebnik[7] on molecular simulation of PA synthesis. The PA film formation takes place in three steps: incipient film formation - a fast process, followed by slow polymerization depending upon the permeability of diamine through the incipient film, and finally a diffusion controlled process. In the initial stage, an incipient thin film is formed at the organic side of the interface, and acts as a barrier layer controlling the separation characteristics of the thin film and divides the film into two regions. Each region is rich in one type of monomer and end group. In the diffusion controlled step, film growth takes place until the monomers diffusing through the film get consumed by other monomers and/or unreacted functional groups of the film.[7]

In the past decades, many studies have been devoted to improving the polyamide (PA) skin layer by using different recipes in order to increase the water permeation flux and membrane stability without sacrificing the salt rejection. Most of the work focused on reducing the thickness of the membrane or modifying the surface morphology and properties, such as grafting hydrophilic polymers on the membrane surface, changing the surface roughness using different solvents, terminating reactive functional groups, and even introducing electric-fields to improve anti-biofouling properties.[8–10] However, unlike traditional RO membranes, our approach is dedicated to adding inorganic components with excellent transport and separation properties into the polymer matrix. Our study found that the approach should be substantially different than previously reported methods in order to produce a durable, high-quality Z-SWNT nanocomposite membrane. Instead of making a thinner, highly-permeable PA matrix, we have to make sure that the skin layer is thick and strong enough to maintain the alignment/ position of CNTs, while minimizing any defects created by the incompatibility of the organic polymer chains and the inorganic CNTs' wall. The factors described in the following sections were systemically studied during Z-SWNT/PA membrane fabrication and can be considered as guidelines for future nanocomposite membrane fabrication using a PA polymer matrix.

## 6.1. pH Condition of Aqueous Solution (MPD Solution)

Triethylamine (TEA) or sodium hydroxide (NaOH) is commonly used as an acid acceptor in amide formation for neutralizing the by-product of hydrochloric acid (HCl) formed during the polymerization. When using Piperazine (PIP) as the diamine monomer it is usually necessary to

include an acid acceptor to neutralize the hydrochloric acid. This is not necessary when using MPD since it is a much weaker base than PIP and is used in a higher excess concentration so that excess MPD serves as its own acid acceptor. Surfactant is commonly added into the aqueous solution as an acid acceptor as well, but Cadotte argues that it did not appear to provide any advantage in the context of invention and it is preferred not to add any surfactant for the purpose of neutralizing the by-product.[11] Surfactant, however, helps the wetting and thus ensures even coverage of PA on the PS support. The effect of the addition of acid acceptor to PA formation was studied by Saha and Joshi,[3] who added 0.9% (w/v) sodium hydroxide to 1% diamine solution (Piperazine) and the resultant PIP-TMC membrane was found to have 14% higher permeation flux compared to the membrane prepared without any acid acceptor, while the sodium chloride rejection remained almost unchanged. In the absence of an acid acceptor, the diamine itself will become the acceptor and thus reduce the polymer yield. On the other hand, (+)-10-camphor sulfonic acid (CSA) or sulfonic acid (shown in Table 6.1) is used in creating acidic conditions in aqueous solution. Adjusting the pH of the aqueous solution to around 8.5 allows better absorption of acid chloride. The addition of CSA is also believed to help protect the microporous skin layer of the support membrane from annealing during thermal curing.

Hoek *et al.* added 4wt% of CSA and 2wt% of triethylamine (TEA) in the MPD solution, and produced polyamide layers with thickness roughly 200 nm and salt rejection as high as 95%.[4] Using the same protocol, I was able to replicate the process and the resultant membrane had a permeation flux of 14.0 LMH (liter per $m^2$ per hour) and salt rejection of 98.1% under the applied pressure of 250 psi. However, when the same procedure was applied in fabricating Z-SWNTs-embedded PA membrane, the salt rejection decreased drastically from 98% down to ~50% whereas the permeation flux increased more than three-fold (shown in Figure 5.7). This demonstrated that the thin skin layer underwent a severe mechanical failure when Z-SWNTs were added. Ahmad *et al.*[12] shows that increasing the concentration of TEA could increase the thickness of PA whereas the pore radius would not be affected. They also show that acidic aqueous conditions can slow down the reaction of interfacial polymerization, which resulted in reduced thickness but increased pore size. However, the skin layer produced was severely compacted and exhibited mechanical strength issues. Their study agreed with our result, in which an aqueous solution containing 4wt% CSA and acidic condition resulted in a thin skin layer during IP. Due to the poor mechanical strength, this thin layer was not able to embed high concentrations of carbon nanotubes and lost

salt rejection ability under increasing pressure across the membrane. Independent study in terms of the change of pH in aqueous solution was conducted in order to verify the change of membrane thickness in terms of the pH condition. The results are shown in the Figure 6.1. The thickness of polyamide exhibited a linear decrease as the concentration of CSA increased.

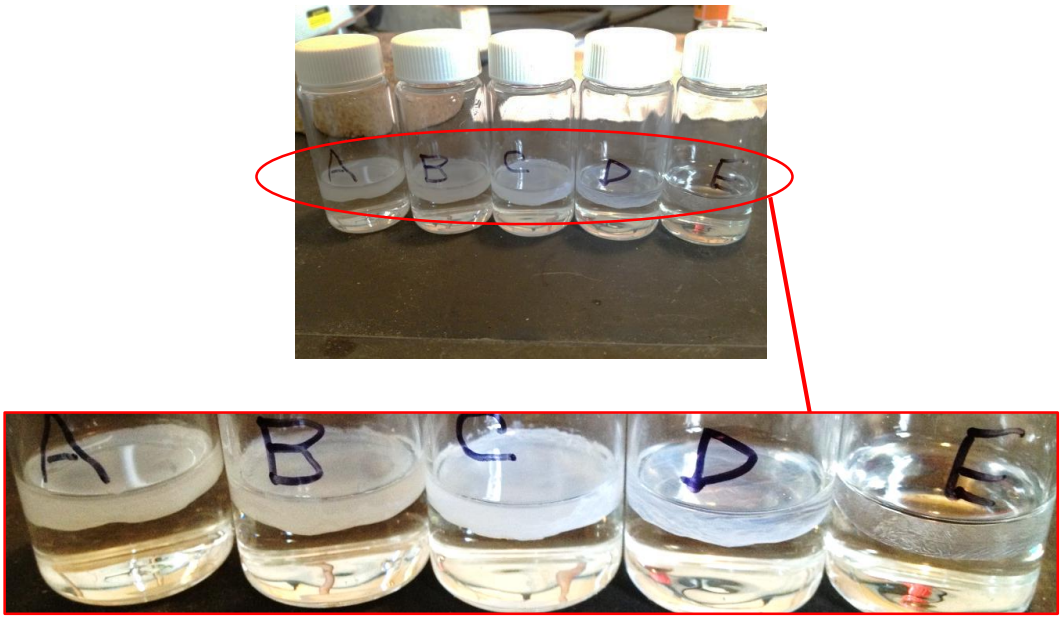


| A | B | C | D | E |
|---|---|---|---|---|
| 2wt% TEA<br>2wt% MPD | 2wt% TEA<br>0.5wt% CSA<br>2wt% MPD | 2wt% TEA<br>1wt% CSA<br>2wt% MPD | 2wt% TEA<br>2wt% CSA<br>2wt% MPD | 2wt% TEA<br>4wt% CSA<br>2wt% MPD |

**Figure 6.1.** Experimental study of the relationship between pH condition in monomer solution and the total thickness of the resulting interfacial polycondensed PA membrane.

Aqueous solutions in A to E (bottom layer) have come in contact with the hexane solution containing 0.05% (w/v) TMC (top layer). Under the basic conditions in solution A with 2wt% of TEA present, the PA film was thick, making the skin layer opaque. As the percentage of CSA increased, the aqueous solution became less caustic, and the thickness of the PA film was reduced correspondingly. At 4wt% of CSA (solution E) the film is completely transparent, indicating that the thickness of PA film is extremely thin. Using the same condition, Hoek *et al.* [4] was able to generate membranes with thicknesses lower than 200 nm. Two other conditions of a) 2wt% MPD only and b) 2wt%-MPD only crosslinked with 0.34% (w/v) TMC were tested as well, and the results showed similar thicknesses to solution E. Without any addition of bases or acids the pH of the aqueous solution will still be relatively high due to the presence of diamine. The thickness of

the PA film did not change with increased crosslinker concentration, but its pore size was reduced significantly (See section 6.3).

In the presence of acid, amine groups in MPD were protonated and resulted in a decrease in its basicity and reactivity towards TMC. The reaction rate of crosslinking was thus slowed and resulted in a skin layer with larger pore size and weaker mechanical strength. Therefore, it is important to choose the right condition to grow the PA film in a nanocomposite membrane. An optimal thickness can offer desired strength without compromising the permeation flux. It should be noted that high acidity (pH~1.85) can cause zwitterionic CNTs to aggregate into bundles in solution, and thus decrease the dispersity of CNTs in the nanocomposite membrane, potentially lowering the separation performance.

## 6.2. The Presence of Surfactant

Adding nanoparticles or carbon nanotubes into thin film composite layers is considered challenging, since the thin PA layer has a low tolerance to impurities. Any foreign substance present in the film could potentially distort the degree of crosslinking of the polymer and lower the rejection performance, even when the quantity of embedded particles is small. Lee *et al.*[13] investigated the effect of $TiO_2$ nanoparticles added into thin film composite (TFC) membranes, and they found that the critical concentration the thin film can bear is near 5.0 wt% of $TiO_2$. If the concentration is above 5.0 wt%, the flux of the thin film nanocomposite (TFN) membrane will abruptly increase while the salt rejection decreases sharply. In their study, the salt rejection of $MgSO_4$ dropped from above 80% to below 30% when $TiO_2$ concentration increased from 5 to 9 wt%. They attributed this to the fact that the interference of $TiO_2$ nanoparticles to interfacial polymerization starts to become significant at high $TiO_2$ concentrations, leading to a lower degree of polymerization of PA. Hoek *et al.*[14] fabricated zeolite-PA TFN membrane, and have studied the composition of the membranes using XPS which showed that all the TFN membranes had lower carbon/nitrogen ratios than the corresponding controlled composite membranes. This demonstrated that fewer amide bonds were formed in TFN membranes where nanoparticles were present, leading to less crosslinking of PA during the IP. Similar to the nanoparticles, the presence of CNTs in PA thin film could result in lower polymer crosslinking.

On the other hand, the hydrophobic nature of CNT makes it incompatible with hydrophilic polyamide chains. Even though Z-SWNTs were functionalized with zwitterion groups which have

high dipole moments (10 – 20 Debye) and substantially increase the hydrophilicity of the nanotubes, the side walls of the tubes remained hydrophobic where carbon atoms dominate most of the surface area. Experimental studies showed that the presence of surfactant in the aqueous diamine solution could help the monomers to impregnate the space between SWNTs as well as the membrane support during the IP. For example, a control membrane was fabricated with the aqueous solution contained only MPD, while another membrane was created using an aqueous solution with MPD and 0.2wt% sodium dodecylbenzenesulfonate (SDBS). All other fabrication conditions, including the contact time between the two different monomers, the curing time, and the temperature, remained unchanged. The membrane produced without the addition of surfactant exhibited poor adhesion to the support layer, in which an uneven surface with tiny water bubbles appeared underneath the thin PA layer when the fresh-made Z-SWNT/PA membrane was dipped into deionized (DI) water. In contrast, the membrane produced with the SDBS-MPD solution had good adhesion and a smooth wet surface after dipping in DI water. We concluded that the hydrophobic wall of the CNTs prevents complete wetting by the MPD solution down to the base of the CNT mat (see Figure 6.2A), which caused the polyamide matrix to grow from midway up the mat of CNTs instead of in between the SWNTs. Therefore, when the membrane was dipped in water, the thin PA layer detached from the nanotubes because the empty space under the skin layer filled with water. In the presence of SDBS (Figure 6.2B), the SWNT mat was fully impregnated by the MPD solution, allowing a continuous PA layer to grow from the bottom of the nanotubes up to the surface.

A control study was conducted separately using pristine SWNTs (end-capped unfunctionalized) embedded in a PA thin film. The aqueous solution contained the same amount of surfactant (0.2wt% SDBS) and the resulting membrane appeared to have a smooth surface after washing in DI water. However, the salt rejection dropped approximately 10% compared to the Z-SWNTs/PA membrane at the same embedded nanotube concentration. We attribute this to the formation of nanochannels around the SWNTs.[15] Even though the surfactant helped the polymerization grow continuously from the bottom to the top, the nonfunctional hydrophobic walls of CNTs have very poor adhesion with the polymer. This leads to the formation of empty voids not at the bottom of the membrane layer, but around the nanotubes themselves. It is these nanovoids that allow fast passage of salt ions through the membrane, resulting in lower salt rejection.

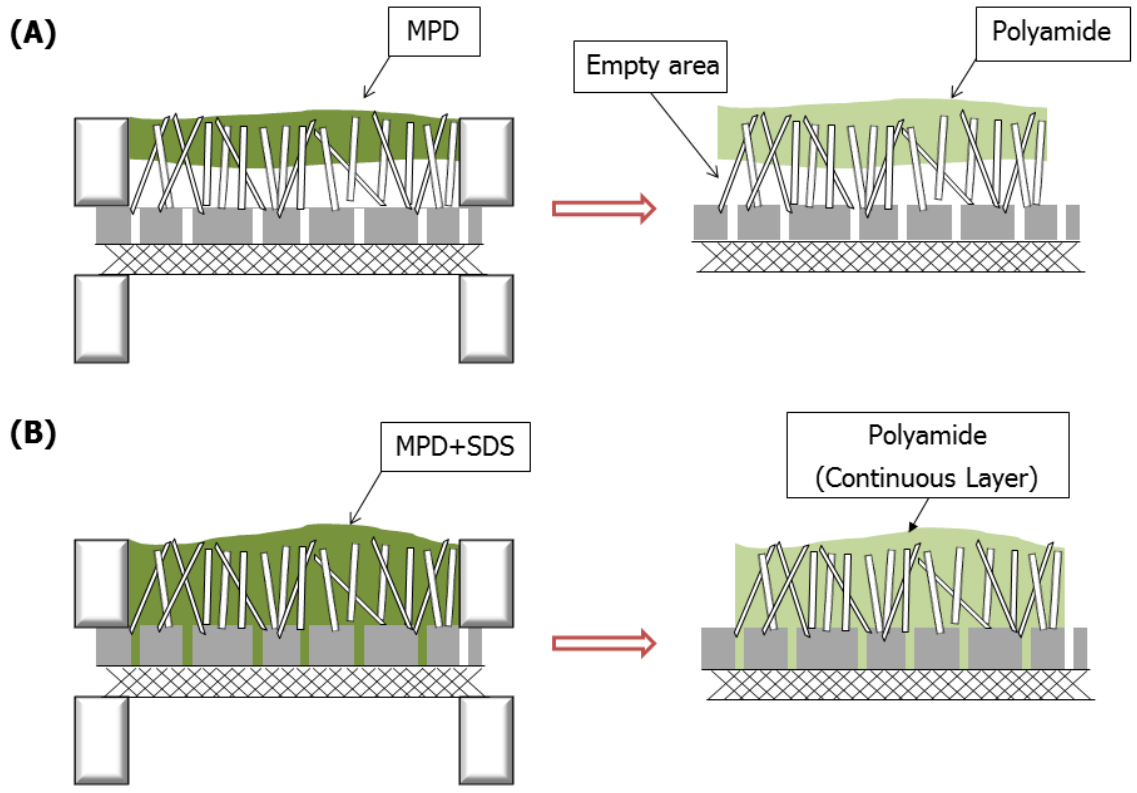


**Figure 6.2.** The schematics of interfacial polymerization with the aqueous solution of (A) monomer of MPD only and (B) monomer with surfactant. The function of surfactant helps the aqueous solution to penetrate through the inner area of CNT bundles.

The presence of surfactant, however, may affect the crosslinking of the polyamide during the interfacial polymerization. Lind *et al.*[16] studied the influence of surfactant molecules on the PA chains and have proposed a mechanism, illustrated in Figure 6.3, based on the hydrogen-bond induced hydration of polyamide in the presence of SDS and water molecules. Amide groups on PA contain electronegative atoms of O and N which hydrogen bond with amide groups in adjacent polyamide chains in an amorphous domain. However, oxygen atoms on the sulfone groups of SDS and the water molecules can also act as hydrogen-bond acceptor and donor sites and can break the inter-chain hydrogen bonds by forming intermolecular H-bonds with the amide groups. A new equilibrium will then exist between the chain-chain, amide-SDS, and amide-$H_2O$ H-bonds resulting in a plasticization of the membrane due to weakening of the chain-chain H-bonding. This allows the chain segments to slip and open the network structure. Moreover, small ions in water can either stabilize or destabilize H-bonding through ionic hydration. In the circumstance of using

SDS as a wetting agent, the presence of salt ions could cause swelling of the polar polyamide skin layer by stabilization and destabilization of hydrogen-bond induced hydration.

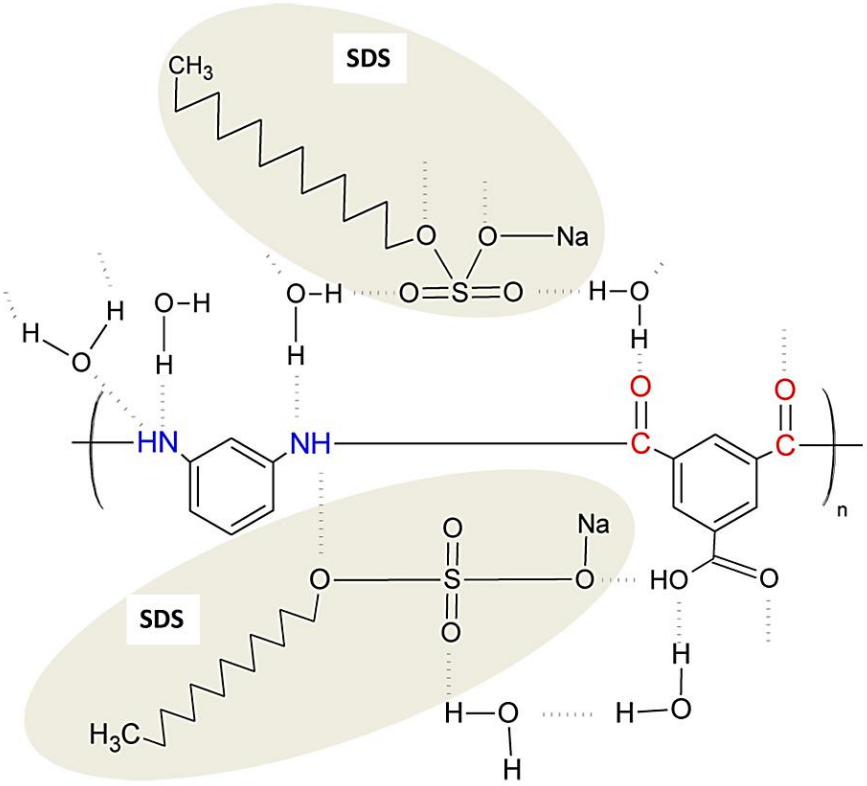


**Figure 6.3.** Illustration of a possible arrangement of hydrogen-bonding hydration (dotted lines) of polyamide in the presence of sodium dodecyl sulfate (shaded areas). Copyright 2011. Reprint with permission from Elsevier Ltd.

## 6.3. Concentration Trade-off between TMC and Z-SWNTs

The overall goal for our study is to increase the water permeation flux without lowering the salt rejection of the membrane. Studies reported in the literature are often aimed at making thinner membranes to obtain higher fluxes. However, in fabricating a nanocomposite membrane, the integrity and stability of the polymer matrix should be the primary concern. This can be characterized by the quantity of nanoparticles the skin layer can contain without membrane failure (e.g. pin holes, cracking, compaction and decreases in mechanical strength). By increasing the concentration of TMC, the crosslinking agent, the density of the PA layer increased and a tough, durable polymer matrix formed around CNTs. Therefore, when high pressure was applied across the membrane, embedded Z-SWNTs are held in position firmly and operate as expected to filter water molecules from salt ions. Nevertheless, this approach reduces the pore size of the skin layer and slows down the diffusion speed of water molecules within the polymer matrix, decreasing the

speed at which they reach the tips of the SWNTs. In contrast, decreasing the density of the PA layer (lower TMC concentration) expands the pores in the matrix and allows waters to have higher diffusion rates, but results in a skin layer that is too weak to allow the inclusion of nanoparticles, and eventually results in the formation of pin holes and cracking inside the skin layer.

As discussed in Chapter 5, Figure 5.7 clearly shows the trade-off between the density of skin layer and the embeddability of Z-SWNTs. In this study, all the data were obtained under an applied pressure at 350 psi, and with a feed solution containing 2000 ppm of NaCl. When there are no Z-SWNTs embedded in the film, lower concentrations of TMC lead to higher permeation fluxes and high salt rejection due to the reduced thickness of the barrier PA layer and loose polymer chains. However, when Z-SWNTs were added to this low-crosslink density film, the rejection dropped down drastically, indicating that this loose skin layer cannot embed nanotubes. On the other hand, higher concentrations of TMC can lead to denser skin layers and thus higher embeddability for CNTs. When the concentration of TMC increased up to 0.34 (v/v)%, the skin layer was able to embed Z-SWNTs up to 26 wt% without significant loss in salt rejection. Among all the TFN membranes, we found the optimal condition to be at 0.34 (w/v)% of TMC and 26 wt% of Z-SWNTs, where the water flux was the fastest at 36.2 LMH and the salt rejection was above 98%. Facing this trade-off, our suggestion for the pursuit of better membranes is to create a highly durable PA layer which can possibly withhold up to 40 wt% of Z-SWNTs. The skin layer itself may become essentially non-permeable, but would offer promising embeddability.

## 6.4. MPD Soaking Time, Removal Methods and IP Contact Time

During the interfacial polymerization, the microporous ultrafiltration (UF) support is first dipped into the MPD solution for a fixed period of time. The pores on the support are completely filled and then came in contact with the hexane solution containing TMC. It is believed that the IP happens within the pores and the polymerization proceeds in the organic phase near the interface, due to the low solubility of acid chloride in water and relatively good solubility of amines in the organic phase. Polyamide thus forms in the hexane solution, crosslinks and pushes outward to the surface. Polyamide from each pore continues to crosslink outside the pores and connects together at the surface, eventually forming a continuous layer. In our TFN fabrication, we separate this polymerization into three steps, which includes the soaking of MPD into the support and the inner

spaces between CNTs, the removal of excess MPD solution, and finally the contact between MPD inside the CNT array and support pores, and TMC in the organic solvent.

### 6.4.1. MPD soaking time

As seen in Table 6.1, Hoek *et al.*[4] suggests only 15 seconds of MPD soaking time for the support microporous layer to be completely impregnated, while Freeman and McGrath's group[5] preferred longer soaking times (5 minutes). Both of their results showed excellent salt rejection with fast permeation flux. Based on our experience, with the presence of CNTs on the support it will require at least 2 minutes of soaking time in order to penetrate through the entire array and pores on the support. Inadequate soaking time will result in a membrane similar to the case in section 0, where the PA layer forms only at the shallow surface instead of continuous growth from the bottom up top.

### 6.4.2. MPD removal

The reason to have a procedure for removing the excess MPD solution from the support is to make sure that PA grows from the substrate's pores, and to avoid any unwanted polymer formation at the interface between water droplets outside the substrate pores and the hexane solution. If PA starts to form far away from the pores, the resulting film will float on top of a layer of water, and collapse to the substrate surface after the water layer is dried. This would drastically decrease the adhesion between the thin film and the substrate, and creates problems similar to the case discussed in section 6.2. Three common methods for removing the excess MPD solution were shown in Table 6.1, namely the air-drying, air-knife and rolling methods. Air-drying of MPD solution requires relatively long times (5 minutes) and the drying speed can be dependent to the humidity in the atmosphere. In our case, we found that the exact drying time for MPD soaked in CNTs' arrays is very hard to determine, because the array is randomly packed with hydrophilic (functional groups) and hydrophobic (CNT walls) voids, which leads to uneven drying at different location in the CNT mat. The resulting TFN membranes exhibited varied performance from batch to batch even though the drying time and fabrication process were identical. This is due to non-uniform crosslinking when part of the CNT mat may have been too dry allow effective crosslinking, while other spots were too wet to insure polymer chains grew near the CNTs' surface instead of at the interface between the water layers and the organic solution. Similar issues were also found when using an air-knife as the drying method. The rolling method was found to be the best way

for removing MPD solution uniformly from the CNT array. Instead of using a rubber-roller as seen in the last example in Table 6.1, we used a clean glass tube as the roller, which prevented CNTs attaching to the roller peeling off the support. This method squeezes the impregnated membrane by rolling over the surface of the CNT array and efficiently removes the MPD as well as any air-bubbles trapped inside the arrays. The resulting membrane showed high salt rejection and good reproducibility.

### 6.4.3. IP contact time

When MPD is contacted with TMC at the organic-inorganic interface, the film forms very quickly and continues to grow for several seconds. The film growth rate increases until diffusion of MPD through the film starts to be limited.[17] The rate of polymer production depends mainly on the solvent, monomer concentration and interfacial area available for reaction. The change of each of these parameters can subsequently affect the contact time of the MPD-TMC required for a complete polymerization. Tsuru *et al.*[10] investigated the relationship between the contact time and the salt rejection, and showed that a minimum of 25 seconds is required to produce a PA membrane with NaCl rejection higher than 90%. Rejection reached their highest values (~98%) when the contact time was between 50 and 60 seconds. Longer contact times may be required when a co-solvent (e.g. acetone, DMSO) is present in the hexane solution. The water-organic miscibility is increased by the co-solvent and may cause hydrolysis of acid chlorides or de-protonation of amines, thereby reducing their reactivity and the extent of crosslinking[18]. For the fabrication of TFN membranes, we suggest allowing 90 seconds of contact time to insure complete crosslinking. Longer contact times eliminate any undesired voids and produce a dense and durable PA film that favors the embeddability of CNTs, as mentioned in section 6.3. Anytime longer than 90 seconds is not required, because experimental studies suggest that it would have no change on the membrane's effective pore size and film thickness.

## 6.5. Other Conditions

### 6.5.1. Pretreatment of the support

A survey of the RO membrane fabrication shows that some researchers prefer making their own UF support membranes by dissolving either polysulfone (PSf) or polyethersulfone (PES) in organic solvents such as N-methyl pyrrolidone (NMP) or N,N-dimethylformamide (DMF), and casting them on a non-woven fabric.[3,4,13] A self-cast membrane usually involves post-treatment in

surfactant solution which helps to remove solvent and increases the surface hydrophilicity. Some membrane fabrication was also done on commercial UF membranes purchased from filtration companies.[5,10,19] In this case, there is a danger that the membranes are refrigerated before shipment and the pores may shrink during the shipping process. A pretreatment is then required for pore cleansing, leftover solvent removal and improvement of soakage properties. Zhao *et al.*[19] dipped their support membranes in SDS solution for at least 48 hours before IP, and Freeman *et al.*[5] immersed their support in DI water overnight. For our Z-SWNT/PA membrane, we purchased the support membrane from Trisep© Co. (Goleta, CA) and soaked them in a 0.5wt% SDBS solution for two days before TFC fabrication. The soaked support has significant improvement in water permeation, which greatly improved the deposition speed of CNTs on top of the support when using the high-vacuum filtration method. However, surfactant presented in the support will contact the back side of the PA layer and may contribute to plasticization. The PA layer is not a symmetric dense film but instead a non-uniform distribution of crosslink density in the polyamide bulk. The backside of the PA layer likely has lower density, and thus, enables deeper penetration of the surfactant. Therefore, plasticization effects that are exacerbated by salt ions may be enhanced and cause a more severe swelling problem for the membrane.

### 6.5.2. Heat curing

Most studies of the MPD–TMC thin film indicate that curing is a necessary step to stabilize polyamide thin films.[20,21] Studies also found that thermally cured polyamide TFC membranes usually exhibited higher salt rejection than untreated analogs.[5,18,22] Heat curing is used after film formation to remove residual inorganic and organic solvents from the film and to promote additional crosslinking. The fresh made film is usually placed in an air-circulating oven at temperatures ranging from 50 to 80˚C, or washed by boiling water at 100 ˚C. Increasing the curing time or temperature could cause a reduction in porosity of the PA film by crosslinking, and thus increase the salt rejection. However, exposure to high curing temperatures or long curing times can potentially damage the microporous layer of the UF support, which tends to decrease both water flux and salt rejection.[22] In our study, the TFN membrane was placed in an air-circulating oven at 68˚C and cured for 5 minutes. Heat-curing turned the surface of the membrane a shiny dark purple color under reflected light, rather than the natural black of the CNTs. This indicates a uniform transparent PA film formed on the surface.

### 6.5.3. Adhesion to Polysulfone Membrane

Bui *et al.*[16] suggest that the –COCl functional groups in TMC (crosslinking agent) play an important role in improving the adhesion of the PA thin film with the polysulfone support. During the IP, some of the –COCl groups do not take part in the cross-linking process. The C–Cl bond in the carbonyl groups is very weak due to the polar distribution of electrons in the structure of TMC. Therefore, it tends to be broken to form a $Cl^-$ ion and an electrophile having a positively charged carbon site. This electrophile can attract an electron-rich group like –OH to form a carboxylic structure via a hydrolysis mechanism. It may also attack the electron-rich aromatic ring in the bisphenol-A moiety of polysulfone. As a result, the electrophile will replace a hydrogen atom at the ortho site of the aromatic ring via the electrophilic aromatic substitution mechanism or, more specifically, the Friedel–Crafts acylation mechanism.

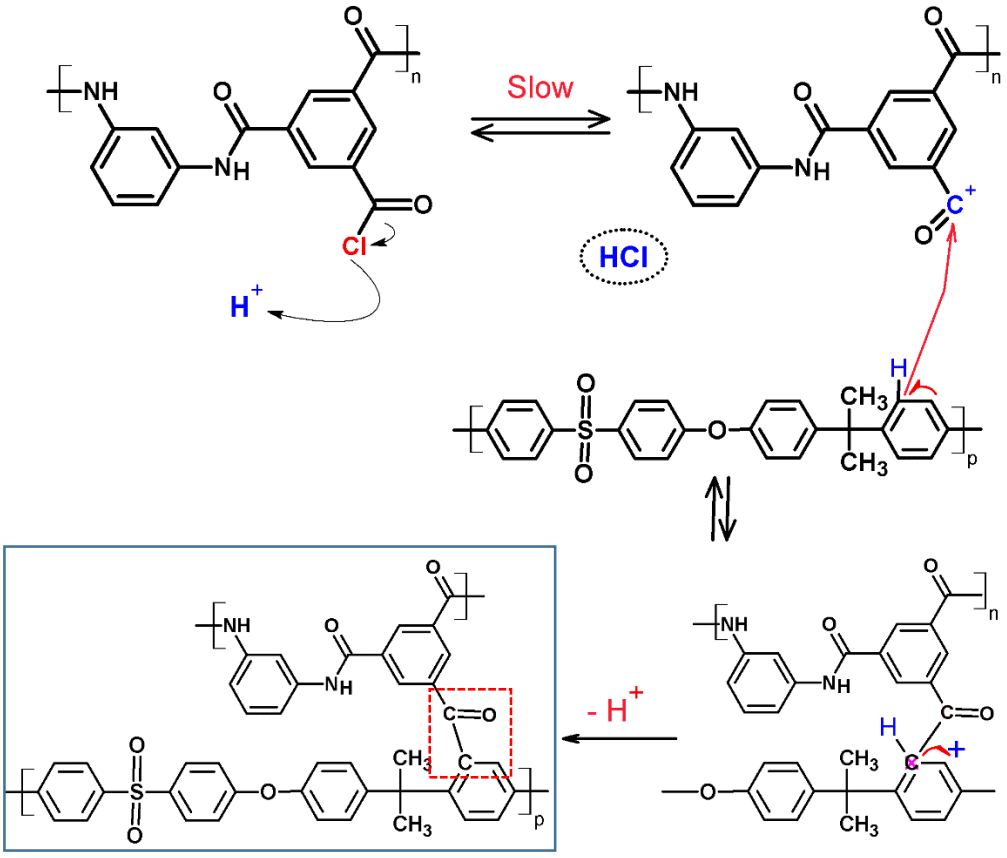


**Figure 6.4.** Diagram of the Friedel-Crafts acylations between unreacted –COCl groups on the polyamide chains and the polysulfone support.

The mechanism, depicted in Figure 6.4, is catalyzed by the presence of hydrochloric acid formed as a by-product of the interfacial polymerization. The hypothesized crosslinking

interaction may not happen for all the unreacted acid chloride groups due to its relatively slow reaction rate. However, even a small number of covalent bonds between the PA film and the support can promote good adhesion when compared to adhesion by non-covalent interactions. It has also been suggested that Polysulfone (Psf) support would be more preferable to be chosen as the substrate over Polyethersulfone, because the presence of the bisphenol-A moiety in the chains of Psf helps to create electron-rich aromatic rings for more crosslinking to occur with the PA film.

## References


(1) Petersen, R. J. Composite Reverse Osmosis and Nanofiltration Membranes. *Journal of Membrane Science* **1993**, *83*, 81–150.

(2) Zhou, Y.; Yu, S.; Liu, M.; Chen, H.; Gao, C. Effect of Mixed Crosslinking Agents on Performance of Thin-Film-Composite Membranes. *Desalination* **2006**, *192*, 182–189.

(3) Saha, N. K.; Joshi, S. V. Performance Evaluation of Thin Film Composite Polyamide Nanofiltration Membrane with Variation in Monomer Type. *Journal of Membrane Science* **2009**, *342*, 60–69.

(4) Ghosh, A. K.; Hoek, E. M. V. Impacts of Support Membrane Structure and Chemistry on Polyamide–polysulfone Interfacial Composite Membranes. *Journal of Membrane Science* **2009**, *336*, 140–148.

(5) Xie, W.; Geise, G. M.; Freeman, B. D.; Lee, H.-S.; Byun, G.; McGrath, J. E. Polyamide Interfacial Composite Membranes Prepared from M-Phenylene Diamine, Trimesoyl Chloride and a New Disulfonated Diamine. *Journal of Membrane Science* **2012**.

(6) Freger, V. Kinetics of Film Formation by Interfacial Polycondensation. *Langmuir* **2005**, *21*, 1884–1894.

(7) Nadler, R.; Srebnik, S. Molecular Simulation of Polyamide Synthesis by Interfacial Polymerization. *Journal of Membrane Science* **2008**, *315*, 100–105.

(8) Allen, R.; Hedrick, J.; Na, Y. Composite Membranes with Performance Enhancing Layers. *US Patent 8,011,517* **2011**, *1*.

(9) de Lannoy, C.-F.; Jassby, D.; Gloe, K.; Gordon, A. D.; Wiesner, M. R. Aquatic Biofouling Prevention by Electrically Charged Nanocomposite Polymer Thin Film Membranes. *Environmental science & technology* **2013**.

(10) Kong, C.; Kanezashi, M.; Yamomoto, T.; Shintani, T.; Tsuru, T. Controlled Synthesis of High Performance Polyamide Membrane with Thin Dense Layer for Water Desalination. *Journal of Membrane Science* **2010**, *362*, 76–80.

(11) Cadotte, J. Interfacially Synthesized Reverse Osmosis Membrane. *US Patent 4,277,344* **1981**.

(12) Ahmad, a. L.; Ooi, B. S. Optimization of Composite Nanofiltration Membrane through pH Control: Application in CuSO4 Removal. *Separation and Purification Technology* **2006**, *47*, 162–172.

(13) Lee, H. S.; Im, S. J.; Kim, J. H.; Kim, H. J.; Kim, J. P.; Min, B. R. Polyamide Thin-Film Nanofiltration Membranes Containing TiO2 Nanoparticles. *Desalination* **2008**, *219*, 48–56.

(14) Lind, M. L.; Ghosh, A. K.; Jawor, A.; Huang, X.; Hou, W.; Yang, Y.; Hoek, E. M. V. Influence of Zeolite Crystal Size on Zeolite-Polyamide Thin Film Nanocomposite Membranes. *Langmuir : the ACS journal of surfaces and colloids* **2009**, *25*, 10139–10145.

(15) Chan, W.-F.; Chen, H.; Surapathi, A.; Taylor, M. G.; Shao, X.; Marand, E.; Johnson, J. K. Zwitterion Functionalized Carbon Nanotube/polyamide Nanocomposite Membranes for Water Desalination. *ACS Nano* **2013**, *7*, 5308–5319.

(16) Bui, N. N.; Lind, M. L.; Hoek, E. M. V; McCutcheon, J. R. Electrospun Nanofiber Supported Thin Film Composite Membranes for Engineered Osmosis. *Journal of Membrane Science* **2011**, *385-386*, 10–19.

(17) Enkelmann, V.; Wegner, G. Mechanism of Interfacial Polycondensation and the Direct Synthesis of Stable Polyamide Membranes. *Die Makromolekulare Chemie* **1976**, *177*, 3177–3189.

(18) Kim, S.; Kwak, S.; Suzuki, T. Positron Annihilation Spectroscopic Evidence to Demonstrate the Flux-Enhancement Mechanism in Morphology-Controlled Thin-Film-Composite (TFC) Membrane. *Environmental science & technology* **2005**, *39*, 1764–1770.

(19) Zhao, J.; Wang, Z.; Wang, J.; Wang, S. Influence of Heat-Treatment on CO2 Separation Performance of Novel Fixed Carrier Composite Membranes Prepared by Interfacial Polymerization. *Journal of Membrane Science* **2006**, *283*, 346–356.

(20) Prakash Rao, a. Interfacially Synthesized Thin Film Composite RO Membranes for Seawater Desalination. *Journal of Membrane Science* **1997**, *124*, 263–272.

(21) Prakash Rao, A.; Joshi, S. .; Trivedi, J. .; Devmurari, C. .; Shah, V. . Structure–performance Correlation of Polyamide Thin Film Composite Membranes: Effect of Coating Conditions on Film Formation. *Journal of Membrane Science* **2003**, *211*, 13–24.

(22) Ghosh, A. K.; Jeong, B.-H.; Huang, X.; Hoek, E. M. V. Impacts of Reaction and Curing Conditions on Polyamide Composite Reverse Osmosis Membrane Properties. *Journal of Membrane Science* **2008**, *311*, 34–45.

# Chapter 7. Conclusion and Future Work

Reverse osmosis water desalination has more than half a century of industrial operation and has become the most effective way to generate fresh water from a wide range of water sources. This makes it a vital process in tackling current and future water shortage problems. At the core of this technology is the reliance on a semipermeable membrane to drive the whole desalting process. Challenges in membrane design, such as low permeation flux, chemical stability, and surface biofouling substantially increase the cost of desalination plants by increasing the capital and operating costs associated with building complex pre-treatment units and extra energy consumption. Thin-film nanocomposite membranes (TFN) aim to resolve these issues by changing the surface and physiochemical properties of the RO membranes. By dispersing nanofillers in the barrier layer the resultant membranes possess both excellent permselectivity properties from the additives and can be easily processed using methods from traditional RO membranes. Molecular simulations and experimental studies have demonstrated that the transport of fluids through CNTs is orders of magnitude faster than through other nanoporous materials due to the unprecedented smoothness and regularity of the CNT pores.[1–7] Functionalized SWNTs have also been predicted to offer complete salt rejection with functional groups at the SWNT tips acting as gatekeepers to block out salt ions from entering the pore of the CNT via steric hindrance and electrostatic interactions.[8,9] In this research study, we have developed a new type of TFN membrane using zwitterion functionalized SWNTs, and have reported on its permeation, salt rejection, and anti-biofouling capabilities. The major contributions from the work are as follows:

1. **Successfully fabricated TFN membranes with a scalable procedure.** Fabrication of zwitterionic SWNT/polyamide membranes requires subtle control over multiple variables (i.e. monomer concentration, crosslinking density, presence of surfactant, drying method and heat-curing treatment) in order to disperse the SWNT in the polymer phase without introducing defects. The vacuum filtration method that aligns SWNT within the barrier layer of the membrane allows one to control the amount of SWNT embedded in the resulting nanocomposite membrane, and the process can be easily scaled up for mass production. Aligned SWNTs were embedded in the polyamide thin layer to form thin-film nanocomposite membranes with the barrier thicknesses of approximately 250 nm. This is close to the thicknesses reported for membranes elsewhere in the literature.[10,11]

2. **Demonstrated that the zwitterionic SWNTs exhibit water/ion separation properties that agree with simulations.** The water permeation flux increased more than 3-fold when the concentration of zwitterionic SWNTs in the thin film increased from 0 to 20 wt%. Furthermore, the salt rejection of the membrane increased slightly, indicating that the increased water flux is not due to an increase in nonspecific pores or free volume in the membrane by chain disruption, but rather due to an additional transport mechanism resulting from the presence of the functionalized SWNTs. The embedded SWNT exhibited salt rejection capacities that agreed with the predictions of MD simulations for nanotubes with diameters the same as those used in the experiments showing that the addition of two zwitterions per nanotube end would result in complete rejection of ions, while still allowing significant water flux.
3. **The structure/property relationship of TFN membrane has been investigated.** The tradeoff between the crosslinking density of the polyamide thin film and the amount of functionalized SWNTs that can put into the film was studied. Increasing the quantity of SWNTs in the films requires higher crosslinking density to maintain the stability of the nanocomposite. Thin films with higher crosslinking density lowered the diffusivity of water through the polymer phase, forcing the water molecules to be transported through pores introduced by the SWNTs. These pores are selective and prevent ions from entering. They could be the inner core of the SWNT, or nanochannels formed at the interface between SWNT and the polymer phase. Nanochannels on the outer surfaces of the SWNTs could also reject ions while allowing water to permeate through, and are not considered to be defects or pinholes in the film that would lower the selectivity. The pore size and pore size distribution of the membranes indicated that the size of the pores in the pure polyamide phase are close to those of the CNT cores and the nanochannels.
4. **The rejection mechanism has been identified.** Unlike singly-charged functional groups that suffer electrostatic screening effects at higher salt concentrations, the zwitterionic SWNT/PA membranes used in this study maintained high salt rejection even in the presence of high salinity feed solutions. This suggest that the gatekeeper mechanism preventing ions from permeating is dominated by the steric hindrance of the zwitterionic groups, rather than a combination of steric effects and electrostatic interactions between the fixed charges on the zwitterions and the charged salt ions. Furthermore, this indicates that the effective pore size of

the functionalized SWNT remains constant regardless of changes in the ionic strength of the feed solution.

5. **Anti-biofouling properties of the zwitterionic SWNT membranes were demonstrated.** The nanocomposite membranes exhibited increased surface biofouling resistance after the zwitterionic SWNT was embedded in the thin film. This indicated that zwitterionic groups exposed at the membrane surface interacted with the water in the feed solution to form a hydration layer and prevent strong binding of the foulant. After washing, the nanocomposite membrane regained 100% of the original water flux, indicating that foulants were not strongly adsorbed on the hydrated surface and were easily removed when flushed with clean water. We have demonstrated that advanced materials like CNTs can be synthesized with desired functional groups, and can be embedded into traditional RO membranes to simultaneously resolve the challenge of low flux and surface fouling in the current desalination process.
6. **Developed guidelines for fabrication of thin-film nanocomposite membranes.** Detailed fabrication procedures and troubleshooting methods have been developed that allow the fabrication of CNT based thin film nanocomposited membranes in a systematic and reproduceable fashion.

The following sections include a brief discussion of areas for ongoing research based on the results of this work.

## 7.1. Adhesion Study of CNTs to Polyamide

Interactions between the embedded nanomaterials (NMs) and the polymer matrix has been demonstrated to be the key factor in structural nanocomposites, which aim to take advantage of the superior mechanical properties of nanomaterials like carbon nanotubes.[12] Poor adhesion results in delamination of CNTs and polymer when the composite is under stress. In the fabrication of TFN membranes, NM-polymer interactions also have a direct relationship to the membrane permselectivity. Kim *et al.*[13] embedded oxidized carbon nanotubes in polyamide (PA) thin films and their results suggest that CNTs with highly oxidized surfaces interact more with the polymer chain, and form TFN membranes with more uniformly dispersed nanotubes and fewer defects at the interface between CNTs and the PA. Measurements of the interaction force are performed by using a modified AFM tip to scan across a surface coated with CNTs. A short chain of polyamide

was attached to the silicon tip and comes in contact with the surface of the oxidized CNTs. CNTs with poor interaction force with PA resulted in a TFN membrane with almost no ability to reject monovalent ions, but with a more than 2-fold increase in permeation flux compared to a plain PA membrane. Higher interaction forces yielded higher salt rejection and smaller increases in flux in the membranes. CNTs with the highest interaction force with PA exhibited similar or higher salt rejection compared to the control membrane, and also exhibited a more than 40% increase in water flux. It is believed that the improvement of the interaction force is solely due to noncovalent bonding such as hydrogen bond between the amide groups on the tip and the –COOH functional groups on the surface of CNTs introduced by the acid oxidization process.

Kim *et al.* also suggested that the compatibility between the PA chains and the embedded CNTs is improved by both the increase in interfacial interaction force as well as the degree of dispersion of CNTs in the polymer phase. Raman spectroscopic mapping images show that poorly oxidized CNTs formed agglomerations in the polymer phase, while strongly oxidized CNTs were well-dispersed. To study the NM-polymer interaction, we need to first understand the characteristics of both constituents and how they interrelate with each other. The adhesion forces come from several kinds of interaction: covalent or noncovalant bonding (i.e., hydrogen bond, electrostatic force, Van der Waals force, and $\pi$ - $\pi$ stacking). Therefore, the objective of this proposed work is to investigate the key factors that control the interaction forces between nanomaterials and the polyamide, and how this relates to the overall performance of the TFN membrane in terms of its pore size, permselectivity, surface roughness, etc.

### 7.1.1. Plan of investigation

**(A) Interaction measurement using polymer modified AFM tip.** In this study, the tip of AFM will be modified with the aromatic polyamide used in most of RO membranes. Three different types of CNTs (pristine, -COOH functionalized and zwitterion functionalized) will be dispersed in solvent and uniformly deposited onto a filter substrate via the vacuum filtration method. This CNT-coated substrate will then be scanned by the PA-modified AFM tip in contact mode. A force curve can be generated and the interaction force between CNTs and PA can be calculated by multiplying the spring constant of the cantilever with the deflection distance. Figure 7.1 illustrates the idea of the experiment. Due to the fact that the functional groups at the surface of the CNTs can attract water molecules and form a strong hydration layer at the surface through hydrogen bonding, the polymer chain at the AFM tip has a chance of scanning the hydration layer while not

coming directly in contact with the CNT sample. Therefore, a control study is required to investigate how changing the humidity at the sample surface changes the interaction force. The following table shows three different environments to conduct the scanning experiment.

| **Chamber filled with** | **Relative Humidity (%)** |
|---|---|
| Mild organic solvent | 0 |
| Nitrogen gas | 0 |
| Water moisture | 100 |

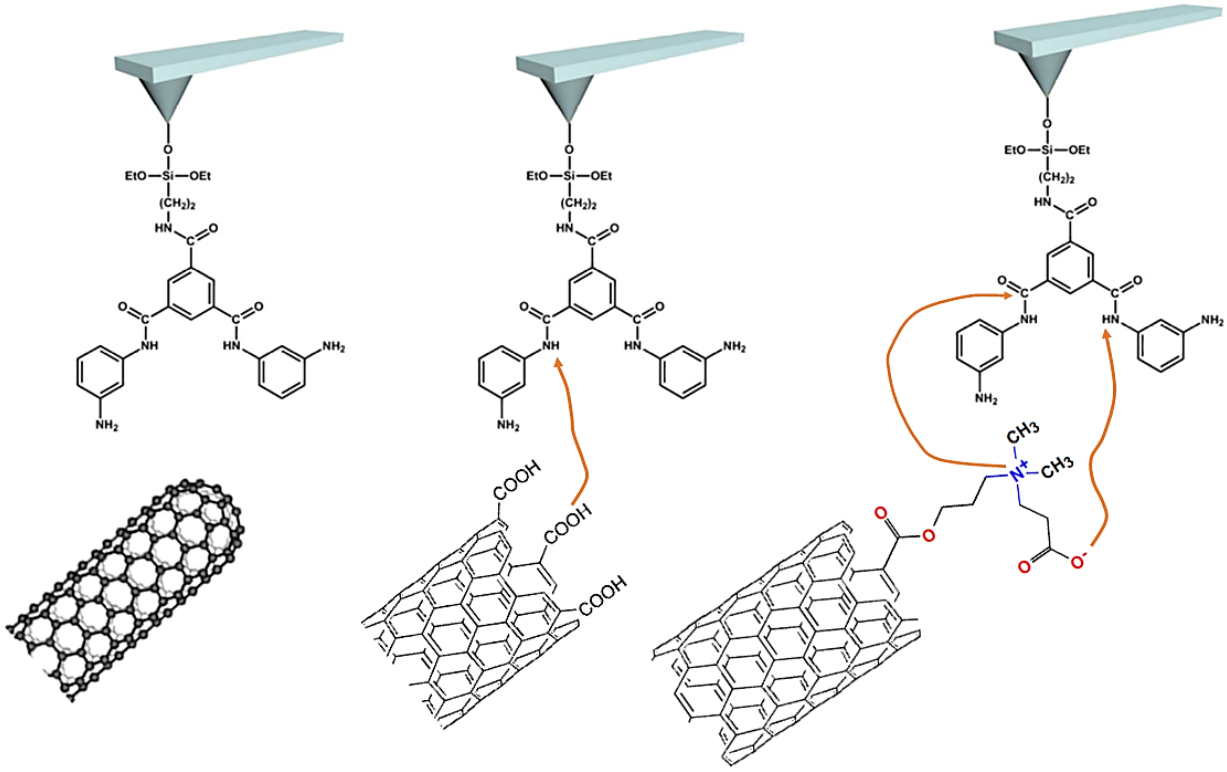


**Figure 7.1.** Diagram of the functionalization of AFM tip with short polyamide chains. The AFM tip will then be used to interact with carbon nanotubes with different functional groups.

**(B) pH effect on interaction force.** Dai *et al.*[14] modified AFM tips with polypeptide (polylysine) and used it to scan across a substrate where oxidized CNTs were deposited. The scanning was performed in a buffer solution with pH ranging from 1 to 12. The adhesion force measured by the AFM varies as a function of pH, in which the adhesion between polypeptide chains and the CNTs decreases as the pH of the buffer solution increases. They attributed this to the protonation/deprotonation of –COOH groups on the oxidized CNTs and the $–NH_2$ groups on the polypeptide. At low pH values, the protonated $–NH_3^+$ groups of polylysine attract –COOH ($–COO^-$

+ $H^+$) groups on oxidized CNTs through electrostatic interaction. At high pH values, both groups are deprotonated into $–NH_2$ and $–COONH_4$ ($–COO^–$ + $Na^+$; with $Na^+$ from the buffer solution) moieties and greatly reduce the adhesion force between them.

In the proposed study, the interaction force will be measured between PA and two types of functionalized CNTs (–COOH and zwitterion). The testing will proceed with both modified tips and the substrate with CNTs submerged in buffer solutions of different pH values. The adhesion force between the tip and CNTs is expected to vary not just with pH, but also with the tip modification. If the final step of PA-tip modification is to crosslink TMC with diamine solution, unreacted $–NH_2$ functional groups will be left on the tip and will be converted to $–NH_3^+$ at low pH as shown on the left side in Figure 1.2. This should then have a strong interaction with –COOH-CNTs through hydrogen bonds between amide groups and carboxylic groups, but negative interactions with the zwitterion CNTs due to electrostatic repulsion between the positive nitrogen atoms on both the zwitterion and $–NH_3^+$. At high pH values, the tip should show higher adhesion forces with the zwitterionic groups because the electrostatic repulsion is diminished and replaced by hydrogen bonds formed between amide group and $–COO^–$ at the end of the zwitterion group.

In contrast, if the final step of tip modification is to crosslink the amine group on the tip with TMC solution, carbonyl groups on TMC will be hydrolyzed and form –COOH groups as shown on the right side in Figure 1.2. At low pH, no electrostatic force is shown between CNTs and the tip for both functionalized CNTs. However, both CNTs should exhibit strong repulsion forces at high pH due to repulsion between negative charges.

**Low pH**

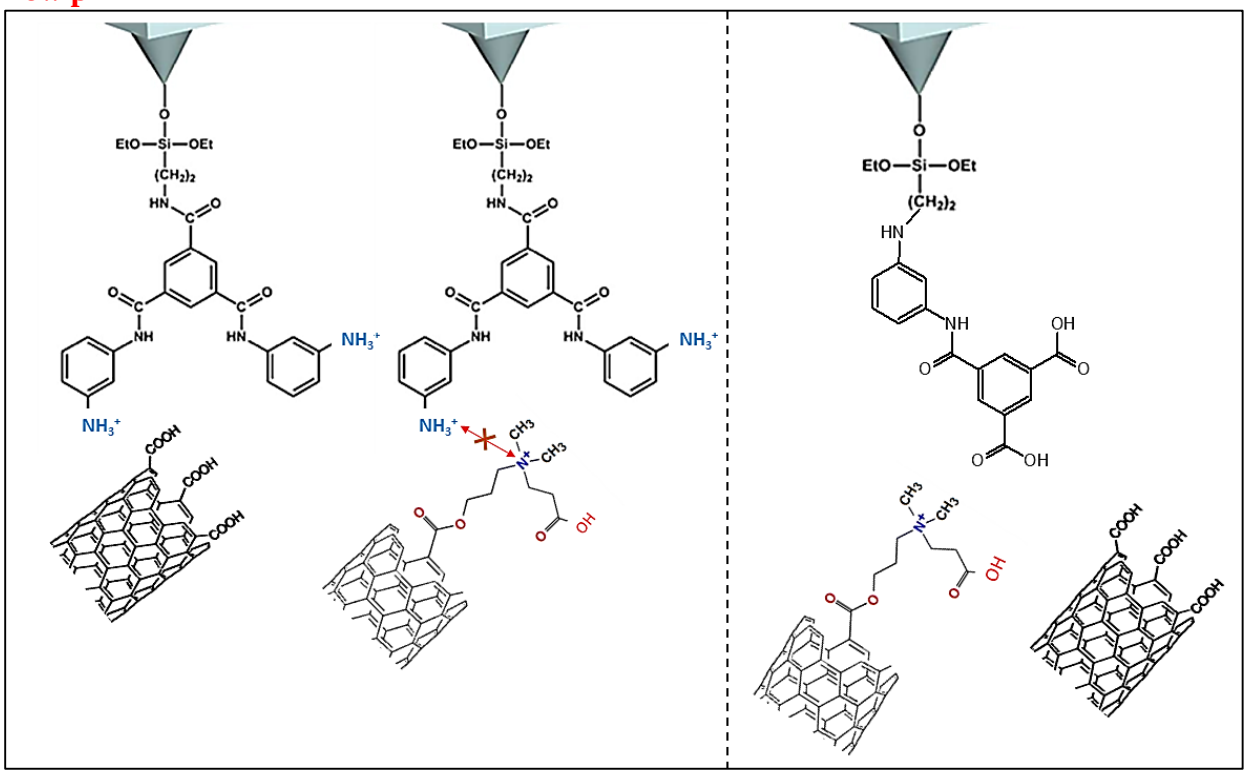


**High pH**

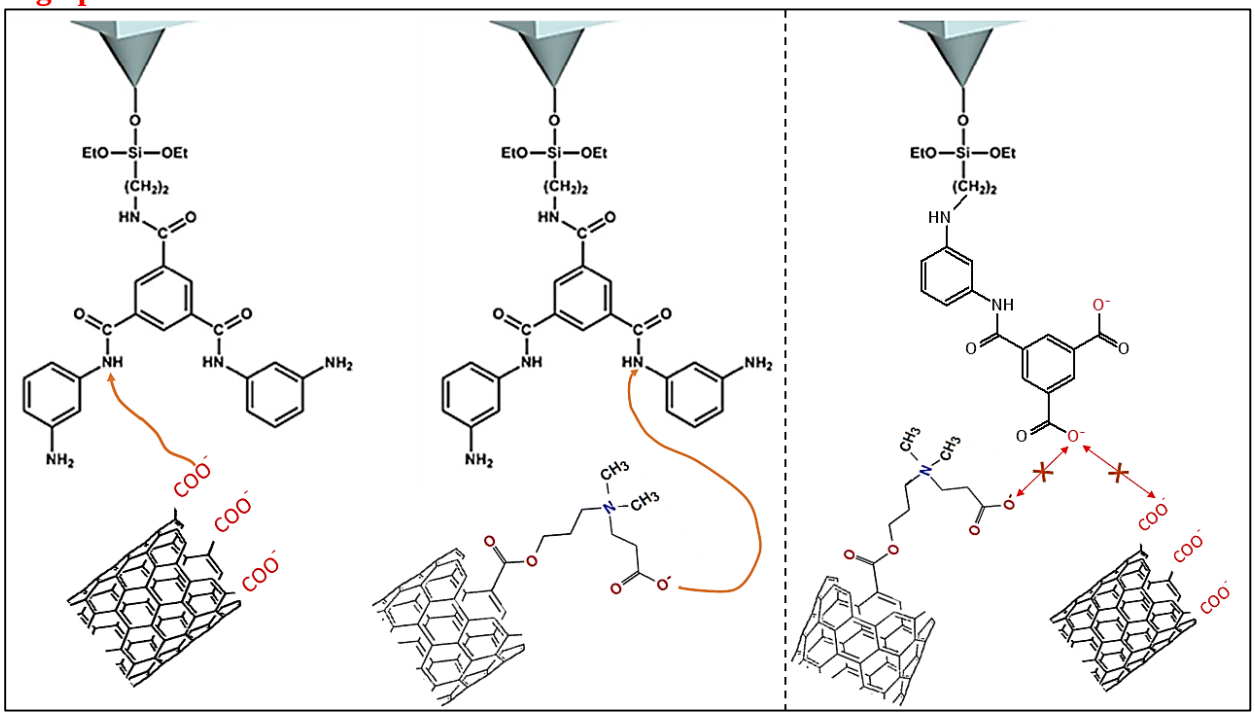


**Figure 1.2.** Possible interactions between PA-coated AFM tip and functionalized CNTs.

## 7.2. Study of the Functionalization of SWNTs

In addition to our study using zwitterions as the functional group on CNTs for water desalination applications, recent simulation studies[8] also provide insight into using other charged functional groups to enhance the RO performance of hydrophobic channels. Functional groups in CNTs generally (i) serve as a gatekeepers at the end of the tubes which provide steric hindrance at the entrance and prevent undesired ionic transport, and (ii) offer special properties like electrostatic interactions with solvents/solutes or anti-biofouling capability. Simulation data shown in Table 7.1 demonstrates that the effect of the gatekeeper reduces the effective pore diameter of the CNT by adding chemical groups at the entrances of the tubes. The net interaction between the functional groups and water and ion molecules becomes more significant as the number of functional groups increase, and could eventually offer complete blockage of salt ions while allowing water to transport through the tubes many times faster than existing technologies. As the number of functional groups attached at the end of the tube increases, the rejection rate generally increases proportionally but is accompanied by a significant drop in the water flux. It has also been observed that too many single-charged functional groups at the end of CNTs can actually favor the transport of counter-charged ions. For example, perfect rejection is achieved for both for $Na^+$ and $Cl^-$ ions when a CNT has four $NH_3^+$ groups at the tube end. However, with 8 $NH_3^+$ groups attached to the end, the passage for $Cl^-$ increases and the salt rejection is essentially lowered from 100% to 66%. The overwhelming positive charge due to the $NH_3^+$ groups attracts negatively-charged chloride ions and overcomes the strong energy barrier created by the steric hindrance of the functional groups. On the other hand, Corry *et al.* concluded that the rejection of $Cl^-$ is easier to achieve than that of $Na^+$ due to the inherently greater dehydration energy required for it to enter the pore. Thus, the inclusion of negatively charged groups can reject ions more effectively.

**Table 7.1.** Water flux and ion rejection through functionalized carbon nanotubes under a hydrostatic pressure difference of 246 MPa. All flux values are in number of molecules per tube per ns and are calculated from 40 ns of simulation. Regenerated table from the simulation data of B. Corry, Water and ion transport through functionalised carbon nanotubes: implications for desalination technology, *Energy & Environmental Science*, **2011**.[8]

| **Tube type** | **Water Flux** | **$Na^+$ rejection** | **$Cl^-$ rejection** |
|---|---|---|---|
| Non func | 107.8 ± 0.6 | 28% | 86% |
| $4COO^-$ | 35 ± 2 | 32% | 100% |
| $8COO^-$ | 14 ± 3 | 100% | 100% |
| $2NH_3^+$ | 60 ± 2 | 86% | 87% |
| $4NH_3^+$ | 22.1 ± 0.7 | 100% | 100% |
| $8NH_3^+$ | 18.9 ± 0.8 | 100% | 66% |
| $2NH_3^+2COO^-$ | 46 ± 2 | 82% | 82% |
| $4NH_3^+4COO^-$ | 18 ± 1 | 55% | 100% |
| 3 x ($2NH_3^+$) | 59 ± 1 | 94% | 92% |
| 3 x ($4NH_3^+$) | 23 ± 1 | 100% | 100% |

It is impossible to have precise control over the number of functional groups attached to each CNT experimentally in order to achieve the perfect rejection shown above. The walls of pristine CNTs always contain defects created by the catalyst during the fabrication process, in which the defect sites are active in reacting with the chemical groups. The resulting functionalized CNTs contain many more functional groups than those at the CNT tips. However, we can study functional groups that have similar length and size structurally but with different fixed charges (i.e. valency and sign) in order to explore the effect of charge-charge interactions on the water flux and salt rejection. MD simulation studies by Johnson *et al.*[9] showed that by turning off the charges on the zwitterion functional groups, the ion and water conductance through the CNTs will increase approximately 30% when only one functional group is present at the tube end. However, when the number of chemical groups present at the tube ends reach a threshold that can completely block the ions from entering the CNTs (two groups in this case), the absence of charges does not change the rejection of ions. They concluded that the steric hindrance of the chemical group provides the majority of the salt ion rejection.

**Table 7.2.** Possible functional groups to be introduced to the SWNT.

| Functional Group | Approximate Size (nm) | Charge |
|---|---|---|
| $-COO^-$ (high pH) | <0.4 | -1 |
| -COOH (low pH) | <0.4 | neutral |
| $-CONH-(CH_2)_2-NH_2$ (high pH) | 0.58 | neutral |
| $-CONH-(CH_2)_2-NH_2^+$ (low pH) | 0.58 | neutral |
| $-COO-(CH_2)_2-N^+(CH_2)_2-(CH_2)_2COO^-$ | 1.1-1.2 | Zwitterion (+1,-1) |
| $-CONH-(CH_2)_4-CH_3$ | 0.69 | neutral |
| $-CONH-(CH_2)_8-CH_3$ | 1.14 | neutral |

### 7.2.1. Plan of Investigation

**(A) Charge of the functional group.** As shown in Table 7.2, the charge effect of the chemical groups can be studied by introducing groups that have similar lengths but different charges. For example, the group of $-CONH-(CH_2)_8-CH_3$ has a length of 1.14 nm that is close to that of the zwitterion group, but contains plain alkane chains that have no charge. This will therefore be a good candidate to functionalize CNTs in order to study the change of water flux and salt rejection of the resulting membranes when the charge effect is completely absent. According to the simulation study, the resulting membranes should show faster permeation flux due to the slightly larger size of the effective pores, but remain identical in salt rejection since the change of the pore size due to the absence of charge will not be enough for any salt passage.

**(B) Length and configuration of the group.** To study the effect of length of the functional group, CNTs can be functionalized with a $-CONH-(CH_2)_4-CH_3$ (group 1) and $-CONH-(CH_2)_8-CH_3$ (group 2), whose lengths are 0.69 nm and 1.14 nm respectively. Both functional groups are neutral in charge. Hence the effective pore diameter of their respective functionalized SWNTs will be different. For example, assuming that the average diameter of the SWNT is 1.5 nm, the effective pore diameter after functionalization will be 0.81 nm for CNTs with group 1, and 0.36 nm for those with group 2. We should expect that the resulting membranes from group 1 will have no rejection ability since their pore size is larger than the hydrated diameter of the salt ions, while that

for group 2 will result in high salt rejection since it is between the molecular diameter of salt ions and water molecule.

Studies from Johnson *et al.*[9] have also shown another interesting phenomenon concerning the flexibility of long functional groups. For example, functional groups like the zwitterion groups shown in Table 7.2 adopt two configurations: (i) an extended configuration from the tube ends into the solution phase and (ii) a folded configuration inside the nanotube. Thermodynamically, the folded configuration is more favorable than extending into the bulk. This folded configuration changes the effective pore diameter "internally". Therefore, we expect to see the folded configuration in other long functional groups and a reduction of pore size within the nanotubes. Hence, the effective pore diameter also depends on the configuration and the folding of the functional group, potentially minimizing the effect of pore size reduction by the functional groups, and making it hard to observe differences in the performance of the functionalized CNTs with functional groups of different lengths.

## 7.3. Orientation of CNTs

One of the reasons that Z-SWNT/PA membranes do not achieve their expected maximum performance is due to the lack of alignment of the CNTs within the polymer matrix. As shown in Chapter 4, the cross-sectional scanning electron microscope (SEM) image of the TFN membrane reveals partial alignment of Z-SWNTs within the polymer matrix, with many other undesired microstructures such as nanotube bundling, curling and poor orientation. When water and salt molecules permeate inside the nanocomposite membrane, they will then be required to first diffuse through a thin polymer layer in order to reach for the entrance of the Z-SWNTs buried beneath the surface (Figure 7.3). This can drastically slow down the overall transport of water molecules and greatly reduces the water flux.

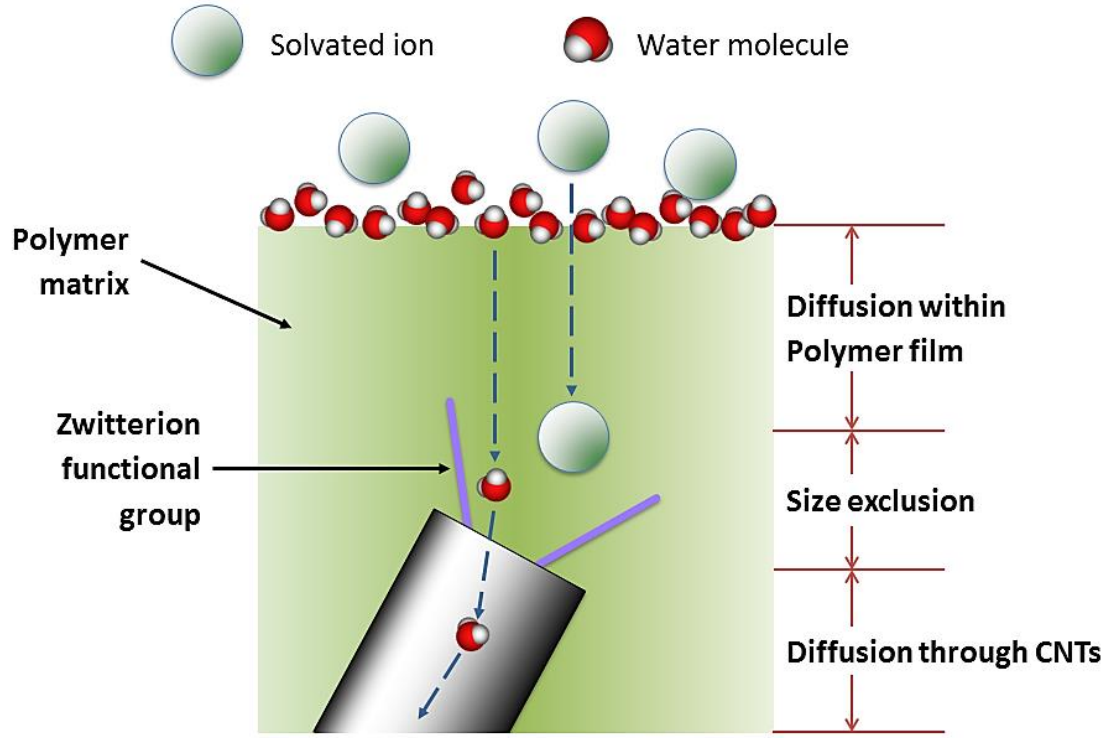


**Figure 7.3.** Transport of water and ion molecules within the Z-SWNTs/PA nanocomposite membrane.

**Characterization of SWNT Alignment.** The alignment of the CNTs inside the polymer layer needs to be characterized in greater detail. Qualitative measurements were attempted using scanning electron microscopy, however, the characterization was limited within the area imaged. In addition, artificial defects may be introduced during the sample preparation process. The image for the cross-sectional area of the membrane is prepared by using a small piece of fabric-free membrane sample and freezing it in liquid nitrogen to fracture cryogenically. This process may artificially align the CNTs around the cross section and generate false evidence of alignment. It is important to have a reliable method for characterizing the nanotube alignment quantitatively. One way to overcome this is to first prepare our samples in an epoxy resin and then slice the samples into several very thin films along the cross-section of the sample after the epoxy is cured. This would guarantee that the cross-section of the membrane is untouched before any imaging. Transmission electron microscopy (TEM) imaging can also perform over the cross-sectional area for the samples prepared in this method. The average diameter of our CNTs is 1.5 nm, which is lower than the detection limit for most high definition SEM imaging. TEM imaging can provide resolution down to the sub-nanometer level and reveal more CNTs which cannot be seen in SEM.

**Alignment of SWNTs by Electric Field.** SWNTs in the polymer CNT nanocomposite membranes can be aligned using electric fields[15–17] and magnetic fields[18–20]. However, high magnetic field strengths are required for SWNT alignment in nanocomposites. Fischer *et al.*[18] and Smith *et al.*[19] used magnetic field strengths of 7 T and 25 T respectively for SWNT alignment, which is achievable only in certain specially equipped laboratories. Hence, for future studies in aligning the Z-SWNTs in PA membranes, the possibility of using electric fields should be investigated.

## References


(1) Holt, J. K.; Park, H. G.; Wang, Y.; Stadermann, M.; Artyukhin, A. B.; Grigoropoulos, C. P.; Noy, A.; Bakajin, O. Fast Mass Transport through Sub-2-Nanometer Carbon Nanotubes. *Science (New York, N.Y.)* **2006**, *312*, 1034–1037.

(2) Majumder, M.; Chopra, N.; Hinds, B. J. Effect of Tip Functionalization on Transport through Vertically Oriented Carbon Nanotube Membranes. *Journal of the American Chemical Society* **2005**, *127*, 9062–9070.

(3) Skoulidas, A. I.; Sholl, D. S.; Johnson, J. K. Adsorption and Diffusion of Carbon Dioxide and Nitrogen through Single-Walled Carbon Nanotube Membranes. *The Journal of chemical physics* **2006**, *124*, 054708.

(4) Holt, J. K. Carbon Nanotubes and Nanofluidic Transport. *Advanced Materials* **2009**, *21*, 3542–3550.

(5) Holt, J. K.; Noy, A.; Huser, T.; Eaglesham, D.; Bakajin, O. Fabrication of a Carbon Nanotube-Embedded Silicon Nitride Membrane for Studies of Nanometer-Scale Mass Transport. *Nano Letters* **2004**, *4*, 2245–2250.

(6) Skoulidas, A. I.; Sholl, D. S. Transport Diffusivities of CH4, CF4, He, Ne, Ar, Xe, and SF6 in Silicalite from Atomistic Simulations. *The Journal of Physical Chemistry B* **2002**, *106*, 5058–5067.

(7) Kalra, A.; Garde, S.; Hummer, G. Osmotic Water Transport through Carbon Nanotube Membranes. *Proceedings of the National Academy of Sciences of the United States of America* **2003**, *100*, 10175–10180.

(8) Corry, B. Water and Ion Transport through Functionalised Carbon Nanotubes: Implications for Desalination Technology. *Energy & Environmental Science* **2011**, *4*, 751.

(9) Chan, W.-F.; Chen, H.; Surapathi, A.; Taylor, M. G.; Shao, X.; Marand, E.; Johnson, J. K. Zwitterion Functionalized Carbon Nanotube/polyamide Nanocomposite Membranes for Water Desalination. *ACS Nano* **2013**, *7*, 5308–5319.

(10) Ghosh, A. K.; Jeong, B.-H.; Huang, X.; Hoek, E. M. V. Impacts of Reaction and Curing Conditions on Polyamide Composite Reverse Osmosis Membrane Properties. *Journal of Membrane Science* **2008**, *311*, 34–45.

(11) Saha, N. K.; Joshi, S. V. Performance Evaluation of Thin Film Composite Polyamide Nanofiltration Membrane with Variation in Monomer Type. *Journal of Membrane Science* **2009**, *342*, 60–69.

(12) Rahmat, M.; Hubert, P. Carbon Nanotube-Polymer Interactions in Nanocomposites: A Review. *Composites Science and Technology* **2011**, *72*, 72–84.

(13) Kim, H.; Choi, K.; Baek, Y.; Kim, D. High-Performance Reverse Osmosis CNT/Polyamide Nanocomposite Membrane by Controlled Interfacial Interactions. *ACS applied materials & interfaces* **2014**, 2819–2829.

(14) Li, X.; Chen, W.; Zhan, Q.; Dai, L.; Sowards, L.; Pender, M.; Naik, R. R. Direct Measurements of Interactions between Polypeptides and Carbon Nanotubes. *Journal of Physical Chemistry B* **2006**, *110*, 12621–12625.

(15) Chen, X. Q.; Saito, T.; Yamada, H.; Matsushige, K. Aligning Single-Wall Carbon Nanotubes with an Alternating-Current Electric Field. *Applied Physics Letters* **2001**, *78*, 3714–3716.

(16) Martin, C. a. a.; Sandler, J. K. W. K. W.; Windle, a. H. H.; Schwarz, M.-K. K.; Bauhofer, W.; Schulte, K.; Shaffer, M. S. P. S. P. Electric Field-Induced Aligned Multi-Wall Carbon Nanotube Networks in Epoxy Composites. *Polymer* **2005**, *46*, 877–886.

(17) Park, C.; Wilkinson, J.; Banda, S.; Ounaies, Z.; Wise, K. E.; Sauti, G.; Lillehei, P. T.; Harrison, J. S. Aligned Single-Wall Carbon Nanotube Polymer Composites Using an Electric Field. *Journal of Polymer Science Part B: Polymer Physics* **2006**, *44*, 1751–1762.

(18) Fischer, J. E. Magnetically Aligned Single Wall Carbon Nanotube Films : Preferred Orientation and Anisotropic Transport Properties. *Structure* **2003**, *93*, 2157–2163.

(19) Smith, B. W.; Smith, B. W.; Benes, Z.; Benes, Z.; Luzzi, D. E.; Luzzi, D. E.; Fischer, J. E.; Fischer, J. E.; Walters, D. a; Walters, D. a; *et al.* Structural Anisotropy of Magnetically Aligned Single Wall Carbon Nanotube Films. *Applied Physics Letters* **2000**, *77*, 663–665.

(20) Mauter, M. S.; Elimelech, M.; Osuji, C. O. Nanocomposites of Vertically Aligned Single-Walled Carbon Nanotubes by Magnetic Alignment and Polymerization of a Lyotropic Precursor. *ACS Nano* **2010**, *4*, 6651–6658.

# Appendix A

## A.1. Detailed Membrane Fabrication

The interfacial polymerization (IP) of polyamide (PA) is very sensitive to the operating condition and reaction time. Moreover, there are many ways to carry out the procedure. Different publications report different recipes in terms of the concentration of monomers, contact time, air-drying time, curing temperature, etc.[1–4] A schematic of our recommended fabrication procedure is shown in Figure 4.2. The polyethersulfone PES membrane support was first pretreated by soaking in a 0.5 wt% sodium dodecylbenzenesulfonate (SDBS) solution (Figure 4.2A) for two days to increase the hydrophilicity and to open the pores of the support. The support was then soaked in deionized (DI) water for one day to remove any excess surfactants. This soaking pretreatment guaranteed that there was no SBDS solution left in the pores. The absence of this step may introduce air bubbles underneath the later PA layer. The support was then sandwiched in between two round Poly(tetrafluoroethylene) (PTFE) holders. Before being poured on the top of the membrane support, a predetermined weight of zwitterion-functionalized CNTs was dispersed in 40 ml of deionized (DI) water by sonication. During the sonication step, the CNT solution was heated by the sonicator horn and therefore required cooling to room temperature. As shown in Figure 8, the functionalized CNTs were deposited and semi-aligned on the membrane support using high-vacuum filtration.[5] The support and CNTs were then dried for an hour in a vacuum oven. This insured that all water was removed from the nanotubes before the interfacial polymerization took place. An alternative way to filter the CNT solution was to use a solvent-resistant stirred cell (XFUF04701; Millipore, MA). This apparatus utilized a dead-end filtration method, in which the support was held at the bottom of the cell and the CNTs solution was stored within the cell above the support. The cell was pressurized up to 6 bar with inert gas on the top of the solution. Under this relatively high pressure the CNT solution also filtered through the support leaving the CNT behind. As shown in Figure 8C, IP was subsequently carried out on the CNT covered support by wetting the fabrication side (with CNTs) with an aqueous diamine solution containing 2 wt% MPD and 0.2 wt% of SDBS at ambient temperature for 2 min and then the membrane was unclamped and immediately placed on a glass plate. A glass roller was rolled over the membrane once to remove all the excess MPD solution. The membrane was then sandwiched again into the holder and wetted by a n-hexane solution containing 0.5% (w/v) TMC for 90 seconds.

The resulting PA thin film nanocomposite membrane was subsequently heat cured at 68°C for 5 min. After the membrane had cooled down, it was washed thoroughly with DI water, submersed in fresh DI water and stored in a laboratory refrigerator at 4°C.

## A.2. Estimation of Flux Through an Ideal Membrane

In an ideal membrane all water flux will be through the carbon nanotubes and no water or ions would permeate through the polymer matrix. All the nanotubes would be semi-aligned so that they provided a pathway from one side of the membrane to the other. Taking the experimental membrane having 20 wt% (0.75 mg) CNTs, and assuming a nominal (20,0) CNT as the average nanotube having a length of 1000 nm, we can compute the average number of CNTs per membrane. The diameter of the membrane is 3.7 cm, so that the total area is 10.75 $cm^2$. This membrane would have a density of $1.86\times10^{13}$ CNT/$cm^2$. Assuming a linear flux of water with pressure drop,[6] we get a flux of 1.75 water molecules per CNT per ns. Converting to units of gallons per square foot per day gives a flux of about 20,000 GFD at a pressure drop of 530 psi.

## A.3. Estimation the Number of Zwitterions per CNT

In the experiment, the average diameter of CNTs is about 15 Å, close to the diameter of a CNT (20,0) which is 15.66 Å. Thus, we consider the (20,0) CNT in the estimation of the number of zwitterions per CNT. In a CNT with indices (*n*,*m*), the length of one unit cell is calculated as $L=\frac{\sqrt{3}\pi d_{cnt}}{d_R}$, where $d_R$ is the common divisor for (2*n*+*m*, 2*m*+*n*) and $d_{cnt}$ is the diameter of a CNT. For a (20,0) CNT, L is given as 4.26 Å. The number of atoms in one unit cell of a CNT is calculated as $n_c=\frac{4(n^2+m^2+n\times m)}{d_R}$. Thus, in a (20,0) CNT, the number of atoms per unit cell is 80. The length of the CNTs used in experiments is around 1000 nm, so that the number of C atoms in one CNT is $\frac{80}{0.426\text{nm}}\times1000\text{nm}=1.88\times10^5$ C atoms/CNT. The atomic percentages of C and N in zwitterion functionalized CNTs were measured by x-ray photoelectron spectroscopy. The results show that for every 100 atoms of the sample, 77 are C atoms and 2 are N atoms. Zwitterion groups we used have the structure: -COO-$(CH_2)_3$-$N^+(CH_3)_2$-$(CH_2)_2$COO-. Thus, each zwitterion group has one nitrogen atom and hence there are 2 zwitterion groups per 77 carbon atoms. For 77 carbon atoms, 18 of them are carbon atoms contained in the zwitterion groups. Let the number of

zwitterion groups in a typical CNT be *x*. Using proportionality, *x* is calculated as $\frac{77-18}{2} = 29.5 = \frac{1.88\times10^5}{x}$. Therefore, the number of zwitterions is estimated to be 6400 per CNT. Given that there are only 20 dangling bonds at each end of a (20,0) CNT, the maximun number of zwitterions attached at the ends is 40. Thus, most of zwitterions must be bound to the tube wall, presumably at defect sites along the length of the nanotube.

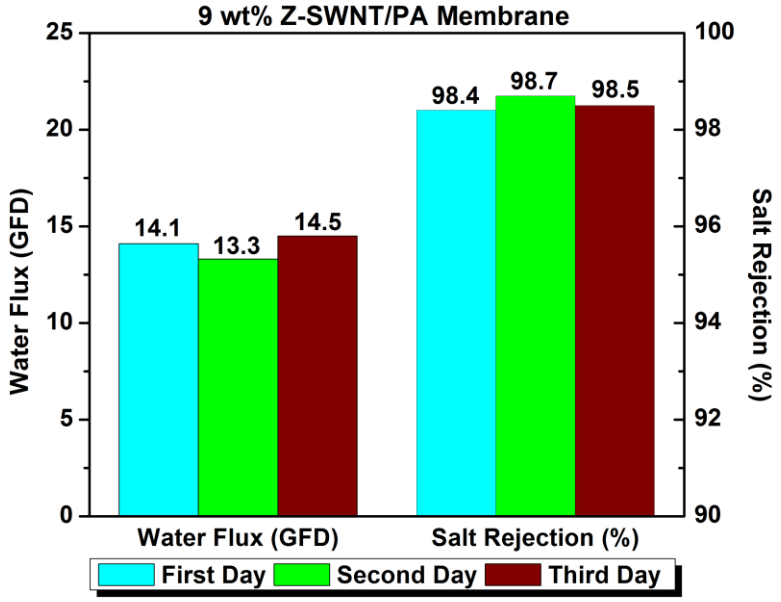


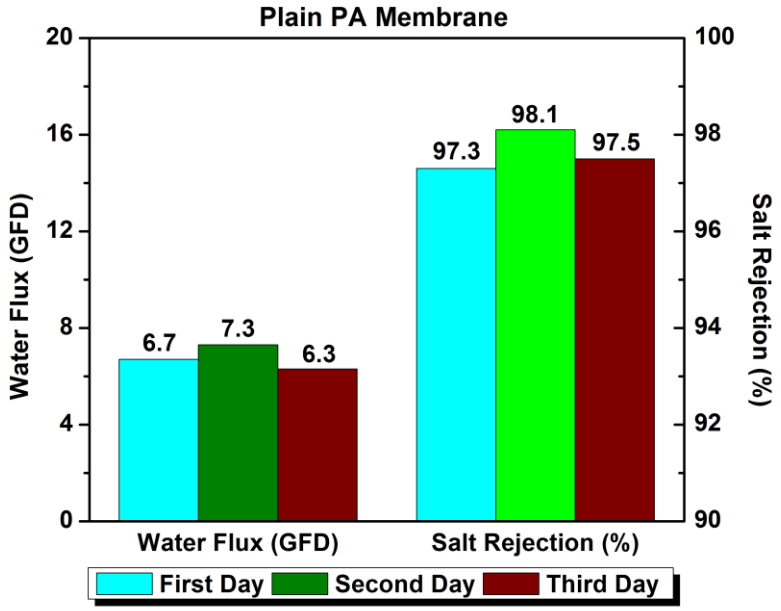

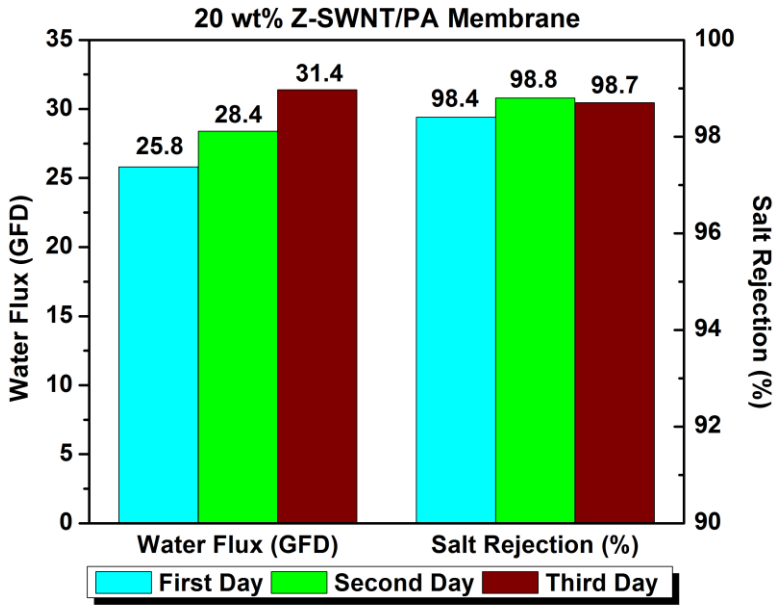


**Figure A.1.** Water flux and salt rejection for pure PA membrane 9 wt% Z-SWNT/PA and 20 wt% Z-SWNT/PA membrane operated for a pressure drop of 530 psi.

## A.4. Reynolds number Calculation

The geometry of our reverse osmosis system fits the model of rectangular duct, and the fluid moving in this geometry has the characteristic linear dimension equals to its hydraulic diameter, $D_H$.

$$D_H = \frac{4ab}{2(a+b)} \tag{A.1}$$

where a and b are the width and the height of the cross sectional area.

The equation for Reynolds number in rectangular duct is shown as follow.

$$Re = \frac{D_H v_0 \rho}{\mu} \tag{A.2}$$

Where $v_0$ is the fluid velocity in the duct, and $\rho$ and $\mu$ are the density and viscosity of the solution, respectively. All the salts used in this study contained light metal cations and the weight percentage in water were all less than 1wt%. Therefore, we can safely assume that the density of all the feed solution is approximately 1.0 g/ml.

The volumetric flow rate in the duct is 2.5 L/min = $4.17 \times 10^{-5}$ $m^3/s$. The height of the space inside the stainless steel cell is 2 mm, and the length and width are 7.5 and 5.5 cm, respectively. Since the flow travels along the length direction, the cross sectional area A will be equal to $a * b$, and the fluid velocity will be

$$v_0 = \frac{Q}{A} = \frac{Q}{ab} \tag{A.3}$$

where Q is the volumetric flow rate.

The kinematic viscosity, $\mu_C = (\mu/\rho)$ is[7]

| Temperature (˚C) | Salinity (ppm) | $\mu_C$, kinematic viscosity ($m^2/s$) |
|---|---|---|
| 25 | 2000 | $8.950 \times 10^{-7}$ |

After a rearrangement of the equation (A.2), the new equation is as follow.

$$\mathrm{Re} = \frac{2Q}{(a+b)\mu_C} \tag{A.4}$$

Re is calculated to be 1633, which means flow inside the cell is laminar.

## A.5. ATR-FTIR Reference Peak

We have noticed that peak at 1543 $cm^{-1}$ appeared in both PA and Z-SWNT/PA spectra, but not in the spectrum of PES support; therefore, it is safe to use it as a reference peak for cross comparison between PA and nanocomposite membranes, because this signal did not come from the base support and is irrelevant to what substrate we used to coat on. The total area under this peak should be identical after normalization. One may argue of using the peak at 1240 $cm^{-1}$ as the reference peak since it appeared in all three spectra. This signal therefore is solely from the PES support and should remain unchanged even after coating by a very thin transparent film of PA. However, the signal of this peak in Z-SWNT/PA can be diminished drastically after the surface was totally covered by the CNTs. The total black appearance of the embedded SWNTs makes it difficult for the infrared light to reflect back to the sensor after hitting the CNTs' wall. The reflection from the support is therefore blocked which makes this peak incomparable.

## A.6. Hydrated layer of the pore walls

In the study of Otero *et al.*[8], the theoretical pore sizes were obtained by using the steric-friction model for each uncharged solute, and are compared with the Stokes' radii of the solutes used. There is a correlation found in study which is close to

$$r_p = r + \alpha d_W \qquad \text{(A.5)}$$

where $r_p$ is the theoretical pore radius, $r$ is the Stokes' radius of the solutes used, and $d_W$ is the size of the water molecule. This shows that a molecule of a given solute cannot approach the walls of a pore closer than a certain interaction length. The distance of nearest approximation for the molecule of solute and the pore walls is 0.14 nm according to the study, thus leading to α = 1/2. This length was interpreted as referring to the hydration layer of the pore walls.

**Table A.1.** Molecular radii of organic solutes used in the pore size distribution test.[8]

| 500 ppm feed solution | r (nm) |
|---|---|
| Ethanol | 0.2 |
| Galactose | 0.35 |
| Maltose | 0.47 |
| Rafinose | 0.58 |
| α-Cyclodextrine | 0.77 |

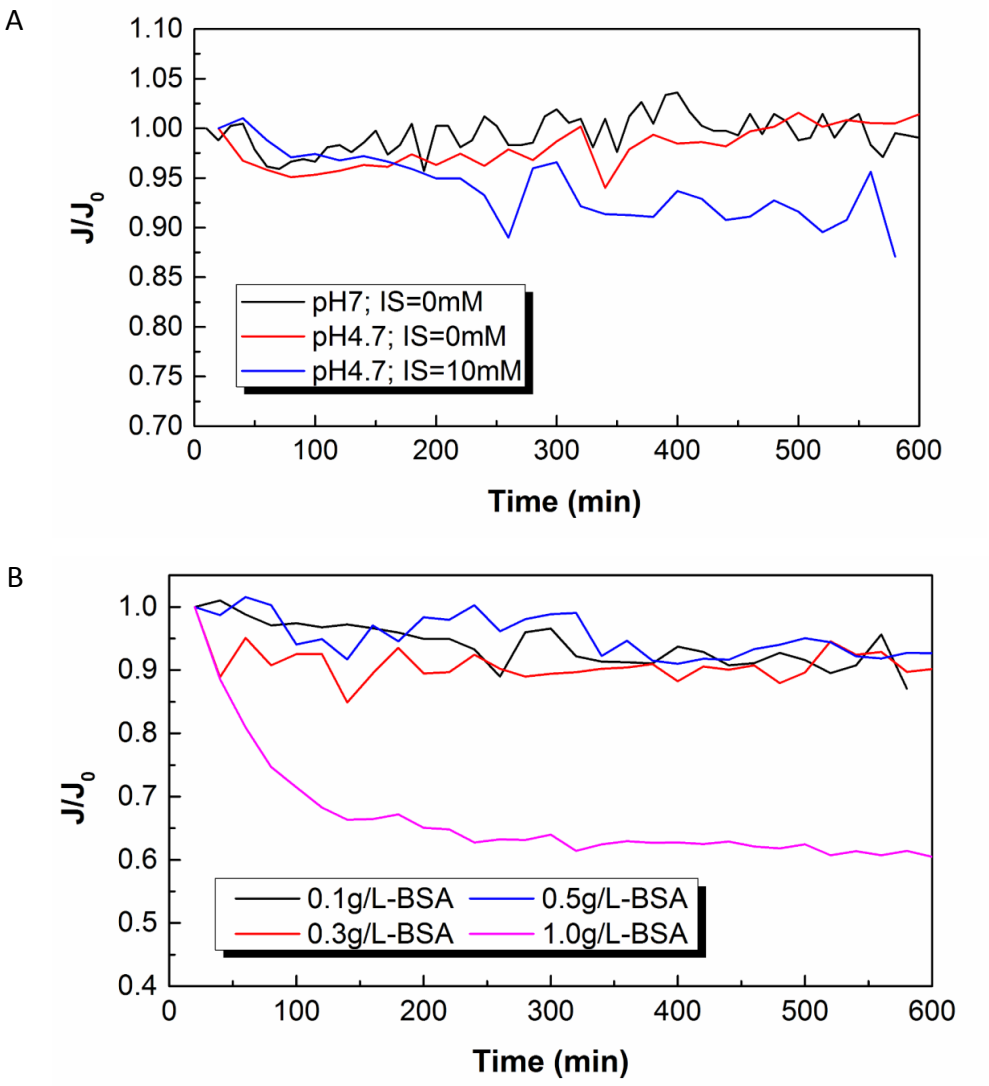


**Figure A.2.** Normalized flux of the plain PA membrane as a function of time during BSA fouling. (A) Effect of ionic strength (IS) and pH of the feed solution on membrane fouling. The concentration of bovine serum albumin (BSA) was kept at 0.1g/L for all three fouling tests. (B) Effect of the concentration of BSA on fouling, where pH and IS of the feed solution were adjusted to 4.7 and 10mM, respectively. Total ionic strength of the feed solution was adjusted by varying Ca2+ and NaCl concentration. AAS (100 mg/L) was added to the solution in every testing to enhance the fouling.

## References

(1) Ghosh, A. K.; Hoek, E. M. V. Impacts of Support Membrane Structure and Chemistry on Polyamide–polysulfone Interfacial Composite Membranes. *Journal of Membrane Science* **2009**, *336*, 140–148.

(2) Saha, N. K.; Joshi, S. V. Performance Evaluation of Thin Film Composite Polyamide Nanofiltration Membrane with Variation in Monomer Type. *Journal of Membrane*

*Science* **2009**, *342*, 60–69.

(3) Kong, C.; Kanezashi, M.; Yamomoto, T.; Shintani, T.; Tsuru, T. Controlled Synthesis of High Performance Polyamide Membrane with Thin Dense Layer for Water Desalination. *Journal of Membrane Science* **2010**, *362*, 76–80.

(4) Xie, W.; Geise, G. M.; Freeman, B. D.; Lee, H.-S.; Byun, G.; McGrath, J. E. Polyamide Interfacial Composite Membranes Prepared from M-Phenylene Diamine, Trimesoyl Chloride and a New Disulfonated Diamine. *Journal of Membrane Science* **2012**.

(5) Kim, S.; Jinschek, J. R.; Chen, H.; Sholl, D. S.; Marand, E. Scalable Fabrication of Carbon Nanotube/Polymer Nanocomposite Membranes for High Flux Gas Transport. *Nano Letters* **2007**, *7*, 2806–2811.

(6) Corry, B. Designing Carbon Nanotube Membranes for Efficient Water Desalination. *Journal of Physical Chemistry B* **2008**, *112*, 1427–1434.

(7) GWQR. FLUID VISCOSITY TABLES http://home.global.co.za/~fluid/GWIS Fluid_Viscosity_Table.htm.

(8) Otero, J. a.; Mazarrasa, O.; Villasante, J.; Silva, V.; Prádanos, P.; Calvo, J. I.; Hernández, a. Three Independent Ways to Obtain Information on Pore Size Distributions of Nanofiltration Membranes. *Journal of Membrane Science* **2008**, *309*, 17–27.

# Appendix B

## B.1. Cross-Flow Reverse Osmosis Operating Procedure

**Set-up:**

1. Place a clean feed spacer in the cavity inside the bottom-half SS cell
2. Place a pre-cut permeate carrier (white mesh) in the cavity at the top-half SS cell (Wet the cavity with deionized water so that the mesh can stick on it)
3. Place the masked membrane in the cell and align it so that the membrane covers the whole inner O-ring
4. Close the cell and screw all the corners (hand-tight)
5. Put it into the cell holder and pressurize the holder up to 45 bars
6. Connect all the tubings and pipings to the cell.

**Start-up Procedure:**

- Open all the valves including the valve between the pump and the cell inlet and the one at the concentrated outlet.
- Start the pump and slowly increase the flow rate up to 2 LPM.
- Gently close the concentrated outlet valve to build the pressure up to 50 psi.
- Allow **5** minutes to stabilize the system and make sure the water flow is continuous with no air bubbles rushing through the tube (visible through the flow meter).
- Increase the flow rate to 2.5 LPM and adjust the pressure to the designated testing pressure.

**Testing Protocol:**

- For testing any **fresh membrane**, increase the pressure until the permeation flux is ~ **5g/hr** (effective area: ~1.7 cm in diameter) and keep permeating for **one hour** before testing it at the desired pressure. This process can make sure the concentration of the permeance reaches its equilibrium.
    - e.g. 350 psi for 26wt% Z-SWNTs/PA and 500 psi for 0.34(v/v)% TMC-PA
- At each testing pressure, allow **30** minutes of continuous permeation in order to reach equilibrium before taking any sample.
- When the testing pressure can only provide less than **3 g/hr** of permeance through the membrane, allow 1 hour of continuous permeation before taking any sample.

**Clean-up:**

1. Slowly release the pressure by turning the outlet valve counter-clockwise until the pressure gauge shows **0**
2. Reduce the flow rate slowly until it reaches **0**
3. To drain out all the fluid inside the tubes, pump and cell...
    A. Remove the rotameter and collect the fluid within it
    B. Make sure the inlet of the pump has been disconnected from the feed tank
4. Start the pump and slowly drain the fluid inside the system to an extra container (collect them at the outlet of the SS cell)

5. Exchange the feed to other salt solutions if for further testing using the same membrane
6. If not, replace the membrane with a plastic sheet, reconnect all the tubings and flush deionized water through the system to clean out any salt residues

TO CLEANSE any **Calcium deposit** in the system....

- Use the mixture of nitric acid (70%) and tap water in the ratio of 1 to 25 (e.g. add 20 ml of $HNO_3$ into 500 ml of tap water)
- Flush the mixture through the system overnight

## B.2. Functionalization procedure for Zwitterionic CNT

### B.2.1. Acylation of SWNTs with Thionyl Chloride

1. Take a 100 ml round bottomed flask and put 200 mg of SWNTs
2. Setup the condenser (straight) with water flowing
3. Also, make a blockage using sulfuric acid for the gas that comes out during reaction and attach it to the top end of the condenser
4. Now, add 25 ml of SOCl2 and 1 ml of DMF to the flask
5. Close immediately with a stopper (SOCl2 should not be exposed to atmosphere. Otherwise it will get hydrolyzed)
6. Add a stirrer bar and attach the flask to the lower end of the condenser
7. Bring the stirring hot plate with a bowl of paraffin oil in it
8. Pull it up until the flask submerges around two-third
9. Check that the thermometer is inside the paraffin oil and not touching the flask
10. Put the speed for RPM at the first sector and the temperature at 6 sectors (65 C) on the stirring hot plate
11. Run the reaction at those particular settings for 3 days until gas bubbles in sulfuric acid stops coming.
12. When cooling down, the vacuum in the flask will pull the sulfuric acid inside. Be careful at this step. I can close with a stopper to avoid this situation.
13. Once the reaction ends, remove the sulfuric acid gas outlet
14. Attach the outlet pump with a trap to the flask and no condenser is required this time
15. Increase the temperature to around 70 degrees and then, try to vacuum distill the thionyl chloride.
16. Keep checking the trap and if it is fill, empty it.
17. Once it is semi dry, add around 30 ml of anhydrous THF and mix it well.
18. Then, add this solution to centrifuge tubes
19. Centrifuge at around 10000 RPM and wash at least twice.
20. The supernatant will be brown- black and it is hard to see that SWNTs has settled down in the tubes.
21. Drain the supernatant solution and vacuum dry overnight in the oven.

### B.2.2. Reaction of Acylated SWNTs with the 3-Dimethyl Amino-1-Proponol

1. Clean all the glassware that will be used in this experiment with ethanol, then acetone and dry it in the heat oven which will ensure no traces of any water in the glassware
2. Any traces of water will react with the acylated SWNTs and convert them back to carboxylic acids
3. Take a round bottome flask 100 ml and add 3 ml of DMAP, and 3 ml of Triethyl Amine (TEA).
4. Now, crush the pellets of SWNTs formed in the centrifuging tube using a spatula and add the SWNTs to the reaction mixture
5. Take a stopper and put some lubricant to it
6. Add a suitable stirrer and close the flask.
7. Stir for 6 days under ambient conditions.

### B.2.3. Reaction of SWCNT with 3-Dimethylamino-1-propanol

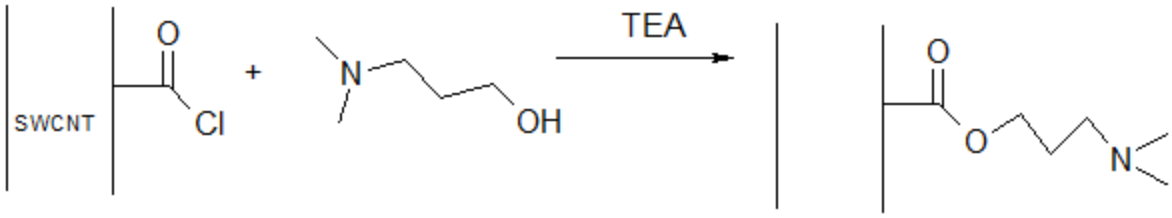


In the first step the SWCNTs were modified by thionyl chloride and carboxyl groups were converted to more reactive chloride groups.

The following step – ester preparation:

3-Dimethylamino-1-propanol – $M_w$=101.2, r=0.726
Triethyl amine - $M_w$=103.16, r =0.872

100 mg of SWCNT-COCl (~0.1 mmol of COCl groups) was reacted with 1.2 ml 3-Dimethylamino-1-propanol (10 mmol) in the presence of 1.4 ml triethyl amine (10 mmol). [The amount of amines used was 100 times higher than chloride]. Reaction mixture was kept under stirring at room temperature for 6 days. The modified SWCNT were filtered of (or centrifuged) to remove unreacted excess of the initial amines and washed with water or ethanol to remove Triethylamine hydrochloride and dried under vacuum.

1. Take 'x' amount go SWNTs in 50 ml flask and drop the stirrer
2. Add 20 ml of dry THF to the flask with the stopper
3. Run the nitrogen protection
4. Remove the stopper and add beta-propiolactone (1000 ul)
5. Keep stirring for 5 hours

Washing: Wash with dry THF (using centrifuge)

## B.3. Membrane Masking Using aluminum Tape

During the fabrication of Z-SWNT/PA membrane the size of the membrane was limited by the depositing area of the filtration system. The largest membrane we are able to synthesize is 3.7 cm in diameter, which leads to a problem in testing the membrane. Using our designated permeation cell, the effective area is much larger than the membrane. It requires proper masking for membrane in order to extend the total area of the film and seal the gap of empty area preventing any sorts of leaking.

NO wonder the masking is the most important step during the characterization. The failure of proper masking will open so many doubtful questions for your data, rather the bad performance in water flux and salt rejection rate really due to your membrane, or some leaks at your masking. Therefore, aluminum foil duct tape (McMaster-Carr; 76145A36) became our prior choice because of its heavy-duty performance against high hydraulic pressure and inert behavior to the salt water.

For small membrane permeation cell, a piece of Al tape, dimension of 21 cm in length and 7.2cm in width (the width of the tape), is cut. The tape was then fold in half, following with a circle of 2.2cm in diameter cut back and front at the center of the tape. The edge of the cut circle may be quite sharp due to some bad cutting. Make the edge become even and smooth using the back of a razer blade. After that the tape protecting sheet was peeled off and the TFC membrane was placed in between the Al tape. Align the center of the membrane to that of the hole. Afterwards, use the back of razer blade to squeeze the tapes tight to each other and make sure no air gaps or bubbles in between.

2 Ton® Epoxy from Devcon Inc. was then applied between the edge of the hole and the membrane to seal off any possibility of leaking. This epoxy requires at least 2-3 hours of curing time. The membrane will then be saved to test in the cell. This type of masking is proven to be the safest and effective method. Almost all the experiments carried out perfectly after using this masking method.

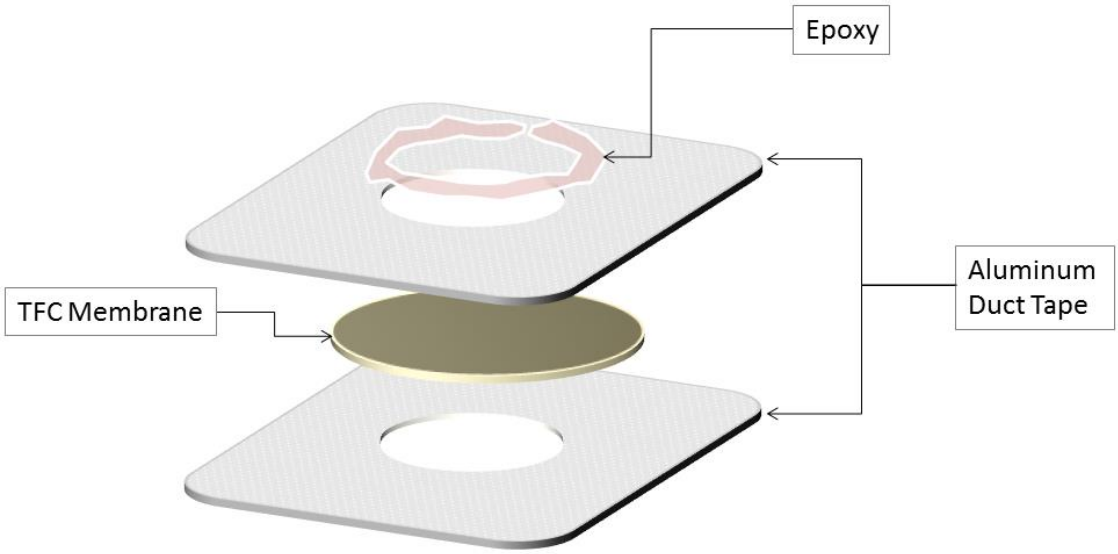

# Appendix C: Journal Permissions for Reprinting

## C.1. Figure 6 in McGrath et al. Water permeability and water/salt selectivity tradeoff in polymers for desalination Journal of Membrane Science. 369 (2011) 130–138.

ELSEVIER LICENSE
TERMS AND CONDITIONS

Mar 24, 2015

This is a License Agreement between Waifong Chan ("You") and Elsevier ("Elsevier") provided by Copyright Clearance Center ("CCC"). The license consists of your order details, the terms and conditions provided by Elsevier, and the payment terms and conditions.

All payments must be made in full to CCC. For payment instructions, please see information listed at the bottom of this form.

| | |
|---|---|
| Supplier | Elsevier Limited<br>The Boulevard,Langford Lane<br>Kidlington,Oxford,OX5 1GB,UK |
| Registered Company Number | 1982084 |
| Customer name | Waifong Chan |
| Customer address | 1400 UNIVERSITY CITY BLVD APT J<br>BLACKSBURG, VA 24060 |
| License number | 3595411333184 |
| License date | Mar 24, 2015 |
| Licensed content publisher | Elsevier |
| Licensed content publication | Journal of Membrane Science |
| Licensed content title | Water permeability and water/salt selectivity tradeoff in polymers for desalination |
| Licensed content author | Geoffrey M. Geise,Ho Bum Park,Alyson C. Sagle,Benny D. Freeman,James E. McGrath |
| Licensed content date | 1 March 2011 |
| Licensed content volume number | 369 |
| Licensed content issue number | 1-2 |
| Number of pages | 9 |
| Start Page | 130 |
| End Page | 138 |

| | |
|---|---|
| Type of Use | reuse in a thesis/dissertation |
| Portion | figures/tables/illustrations |
| Number of figures/tables/illustrations | 1 |
| Format | both print and electronic |
| Are you the author of this Elsevier article? | No |
| Will you be translating? | No |
| Original figure numbers | figure 6 |
| Title of your thesis/dissertation | Functionalized Carbon Nanotube nanocomposite membrane for water desalination |
| Expected completion date | Jun 2015 |
| Estimated size (number of pages) | 100 |
| Elsevier VAT number | GB 494 6272 12 |
| Permissions price | 0.00 USD |
| VAT/Local Sales Tax | 0.00 USD / 0.00 GBP |
| Total | 0.00 USD |
| Terms and Conditions | |

**C.2. Figure 2 and 5 in Coronell et al. Investigating the void and nodular structure of the polyamide active layers of thin-film composite membranes, Journal of Membrane Science. In review (2016) 365–376.**

ELSEVIER LICENSE
TERMS AND CONDITIONS

Sep 26, 2015

This is a License Agreement between Waifong Chan ("You") and Elsevier ("Elsevier") provided by Copyright Clearance Center ("CCC"). The license consists of your order details, the terms and conditions provided by Elsevier, and the payment terms and conditions.

All payments must be made in full to CCC. For payment instructions, please see information listed at the bottom of this form.

| | |
|---|---|
| Supplier | Elsevier Limited<br>The Boulevard,Langford Lane<br>Kidlington,Oxford,OX5 1GB,UK |
| Registered Company Number | 1982084 |
| Customer name | Waifong Chan |
| Customer address | 1400 UNIVERSITY CITY BLVD APT J<br>BLACKSBURG, VA 24060 |
| License number | 3716801234214 |
| License date | Sep 26, 2015 |
| Licensed content publisher | Elsevier |
| Licensed content publication | Journal of Membrane Science |
| Licensed content title | Investigating the void structure of the polyamide active layers of thin-film composite membranes |
| Licensed content author | Lin Lin,Rene Lopez,Guy Z. Ramon,Orlando Coronell |
| Licensed content date | Available online 15 September 2015 |
| Licensed content volume number | n/a |
| Licensed content issue number | n/a |
| Number of pages | 1 |
| Start Page | 0 |

| | |
|---|---|
| End Page | 0 |
| Type of Use | reuse in a thesis/dissertation |
| Portion | figures/tables/illustrations |
| Number of figures/tables/illustrations | 2 |
| Format | both print and electronic |
| Are you the author of this Elsevier article? | Yes |
| Will you be translating? | No |
| Original figure numbers | figure 2,5 |
| Title of your thesis/dissertation | Functionalized Carbon Nanotube nanocomposite membrane for water desalination |
| Expected completion date | Jun 2015 |
| Estimated size (number of pages) | 100 |
| Elsevier VAT number | GB 494 6272 12 |
| Permissions price | 0.00 USD |
| VAT/Local Sales Tax | 0.00 USD / 0.00 GBP |
| Total | 0.00 USD |
| Terms and Conditions | |

**C.3. Figure 1 in Lee et al. Modification to the polyamide TFC RO membranes for improvement of chlorine-resistance, Journal of Membrane Science. 376 (2011) 302–311.**

ELSEVIER LICENSE
TERMS AND CONDITIONS

Oct 06, 2015

This is a License Agreement between Waifong Chan ("You") and Elsevier ("Elsevier") provided by Copyright Clearance Center ("CCC"). The license consists of your order details, the terms and conditions provided by Elsevier, and the payment terms and conditions.

All payments must be made in full to CCC. For payment instructions, please see information listed at the bottom of this form.

| | |
|---|---|
| Supplier | Elsevier Limited<br>The Boulevard,Langford Lane<br>Kidlington,Oxford,OX5 1GB,UK |
| Registered Company Number | 1982084 |
| Customer name | Waifong Chan |
| Customer address | 1400 UNIVERSITY CITY BLVD APT J<br>BLACKSBURG, VA 24060 |
| License number | 3723130191961 |
| License date | Oct 06, 2015 |
| Licensed content publisher | Elsevier |
| Licensed content publication | Journal of Membrane Science |
| Licensed content title | Modification to the polyamide TFC RO membranes for improvement of chlorine-resistance |
| Licensed content author | Dong Ho Shin,Nowon Kim,Yong Taek Lee |
| Licensed content date | 1 July 2011 |
| Licensed content volume number | 376 |
| Licensed content issue number | 1-2 |
| Number of pages | 10 |
| Start Page | 302 |
| End Page | 311 |
| Type of Use | reuse in a thesis/dissertation |
| Portion | figures/tables/illustrations |

| | |
|---|---|
| Number of figures/tables/illustrations | 1 |
| Format | both print and electronic |
| Are you the author of this Elsevier article? | Yes |
| Will you be translating? | No |
| Original figure numbers | figure 1 |
| Title of your thesis/dissertation | Functionalized Carbon Nanotube nanocomposite membrane for water desalination |
| Expected completion date | Jun 2015 |
| Estimated size (number of pages) | 100 |
| Elsevier VAT number | GB 494 6272 12 |
| Permissions price | 0.00 USD |
| VAT/Local Sales Tax | 0.00 USD / 0.00 GBP |
| Total | 0.00 USD |
| Terms and Conditions | |

**C.4. Figure 8 in Gao et al. Aromatic-cycloaliphatic polyamide thin-film composite membrane with improved chlorine resistance prepared from m-phenylenediamine-4-methyl and cyclohexane-1,3,5-tricarbonyl chloride, Journal of Membrane Science. 344 (2009) 155–164.**

ELSEVIER LICENSE
TERMS AND CONDITIONS

Oct 12, 2015

---

This is a License Agreement between Waifong Chan ("You") and Elsevier ("Elsevier") provided by Copyright Clearance Center ("CCC"). The license consists of your order details, the terms and conditions provided by Elsevier, and the payment terms and conditions.

All payments must be made in full to CCC. For payment instructions, please see information listed at the bottom of this form.

| | |
|---|---|
| Supplier | Elsevier Limited<br>The Boulevard,Langford Lane<br>Kidlington,Oxford,OX5 1GB,UK |
| Registered Company Number | 1982084 |
| Customer name | Waifong Chan |
| Customer address | 1400 UNIVERSITY CITY BLVD APT J<br>BLACKSBURG, VA 24060 |
| License number | 3726671053431 |
| License date | Oct 12, 2015 |
| Licensed content publisher | Elsevier |
| Licensed content publication | Journal of Membrane Science |
| Licensed content title | Aromatic-cycloaliphatic polyamide thin-film composite membrane with improved chlorine resistance prepared from mphenylenediamine-4-methyl and cyclohexane-1,3,5-tricarbonyl chloride |
| Licensed content author | Sanchuan Yu,Meihong Liu,Zhenhua Lü,Yong Zhou,Congjie Gao |
| Licensed content date | 15 November 2009 |
| Licensed content volume number | 344 |
| Licensed content issue number | 1-2 |
| Number of pages | 10 |
| Start Page | 155 |
| End Page | 164 |

| | |
|---|---|
| Type of Use | reuse in a thesis/dissertation |
| Portion | figures/tables/illustrations |
| Number of figures/tables/illustrations | 1 |
| Format | both print and electronic |
| Are you the author of this Elsevier article? | No |
| Will you be translating? | No |
| Original figure numbers | figure 8 |
| Title of your thesis/dissertation | Functionalized Carbon Nanotube nanocomposite membrane for water desalination |
| Expected completion date | Jun 2015 |
| Estimated size (number of pages) | 100 |
| Elsevier VAT number | GB 494 6272 12 |
| Permissions price | 0.00 USD |
| VAT/Local Sales Tax | 0.00 USD / 0.00 GBP |
| Total | 0.00 USD |
| Terms and Conditions | |

## C.5. Figure 10 in Hoek et al. Electrospun nanofiber supported thin film composite membranes for engineered osmosis, Journal of Membrane Science. 385-386 (2011) 10–19.

ELSEVIER LICENSE
TERMS AND CONDITIONS

Oct 28, 2015

This is a License Agreement between Waifong Chan ("You") and Elsevier ("Elsevier") provided by Copyright Clearance Center ("CCC"). The license consists of your order details, the terms and conditions provided by Elsevier, and the payment terms and conditions.

All payments must be made in full to CCC. For payment instructions, please see information listed at the bottom of this form.

| | |
|---|---|
| Supplier | Elsevier Limited<br>The Boulevard,Langford Lane<br>Kidlington,Oxford,OX5 1GB,UK |
| Registered Company Number | 1982084 |
| Customer name | Waifong Chan |
| Customer address | 1400 UNIVERSITY CITY BLVD APT J<br>BLACKSBURG, VA 24060 |
| License number | 3737701207611 |
| License date | Oct 28, 2015 |
| Licensed content publisher | Elsevier |
| Licensed content publication | Journal of Membrane Science |
| Licensed content title | Electrospun nanofiber supported thin film composite membranes for engineered osmosis |
| Licensed content author | Nhu-Ngoc Bui,Mary Laura Lind,Eric M.V. Hoek,Jeffrey R. McCutcheon |
| Licensed content date | 1 December 2011 |
| Licensed content volume number | 385 |
| Licensed content issue number | n/a |
| Number of pages | 10 |
| Start Page | 10 |
| End Page | 19 |
| Type of Use | reuse in a thesis/dissertation |
| Portion | figures/tables/illustrations |

| | |
|---|---|
| Number of figures/tables/illustrations | 1 |
| Format | both print and electronic |
| Are you the author of this Elsevier article? | No |
| Will you be translating? | No |
| Original figure numbers | Figure 10 |
| Title of your thesis/dissertation | Functionalized Carbon Nanotube nanocomposite membrane for water desalination |
| Expected completion date | Jun 2015 |
| Estimated size (number of pages) | 100 |
| Elsevier VAT number | GB 494 6272 12 |
| Permissions price | 0.00 USD |
| VAT/Local Sales Tax | 0.00 USD / 0.00 GBP |
| Total | 0.00 USD |
| Terms and Conditions | |